# SYNTHESIS OF MULTI-COMPONENT POLYMER PARTICLES VIA SEEDED-EMULSION POLYMERIZATION

**YAM CHUN HO**

**Ph.D**

**The Hong Kong Polytechnic University**

**2015**

The Hong Kong Polytechnic University

Department of Applied Biology

and Chemical Technology

# Synthesis of Multi-Component Polymer Particles via Seeded-Emulsion Polymerization

YAM CHUN HO

A thesis submitted in partial fulfillment of

the requirements for the degree of Doctor of Philosophy

May 2014

# Certificate of Originality

I hereby declare that this thesis is my own work and that, to the best of my knowledge and belief, it reproduces no material previously published or written, nor materials that has been accepted for the award of any other degree or diploma, except where due acknowledgement has been made in the text.

Yam Chun Ho

(May 2014)

# Abstract

Development of novel strategies to prepare multi-component polymeric (MCP) particles is scientifically and technologically important because the MCP particles can possess multi-functionalities, intriguing hierarchical nanostrustures and synergistic properties of different components. Current synthetic approaches to prepare this kind of particles often suffer from some major drawbacks such as time-consuming solvent treatment, addition of large amount of stabilizers and emulsifiers, complicated multi-stage polymerization, and formation of relatively large particles. Thus, this thesis aims to develop a versatile and robust synthetic approach to synthesize multi-component amphiphilic core-shell particles in one-pot polymerization. The new approach is based on semi-batch seeded emulsion polymerization, which could be scale up for mass production. Various types of multi-component polymer nanoparticles were synthesized from different kinds of seed particles, including hard, soft and temperature-sensitive materials. The shell of the particles could be altered from a pH-responsive only to both pH- and temperature-responsive materials. The novel approach developed in this research allows us to fabricate multi-component polymeric particles with different nanostructures and compositions. It opens up an amenable pathway to commercial production of multi-component polymeric particles.

The thesis begins with the definition of multi-component polymer (MCP) particles. Possible morphologies of the MCP particles and key principles for the formation of these special morphologies are discussed in detail. Current approaches to prepare MCP particles and their limitations are presented. Lastly,

the core-shell particle platform technology developed by Li's group and their potential applications are illustrated.

Chapter Two introduces the motivation of this project. Specific objectives of this research to develop three-component amphiphilic core-shell particles are highlighted.

Chapter Three describes the synthesis of MCP particles using PMMA/PEI as the seed particles. The seed particles were initially formed through a graft copolymerization of methyl methacrylate (MMA) from polyethyleneimine (PEI) via a redox initiation. Second hydrophobic monomer, such as styrene or *n*-butyl acrylate (*n*-BA), was subsequently added and polymerized within the seed nanoparticles to form MCP particles. Two types of PMMA/PEI based MCP particles, namely poly(*n*-butyl acrylate)/poly(methyl methacrylate) /polyethyleneimine (PBA/PMMA/PEI) and polystyrene/poly(methyl methacrylate) /polyethyleneimine (PS/PMMA/PEI), were synthesized and systematically characterized by different analytical methods. Under optimum reaction pH, the PBA/PMMA/PEI MCP particles possessed amphoteric property arising from the presence of positively charged amino groups and negatively charged carboxylic acid groups that were formed via the hydrolysis of the ester group. These amphoteric MCP particles were colloidally stable over the whole pH range.

Chapter Four discusses the synthesis of MCP particles using *N,N'*-methylene bis(acrylamide)-crosslinked poly(*N*-isopropyl acrylamide) /polyethyleneimine (PNIPAm-MBA)/PEI as seed particles. The (PNIPAm-MBA)/PEI seed nanogel was first formed by a graft copolymerization of *N*-isopropyl acrylamide (NIPAm) from PEI via a redox initiation. MBA was utilized as a crosslinker for the PNIPAm/PEI seeds. Second hydrophobic monomer, such as MMA, styrene or *n*-BA, was subsequently added and polymerized in the presence of seeded nanoparticles to form MCP particles. Three types of smart MCP particles, namely PMMA/(PNIPAm-MBA)/PEI, PBA/(PNIPAm-MBA)/PEI and PS/(PNIPAm-MBA)/PEI, were successfully synthesized. All of these smart MCP particles exhibited pH- and temperature-responsive properties. Degree of MBA crosslinking was found to affect the pH- and temperature-responsive properties of the MCP particles. The particle morphology and nanostructure were revealed by Field-Emission Scanning Electron Microscopy (FE-SEM) and Transmission Electron Microscopy (TEM). The inner core of MCP particle was constructed with hydrophobic polymer of PMMA, PBA or PS, while the outer shell of MCP particle was an interpenetrated network, comprising of pH-responsive PEI and temperature-responsive PNIPAm. Interestingly, MCP particles with different morphologies were obtained when using different monomers as the second batch of hydrophobic monomers. The PS/ (PNIPAm-MBA)/PEI and PBA/(PNIPAm-MBA)/PEI MCP particles displayed spherical morphology, while PMMA/(PNIPAm-MBA)/PEI MCP particles possessed aerolite-like morphology with many PMMA micro-domains evenly distributed in the particles matrix.

Chapter Five describes further investigation of MCP particles using non-crosslinked PNIPAm/PEI as seed particles based on the previous findings described in chapter Four. PNIPAm/PEI micelle-like seed nanoparticles were first formed by the graft copolymerization of NIPAm from PEI via a redox initiation. Second hydrophobic monomer, MMA or styrene, was subsequently added and underwent seed emulsion polymerization, giving stable MCP particles. Two types

of MCP particles, PS/PNIPAm/PEI and PMMA/PNIPAm/PEI, were successfully prepared. The temperature-responsive properties of MCP particles could be adjusted by varying the weight ratio between seed monomer and second batch monomer. MCP particles with different morphologies were produced when using various second batch hydrophobic monomers. Spherical particles were obtained when styrene was used as the second batch monomer, while the use of MMA gave aerolite-like particles.

The properties of the resulting particles, including particle size and size distribution, surface charge, chemical composition and morphology, have been systematically characterized by dynamic light scattering, ζ-potential measurement, Fourier-transform infra-red spectroscopy, field emission scanning electron microscopy and transmission electron microscopy. The pH-responsive property of the shell of the particles was confirmed by ζ-potential measurement at different pHs.

Chapter Six concludes the essential findings obtained in this thesis. The synthesis and smart responsive properties of MCP particles were also summarized. Mechanism of MCP particle formation leading to various nanostructures was proposed.

The final Chapter provides recommendations for further development of MCP particles. Future works include fabrication of different functional MCP particles and exploration of MCP particles as protective coating.

# List of Publications

## *Referred Journal Articles*

1. Ho, K. M.; Li, W. Y.; Lee, C. H.; Yam, C. H.; Gilbert, R. G.; Li, P. "Mechanistic study of the formation of amphiphilic core-shell particles by grafting methyl methacrylate from polyethylenimine through emulsion polymerization" *Polymer,* **2010,** 51, 3512-3519

## *Conference Presentations and Publications*

1. Yam, C. H.; Ho, K. M.; Li, P. "Smart Multi-Component Polymer Particles with Tunable Surface Charge Density and Size" *Abstract of Papers, Polymers in Dispersed Media 2012, Lyon, France,* pp. P66, 16-19 April 2012

2. Yam, C. H.; Ho, K. M.; Li, P. "Smart Multi-Component Polymer Particles with Polystyrene Core, pH-Sensitive Polyethyleneimine and Temperature-Sensitive Poly(*N*-isopropyl acrylamide) Shell: Synthesis and Characterization" *Abstract of Papers, The 19th Symposium on Chemistry Postgraduate Research in Hong Kong, The Hong Kong University of Science and Technology, Hong Kong,* pp. P-48, 14 April 2012

3. Yam, C. H.; Ho, K. M.; Li, P. “Novel Multi-Component Polymer Particles with pH and Temperature Modulated Surface Charge Density” *Abstract of Papers, The 4th Asian Symposium on Emulsion Polymerization and Functional Polymeric Microspheres, The Hong Kong Polytechnic University, Hong Kong,* pp. P-36, 11-14 December 2011

4. Yam, C. H.; Ho, K. M.; Li, P. “Smart Multi-component Polymer Particles with Temperature-Modulated Surface Charge Density” *Abstract of Papers, The 18th Symposium on Chemistry Postgraduate Research in Hong Kong, City University of Hong Kong, Hong Kong,* pp. P-39, 30 April 2011

5. Yam, C. H.; Ho, K. M.; Li, P. “Synthesis of Multi-Component Polymer Particles via Seeded Emulsion Polymerization” *Abstract of Papers, The 17th Symposium on Chemistry Postgraduate Research in Hong Kong, The Hong Kong Polytechnic University, Hong Kong,* pp. O-41, 24 April 2010

6. Yam, C. H.; Ho, K. M.; Li, P. “Facile Route to Polymer Nanocomposite Particles via Semi-Batch Seeded Emulsion Polymerization” *Abstract of Papers, The 16th Symposium on Chemistry Postgraduate Research in Hong Kong, Hong Kong Baptist University, Hong Kong,* pp. O-85, 18 April 2009

# Acknowledgements

I wish to express my deepest gratitude to my supervisor, Prof. Pei Li, for her supervision, intelligent ideas, professional guidance and continuing encouragements throughout the entire period of my study. Her wise ideas on this research project and valuable comments made my study a rewarding experience.

Special thanks also go to the colleges of Prof. Pei Li’s research group, including Dr. Edmond Kin Man Ho, Dr. Ai Hua Wu, Dr. Cheng Hao Lee, Yuen Shan Siu, Ka Ki Mou, Chiu Man Hung, Noel Peter Tan, Suqing Tan and Chun Him Wong, for their insightful discussions, technical advises and continual support.

In addition, I would like to acknowledge Mr. C. S. Lo of Department of Applied Physics for his training on the operation of field emission scanning electron microscopy (FE-SEM) and technical support on FE-SEM characterization. I am also grateful to the staff in the Department of Applied Biology and Chemical Technology who had helped me a lot in various ways.

I would also like to thank the Research Committee of the Hong Kong Polytechnic University and the Research Grants Council (RGC) of Hong Kong Special Administrative Region for their financial support of my postgraduate study.

Finally, I would like to express my gratitude to my beloved family members for their unconditional love and unstinting supports.

# Table of Content

# Abbreviation and Symbols

| **Symbol** | **Description** |
|---|---|
| AGET | Activator Generated by Electron Transfer |
| AIBN | Azobisisobutyronitrile |
| APS | Ammomium persulfate |
| ATRP | Atom Transfer Radical Polymerization |
| $CDCl_3$ | Deuterated chloroform |
| Conv. % | Monomer conversion |
| $D_2O$ | Deuterated water |
| Dh | Hydrodynamic diameter |
| $D_N$ | Number-average hydrodynamic diameter |
| $D_V$ | Volume-average hydrodynamic diameter |
| $D_V/D_N$ | Polydispersity index of the particle size distribution |
| DLS | Dynamic light scattering |
| DSC | Differential scanning calorimetry |
| DVB | Divinylbenzene |

| | |
|---|---|
| FE-SEM | Field-emission scanning electron microscopy |
| FT-IR | Fourier-Transform Infrared spectroscopy |
| $^1$H NMR | Proton nuclear magnetic resonance spectroscopy |
| IEP | Isoelectric point |
| KPS | Potassium persulfate |
| MBA | *N,N'*-methylenebisacrylamide |
| NMP | Nitroxide Mediated Polymerization |
| PAA | Poly(acrylic acid) |
| PAN | Polyacrylonitrile |
| PANI | Polyaniline |
| PB | Polybutadiene |
| PBA | Poly(butyl acrylate) |
| PBIEM | Poly(2-(2-bromoisobutyryloxy)ethyl methacrylate) |
| PBMA | Poly(butyl methacrylate) |
| PDI | Polydispersity Index |
| PDM | Poly(2-(dimethylamino)ethyl methacrylate) |
| PEDOT | Poly(3,4-ethylenedioxythiophene) |
| PEGm | Poly(ethylene glycol) monomethacrylate |

| | |
|---|---|
| PEI | Poly(ethyleneimine) |
| PEO | Poly(ethylene oxide) |
| PI | Polyisoprene |
| PIDS | Polarization Intensity Differential Scattering |
| PMMA | Poly(methyl methacrylate) |
| PNIPAm | Poly(*N*-isopropylacrylamide) |
| PNVP | Poly(*N*-vinylpyrrolidone) |
| PS | Polystyrene |
| PSS | Poly(Sodium Styrene Sulphonate) |
| PTA | Phosphotungstic acid |
| PVP | Polyvinylpyrrolidone |
| RAFT | Reversible Addition-Fragmentation Chain-Transfer |
| Rh | Hydrodynamic radius |
| S.C.% | Solid content |
| STXM | Scanning transmission X-ray microscopy |
| TBHP | *tert*-butyl hydroperoxide |
| TEM | Transmission electron microscopy |
| $T_g$ | Glass transition temperature |

| | |
|---|---|
| UV-VIS | Ultraviolet-visible spectrophotometer |
| V-50 | 2,2'-Azobis(2-methylpropionamidine)dihydrochloride |
| V-65 | 2,2’-Azobis(2,4-diemthylvaleronitrile) |
| V-65B | 2,2’-azodi(2,4’-dimethylvaleronitrile) |
| VPTT | Volume phase transition temperature |
| $Z_{AVE}$ | Hydrodynamic diameter |
| ζ-potential | *zeta*-potential |

# Chapter 1

## Introduction

### 1.1 Definition of Multi-Component Polymer (MCP) particles

Multi-component polymer (MCP) particles are defined as polymeric particles composed of more than three components. These components could be polymer, organic, inorganic or metallic species, but excluding the initiator and crosslinker. MCP particles exhibited micron or nano-sized dimension and are dispersed uniformly in the continuous solvent medium.

MCP particle is a robust technology platform that allows the design and fabrication of particles with sophisticated nanostructure and specific functionalities. Through combination of various types of components, MCP particles could be tailor-made with specialty performance and stimuli responsive properties. For examples, multi-responsive nanoparticles could be constructed by introducing pH-, temperature-, magnetic- or UV-sensitive materials into the particles. Electric conducting nanoparticles could be formed by embedding conducting polymer or piezo-electric materials in the particles. These stimuli-responsive properties made MCP particles became smart materials and applicable in various specialty areas [1, 2].

The physical and chemical properties of the composite particles could also be easily adjusted [3]. By varying the composition of different components in the particles, hardness or softness could be tuned. This can either improve the rigidity or film forming ability of the resulting particles which made them suitable for anti-stretching or film forming applications. In addition, particle morphologies could be tailor-made to various nanostructures through changing the reaction parameters like temperature, solvent system, sequences of reagent addition and post-treatment. With the control of these processing parameters, spherical-, ellipsoidal-, anisotropic-, dumbbell- and raspberry- shaped particles could be formed. Since morphology is one of the most important factors in determining the terminal application of the materials, controllable particle morphology provides a promising route to prepare particles for different specific applications [4].

Comprising of multi-functionalities, sophisticated nanostructures and high stability, MCP particles have demonstrated great potential in various applications [5], including synthetic rubber, stimuli responsive coatings, painting inks, paper additives, textile additives, construction materials additives, impact modifiers, cosmetics, drug and gene delivery, enzyme immobilization, colloidal catalysts, optics, photonics, chemical sensing and thermal laser imaging [6-16].

## 1.2 Formation of MCP particles based on the principle of phase separation of incompatible polymers

MCP particles are attractive due to their multi-functionalities. These properties are highly dependent on the morphology and nanostructure of the particles. Therefore, controllable morphology and nanostructure has become a key factor in particle design. Before particle design and synthesis, it is necessary to understand the parameters that determine the final morphology and nanostructure of the particles. One of the most important parameters leading to the formation of different morphologies and nanostructures is the phase separation of incompatible polymers during and after the synthesis [17].

To simplify the system for easy understanding, the reaction system was assumed to be a biphasic system comprised of three major components, water as the solvent medium, initiator, and composite latex particles composed of two different types of polymers. The synthesis of the particles was divided into two steps. Seed particles were first formed by the polymerization of one monomer in the presence of initiator and sufficient temperature under nitrogen protection. Another monomer was then added to the seed particles to proceed seeded emulsion polymerization to form the composite latex particles.

### *Particles formation mechanism*

In the first stage, seed particles were formed by homopolymerization. The preformed particles exhibited spherical morphology in order to minimize the interfacial free energy. Another monomer was then introduced to the reaction system to proceed seed emulsion polymerization in the second stage. The monomer would first diffuse from the bulk phase into the seed particles as the monomer had greater compatibility with the seed particles than the bulk phase. The swollen seed particles underwent seeded emulsion polymerization after the addition of the second batch initiator. Upon polymerization of the second monomer, the resulting morphology of the particles was greatly dependent on the compatibility between the newly formed polymer and the seed polymer.

### *Phase separation between polymers*

If the newly formed polymer was compatible with the existing polymer in the seed particles, two types of polymer chains were free to diffuse inside the particles and equilibrium morphology would eventually achieve at the end of reaction. Nevertheless, it would be a totally different situation if the newly formed polymer was incompatible with the existing polymer in seed particles. The incompatibility between the polymers was the driving force for the phase separation [17]. Compatibility between two polymers was determined by their solubility, structural and polarity similarities. The higher the similarity was, the greater the compatibility between the polymers would result.

### *Morphology development*

During seeded emulsion polymerization, the second monomer was polymerized in the seed particles. As the newly formed polymer and the existing polymer were not compatible with each other, phase separation took place and clusters of the newly formed polymer were resulted. After the formation of numerous clusters, they started to migrate within the particles in order to minimize the interfacial tension to achieve minimum interfacial free energy (Gibbs free energy) [18].

Interfacial tension is the measurement of the cohesive energy at the interface due to the imbalanced force between the molecules at the interface. Common interface includes gas/liquid, gas/solid, liquid/liquid, and liquid/solid interface. Molecules located at the interface between two phases experience imbalanced force which results in free energy accumulation at the interface. Interfacial tension is a force which tends to minimize the surface area in contact with the other phase. Commonly used SI units for interfacial tension are dynes/cm and mN/m, which are expressed as force/length measurement.

Due to the tendency of minimization the surface area driven by interfacial tension, polymer composite particles are usually spherical in shape which reaches thermodynamic stable state. For the system comprised of composite polymer particles in aqueous phase, there are two major types of interfacial tension, namely polymer-polymer interfacial tension and polymer-aqueous phase interfacial tension. Generally, polymer-polymer interfacial tension is typically in the range of 1 – 20 mN/m and polymer-aqueous phase interfacial tension is typically in the range of $10^{-4}$ – 0.1 mN/m. Polymer-polymer interfacial tension and polymer-aqueous phase are important factors in determining the terminal morphology during morphology development. Lower interfacial tension corresponds to lower van der Waals force, which implies a slower rate of evolution towards equilibrium morphology, and vice versa.

Interfacial tension is important to morphology development as it determines the total interfacial free energy. Interfacial energy, also called Gibbs free energy, was the thermodynamic potential measuring the process-initiating work obtainable from isothermal and isobaric thermodynamic system. When a system changed from well-defined initial state to well-defined final state, the Gibbs free energy would be equal to the work exchanged by the system with its surroundings, minus the work of the pressure forces, during a reversible transformation of the system from the same initial state to the same final state. When a system reaches equilibrium state under isothermal and isobaric conditions, the Gibbs free energy would be minimized. The Gibbs free energy is a criterion of the spontaneity for chemical or physical process under constant conditions. Upon particle morphology development, the total interfacial free energy is defined as

$$\Delta G = \sum \gamma_{ij} A_{ij} - \gamma_0 A_0 \qquad \text{[Eq. 1.1]}$$

where $\Delta G$ is the change of total Gibbs free energy. $\gamma_{ij}$ is the interfacial tension at the interface between two phases i and j. $A_{ij}$ is the corresponding interfacial area. $\gamma_0$ and $A_0$ are the interfacial tension and area between the initial particle suspended in the continuous phase and the continuous phase respectively. The structural rearrangement is thermodynamic favorable (spontaneous) when $\Delta G$ is negative while it is thermodynamic unfavorable (non-spontaneous) when $\Delta G$ is positive. If $\Delta G$ is equal to zero, the structure of the particles has already reached the equilibrium state.

The determination of Gibbs free energy by [Eq. 1.1] is based on a number of assumptions. 1) Initially, there are three components in the system, including latex seed particle and two other polymers. 2) After morphology development, three component polymer particles are obtained. 3) All the polymer components are suspended in aqueous phase and the bulk phase is a monosolvent system. 4) There are no residual monomers presences in the system. 5) Sufficient time is allowed for the morphology rearrangement.

Morphology development of particles is the interplay between the kinetics and thermodynamics [19]. Thermodynamic factors determine the stability of particle morphology in accordance with minimum surface free energy. Kinetic factors control the ease with which such a thermodynamically preferred morphology could be reached. During morphology rearrangement of polymeric particles, the final morphology usually depends on the balance between the van der Waals attraction-repulsion interaction and viscous force. If van der Waals interaction outweighs the viscous force, thermodynamic favored morphology would be resulted. On the contrary, when viscous force outweighs the van der Waals interaction, kinetic stabilized morphology would be resulted [20]. Depending on the extent of cluster migration, viscosity of the particles, reaction temperature, glass transition temperature ($T_g$) of the polymers, types of initiators, crosslinking degree of the seed particles, selection of monomer etc., two different types of morphologies would be resulted in the synthesis of composite latex particles, namely thermodynamic morphology and kinetic morphology [21-24].

### *Case 1: Thermodynamic morphology (equilibrium morphology)*

Thermodynamic morphology, also called equilibrium morphology, is the morphology that particles exhibited the lowest Gibbs free energy. Particles with thermodynamic morphology are at the most stable state. These particles are spherical in shape so that interfacial tension could be minimized. Depending on the hydrophilicity of the polymer, three types of morphologies would be resulted in thermodynamic morphology under normal circumstances. These three morphologies are known as core-shell, inverted core-shell and occluded morphology and are illustrated in Fig. 1.1.

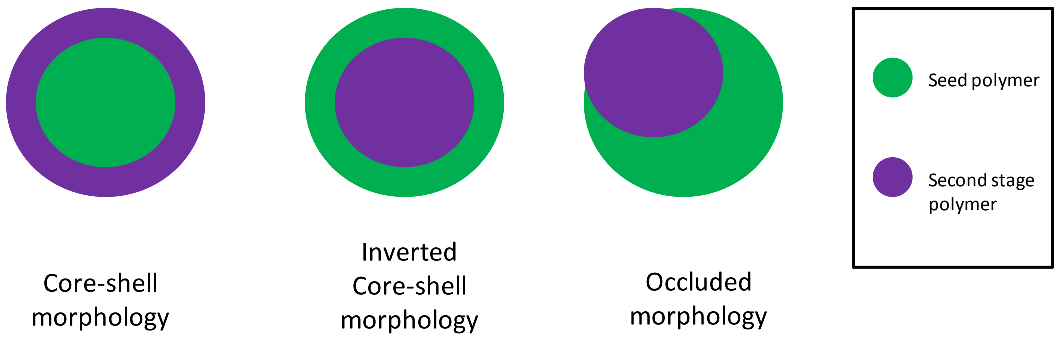

**Fig. 1.1.** Thermodynamic morphologies of two component polymer particles.

In thermodynamic morphology, two polymers would be completely separated in the particle at the end of reaction. Upon seed emulsion polymerization, some clusters of newly formed polymer were formed. These clusters would then migrate and coalescence due to van der Waals attraction and Ostwald ripening. However, the viscosity of the seed polymer would be the greatest restriction for the evolution of equilibrium morphology since it restricted the migration and diffusion of polymer chains in the particles. In order to achieve equilibrium morphology, van der Waals attraction should overcome the viscous force exerted by the particles. Provided that the reaction temperature was higher than the $T_g$ of two individual polymers, and the viscosity of particles was low enough for the clusters migration, well-defined structured particles could be achieved eventually.

Core-shell morphology is resulted when the newly formed polymer is more hydrophilic than the seed polymer. Since the newly formed polymer exhibits greater compatibility with the aqueous phase than the seed polymer, these polymer chains are preferentially migrated to the surface of the particles. Under this circumstance, the newly formed polymer is located at the outermost shell layer and acts as shell component. The seed polymer is less hydrophilic so it is confined at the innermost core and acts as core component. The evolution of the morphology is illustrated in Fig. 1.2.

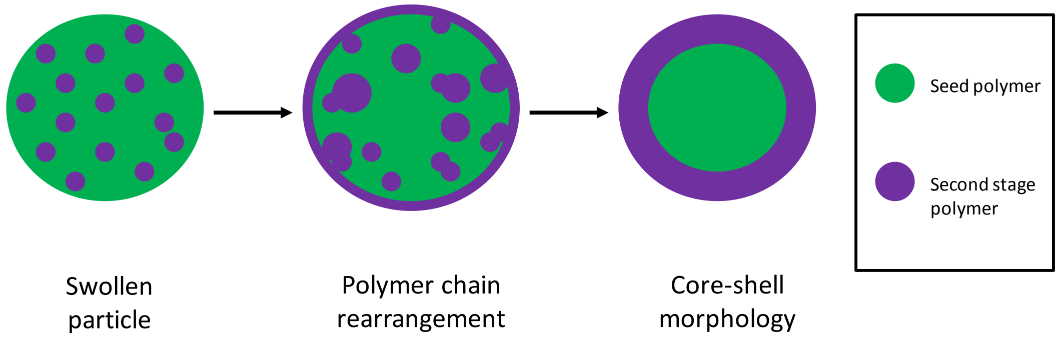

**Fig. 1.2.** Structural rearrangement of core-shell morphology.

Inverted core-shell morphology is resulted when the seed polymer is more hydrophilic than the newly formed polymer. Under this circumstance, the seed polymer exhibits greater compatibility with the aqueous phase. Therefore, the newly formed polymer would be diffused and migrated into the internal part of the particles and then coagulated due to the repulsion by the aqueous phase. Eventually, the shell of the composite particles is constructed by the seed polymer while the core is constructed by the newly formed polymer. The evolution of the morphology is illustrated in Fig. 1.3.

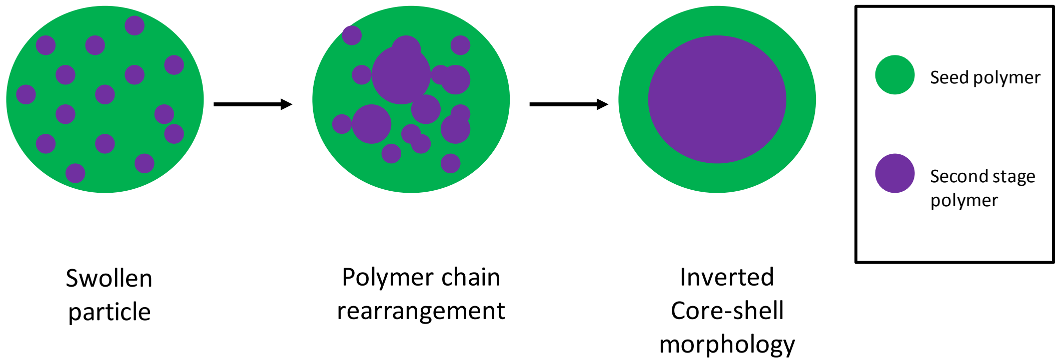

**Fig. 1.3.** Structural rearrangement of inverted core-shell morphology.

Occluded morphology is resulted when the seed polymer and the newly formed polymer possess similar hydrophilicity. As both polymers exhibit similar hydrophilicities, they have similar tendencies to migrate to the core or surface of particles. Depending on the composition of the two components, the dominant polymer would form the majority of the particle shell. The polymer with lower moieties would be embedded in the particles and becomes part of the particle surface. Assuming the seed particles as the dominant polymer, the evolution of the morphology is illustrated in Fig. 1.4.

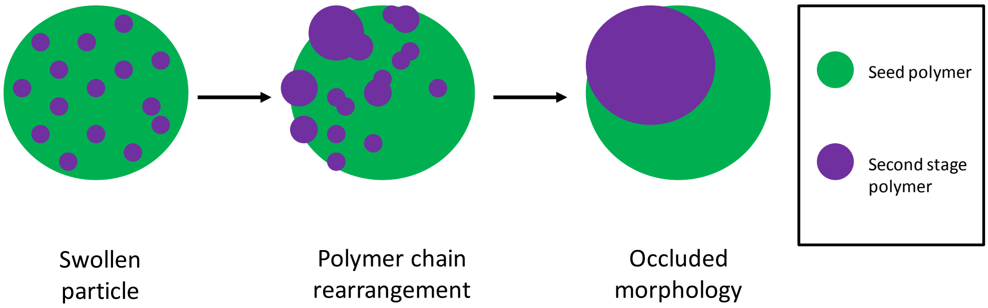

**Fig. 1.4.** Structural rearrangement of occluded morphology.

***Case 2: Kinetic morphology (non-equilibrium morphology)***

In real situation, particles could not achieve the most stable thermodynamic morphology at the end of reaction process, especially in pilot-scale polymerization. At the end of the polymerization process, these particles eventually reach non-equilibrium morphology called kinetic morphology. Under this circumstance, particles are at the metastable state and do not possess minimum interfacial energy. Though they are not at the most thermodynamic favored state, they are still stable to maintain the particle morphology without being deteriorated due to other surrounding physical parameters.

There are two major reasons contributing to the kinetic morphology of polymer particles. First, the viscosity of the seed particles is too high [25-27] that it retards the Ostwald ripening of the newly formed polymer. As the viscosity is too high, second stage polymers are hard to diffuse and coagulate inside the seed particles. Second, the reaction temperature also plays an important role in determining the terminal morphology of particles. Temperature is a key parameter to determine the rate of polymerization. If the temperature is too high, the polymerization kinetics of the second monomer would be too fast during seeded polymerization. Then rate of polymerization will be much faster than the rate of diffusion. Very rigid micro domains are formed and locked inside the seed particles which are not free to diffuse. If the temperature is low, i.e. below the $T_g$ of the both polymers in the composite particles, the polymer chains are free to migrate in the particles without restriction by any rigid polymer domains. Nevertheless, such low reaction temperature usually leads to slow rate of polymerization.

One of the most common types of non-equilibrium morphology is spherical shaped seed particles embedded with numerous micro domains of the second polymers formed during seeded polymerization [28]. A proposed morphology evolution scheme is suggested in Fig. 1.5.

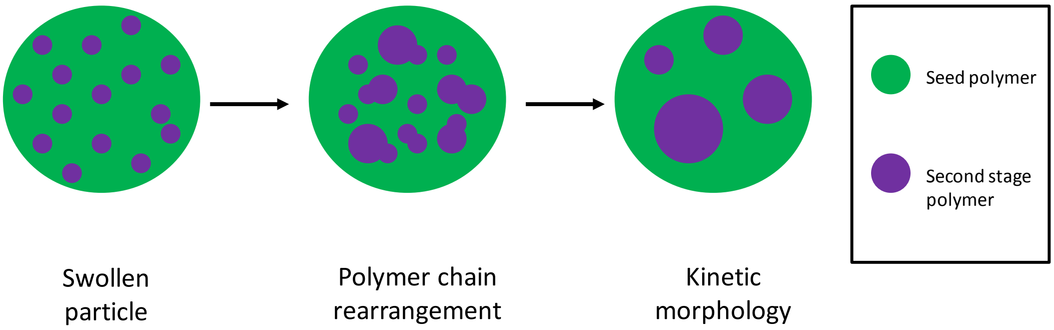

**Fig. 1.5.** Structural rearrangement of kinetic morphology.

### *Other factors affecting the morphology development*

Reaction temperature and viscosity of particles are essential in determining the final morphology of particles. Nevertheless, there are still some other parameters that could affect the morphology development of particles, such as approach of monomer addition [29], feeding rate of monomer [30], the extend of monomer conversion [31], selection of seed polymer [32], presence of compatibilizer [24, 33-35], degree of crosslinking of seed particles [36, 37], selection of initiator [38-40], addition of surfactant [41, 42], presence of chain transfer agent [43], solvent post treatment and postpolymerization [44, 45] etc.

### *Monomer addition approach*

Particle morphology development could be controlled by polymerization processing, such as the approach of monomer addition. There were three most common approaches to introduce monomer to reaction system, namely batch addition, semi-batch or semi-continuous addition, and continuous addition. In batch addition, all monomers are added at once to the reaction system. In semi-batch addition, the addition of monomers is divided into several small batches. Practically, the time interval between additions of each batch of monomers is fixed and monitored. Continuous addition, also called starve feed addition, is a method which monomers are added to the reaction system throughout the reaction process. This approach is widely applied in the preparation of latex particles in industrial-scale production. By utilizing this approach, the problem of autoacceleration originated from simultaneous polymerization under high monomer concentration could be addressed. However, due to different monomer addition methods, the seed particles were swollen by monomers by different extends. The degree of monomer swelling by the seed particles would alter the monomer/polymer composition during seed polymerization. The degree of swelling of seed particles is the highest if batch addition approach is applied. The degree of swelling of seed particles is the lowest if continuous addition approach is applied. Seed particles exhibit lower viscosity if the degree of monomer swelling is high. Polymer chains are freely migrated inside the polymer matrix for morphology rearrangement. Under this circumstance, the rate of evolution to equilibrium morphology is promoted. On the contrary, if continuous addition method is used, the degree of swelling of seed particles is low. High viscosity of the seed particles hinders the cluster migration. As a result, the rate of evolution to equilibrium morphology is retarded.

### *Monomer selection*

As each monomer possesses different rate of polymerization, the selection of an appropriate monomer is then very important to the evolution of particle morphology. The rate of initiation and propagation of the second stage monomer determines the rate of morphology evolution of the particle. Monomers with slow initiation and propagation are beneficial to the progression towards the equilibrium morphology. Due to slow polymerization rate, there is sufficient time for seed particles to be swollen by the monomers. These monomers usually have structure which could stabilize the unstable radicals after initiation by electron delocalization, e.g. styrene and its derivatives. The slow rate of propagation enables high monomer/seed polymer ratio in the initial and middle stages of the polymerization. Due to the slow reaction kinetics of these monomers, seed particles are effectively swelled at the initial stage of polymerization. The viscosity of the polymer matrix is reduced which decreases the retardation force for the cluster migration and coalescence. Therefore, the higher the monomer/seed polymer ratio is, the closer the final particle morphology to the equilibrium morphology would reach. However, if monomers with high polymerization rate are used in the reaction, opposite results would be obtained. Due to the fast reaction kinetics of these monomers, the degree of monomer swelling of seed particles is low. The viscosity in the polymer matrix could not be reduced and thus the motions of clusters formed in seeded polymerization would still be hindered by the retardation viscous drag. Eventually the particles are unable to reach the equilibrium morphology.

### *Smart monomer*

In addition, the presence of stimuli responsive monomers might affect the final morphology of particles. After polymerization, these polymers might change their physical or chemical properties as the surrounding environment changes. For example, if *N*-isopropylacryamide (NIPAm) is selected as a component in particle fabrication, poly(*N*-isopropylacrylamide (PNIPAm) is formed at the end of reaction. This polymer is a temperature-sensitive polymer that exhibits a volume phase transition temperature (VPTT) at about 32°C. Beyond this temperature, the inter-polymer hydrogen bond between PNIPAm would break down. PNIPAm would undergo coil to globule transition which changed from hydrophilic to hydrophobic. When the composite polymer was cooled down from reaction temperature to room temperature after reaction, the latex would pass through the VPTT of PNIPAm which would lead to further morphology rearrangement.

### *Compatilbilizer*

The presence of compatibilizer is another factor that affects the evolution of final particle morphology. Compatibilizer could be regarded as the third component in the latex particle which promotes the compatibility between two polymer components. Traditional compatibilizers include surfactant, macromonomer and graft copolymer. In conventional methods to prepare polymeric particles, surfactants are usually added to promote the stability of particles by reducing the polymer/aqueous phase interfacial tension. Macromonomer is as prepared and introduced to the reaction system during seeded polymerization. Graft copolymers between the two components are originated from the side reaction during seed polymerization or being purposed added to the reaction system. After the formation of the seed particles, some of the radicals of the growing polymer chains are not yet terminated. These radicals are still available for the next stage of polymerization. While second monomers are polymerized in seed polymerization, these radicals react with the monomers and resulted in the formation of graft copolymer. Another pathway for the formation of graft copolymer is the backbone abstraction by initiators. Monomers are swelled in the seed particles and initiators are charged into the reaction mixture to initiate the polymerization. There are two possible pathways for the initiation step. The majority of initiators would react with the unsaturated double bond of the monomers while some of the initiators would abstract the backbone hydrogen from the existing seed polymer chains. Radicals are then generated on the backbone of the seed polymer. Upon seed polymerization, polymers are grafted onto the backbone and hence graft copolymers are generated. Since two ends of graft copolymer exhibit good compatibility with their corresponding polymer, the compatibility between two polymers is aided by the existence of graft copolymer. The presence of macromonomer and graft copolymer reduces the polymer-polymer interfacial tensions and modifies the total surface energy of the whole system by improving the compatibility between two polymer components. Enhanced compatibility promotes the migration of newly formed polymer in the matrix and hence promotes the formation of equilibrium morphology. It is easier for particles to achieve equilibrium morphology in the presence of graft copolymer.

### *Initiator selection*

The selection of initiator and its concentration also affect the final particle morphology. Initiator, one of the most important components in polymerization reaction, is responsible for starting the polymerization. Radical species are generated from initiators at the initial stage of polymerization under sufficient temperature, presence of UV irradiation or presence of redox pairs. The generated radicals are unstable and attack the unsaturated C=C double bond of the monomers. Polymerization begins with this attack. Thus, initiator is important to the particle morphology evolution as it becomes the terminal group of the polymer chains at the end of polymerization. In polymer chemistry, there are many types of initiators which are classified according to their initiation principles and physical properties. Thermal initiators generate radicals under thermal dissociation; UV initiators generate radicals under UV irradiation; and redox initiators generate radicals via redox reaction with its redox pair. Each type of initiator is further categorized into two sub-groups, water soluble initiator and oil soluble initiator, depending on their solubilities. Oil soluble initiator is soluble in hydrophobic solvent while water soluble initiator is soluble in water. Due to the structural difference between different types of initiator, the end group of the second stage polymer varies with the types of initiator. The presence of initiators at the terminal of polymer chains exerts influence on the polymer/polymer and polymer/aqueous phase interfacial tensions and thus affects the final particle morphology. Second stage polymers become more polar as water soluble initiator is used in seeded polymerization. This would subsequently reduce the polymer/aqueous phase interfacial tension and thus favors the migration of the polymer chains towards the particle surface. Eventually, the shell of the particles is constructed by the second stage polymer. On the contrary, the end group of second stage polymer becomes more hydrophobic when oil soluble initiators are used. This would enhance the polymer/aqueous phase interfacial tension and result in the migration of the polymer chains into the particle core. The second stage polymer is localized in the particle core at the end of polymerization.

***Degree of crosslinking***

Degree of crosslinking may inhibit particles from reaching equilibrium morphology under certain circumstances. Crosslinking refers to the chemical reaction which links up the polymer chains in the field of polymer science. This is a usual method occurred to modify the physical properties of the polymers in polymerization. The enhancement of the mechanical properties of the polymers relies on the degree of crosslinking. The higher the degree of crosslinking is, the greater the rigidity of the polymers would be. Commonly used methods for crosslinking include covalent corsslinking, oxidative crosslinking and UV crosslinking, depending on the source of crosslinking. Covalent crosslinking requires a chemical reagent, namely a crosslinker, to kick off the reaction. Crosslinkers are usually unsaturated organic compounds. Oxidative crosslinking requires oxygen, usually from the atmosphere, as the source for crosslinking. UV crosslinking requires UV irradiation as the source for crosslinking. In polymer particles synthesis, covalent crosslinking is the major method to crosslink polymers. During the seed formation stage, seed particles are usually crosslinked to enhance their hardness and rigidity. Depending on the amount of crosslinkers added, polymers are crosslinked in different degrees. The more the crosslinkers are added, the greater the degree of crosslinking of the seed particles would become. The rigidity of the seed particles is also promoted. As a result, the viscosity of the seed polymer is raised due to the high crosslinking degree. During seed polymerization, it is difficult to swell the second stage monomers and newly formed polymer chains are difficult to migrate and coalescence in the polymer matrix. As the restrictive viscous force is increased by high crosslinking degree, the particles are retarded to evolve towards the equilibrium structure. Thus, particles are suggested to have a minimum crosslinking degree in order to achieve equilibrium morphology.

### ***Solvent treatment***

Solvent treatment is a widely applied approach to assist the achievement of equilibrium morphology. In the assumption aforementioned, polymer composite latex particles are synthesized and dispersed in aqueous phase. Water is the continuous phase for polymerization. Equilibrium morphology is not achieved at the end of polymerization. Further post-treatment is carried out to promote the morphology evolution. Postpolymerization by adding booster initiators and solvent post-treatment are commonly used techniques to achieve this goal. In solvent post-treatment, polymer particles are treated with organic solvent after polymerization. Normally, the solvent chosen is the co-solvent between two polymer components. The polymer particles would be swelled after the addition of solvent. As the solvent is the co-solvent between two polymers, it is highly compatible with the two polymers. Benefited from the enhanced compatibility, the viscosity of the polymer matrix inside the particles is reduced. As a result, polymer chains could migrate towards equilibrium morphology due to the reduction of resistive viscous drag.

### ***Reaction time***

In addition, total time for polymerization would result in different kinds of particle morphology. Polymerization kinetics refers to the rate of polymerization, which is regarded as a function of time. The polymerization kinetics for polymer particle synthesis is controlled by a lot of parameters, such as types of monomer, types of initiator, reaction temperature, pressure, and agitation. Sufficient time for reaction is critical to the achievement of equilibrium morphology even all other reaction paprameters are optimized. On the contrary, incomplete reaction would be resulted if there is insufficient time for reaction. Several problems would occur if the reaction time was not enough to complete the polymerization. First, there would be low monomer conversion as only a small portion of monomers is converted into polymer. The remaining unreacted monomers are retained inside the latex particles and the particles are swelled by these monomers. Though trapped monomers could facilitate morphology rearrangement of the monomers, the particles could not reach final equilibrium morphology since a large amount of the reactants remain unreacted. Morphology quenching is the second factor that forbids the equilibrium morphology evolution. As the polymerization is stopped at the middle stage of polymerization, or even earlier, the reaction and the morphology of the particles are being quenched instantaneously. The morphology frozen at the middle stage is not the equilibrium morphology. Sufficient time for polymerization would enable complete morphology rearrangement and thus it is an essential criterion to obtain equilibrium morphology of polymer particles.

## 1.3 Possible morphologies of three component polymers in a particle

Morphology development and rearrangement of polymeric particles containing two components are relatively easy to predict as the reaction system is simple. Based on two-component polymer system, many mathematical simulations have been established by different research groups to predict the final particle morphology, such as Monte Carlo simulation [46, 47]. Some computational simulation methods and software have been developed to elucidate the Gibbs free energy and thus used to predict the final particle morphologies [48, 49]. However, for polymeric particles composed of three components, the prediction of the final morphology is more difficult as the system is more sophisticated. Morphology prediction of three-component polymer particles is not easy to achieve via mathematical or computational modeling. According to the fundamental principle of particle morphology development discussed before, with minimization of the total interfacial tension, some possible morphology of three-component polymer particles are predicted and summarized below. Moreover, some specific nanostructures of three component particles would be discussed, too.

### *Morphology*

Morphology is the study of shape, size, and physical distribution of matters. Three-component polymer particles with various shapes and dimensions could be prepared via different synthetic approaches. Nevertheless, the system of three-component polymers is more complicated than that of two-component polymers; thus the number of possible morphologies of three-component polymer particles is more than that of two-component polymer particles. The greatest challenge on morphology predication of three-component polymer particles arises from the simultaneous phase separation between the three components during morphology development. Polymer particles could be tailor-made with predetermined shape and internal structure if the mechanism of morphology reconstruction is understood. Similar to two-component polymer system, particles with different morphologies could be prepared through adjusting the synthetic approaches and reaction parameters. However, unlike two-component polymer system, the introduction of one more polymer into the system would allow more possibilities in the formation of particles of various morphologies.

Either thermodynamic morphology or kinetic morphology is resulted from the polymerization of composite polymer particles. Thermodynamic morphology is always the interest of scientists because it is the one with the minimum interfacial free energy, implying the particle is at the most stable state. Among the possible thermodynamic morphologies, the most basic and common one is spherical as this kind of morphology possesses the lowest interfacial free energy, which is thermodynamically favored. Besides of spherical shaped particles, there are still a few other possible thermodynamically favored morphologies. To predict all the possible equilibrium morphologies, a system that combines both computational simulations and experimental interpretations is necessary. Based on previous results of computational morphology predictions of two component polymer system, Sundberg and co-workers had established an advanced system to identify the possible morphologies of three component polymer particles and predict the most probable morphology of the three component polymer particles [50]. Same as before, the theory was founded on the most important principle, consideration of Gibbs free energy of the polymer system. Revisiting the equation on determining Gibbs free energy

$$\Delta G = \sum \gamma_{ij} A_{ij} - \gamma_0 A_0 \quad \text{[Eq. 1.1]}$$

The equation is expressed in terms of $\Delta\gamma$ by dividing both sides by $A_o$.

$$\Delta\gamma = \sum \gamma_{ij} A_{ij} / A_0 - \gamma_0 \quad \text{[Eq. 1.2]}$$

where $\Delta\gamma$ is the change of interfacial tension, $\Delta G$ is the change of total Gibbs free energy. $\gamma_{ij}$ is the interfacial tension at the interface between two phases i and j. $A_{ij}$ is the corresponding interfacial area. $\gamma_0$ and $A_0$ are the interfacial tension and area between the initial particle suspended in the continuous phase and the continuous phase respectively. Considering a three-component polymer particle in aqueous phase as the continuous phase, $\Delta\gamma$ of all possible morphologies are elucidated and compared through computational simulations. Theoretically, the one with the lowest $\Delta\gamma$ corresponded to the lowest change in free Gibbs energy, implying the most probable equilibrium morphology of the polymer particle.

From the results of computational simulations, there are six unique categories of particle morphology in three component polymer system, which are defined as core-shell-shell, hemicore, hemishell, trsisectional, snowman and cored hemisphere. Depending on the arrangement and confinement of the polymer components, core-shell-shell particles exhibit 6 possible arrangements. Hemicore particles exhibit 3 possible arrangements. Hemishell particles exhibit 3 possible arrangements. Trisectional particles only have 1 possible arrangement. Snowman particles exhibit 3 possible arrangements. Cored hemisphere particles exhibited 6 possible arrangements. To sum up, there are 22 possible equilibrium morphologies in the three-component polymer system. All the possible morphologies are illustrated from Fig. 1.6 to Fig. 1.12.

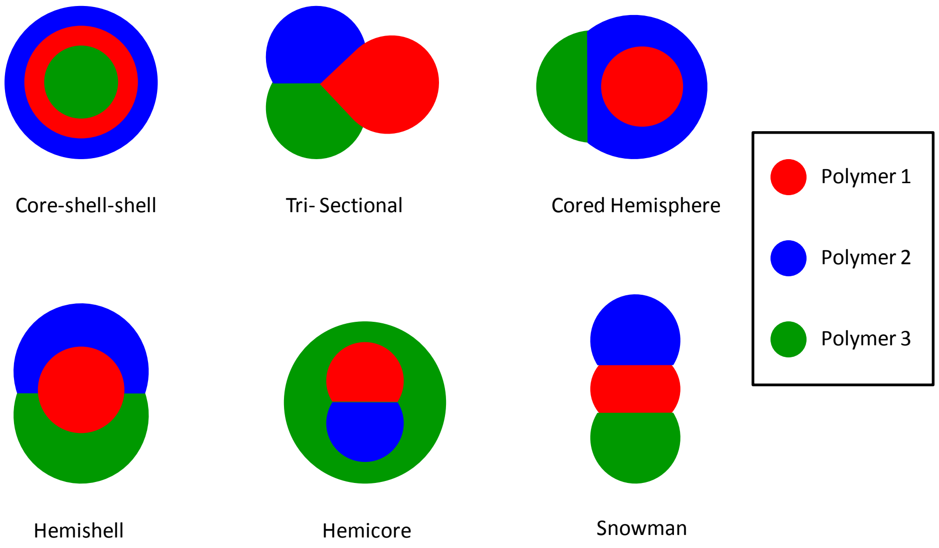

**Fig. 1.6.** Six categories of morphology of three component polymer particles.

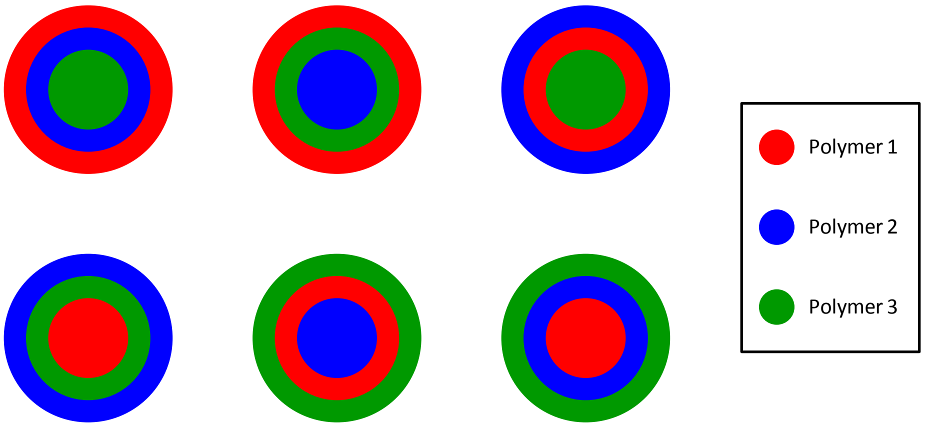

**Fig. 1.7.** Possible morphologies of core-shell-shell polymer particles.

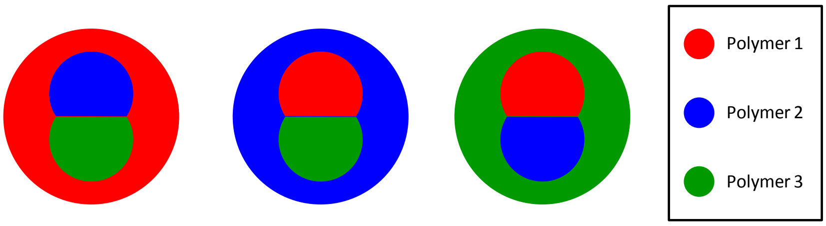

**Fig. 1.8.** Possible morphologies of hemicore polymer particles.

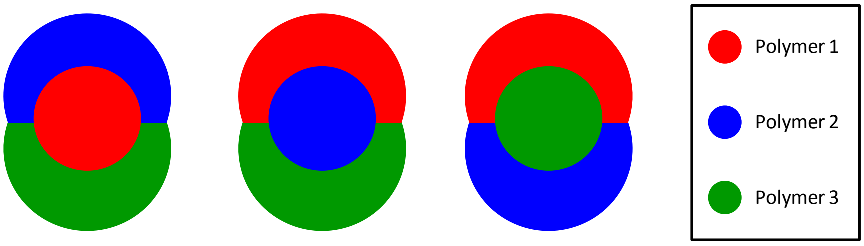

**Fig. 1.9.** Possible morphologies of hemishell polymer particles.

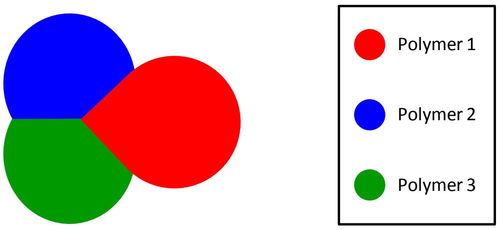

**Fig. 1.10.** Possible morphology of trisectional polymer particles.

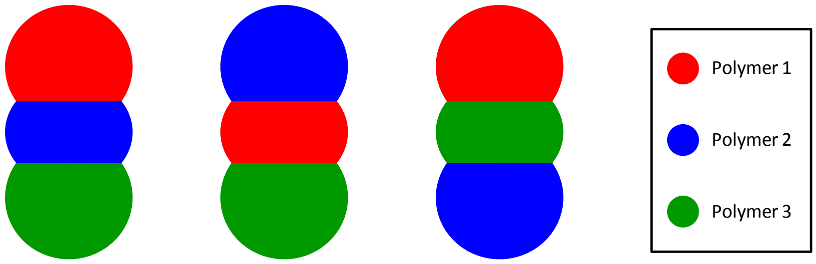

**Fig. 1.11.** Possible morphologies of snowman polymer particles.

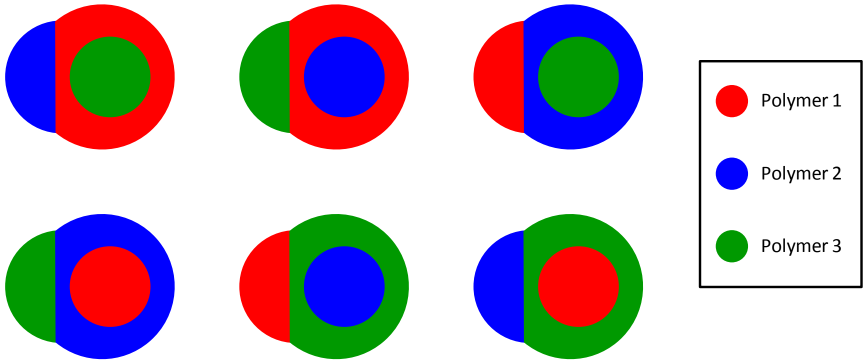

**Fig. 1.12.** Possible morphologies of cored hemishpere polymer particles.

Sundberg investigated the possible morphologies of three-component polymer particles. The three-components were selected out of four polymers, which were poly(methyl methacrylate) (PMMA), polystyrene (PS), poly(dimethyl siloxane) (PDMS) and bisphenol-A polycarbonate (PC) as a model study. Either sodium lauryl sulphate (SLS) or Mexpectin XSS-100 (MXP) was chosen as surfactants. In Sundberg's approach, PMMA, PS, PDMS and PC homopolymers were priory prepared. Homogenization of the three homopolymers was then carried out in the presence of surfactant. The experimental morphologies of the composite particles investigated under light microscope were compared with the results from computational simulations. Similar to two-component polymer system, the terminal morphology of particles relied on the balance between thermodynamics and kinetics consideration. The selection criterion was based on the polymer/polymer interfacial tension and polymer/aqueous phase interfacial tension. More importantly, due to the coexistence of three different polymer components in each particle, polymer/polymer interfacial tension played an even more important role in determining the final particle morphology. In total, there were four possible combinations of three component polymer out of the four polymers. The $\Delta\gamma$ of 22 possible morphologies of each particle was calculated and compared based on equation 1.2. The morphology with the lowest calculated $\Delta\gamma$ value was the thermodynamically favored morphology of the corresponding particle as it provided the minimum interfacial tension. From the comparison between their simulation and experimental results, the equilibrium particle morphology was usually the one with the minimum interfacial free energy calculated. Experimental results were matched with theoretical calculation. Nonetheless, the actual particle morphology was occasionally not the one with the minimum interfacial tension. The resulting morphology was the one with the second lowest $\Delta\gamma$. Because under certain circumstances, the difference in $\Delta\gamma$ calculated between the lowest two possible morphologies was not significant. Due to the similar $\Delta\gamma$ values of these possible equilibrium morphologies, either one of the morphology would be the final morphologies of the particles in real situation. In certain situations, both morphologies with the lowest $\Delta\gamma$ coexisted in the final particle dispersion. Regardless of these phenomena, Sundberg and co-workers established a comprehensive system to predict equilibrium morphology of three-component polymer system.

The mathematical simulation of particle morphology developed by Sundberg and co-workers was based on theoretical and thermodynamic consideration.

Calculation of interfacial area was simplified and some particle morphologies were in simplified sketch from actual morphology. The equilibrium morphology prediction of polymer particles containing more than four components was almost impossible based on mathematical calculation. To obtain a more in-depth understanding on the morphology development of polymer particles composed of three or more components, Asua and coworker [51-53] established a model based on Monte Carlo simulation to predict the equilibrium morphologies of multiphase waterborne polymeric system. This simulation approach provided a robust platform for the understanding of morphology development of multiphase waterborne polymeric systems. This method enabled the prediction of morphology of polymeric particles containing three or even more components. In addition, it also allowed the prediction of morphology evolution of polymer-polymer or polymer-polymer-inorganic system. The simulation method was not restricted to the materials utilized in the reaction. More important was that the kinetics on the formation of particle morphology during polymerization process could be understood. This provided more solid information on the formation of non-equilibrium morphology. The evolution of equilibrium morphology of three-component polymer composites particles was used as a model study in Asua's research. Progress on the particle formation was illustrated in Fig. 1.13.

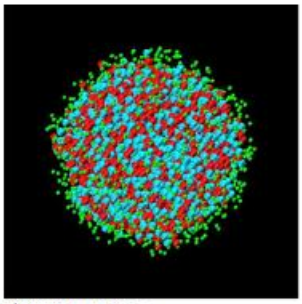

a) initial particle

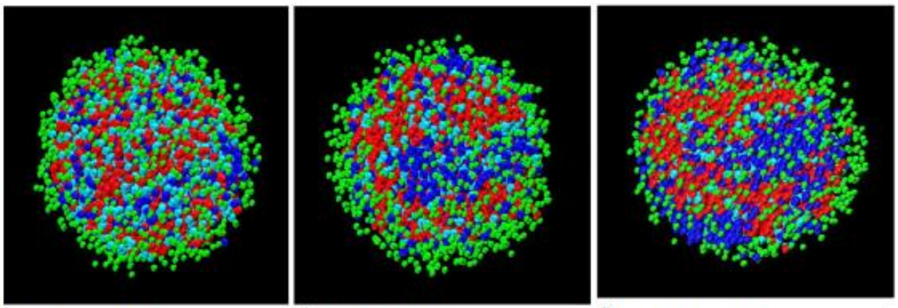

b) x = 0.3; t=1800 c) X = 0.5; t = 3000 d) X = 0.7; t = 4200

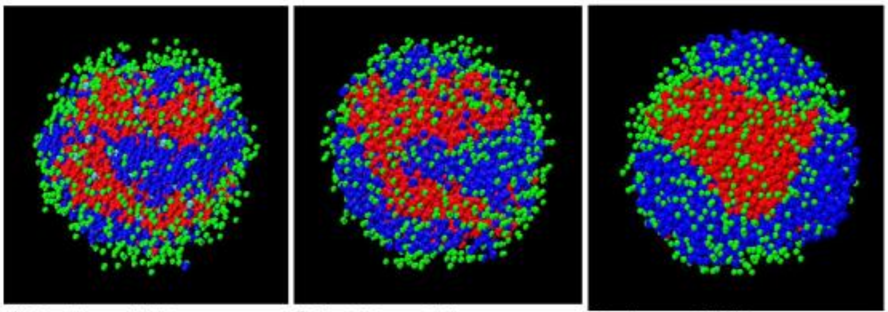

e) X = 0.9; t = 5400 f) X = 1.0; t = 6000 g) aging; t = 15000

**Fig. 1.13.** Equilibrium morphology of three-phase waterborne polymer particle [51, 53].

In Asua's study, each component was divided into many subparticles. More hydrophobic polymer was represented by red subparticles. More hydrophilic monomer and polymer were represented by cyan and blue subparticles respectively. Partial hydrophilic inorganic particle was represented by green subparticles. X corresponded to the monomer conversion and t referred to the time in reduced units. In the initial stage, the hydrophobic seed polymer was swelled by the monomer with the inorganic particles located at the particle surface. As the polymerization progressed, the monomer was consumed as could be seen from the conversion of the cyan subparticles into blue subparticles. Meanwhile, phase separation between each component also took place. During the process, the hydrophobic polymer in red was the most hydrophobic component, and it migrated to the innermost core of the particle. The hydrophilic polymer in blue formed during polymerization was incompatible with the hydrophobic polymer in red. Phase separation took place and the more hydrophilic polymer was migrated towards the outer shell of the particles. Since it was less hydrophilic than the inorganic particle, it was located at the middle layer of the particle eventually. The inorganic particle was the most hydrophilic component among three components so it was located at the outermost shell of the particle. At the end of polymerization, spherical particle with layered nanostructure was formed. Simulation revealed that thermodynamic morphology was eventually not achieved. Non-equilibrium morphology was reached instead and this was due to the high internal viscosity developed during the polymerization process.

### ***Nanostructure***

Nanostructure is the study of the internal structure and phase distribution of different components inside a particle. Well-defined nanostructure particles are essential in applications as they demonstrate better performance than particles with amorphous structure. In-depth understanding of the nanostructure formation of polymer particles is very important to particle designation for various applications. When two-component polymer particles have reached equilibrium morphology, they possibly possessed one of the following nanostructures, core-shell, inverted core-shell, or occluded. Structural development of particles is based on the phase separation between two components. However, nanostructure formation of three-component polymers is more complicated as the selection and combination of monomers exert greater impact on the structural formation during particle synthesis.

Three-component polymer particles had plenty of possible equilibrium morphologies based on the correlation between theoretical simulation and experimental findings. Prediction of possible nanostructures for particles of different shapes was not possible. Therefore, only the nanostructures of spherical particles would be discussed here. Nanostructure of three component polymer particles came from the distribution and confinement of each polymer inside the particles. Considering spherical polymer particles, there were basically five types of possible nanostructures depending on the compatibility between each component and the polymerization kinetics. The possible nanostructures of the spherical three component polymer particles are listed in the Table 1.1.

**Table 1.1** Possible nanostructures of spherical three component polymer particles

| Compatible Polymer | Incompatible Polymer | Partly Compatible | Predicted Naonostructure |
|---|---|---|---|
| Polymer A,<br>Polymer B,<br>Polymer C | N/A | N/A | 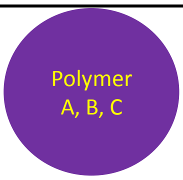 <br>Homogeneous particles |
| Polymer A<br>(Hydrophilic) | Polymer B,<br>Polymer C<br>(Hydrophobic) | N/A | 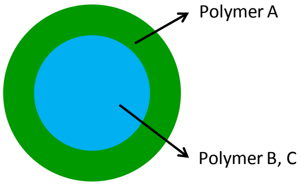 <br>Amphiphilic core-shell particles |
| Polymer A,<br>Polymer B<br>(Hydrophilic) | Polymer C<br>(Hydrophobic) | N/A | 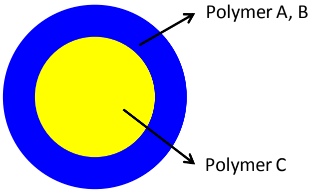 <br>Amphiphilic core-shell particles with interpenetrated shell |
| Polymer A,<br>Polymer B<br>(Hydrophilic) | N/A | Polymer C | 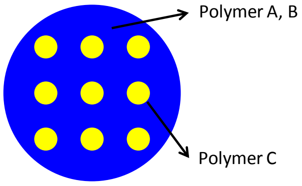 <br>Amphiphilic particles with micro-domains |
| N/A | Polymer A,<br>Polymer B,<br>Polymer C | N/A | 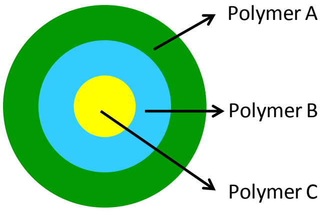 <br>Multi-layered particles |

The first case was the simplest situation as all the polymer components were compatible with each other. Due to the excellent compatibility between each polymer, no phase separation took place during polymerization. Spherical and homogeneous particles were formed at the end of polymerization. Three polymer components were freely and randomly distributed in the particles.

The second and third cases were similar as both had amphiphilic core-shell particles with well-defined core-shell nanostructure at the end of polymerization. Provided that water was used as the continuous phase, the outer shell layer of the particles was constructed by hydrophilic polymer. The inner core of the particles was constructed by hydrophobic polymer. These core-shell nanostructures could be easily revealed under transmission electron microscopy (TEM).

In the second case, the system was composed of one hydrophilic polymer and two hydrophobic polymers. The compatibility between the two hydrophobic polymers was good enough that no phase separation occurred during particle formation. Therefore, upon polymerization, phase separation between hydrophilic polymer A and hydrophobic polymers B and C took place due to high interfacial tension between them. The hydrophilic polymer chains of polymer A migrated towards the particle surface as it possessed lower polymer-aqueous phase interfacial tension. The outer shell of the particles was thus composed of polymer A solely. On the contrary, the polymer chains of hydrophobic polymers B and C migrated inside to the particle core. The inner core of the particles was composed of a hybrid of two hydrophobic polymer, polymers B and C.

In the third case, the system was composed of two hydrophilic polymers (polymers A and B) and one hydrophobic polymer (polymer C). Similarly, it was assumed that the two hydrophilic polymers were highly compatible with each other which did not result in phase separation during particle formation. During polymerization, phase separation between hydrophobic polymer C and hydrophilic polymers A and B occurred due to the high interfacial tension induced. As the polymer-aqueous phase interfacial tension of polymer C was the highest among the three polymers, hydrophobic polymer C then migrated to the core of the particles. Thus the inner core of the polymer was composed of polymer C solely. Hydrophilic polymers A and B migrated towards the particle surface and constructed the outer shell of the particles. As the shell layer of the particles was composed of the two polymers with good compatibility, the polymer chains of the two components were freely and randomly distributed. The outer layer was regarded as an interpenetrated shell.

In the forth case, the system was similar to that of the third case in which polymeric particles were composed of two hydrophilic polymers (polymers A and B) and one hydrophobic polymer (polymer C). These two hydrophilic polymers were highly compatible with each other so that no phase separation between them occurred during polymerization process. As polymers A and B exhibited lower polymer-aqueous phase interfacial tension than polymer C, they were preferentially migrated to the outer shell of the particle. The shell of the composite particles was thus constructed by polymers A and B. Due to the similar polymer-aqueous interfacial tension of polymers A and B, they were randomly distributed in the shell layer and the outer shell was regarded as an interpenetrated shell. On the other hand, polymer C possessed higher polymer-aqueous interfacial tension than polymers A and B because it was more hydrophobic. Consequently, polymer C migrated into the inner core of the particles. Spherical particles with several micro domains of polymer C were formed at the end of polymerization. The formation of such kind of nanostructure was contributed by two major factors, polymerization kinetics and internal viscosity of the particles. First, the rate of polymerization of monomer C was very fast so that nucleation of polymer C clusters occurred instantaneously after the introduction of an initiator. The quick nucleation and particle formation thus inhibited the movement of the polymer chains and resulted in forming numerous micro domains inside the particles. In addition, the fast rate of polymerization of monomer C led to an abrupt increase in the internal viscosity inside the particles. This sudden rise in internal viscosity forbade the migration of polymer chains inside the particles. Consequently, polymer C was confined in the area where it was nucleated and a micro-domain nanostructure was formed eventually. In this circumstance, the particle did not reach minimum interfacial free energy at the end of polymerization. This nanostructure was regarded as a kinetically favored structure.

In the last case, a very specific type of nanostructure was observed. Polymeric particles with onion-like multi-layered nanostructure were formed at the end of polymerization. The formation of such nanostructure originated from the incompatibility between the three polymer components. Since all the polymer components were incompatible with each other, phase separation between the three components took place during polymerization. The polymer component with the lowest polymer-aqueous interfacial tension migrated to the outer shell of the particles as it was a thermodynamically favored process. The most hydrophobic polymer possessed the highest polymer-aqueous interfacial tension and thus it migrated into the innermost core of the particles. The middle layer of the particles was constructed by the polymer with the lowest polymer-polymer interfacial tension with the shell polymer and core polymer. This polymer acted as a compatibilizer between the shell polymer and core polymer. As a result, the polymer composite particle was constructed by three distinct layers of incompatible polymers. This nanostructure was achieved when sufficient time was allowed for the rearrangement of polymer chains. Another reaction pathway to achieve multi-layered nanostructure particles was via sequential seeded emulsion polymerization. Seed homopolymer was priory formed through conventional polymerization approach. After particles purification, second monomer and initiator were then introduced into the reaction system to conduct seeded emulsion polymerization. Polymerization took placed at the surface of the particles and the outer shell of the particles was formed by the second polymer. The core-shell structured polymer particles were purified again and used as seed particle for further seeded emulsion polymerization. Third monomer was added to the reaction system together with the initiator to proceed the seeded emulsion polymerization. Polymerization took place at the particle surface again the outermost shell of the particles was constructed by the third polymer. Particles with multi-layered structures were formed by multi-step seeded emulsion polymerization.

## 1.4 Literature approaches to prepare MCP particles

Since the performance of a polymeric composite particle depends heavily on its morphology, there is strong attraction in preparing polymer particles with various morphologies. Polymer composite particles with multiple components, tailor-made morphology and well-defined nanostructure are tomorrow’s novel materials for various advanced applications. Thus, many researches have been conducted by scientists all over the world in the past decades to fabricate MCP particles with various morphologies and nanostructures. With their contributive works, many approaches have been explored to prepare MCP particles. Herein, some of the representative works are summarized according to the synthetic methods, tailor-made morphologies and well-defined nanostructures.

The preparation of MCP particles is normally based on polymerization. Various types of polymerization approaches are implemented to prepare MCP particles, including precipitation polymerization, emulsion polymerization, emulsifier-free emulsion polymerization, miniemulsion polymerization, seeded polymerization, and controlled living radical polymerization such as atom transfer radical polymerization (ATRP), nitroxide mediated polymerization (NMP) and reversible addition-fragmentation chain transfer polymerization (RAFT). MCP particles are synthesized with different morphologies, such as spherical, ellipsoidal, disc-, raspberry-, mushroom-, snowman-, and dumbbell-shaped. Moreover, anisotropic and Janus polymeric particles also could be prepared. Not only the morphology, the nanostructure of the MCP particles also could be tailor-made by various approaches like core-shell, multi-layered, micro-domain and interpenetrating network.

### *Spherical MCP particles*

From the point of view in thermodynamic consideration, spherical shape is the most abundant morphology of particles as this morphology exhibits the minimum interfacial free energy. Thus, most of the MCP particles possesses a spherical morphology at the end of polymerization. There are in general two types of nanostructures observed in spherical particles, namely multi-layered and core-shell structures. Typical methodologies to fabricate MCP particles with these structures are discussed here.

### *Multi-layered MCP Particles*

Polymer composite particles with multilayered nanostructure have drawn numerous polymer chemists' attention as these particle possess great potential applications in optics, photonics and electronics [54-58]. Several synthetic approaches towards multi-layered structured particles, also named as onion-like polymeric composite particles, have been investigated in the past decades.

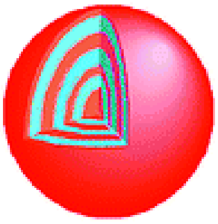

**Fig. 1.14.** Nanostructure of multi-layered polymer particles [59].

### *Multistep seeded polymerization*

The most common and direct approach to prepare polymer composite particles with multi-layered nanostructure is by using multistep seeded polymerization. Seed particles were priory prepared by conventional polymerization method with subsequent seeded polymerization. Polymerization then takes place step by step and polymer particles with multi-layered architecture are resulted consequently.

Hu and coworker fabricated multi-component polymer particles via emulsion polymerization [60]. The synthesized particles exhibited either interpenetrating network (IPN) core-shell structure or multi-layered structure. The preparation of multi-layered MCP particles involved a three-step emulsion polymerization. The core latex, poly(butadiene-*stat*-styrene), was first synthesized by batch emulsion polymerization with 90/10 w/w ratio between butadiene and styrene monomers. Starve feed emulsion polymerization of mixed monomer of 2-ethylhexylmethacrylate and styrene (60/40 w/w) was then conducted in the presence of potassium persulphate. The latex was thus coated with a layer of P(EHMA/S) on the P(Bd/S) core. In the last step, starve feed emulsion polymerization of mixed monomer of styrene and acrylonitrile in a w/w ratio of 72/28 was conducted. The poly(styrene-*stat*-acrylonitrile), SAN, formed from the semicontinuous emulsion polymerization was confined at the outermost shell of the multi-layered MCP particles. The P(EHMA/S) was located at the middle layer of the particles while P(Bd/S) was located at the innermost core. This MCP particle was proposed to be a potential damping and toughening agent for thermoplastics. Each component of this MCP particles exhibited different functionalities in damping and toughening modification of thermoplastics. The innermost P(Bd/S) core had great impact resistant properties. The middle layer, P(EHMA/S), was a layer rich in acrylic polymer that had excellent damping modification properties. The outermost SAN shell had good compatibility with the bulk thermoplastic phase, polycarbonate (PC). Preliminary results from dynamic mechanical spectroscopy (DMS) revealed that MCP particles with both IPN core-shell and multi-layered structure possessed great potential to be toughening and damping modifiers in thermoplastics. The damping and mechanical properties of these MCP polymer particles were further studied in a later publication [61].

**Fig. 1.15.** Schematic diagram of the nanostructures of the MCP particles (left : IPN; right : multi-layered) [61].

Okubo and coworkers had prepared four layered PMMA/PS/PMMA/PS particles via multistep seeded dispersion polymerization [62]. PMMA/PVP seed particles were produced by dispersion polymerization. The seed particles possessed micron sized dimension (1.77 μm) with narrow size distribution. After purification and characterization, the seed particles were brought to seeded dispersion polymerization. Multi-layered PMMA/PS/PMMA/PS particles were fabricated by thrice stepwise seeded dispersion polymerization via alternative addition of styrene and MMA monomers. Supported by the data from TEM micrographs, gradual increase of particle size and narrow particle size distribution implied that no secondary nucleation took place and thus confirming the multi-layered structure of the polymer particles.

Lee also reported the synthesis of latex particles with multi-layered structure via multistage soapless seeded emulsion polymerization [63]. PMMA/PS/PMMA/PS composite polymer particles prepared from four-stage soapless emulsion polymerization was selected as a model study for the construction of multi-layered architecture. PMMA seed latex particles were first prepared by soapless emulsion polymerization using potassium persulphate as initiator. The synthesized PMMA seed latexes had a number-average diameter of 303 nm. Seeded emulsion polymerization of styrene was conducted in the presence of PMMA seed latex to form core-shell structured latex particles. Ethyl glycol dimethylacrylate (EGDMA) was added as a crosslinking agent to confine the PS in the shell layer. Alternative swelling and polymerization of MMA and styrene was then carried out in the presence EGDMA. Eventually, a four-layered PMMA/PS/PMMA/PS composite latex particle was formed with alternating PMMA and PS layer. Subsequent increase in the number-average diameter of the particles from 303 nm to 558 nm illustrated that multistage seeded emulsion polymerization had occurred without secondary nucleation.

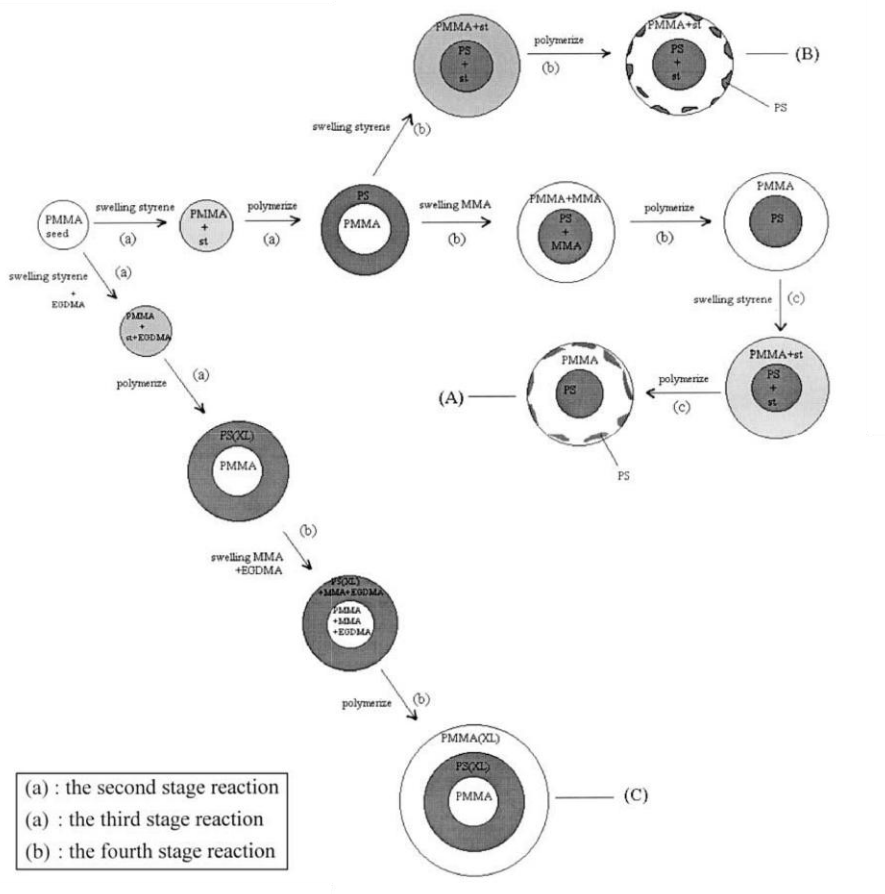

**Fig. 1.16.** Schematic diagram for the preparation of PMMA/PS/PMMA/PS composite particles by a four-stage polymerization process [63].

Lee also reported the preparation of multi-layered PS/PBA/PMAA via sequential multistage semicontinuous emulsion polymerization [64]. Carboxylated PS seed particles were prepared by polymerization of styrene and methacrylic acid. The dimension of the carboxylated PS seed particles was 28 nm. Alternative feeding of styrene and *n*-BA monomer was repeated five times to fabricate multi-layered onion-like composite particles. The reaction was carried out at 90℃ and all the monomers were fed within 4 hours. Methacrylic acid was fed to the reaction mixture for carboxylate functionalization and allyl methacrylate was added as crosslinker. Ten-layered PS/PBA/PMAA composite particles were synthesized at the end of polymerization with a dimension of 150 nm. Experimental results revealed that this onion-like polymer composite possessed pseudopolymer alloy behavior. Through constructing alternative layers with high $T_g$ and low $T_g$, PS/PBA/PMAA possessed excellent film formation properties and mechanical strength that allowed them to be used in adhesives and coating industries.

Recently, Li and Oiu reported the preparation of multi-layered polymer particles by semicontinuous emulsion polymerization [65]. Emulsion polymerization of styrene and *n*-BA monomer was conducted to prepare the P(BA-S) seed particles. Monomer mixture comprising styrene, MMA and *n*-BA with different weight ratios was added sequentially for seeded emulsion polymerization. Divinylbenzene, a crosslinking agent, was added in the first, third and fifth stages of seeded emulsion polymerization to synthesize hard polymer layers via surface crosslinking emulsion polymerization. The crosslinking reaction underwent to prevent the interlayer migration of the polymer chains. As a result, the synthesized polymer was fabricated with alternating hard/soft layers. Gradual increase in the hydrodynamic diameter with narrow particle size distribution from particle size measurement implied that seeded emulsion polymerization had taken place on the seed particles without secondary nucleation. At the end of the fifth seeded emulsion polymerization, the P(BA-S-MMA-DVB) was measured to be 262.5 nm. The layer-by-layer structure of the composite particle was confirmed by multifrequency temperature-modulated differential scanning calorimetry (TOPEM-DSC).

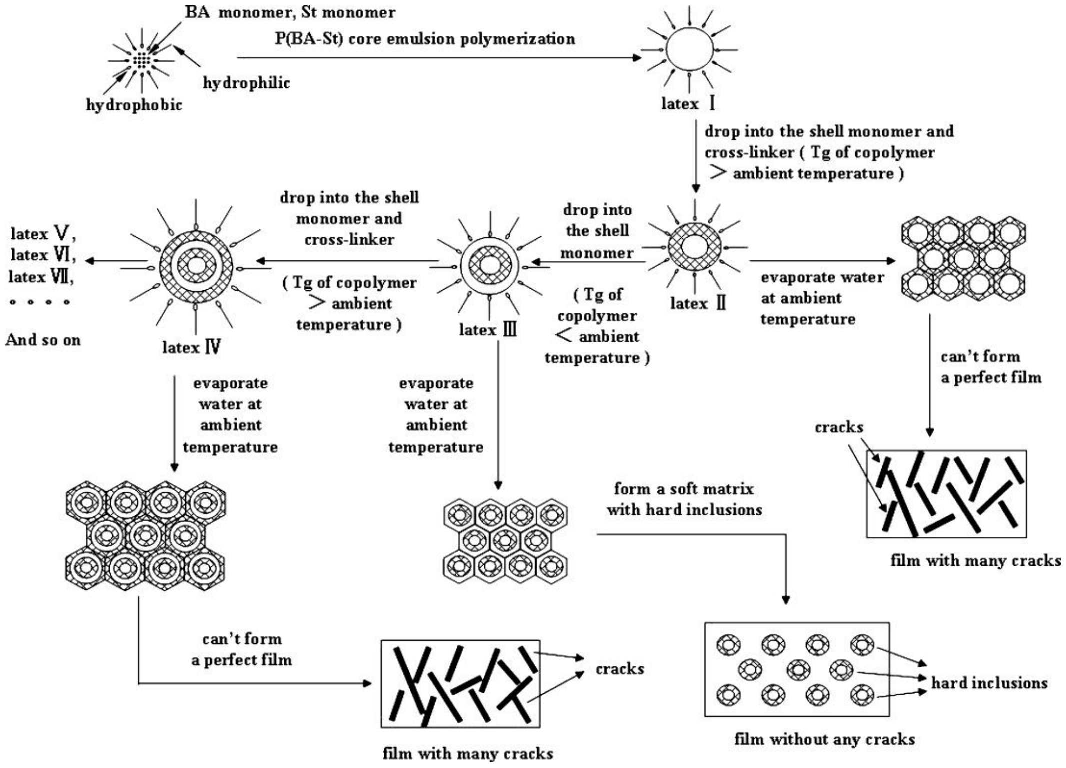

**Fig. 1.17.** Schematic diagram for the preparation of multi-layered P(BA-S-MMA-DVB) [65].

Bon's research group had reported the preparation PMMA-PBA-PUPy polymer colloidal particles as high internal phase emulsion gels (HIPE-gels) [66]. The three components polymer colloidal particles were prepared by a two-step synthetic approach. First step is the functionalization of polyethylene glycol methacrylate (PEGM) by 2-ureido-4[1H] pyrimidinone (UPy) using dibutyltindilaurate as catalyst. Second step is the soap-free emulsion copolymerization of MMA, *n*-BA and UPy functionalized PEGMA macromonomer using potassium persulfate as initiator. The polymerization is carried out at 70℃ for 6 hours. The hydrodynamic diameter and particle size distribution of prepared colloidal particles are 223 nm and 0.025 respectively. The prepared latex particles are capable to form HIPE gels to stabilize water in toluene even at very low solid content (0.1 wt.%). The self-complementary quadruple hydrogen bond interactions of the pendant UPy groups had reinforced the gel network in continuous toluene phase. No rupture of the gel network is observed after solvent evaporation, which allows these particles to be applied in controlled released vehicles, pressure sensors, and compartmentalized chemical reaction microenvironments.

### ***Controlled/living radical polymerization***

Controlled/living radical polymerization is a robust technique developed in recent decades to achieve precise control over the molecular weight ($M_w$) of synthetic polymers [67-70]. Control the growth of polymerization chains is essential and beneficial to the morphological development of polymeric particles. Therefore, with the rapid growth in the research of controlled free radical polymerization, polymer chemists have started to implement controlled free radical polymerization to construct multi-layered polymer nanocomposites.[71] Basically, there are three categories of controlled free radical polymerization, atom transfer radical polymerization (ATRP) [72-74], nitroxide mediated polymerization (NMP) [75-77], and reversible addition-fragmentation chain transfer polymerization (RAFT) [78-80].

### ***ATRP***

Okubo and coworkers reported the synthesis of multi-layered poly(*iso*-butyl methacrylate)-*block*-polystyrene (P*i*BMA-PS) particles via a two-step atom transfer radical polymerization (ATRP) [81]. P*i*BMA-Br macroinitiator was first synthesized by miniemulsion-ATRP in the presence of ethyl 2-bromoisobutyrate (EB*i*B), copper (II) chloride ($CuCl_2$) and DNdpy. EB*i*B, $CuCl_2$ and DNdpy were functioned as initiator, catalyst and ligand respectively. Seeded ATRP between styrene monomer and macroinitiator was then conducted to synthesize P*i*BMA-PS particles. Well-defined onion-like multi-layered structure was formed after polymerization without any post-treatment. Effect of blocking efficiency (the number fraction of block copolymer formed) [82] and polymerization temperature in seeded-ATRP [83] on the formation of onion-like structure was studied. Their findings revealed that well-defined multi-layered particle structure was achieved when the blocking efficiency was high (60%). Disordered sea-island morphology would be resulted if the blocking efficiency was low. Multi-layered structure was achieved when the seeded-ATRP was proceeded at 70℃ and 90℃. Disordered sea-island structure was achieved if the second-step polymerization temperature was carried out at 110℃. Multi-layered structure was not obtained as spontaneous homopolymerization of styrene occurred under high polymerization temperature instead of controlled radial polymerization. The low content of P*i*BMA-PS block copolymer resulted in a disordered sea-island structure. At 70℃ and 90℃, seeded-ATRP was the major pathway of polymerization and the content of block polymer was kept at high level, leading to a multi-layered structure. The relationship between the livingness and the compartmentalization on the ATRP kinetics was also studied based on a simulation modeling method called modified Smith-Ewart approach [84].

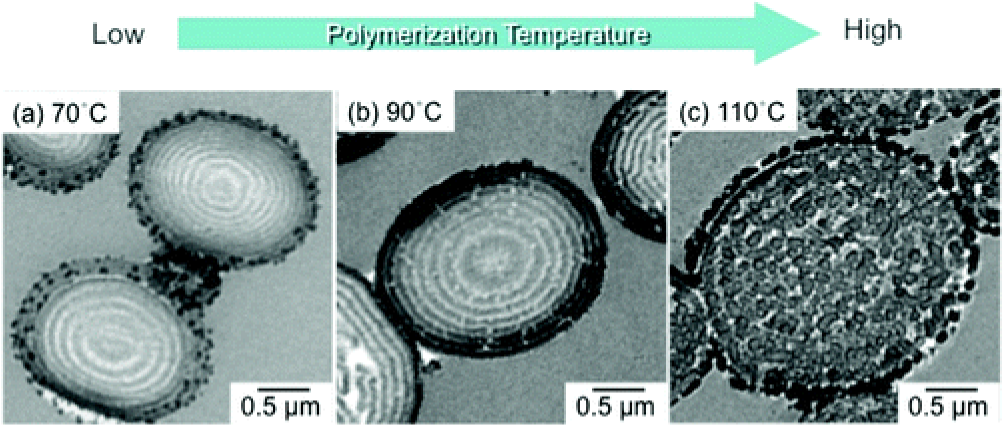

**Fig. 1.18.** Effect of second step polymerization temperature (left: 70℃; middle: 90℃; right: 110℃) on the nanostructure of P*i*BMA-*b*-PS particles [83].

### *NMP*

Charleux and coworker reported the synthesis of multi-layered triblock copolymer particles, (PS-PBA-PS) and (PMMA-PBA-PMMA), by *ab initio* emulsion NMP [85]. Based on the success in the fabrication of core-shell polymeric particles with the use of *N*-*tert*-butyl-*N*-(1-diethyl phosphono-2,2-dimethylpropyl) nitroxide (SG1), Charleux implemented this alkoxyamine and its derivatives to fabricate nanostructured latex particles with a multi-layered structure [86-88]. Derivatives of alkoxyamine SG1 were modified prior to NMP. Seed particles were prepared by polymerization of *n*-BA monomers in the presence of modified alkoxyamine at 90℃. After the formation of seed particles, subsequent addition of *n*-BA and MMA monomers took place to construct triblock copolymer particles by NMP. As the monomer conversion achieved was relatively low (about 50%), a shot of potassium persulphate (KPS) was introduced to the reaction system as the booster at the end of polymerization to fully convert the residual monomer. The mircophase separation between the polymer segments contributed to the formation of multi-layered structure. Therefore, the residual monomer in the particles exerted great impact on the nanostructure formation. Considering a large amount of residual monomers had remained in the previous stage of polymerization, these monomers would be polymerized together with the newly added monomer in a random manner. The presence of copolymer segment could affect the segregation strength and thus the microphase separation. From Charleux's study, addition of styrene monomer when *n*-BA conversion reached 81% resulted in high segregation strength. Microphase separation was strong that resulted in multi-layered structure. When styrene was added at low *n*-BA conversion (55%), low segregation strength would be resulted. In this circumstance, microphase separation was weak and sea-island structure would be formed.

### ***RAFT***

Luo and coworker prepared PS-*b*-(PS-co-PBd) multi-layered nanoparticles successfully via RAFT seeded emulsion polymerization [89]. There were two steps in their approach to prepare the nanostructured materials. The first step was the RAFT-mediated polymerization of the seed latex. In this seed forming step, styrene monomer was dissolved in hexadecane and the RAFT agent. The RAFT agent used in their approach was 1-phenylethyl phenyl dithioacetate (PEPDTA). The solution mixture was transferred to an aqueous solution containing sodium dodecyl sulphate (SDS) and then homogenized for 20 mins. The RAFT-mediated polymerization of the prepared emulsion solution was initiated by potassium persulphate (KPS) at 70℃ with sodium bicarbonate ($NaHCO_3$) as pH buffer. The macro-RAFT agent, PS-PEPDTA, seed latex was prepared after 2.5 hours RAFT polymerization. The second step was the RAFT-mediated seed emulsion polymerization of butadiene (Bd) in the presence of PS-RAFT seed latex. The RAFT-mediated seeded emulsion polymerization of Bd monomer was carried out in an autoclave containing PS-RAT seed latex, KPS and $NaHCO_3$. The polymerization was carried out at 70℃ under vacuum pressure for 1 day. According to the result in their study, the nanostructure of the PS-*b*-(PS-co-PBd) could be adjusted by tuning the composition of PS-co-PBd segment. Under optimal composition of PS-co-PBd, from 0.47 to 0.58, well defined multi-layered nanostructure particles were obtained. The formation of multi-layered particles was proven by TEM investigation with the aid of osmium tetraoxide ($OsO_4$) staining.

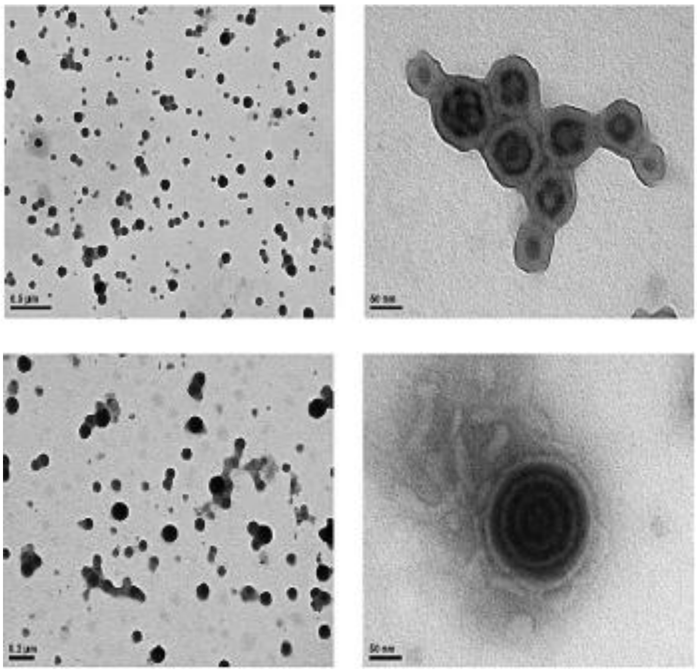

**Fig. 1.19.** TEM micrographs of multi-layered PS-*b*-(PS-co-PBd) with different segment compposityion of PS-co-PBd (upper: 0.47; lower : 0.58) [89].

Chen had presented a mixed approach to fabricate multi-layered polymer microsphere [90, 91]. Chen prepared onion-like microspheres by first synthesizing functional triblock terpolymer via RAFT polymerization followed by aerosol-assisted self assembly. Before block copolymerization, poly(3-(trimethoxysilyl)propyl methacrylate) (PTEPM) based marco-RAFT agent was priory prepared by bulk RAFT polymerization using 2-cyanoprop-2-yl dithiobenzoate (CPDB) as chain transfer agent. The polymerization was initiated by 2,2'-azoisobutylronitrile (AIBN) at 60℃ under vacuum for 20 hours. RAFT polymerization of styrene monomers in the presence of PTEPM macro-RAFT agent was then carried out in 90℃ under vacuum for 15 hours to prepare PTEPM-*b*-PS diblock copolymer. PTEPM-*b*-PS-*b*-P2VP triblock terpolymer was synthesized by further RAFT-mediated polymerization of 2-vinylpyridine monomer with PTEPM-*b*-PS as macro RAFT agent. The polymerization was proceeded at 60℃ under vacuum for 16 hours. With the aid of an aerosol generator, multi-layered microspheres were formed by self-gelation reaction of PTEPM. The multi-layered structure of the PTEPM-*b*-PS-*b*-P2VP microspheres was revealed under TEM microscopy. From their results, this multi-layered functional particle could be applied as template for gold immobilization. Gold salt was immobilized on the P2VP layer and gold nanocluster formation was achieved by subsequent addition of reducing agent like sodium borohydride.

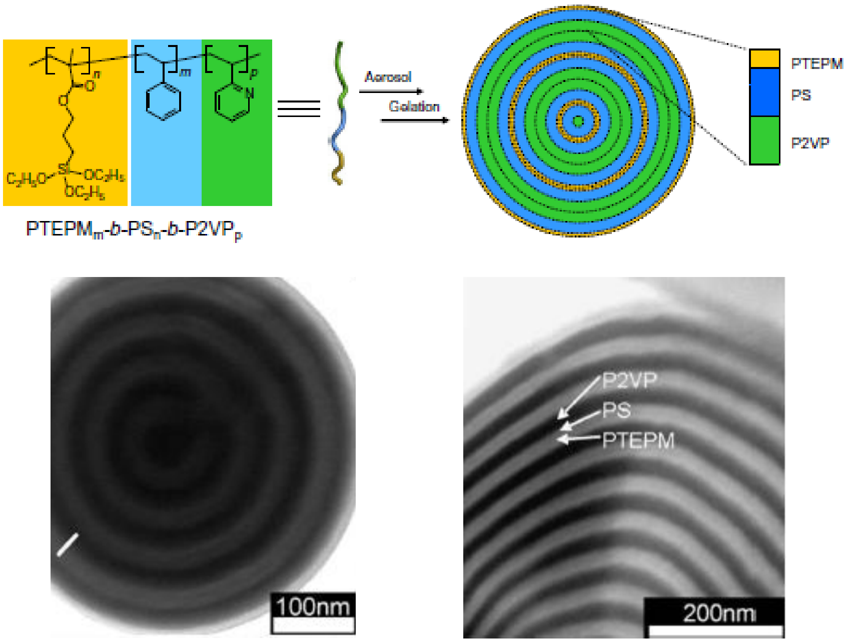

**Fig. 1.20.** Schematic illustration of onion-like PTEPM-*b*-PS-*b*-P2VP microsphere (upper) and TEM micrograph of the microspheres with multi-layered structure (lower) [91].

Mayes and coworker prepared four components multi-layered polymer nanoparticles via sequential surface initiated living-radical polymerization [92, 93]. The proposed approach was a combined method of surface initiated polymerization (SIP) and RAFT polymerization. The fabrication of the multi-layered particles started from seed formation. Seed particles were synthesized by conventional batch emulsion polymerization of monomer/crosslinker/vinylbenzene chloride (VBCl) in a mole ratio of 75 : 5 : 20 using ammonium persulphate (APS) as initiator. Two types of seed particles, styrene based (PS/PDVB/PVBCl) and methacrylate based (PMMA/PEDMA/PVBCl), were prepared as the core materials at this stage. Surface modification of vinylbenyl chloride on the surface of seed particles was then conducted. *In situ* formation of RAFT agent on the seed particle surface was achieved by coupling reaction with sodium diethyldithiocarbamate trihydrate (DEDTC). After surface modification, photo-induced surface initiated polymerization (SIP) of the second monomer was carried out together with a template (morphine, propranolol of *(S)*-naproxen) in argon atmosphere under UV irradiation. The RAFT agent was still retained on the particle surface after the polymerization and was capable for further SIP. Multi-layered polymer particles were thus prepared via sequential photo-induced surface initiated living-radical polymerization. Through this method, drug molecules like morphine, propranolol and naproxen could be molecularly imprinted in different shell layers, resulting in multi-layered functional polymer particles. These functional particles were capable of producing ‘antibody mimics’ by molecular imprinting.

Lim’s research group had synthesized PEO-*b*-PDVB-*b*-PS multi-layered polymer nanoparticles via interblock crosslinking RAFT polymerization [94]. There were three steps in the synthesis of the multi-layered PEO-*b*-PDVB-*b*-PS. PEO-based macro-RAFT agent was synthesized in the first step. Poly(ethylene oxide) was reacted with an excess chain transfer agent, 3-benzylsulphanylthiocarbo propionyl chloride (BSPAC), in anhydrous pyridine at room temperature for 12 hours. RAFT polymerization of styrene was then proceeded in THF at 70°C. 2,2'-azobisisobutyronitrile, AIBN, was applied as the initiator in this polymerization. Amphiphilic PEO-*b*-PS copolymer was synthesized after 12 hours of polymerization process. In the last step, the low molecular weight PEO-*b*-PS was dispersed in isopropyl alcohol (IPA) to form core-shell micelles. Then the crosslinker divinylbenzene (DVB), and initiator AIBN, were introduced to the reaction mixture to initiate the reaction. Core-shell interface crosslinking took place so that the dinvylbenzene was crosslinked at the interblock between PEO and PS. As a result, multi-layered amphiphilic nanoparticles were fabricated with a hydrophobic PS core, a crosslinked PDVB intermediate layer and a hydrophilic PEO shell.

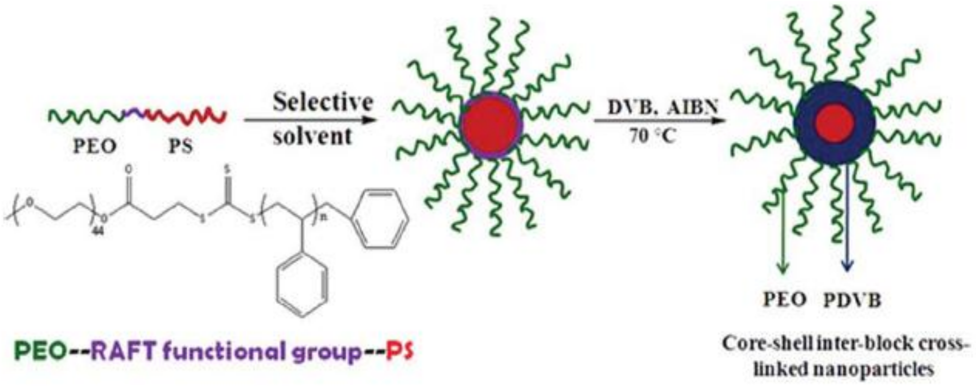

**Fig. 1.21.** Schematic illustration for the synthesis of interblock crosslinked PEO-*b*-PDVB-*b*-PS nanoparticles [94].

Hawkett and Gilbert's research group also had reported an approach that applied ab initio emulsion polymerization to synthesize multi-layered polymer particles via RAFT controlled self-assembly [95]. The first step of this approach was the preparation of the poly(acrylic acid) based macro-RAT agent by RAFT-mediated polymerization of acrylic acid. After formation of a small hydrophilic segment of PAA, hydrophobic monomer such as *n*-butyl acrylate or styrene was added subsequently as second monomer. RAFT-mediated polymerization of the hydrophobic monomer was proceeded to form a hydrophobic segment. When the segment of the hydrophobic polymer was long enough to reach the hydrophilic/hydrophobic balance, self-assembling of the diblock copolymer took place to form core-shell like micelles. The hydrophobic third monomer, styrene or *n*-butyl acrylate, was introduced into the reaction system by starve feed method for RAFT emulsion polymerization. Multi-layered particles constructed by triblock copolymer (PAA-PS-PBA or PAA-PBA-PS) were obtained at the end of polymerization. This approach enabled the preparation of MCP particles with well-controlled shell thickness and core diameter. Well-defined layered structure could be obtained if homopolymerization was absent. Further fundamental study on the mechanism of particle formation [96] and raidical entry [97] were investigated to achieve more in-depth understanding on RAFT-mediated emulsion polymerization with controlled self-assembly.

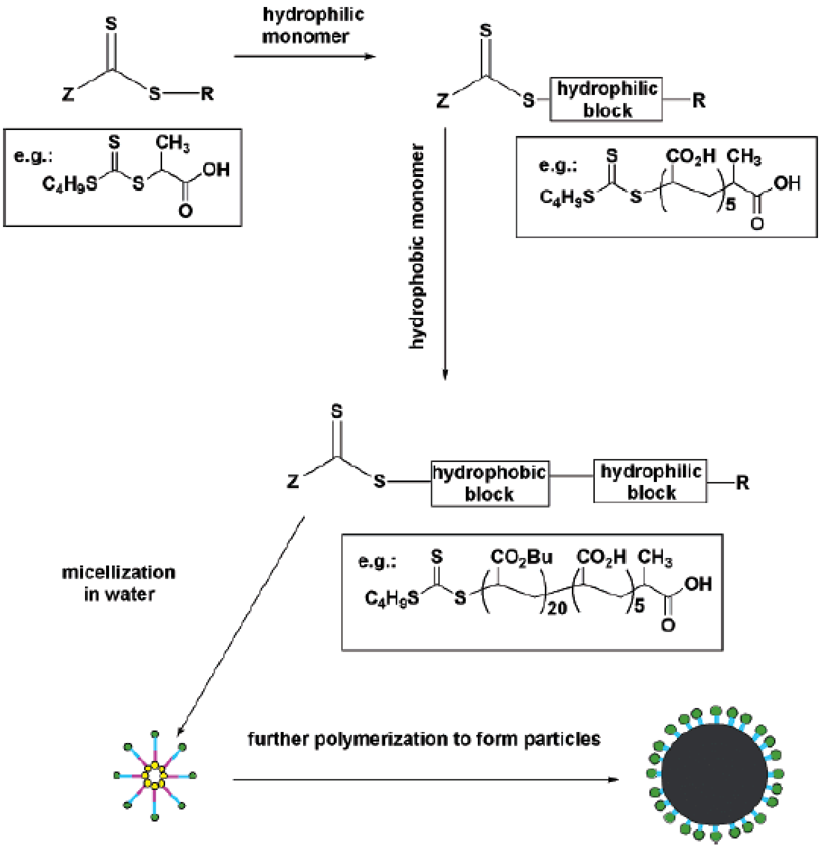

**Fig. 1.22.** Reaction scheme of the formation of amphiphilic polymer particle via RAFT emulsion polymerization under controlled self assembly [95].

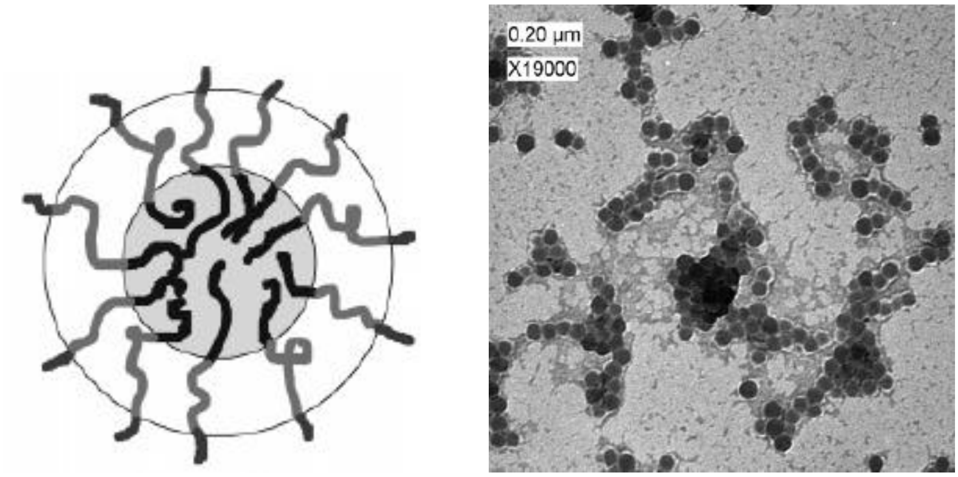

**Fig. 1.23.** Schematic drawing (left) and TEM micrograph (right) of amphiphilic polymer particle by RAFT emulsion polymerization [95].

### *Chemical oxidative seeded dispersion polymerization*

Recently, Fujii had reported a facile route to prepare conducting polymer nanocomposite via chemical oxidative seeded dispersion polymerization [98]. This approach had two steps, seed latex formation followed by chemical oxidative polymerization. Colloidally stable polystyrene/poly(*N*-vinylpyrrolidone) (PS/PNVP) core-shell particles were prepared by dispersed polymerization in the first step. From laser diffraction particle analysis, PS/PNVP seed latex had a volume average diameter of 1.52 μm. The chemical oxidative polymerization was conducted by adding 3,4-ethylenedioxythiophene (EDOT) monomer with palladium chloride as oxidant at 70°C. The resulting PS/(PEDOT-Pd)/PNVP nanocomposite had a rigid PS in the innermost core as solid support, PEDOT-Pd deposited on the PS core and PNVP at the outer shell as stabilizer. The formation of PEDOT-Pd nanocomposite on the seed was proved by the increase in particle diameter from 1.52 μm to 1.96 μm and by the result from X-ray diffraction studies. Findings from previous results proposed that nanocomposites comprising Pd could be applied as an effective recyclable catalyst for Suzuki-Miyaura coupling reaction. [99, 100]

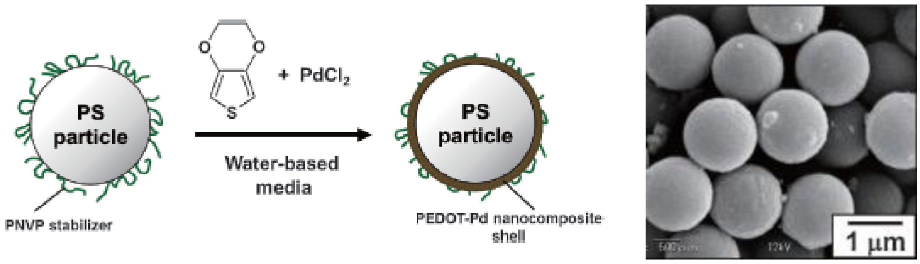

**Fig. 1.24.** Schematic illustration of the chemical oxidative seeded dispersion polymerization (left) and SEM micrograph of PEDOT-Pd coated nanocomposite (right) [98].

### *Solvent-absorbing/releasing method*

The solvent-absorbing/releasing method is a technique to construct multi-layered nanostructured particles via solvent post-treatment after particle synthesis. This approach is raised by Okubo [101]. Okubo and coworkers have developed a post-treatment system to prepare spherical polymeric particles with well-defined multi-layered nanostructure by utilizing the solvent-absorbing/releasing method. They had prepared two types of MCP particles with multi-layered nanostructures. These multi-layered MCP particles were PMMA/PS/PVP and PS/PMMA/PAA. There are three steps in the preparation of these multi-layered polymer particles: i) seed particle formation, ii) core-shell particle formation, and iii) morphology rearrangement by solvent treatment.

The first step of their approach is the preparation of seed particles by dispersion polymerization. PMMA/PVP seed particles are formed by MMA polymerization in the presence of water soluble polymer, poly(vinyl pyrrolidone) (PVP). PS/PAA seed particles are formed by styrene polymerization in the presence of the water soluble polymer, poly(acrylic acid) (PAA). Monodispersed seed particles are prepared and purified for the next stage, seeded dispersion polymerization.

In seeded dispersion polymerization of PMMA/PVP, styrene is used as the second monomer while MMA is used as the second monomer for the seeded dispersion polymerization of PS/PAA [102, 103]. PMMA/PS/PVP and PS/PMMA/PAA core-shell microspheres are subsequently formed. During the seeded dispersion polymerization, *in situ* formation of PS-*b*-PMMA and PMMA-*b*-PS copolymers takes place. Block copolymer acts as compatibilizer to promote the formation of the multi-layered structure in the solvent-absorbing/releasing step. The prepared MCP particles were monodispersed with micron sized dimension about 2 μm.

After purification, the MCP particles are treated with toluene, a common solvent for both PMMA and PS. MCP particles are swelled by the solvent at this stage which refers to a solvent absorbing step. The solvent swelled by particles is then evaporated under room temperature with gentle stirring. This step is solvent releasing step and multi-layered nanostructure is constructed in this step [104]. Effects of graft copolymer [105], internal viscosity [106], surfactant [107], molecular weight [108], and rate of evaporation of solvent [59, 109] were studied on the nanostructure formation of MCP particles. The morphology and nanostructure of the multi-layered particles were investigated by scanning electron microscopy (SEM), transmission electron microscopy (TEM) and scanning transmission X-ray microscopy (STXM) [110, 111]. A schematic diagram on the structural reconstruction on MCP particles was illustrated in the Fig. 1.25.

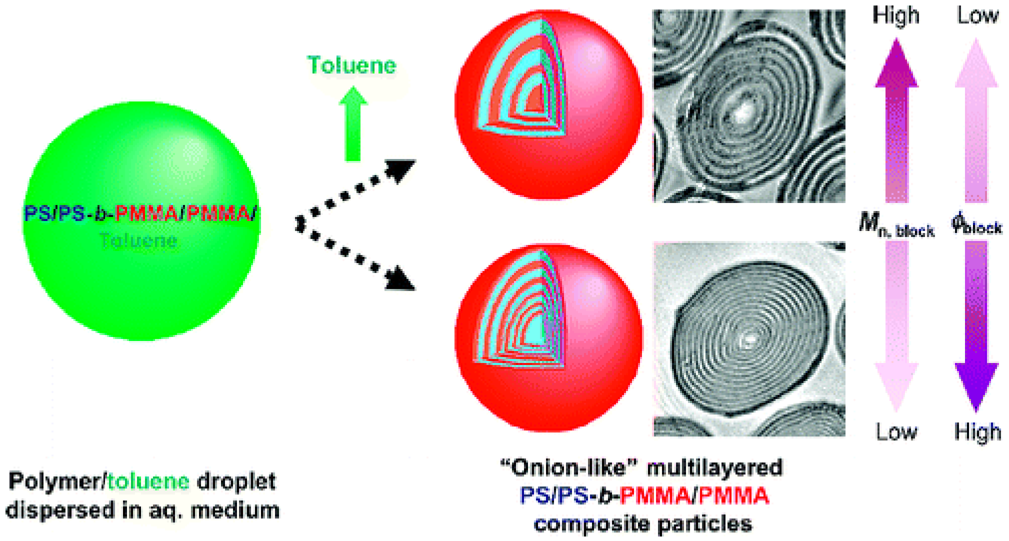

**Fig. 1.25.** Nanostructure reconstruction of multi-layered polymer particles [59].

### *Self-assembling of block copolymers*

Self-assembling of block copolymers is another commonly applied technique to fabricate polymer particles with multi-layered structures. Block copolymer is priory formed by various polymerization methods. Self-assembling of block copolymers is triggered by either introducing another polymer or adding another solvent. Due to the difference in the interfacial tension between polymer and continuous phase, self-assembly of the polymer components takes place to minimize the interfacial free energy.

Yi and Yang have reported an approach to prepare functional polymer particles with lamellar or onion-like multi-layered nanostructures via self-assembly of block copolymers in emulsion droplets [112]. They have prepared three types of multi-layered polymer particles, which are PS/(PS-PB)/(PS-PEO), PS/(PS-PB)/(PB-PEO) and PS/(PS-PB)/(PS-PEO)/(PB-PEO). The prepared polystyrene (PS) homopolymer and poly(styrene-*b*-butadiene) PS-PB block copolymer are first dissolved in toluene and then emulsified in water containing amiphiphilic poly(styrene-*b*-ethylene oxide) (PS-PEO) or poly(butadiene-*b*-ethylene oxide) (PB-PEO) diblock copolymer surfactant. The emulsification is achieved by using homogenization. The oil-in-water emulsion is then carried to solvent removal by treating the emulsion at 95℃ for 2 hours under reduced pressure. During toluene evaporation, self-assembly of the block copolymer and homopolymer is induced to result in colloidal particles with lamellar or onion-like structure. The selection rule for the final morphology and nanostructure mainly depends on the surfactant system chosen during emulsification. By simply varying the composition of amphiphilic diblock copolymer surfactants, tulip-like, ellipsoidal or spherical particle with micro-domain, lamellar or onion-like nanostructured colloidal particles can be fabricated.

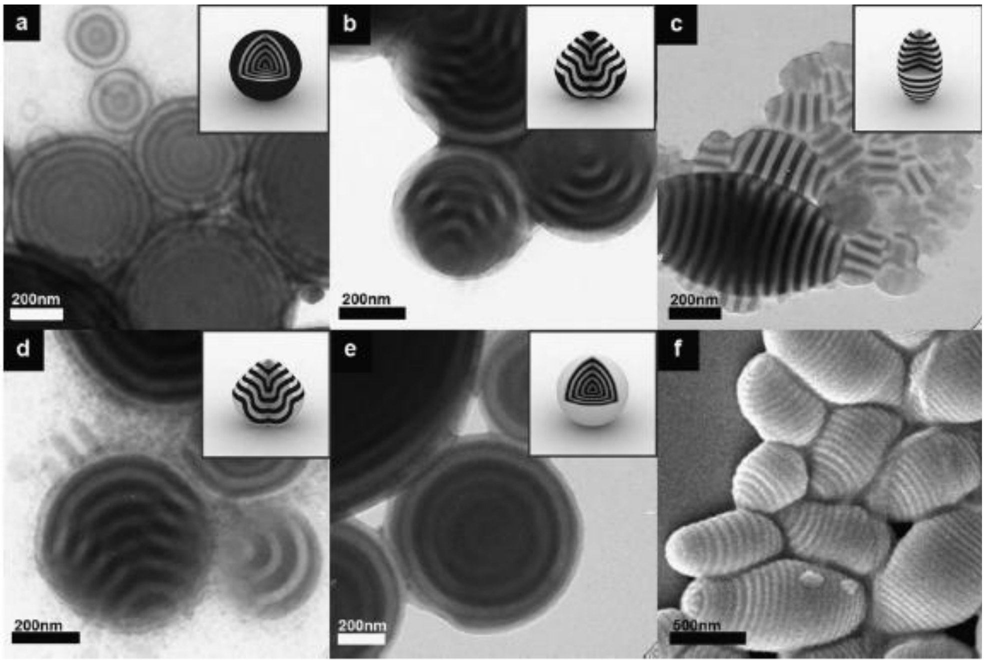

**Fig. 1.26.** TEM micrographs of colloidal particles prepared from evaporation induced self-assembly: spherical particle with onion-like structure (a, e); tulip-like particle with lamellar structure (b, d); ellipsoidal particle with lamellar structure (c, f) [112].

### *Self-organized precipitation*

Yabu and coworker have developed a solvent post treatment method called self-organized precipitation to construct polymer nanoparticles with various hierarchical nanostructures [113-115]. This multi-layer structured nanoparticle is composed of three components, polystyrene (PS), polyisoprene (PI) and poly(styrene-*b*-isoprene) block copolymer. PS, PI homopolymer and PS-PI block copolymer are dissolved in tetrahydrofuran (THF) in the first step of preparation.

An appropriate amount of water was then added to the polymer mixture solution in a continuous feed manner under stirring. When the addition of water is completed, solution mixture agitation is also stopped. THF is evaporated under atmospheric pressure for 2 days. Nanostructure construction occurs during THF evaporation. Onion-like multi-layered structured polymer particles are fabricated after complete removal of THF. Various types of nanostructures such as onion-like, lamellar, cylinder, network and Janus can be fabricated by the self-organized precipitation method by changing the composition of each component and varying the segment length of block copolymer. Particles with network structure possess improved mechanical properties. These particles with multi-layered nanostructure should have high potential to be applied as novel photonic materials.

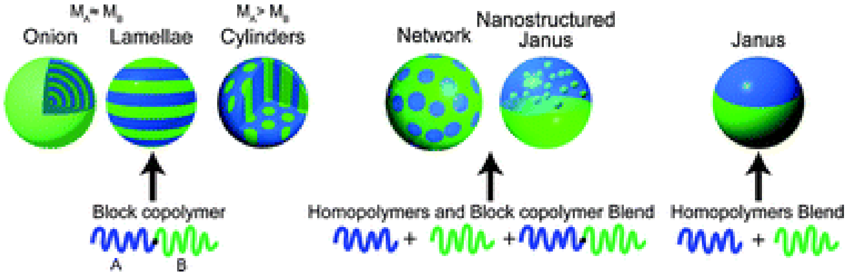

**Fig. 1.27.** Possible nanostructures of colloidal nanoparticles prepared by self-organized precipitation method [114].

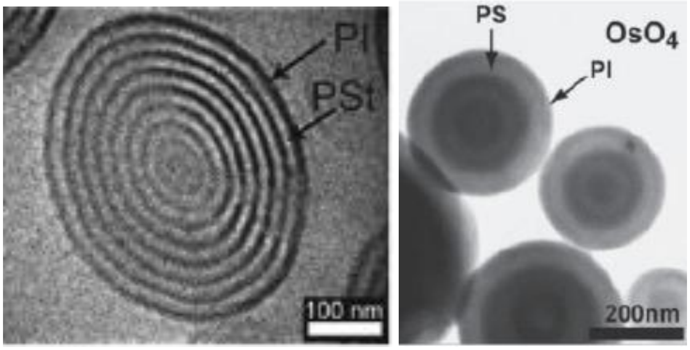

**Fig. 1.28.** TEM micrographs of onion-like multi-layered polymer particles [114, 115].

### *Thermal imprinting*

Stover and coworker have reported the preparation of multi-layered polymeric microsphere via precipitation copolymerization with periodic temperature oscillation [116]. These multi-layered microspheres are fabricated by the copolymerization of chloromethylstyrene (CMS) and divinylbenzene (DVB-55) in acetonitrile. The initiator selected is azobisisobutyronitrile (AIBN). The polymerization is first initiated at 65℃, and the temperature is elevated to 75℃ after being reacted for 1 hour. The reaction temperature is adjusted back to 65℃ after 1 hour reaction at 75℃. This periodic temperature oscillation is repeated for 16 hours. Polymeric microspheres with well controlled radial structure are prepared and this nanostructure is revealed under optical and electronic microscopy. The layer thickness of the particles can be easily adjusted by tuning the frequency of the temperature oscillation. This multi-layered particle exhibited great potential in the photonic application due to periodic modulation of the refractive index.

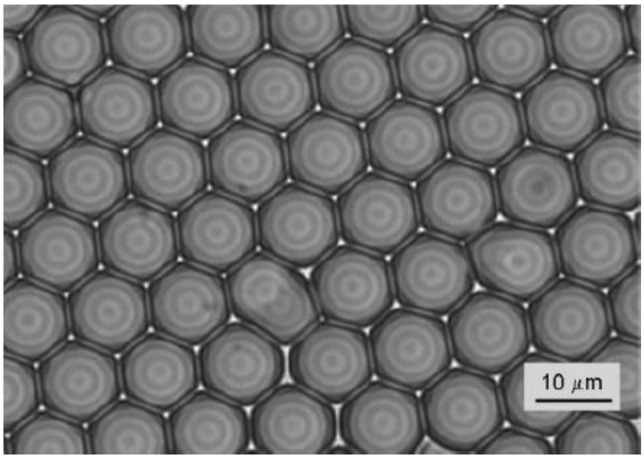

**Fig. 1.29.** TEM micrograph of the multi-layered polymer microspheres [116].

### *Core-shell structured MCP particles*

Well-defined multi-layered structure is not observed in MCP particles under certain cicrcumstances. Simplified layered structure, i.e. core-shell structure, is revealed in spherical MCP particles instead. The formation of core-shell structure is due to the high compatibility between polymer components which originated from the low polymer-polymer interfacial tensions. Usually, core-shell structured MCP particles possess either a mixed component shell or a mixed component core, depending on the polymer-aqueous phase interfacial tension and polymer-polymer interfacial tension of each component. Selected reports on the preparation of core-shell structured MCP particles will be discussed here.

### *One step polymerization*

Penlidis et al have presented a series of studies on the synthesis of multi-component polymer poly(butyl acrylate)/poly(methyl methacrylate)/poly(vinyl acetate) (PBA/PMMA/PVA) [117-120]. The methodology they presented for the preparation of MCP particles is simple that all the monomers (*n*-BA, MMA and VAc), chain transfer agent (*n*-dodecyl mercaptan), and emulsifier are introduced to the reactor before polymerization begins. The emulsion polymerization is initiated by adding a thermal initiator (ammonium persulphate) to the reaction mixture at the onset temperature. Comprehensive investigation on the polymerization kinetics such as the reactivity ratio between each monomer and polymerization approaches have been well studied. Moreover, the synthesis of PBA/PMMA/PVA can be scale up to pilot scale production by a 5L jacketed stainless steel pilot reactor.

### ***Multistep seeded polymerization***

Yang et al have reported the synthesis of amphiphilic core-shell latex particles and their novel application in chemical-free thermal laser imaging [121]. The amphiphilic core-shell particles possess a mixed polymer hydrophobic core and a thin hydrophilic layer. Preparation of these particles is divided into three steps. Poly(butyl methacrylate)-*co*-poly(methyl methacrylate) is prepared by batch emulsion polymerization which is initiated by potassium persulphate (KPS). Subsequent semi-continuous seeded polymerization of glycidyl methacrylate (GMA) monomers is then conducted under a redox initiated system. This initiation system is composed of *tert*-butyl hydroperoxide (oxidizing agent, radical source), L-ascorbic acid (reducing agent) and vanadium (IV) oxide sulphate ($VOSO_4$) (catalyst). The polymerization is carried out at a lower temperature (60℃) which prevented the reaction of active epoxy group of GMA monomers. After the formation of (PBMA-PMMA)/PGMA core-shell particles, surface modification of the epoxy group of PGMA is conducted by treating the core-shell particles with triethanolamine hydrochloride. Part of the epoxy groups undergo ring opening reaction and are converted into quarternary salt and become cationic. A latex film is formed by (PBMA-PMMA)/PGMA particles, binder polymer and IR absorbing dye to demonstrate the thermal laser imaging properties of the core-shell particles. The formed latex film is irradiated by IR laser beam and washed by neutral water. The non-irradiated latex film domain is easily washed in water while the irradiated latex domain cannot be removed. Negative images are obtained, showing that (PBMA-PMMA)/PGMA can be applied as water-developable laser thermal imaging materials.

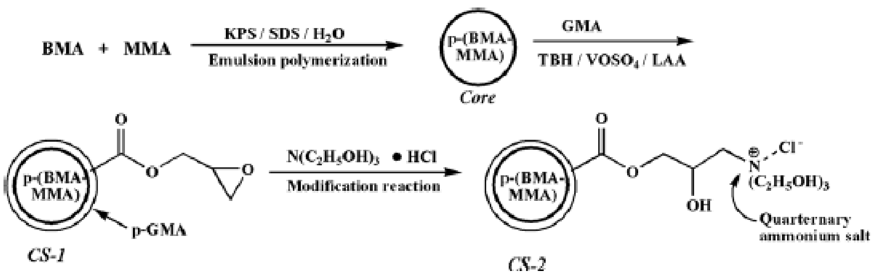

**Fig. 1.30.** Reaction scheme for the synthesis of amphiphilic (PBMA-PMMA)/PGMA core-shell particles [121].

Chiu's research group have prepared (PBA-PMMA)/PANI functional composite particles via two-step soapless emulsion polymerization [122]. These functional composite particles possess a mix core of poly(butyl acrylate) and poly(methyl methacrylate) and an electric conducting shell of polyaniline. (PBA-PMMA) seed particles are prepared by soapless emulsion polymerization of *n*-BA and MMA monomers using 2,2'-azobis(isobutyramidine) dihydrochloride (AIBA) as initiator. Ethylene glycol dimethacrylate (EGDMA) is employed as corsslinker during seed formation. From the TEM micrographs, the seed particles had diameters ranging from 170 to 200 nm. In the next step, aniline monomers are polymerized using ammonium persulphate (APS) as initiator. Dodecyl benzene sulphonic acid is added as an additive to promote the conductivity of the core-shell latex film during film formation. According to the TEM results, (PBA-PMMA)/PANI core-shell complex particles have diameters ranging from 200 to 400 nm. Furthermore, Chiu's research group investigated the electric conducting properties of the (PBA-PMMA)/PANI core-shell complex particles. A continuous film of (PBA-PMMA)/PANI is first formed by dip coating. The presence of the low $T_g$ polymer component, PBA, facilitates the film formation and thus improves the processability of the core-shell latex particles. Under optimum composition, the core-shell latex film exhibites a conductivity of 0.16 S/cm which demonstrating desirable electrical conductivity.

Ma and coworkers have presented the synthesis of core-shell structured poly(4-vinylpyridine-*co*-butyl acrylate)/poly(styrene-*co*-butyl acrylate) (P4VP-PBA)/(PS-PBA) MCP particles via soapless seeded emulsion polymerization [123]. The composite microspheres are prepared by two-step polymerization. Positively charged (P4VP-PBA) seed particles are prepared in the first step. The monodispersed cationic seed particles are synthesized by soapless emulsion polymerization of 4-vinylpyridine and butyl acrylate monomers crosslinked by divinylbenzene (DVB) or ethylene glycol methacrylate (EGMA). The positive charge of the seed particles is contributed by the cationic initiator 2,2'-azobismethyl(propionamidine) dihydrochloride (V-50). Seeded emulsion polymerization of styrene and *n*-BA monomers is carried out in the second step with (P4VP-PBA) as seed particle. Micron-sized composite particles with P4VP-PBA rich core and PS-PBA rich shell are formed and the particles' nanostructure is examined by TEM studies. Extended studies on the effect of monomer composition, monomer feeding rate, crosslinker type, degree of crosslinking and initiator type are also investigated in their publications. Most importantly, the morphology of the composite particles greatly depends on the type of initiator. Spherical core-shell particles are formed if cationic V-50 initiator is used. Nonetheless, popcorn-like or sandwich-like particles are formed if the cationic initiator is replaced by nonionic AIBN initiator. Such difference is due to changes in polymer-polymer and polymer-aqueous phase interfacial tension. The polymer-aqueous phase interfacial tension of particles would be effectively reduced by the positively charged polymer chains if V-50 is used as initiator. On the other hand, if AIBN initiator is used, nonionic polymer chains have lower polarity and thus lead to higher polymer-aqueous phase interfacial tension. The seed particles thus can not be engulfed by the newly formed polymer chains, resulting in different non-equilibrium morphologies.

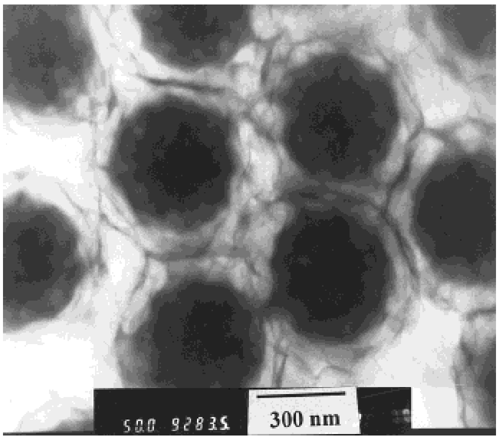

**Fig. 1.31.** TEM micrograph of (P4VP-PBA)/(PS-PBA) composite microspheres [123].

Lee has presented another synthetic pathway to prepare amphiphilic MCP core-shell particles via soap-free seeded emulsion polymerization [124]. The three component polymer system consists of polystyrene (PS), poly(methyl methacrylate) (PMMA) and poly(acrylic acid) (PAA). PMMA seed particles are prepared in the presence of PAA as stabilizer at 80℃ under nitrogen atmosphere. PMMA seed particles with surface stabilized by PAA are formed with an average diameter of 207.8 nm. Seeded emulsion polymerization of styrene monomers is then carried out to form the resulting composite particles. The formed composite particles have an average diameter of 316.6 nm. The evolution of particle morphology is monitored by TEM studies of particle samples withdrawn at different reaction time intervals. Upon seeded emulsion polymerization, composite particles have a mixed core of PMMA and PS and a PS shell in the initial period.

Layer by layer structured PS/PMMA/PS composite particles are obtained in the middle stage of polymerization. At the end of polymerization, core-shell structure particles with PS core and PMMA shell are obtained. Throughout the polymerization process, PAA is adsorbed on the particle surface which acts as stabilizer. The final morphology reached at the end of polymerization should be equilibrium morphology. The evolution of equilibrium morphology is attributed by the presence of PAA as PAA effectively reduces the polymer-aqueous phase interfacial tension.

Liu and coworkers have reported the synthesis amphiphilic MCP particles via semicontinuous seeded emulsion polymerization [125]. These MCP nanoparticles are composed of three components, polystyrene (PS), poly(ethyl acrylate) (PEA) and poly(acrylic acid) (PAA). PS/PEA/PAA seed particles are first prepared by emulsion polymerization of St, EA and AA monomers. The monodispersed seed particles prepared are spherical in shape with a dimension of 415 nm. Semicontinuous seeded emulsion polymerization is then proceeded by adding initiator into the reaction mixture under continuous feed of St/EA/AA mixed monomer. After 11 hours of polymerization, spherical PS/PEA/PAA MCP particles are obtained with high monomer conversion of 94% and dimension of 800 nm. Under alkali post-treatment process, the nanostructure of the PS/PEA/PAA particles is evolved to spherical with multi-hollow. This approach provides a simple route to prepare MCP particles with multi-hollow nanostructure.

### *Controlled/living radical polymerization*

Monteiro et al have reported the synthesis and application of core-shell structured MCP particles [126]. Polystyrene/poly(butyl acrylate-acetoacetoxyethyl methacylate), PS/(PBA-PAAEMA), core-shell nanoparticles are synthesized by two step RAFT emulsion polymerization. Macro-RAFT agent is first prepared by controlled free radical emulsion polymerization of styrene with RAFT agent, (1-(*O*-ethylxanthyl) ethylbenzene). The polymerization is initiated by sodium persulphate (SPS) at 70℃ with a sodium dodecyl sulphate (SDS) surfactant. MCP particles are prepared by second-stage RAFT polymerization of BA and AAHEMA mixed monomer with PS-RAFT macro-RAFT agent under stave-fed condition. Nanoparticles with dimension less than 100 nm are obtained after polymerization. Under cryo-TEM analysis, core-shell structured material with PS core and P(BA-AAEMA) shell is clearly observed. Effects of RAFT agent content, SDS content and initiator content on particle size, size distribution and molecular weight of the MCP particles are also studied. The synthesized MCP particles are found to have superior film properties than conventional polymer blends. By adjusting the location of PAAEMA, the mechanical properties of the film can be further tuned [127].

### *Anisotropic MCP particles*

Apart from spherical particles, non-spherical and anisotropic particles are another major category of MCP particles. From the point of view of thermodynamic consideration, spherical polymer particle is the most stable particle morphology as it possesses the minimum interfacial free energy. This morphology is regarded as the preferred morphology if the polymerization process is allowed to reach equilibrium morphology. Nonetheless, not every polymerization process can reach equilibrium morphology eventually. Kinetic preferred morphology such as non-spherical and anisotropic is achieved at the end of polymerization instead. Such anisotropic morphologies include raspberry, dumbbell, snowman, mushroom, hemispherical, Janus, golf-ball, disc, confetti, multi-hollow, speckled and even particle with a dent [128-143]. Recently, numerous literatures have reported the synthesis, characterization and application of particles with these morphologies. Selected approaches to prepare polymer particles with different types of non-spherical and anisotropic morphology are discussed in detail below.

### ***Raspberry particles***

Akashi and coworkers have fabricated MCP particles with raspberry-like nanostructures by a simple one-step dispersion terpolymerization [144]. Polystyrene-*co*-polyacrylonitrile-*co*-poly(ethylene glycol) monomethacrylate (PS-*co*-PAN-*co*-PEGm) MCP nanoparticles are prepared via batchwise dispersion polymerization of styrene, acrylonitrile monomers and PEGm. The polymerization is carried out at 60°C for 24 hours in an ethanol/water solvent system. Upon polymerization, spherical nanoparticles are formed at the initial stage. As the polymerization progresses, surface roughness is observed on the nanoparticles after 2 hours of reaction. Raspberry-like (PS-*co*-PAN-*co*-PEGm) nanoparticles are formed after 5 hours of polymerization. The formation of raspberry-like particles morphology is attributed to the presence of AN monomers according to Akashi and coworkers previous research on the preparation of spherical PS/PEGm particles. In addition, non-equilibrated swelling of AN monomer and PEGm on the spherical particles surface also plays an important role in the formation of raspberry-like structure. Thorough investigation of reaction time and styrene/AN monomer composition have been conducted on the morphology development of the raspberry-like nanoparticles. From their findings, under optimal AN composition (mole composition of AN to the total monomers ranged from 0.49 to 0.66) and 3-5 hours of polymerization, raspberry-like (PS-*co*-PAN-*co*-PEGm) nanoparticles with uniform particle size and a fixed number of projections are produced, demonstrating a facile synthetic route to prepare raspberry-like nanoparticles.

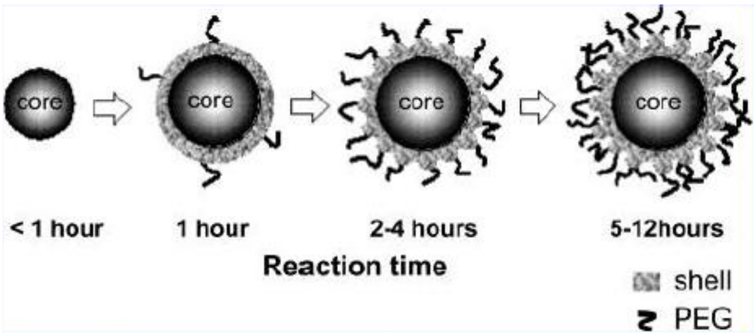

**Fig. 1.32.** Reaction scheme for the formation mechanism of (PS-*co*-PAN-*co*-PEGm) nanoparticles [144].

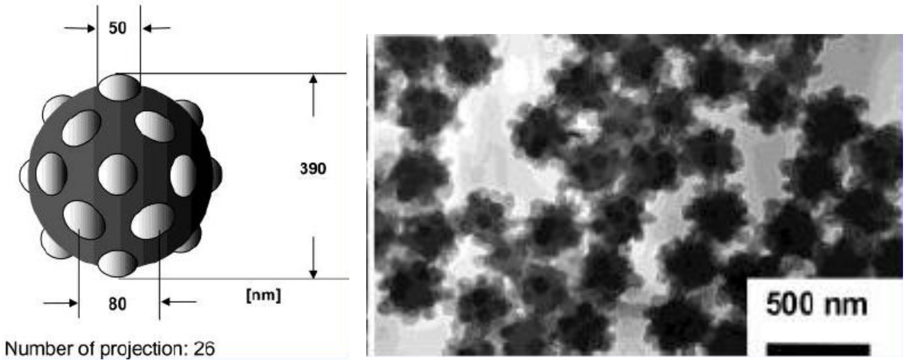

**Fig. 1.33.** Schematic illustration (up) and TEM micrograph (down) of (PS-*co*-PAN-*co*-PEGm) nanoparticles [144].

Seeded emulsion polymerization and self-assembled coagulation are two major conventional strategies to fabricate anisotropic polymeric particles with raspberry-like structure. These methods are based on chemical initiated polymerization at high reaction temperature. Recently, Liu et al have presented a novel approach to fabricate raspberry-like (polystyrene-polydivinylbenzene-poly(acrylic acid))/polyacrylonitrile (PS-PDVB-PAA)/PAN particles via γ-ray radiation-induced seeded emulsion polymerization at room temperature [145]. In the two-step synthesis, spherical PS-PDVB-PAA seed particles are prepared through soapless emulsion polymerization using potassium persulphate (KPS) as initiator in the first step. The particle size and size distribution of seed particles are characterized by SEM, which show a number-average diameter of 307 nm and polydispersity index (PDI) of 1.003, respectively. In the second step, AN monomers are polymerized via γ-radiation-induced seeded emulsion polymerization under ambient pressure at room temperature. $^{60}$Co γ-ray is utilized as the source of irradiation. Morphology, particle size and size distribution of the (PS-PDVB-PAA)/PAN particles are characterized by SEM and TEM. The particles possess a number-average diameter of 415.2 nm and a polydispersity index of 1.003, illustrating the nanosized dimension and absence of secondary nucleation during seeded emulsion polymerization. More importantly, composite particles with raspberry-like structure are revealed from SEM and TEM micrographs. Liu also interprets the formation mechanism of this specific structure. The formation of raspberry-like particles is due to high polymer-polymer interfacial tension and between PS and PAN and the elastic retractile force of crosslinked (PS-PDVB-PAA) seed particles during seeded emulsion polymerization. As AN monomers are introduced into the seed particles, part of the monomers is swollen by the seed particles due to partial compatibility between the monomer and the (PS-PDVB-PAA) seed particles. Upon seeded emulsion polymerization, AN monomers are polymerized and then segregate from the seed particles because of the high polymer-polymer interfacial tension between PS and PAN. The elastic retractile force of seed particles during seeded emulsion polymerization also assists the phase separation of PAN from seed particles, forming many bulges on the seed particle surface. On the other hand, since AN monomers exhibits certain solubility in water, polymerization of AN monomers also takes place in aqueous phase upon radical generation by radiolysis of water. When the growing chains of PAN reach the critical chain length, precipitation of PAN polymer occurred and these PAN chains are preferentially deposited and coagulate on the small PAN nano-domains on the particles in order to minimize the interfacial surface energy. This process continues until all the monomers are consumed, resulting in the formation of raspberry-like (PS-PDVB-PAA)/PAN anisotropic particles.

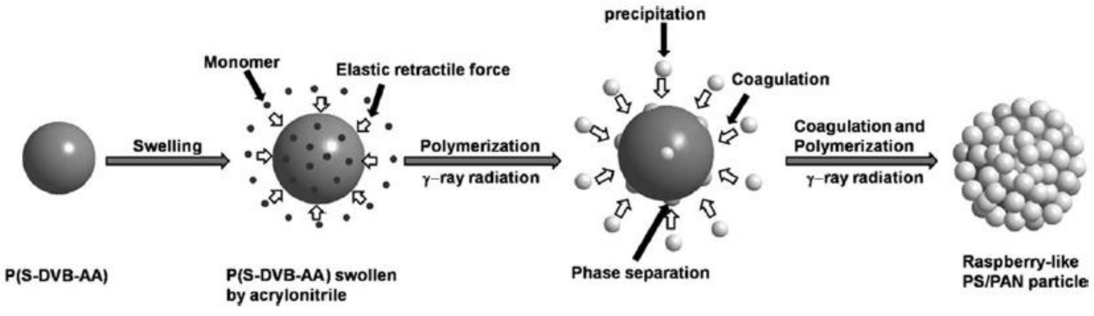

**Fig. 1.34.** Schematic illustration for the preparation of raspberry-like (PS-PDVB-PAA)/PAN particles [145].

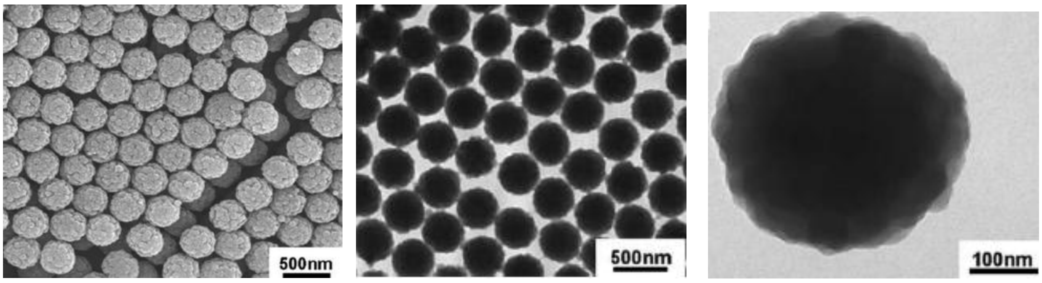

**Fig. 1.35.** SEM (left) and TEM micrographs (middle and right) of raspberry-like (PS-PDVB-PAA)/PAN particles [145].

Kuroda et al have prepared two types of raspberry-like polymeric particles, poly(2-acetoxylethyl methacrylate)/polystyrene (PAEMA/PS) and poly(methyl methacrylate)/ polyacrylonitrile (PMMA/PAN), by two different polymerization approaches. Raspberry-like PAEMA/PS particles are synthesized by two-step soapless seeded emulsion polymerization [146, 147]. PAEMA seed particles are firstly formed by soapless emulsion polymerization of AEMA monomers crosslinked by ethylene glycol dimethacrylate (EGDMA). Anionic initiator, potassium persulphate (KPS) is applied to initiate the polymerization. Seeded emulsion polymerization takes place by introducing styrene monomer and initiator into seed particles. Effects of second monomer composition, addition approach of second monomer and types of initiator are investigated to study the morphology of the particles. Various kinds of morphologies, confetti-like, popcorn-like, void containing, doublets and triplets particles, are formed by adjusting the a fore-mentioned synthetic parameters. Under optimal reaction parameters, raspberry-like particles are fabricated. Kuroda infers that the formation of non-spherical particles is due to the deformation of the polymer network of the seed particles.

Another type of raspberry-like particles, PMMA/PAN is synthesized by two-step seeded precipitation polymerization [148]. In the first step, PMMA seed particles are prepared by soapless emulsion polymerization. The seed particles are synthesized with a number-average diameter of 307 nm and narrow particle size distribution. In the second stage, precipitation polymerization of AN monomers proceeds to form a PAN shell on the seed particles since PAN is more hydrophilic than PMMA. Due to the considerable water solubility of AN monomers, these monomers are first initiated in the aqueous phase. Propagation of the AN polymerization continues until the polymer chains reached hydrophilic-hydrophobic balance. Upon reaching the critical chain length, the growing chains collapse to a globular structure and then precipitated from the aqueous phase onto the seed particle surface. Due to the zero co-solubility of PAN with both AN monomer and water, AN monomers are initiated and propagated in aqueous phase instead of being swollen by the newly generated PAN polymers. In addition, PAN polymers are found to form crystallites during radical polymerization. The zero co-solubility and crystalline nature of PAN polymers should be the major reason for the high degree of roughness on the particle surface, i.e. raspberry-like morphology.

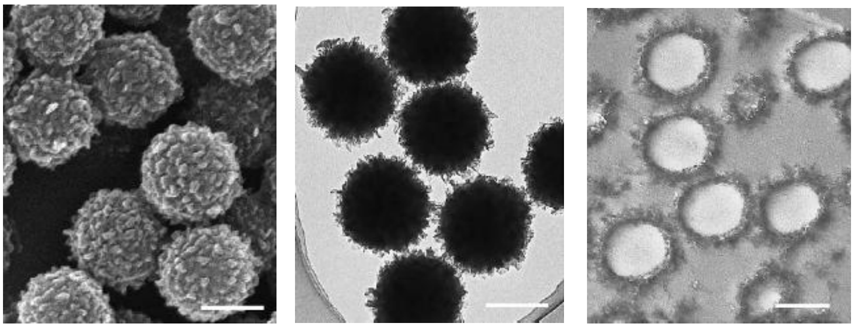

**Fig. 1.36.** SEM (left) and TEM (middle and right) micrographs of raspberry-like PMMA/PAN particles [148].

### *Dumbbell particles*

Balluaff and coworkers have developed a versatile system in preparation of smart dumbbell-shaped anisotropic particles. They have reported three types of dumbbell-shaped particles, PMMA/PS/PSS [149], PMMA/PS/PNIPAm [150] and PS/PS-MPS/PNIPAm [151]. General approach towards these anisotropic particles is comprised of three steps. First, spherical seed particles are prepared by conventional emulsion polymerization. Next, seeded emulsion polymerization is carried out by adding hydrophobic second monomers under starved-fed conditions. Dumbbell-shaped core particles are prepared at this stage. Finally, the surface of dumbbell-shaped core particles is functionalized by anchoring a layer of pH-responsive or thermal responsive polymer via different polymerization methods. In the case of pH-responsive dumbbell-shaped polymer particles, the surface of the core seed particles is modified by photoemulsion polymerization of sodium styrene sulphonate (NaSS) triggered by photoinitiator 2-[*p*-(2-hydroxy-2-methylpropiophenone)]-ethyleneglycol methacrylate (HEHM). In the case of thermal responsive dumbbell polymer particles, the surface of the core seed particles is modified by seeded emulsion polymerization of *N*-isopropylacrylamide (NIPAm) crosslinked by *N*,*N'*-methylenebisacrylamide (MBA). The morphology and nanostructure of the dumbbell-shaped particles are investigated under SEM and cryo-TEM. The thermal responsive properties of the particles are confirmed by dynamic light scattering. Balluaff attributed the formation of these anisotropic particles to three important parameters. First, the relatively high interfacial tension between the spherical PMMA seed particles and the styrene monomers favored the formation of dumbbell-shaped particles. Second, proper selection of surfactants plays an important role in preventing the formation of spherical particles. Finally, the rate of addition of second monomer also affects the terminal morphology of the particles. In Balluaff's approach, hydrophobic styrene monomer is added to the seed dispersion in starve-fed conditions at low reaction temperature (60°C). The diffusion of styrene monomer into the seed particle core is inhibited under such reaction condition.

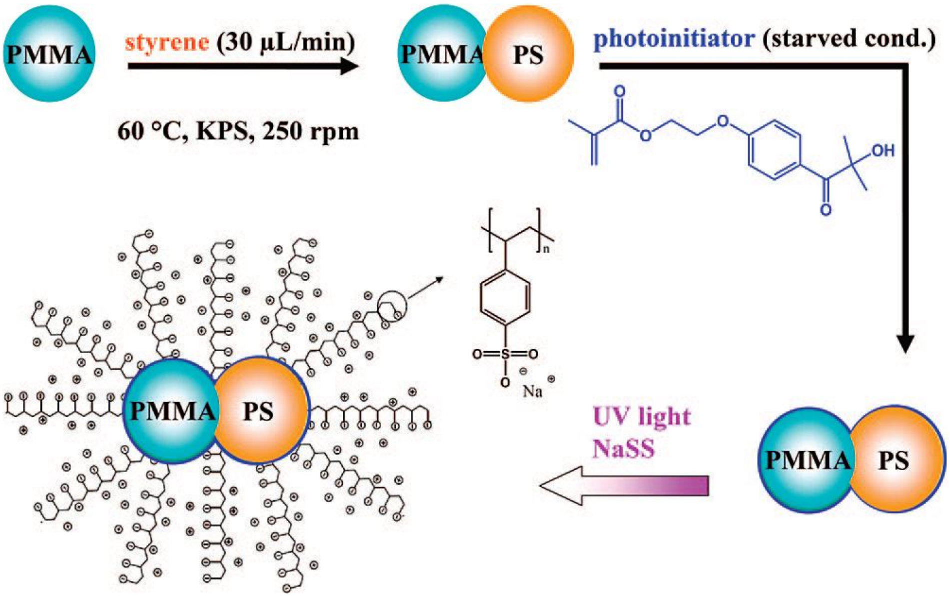

**Fig. 1.37.** Reaction scheme on the synthesis of pH responsive dumbbell-shaped particle [149].

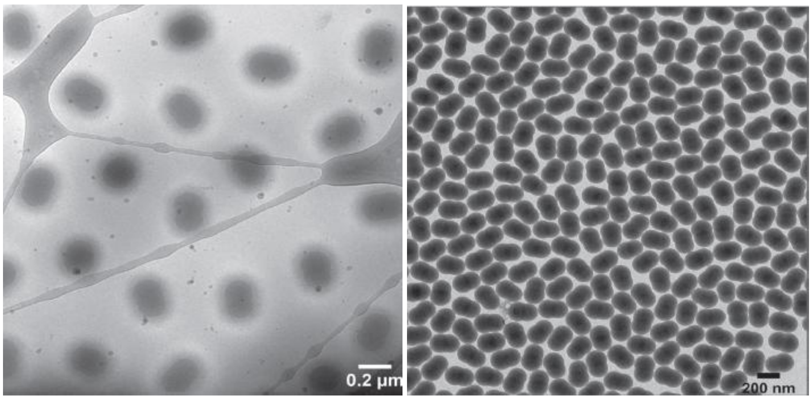

**Fig. 1.38.** cyro-TEM micrographs of PS/PS-MPS seed particle (left) and thermo-responsive dumbbell-shaped PS/PS-MPS/PNIPAm (right).

Weitz and coworkers have established a facile and versatile platform to fabricate dumbbell-shaped polymeric particles with anisotropic properties based on seeded polymerization [152]. Two types of anisotropic dumbbell-shaped particles are fabricated in Weitz publication. Crosslinked polystyrene (PS) seed particles are formed by seeded polymerization in the first step. Functional monomers such as glycidyl methacrylate (GMA), vinylsilane and 9-vinylanthracene are incorporated in the seed forming stage for further surface functionalization or microscopic imaging. The crosslinked seed particles are then swollen by a second monomer, styrene, methyl methacrylate (MMA) or butyl methacrylate (BMA), at the second stage. After swelling with the second monmer for a period of time, seeded polymerization of PS seed particles is triggered by addition of 2,2'-azodi(2,4'-dimethylvaleronitrile) (V-65B). Phase separation takes place during seeded polymerization to form anisotropic dumbbell-shaped particles. Weitz's result points out that the phase separation between seed particle and newly generated polymer is driven by elastic contraction of the swollen polymer particles induced by elevated polymerization [153]. Chemical anisotropic (PS-PDVB)/PMMA/(PS-PMMA) and (PS-PDVB)/PBMA/(PS-PBMA) particles are formed with a new bulb of interpenetrated PS/PMMA or PS/PBMA.

To demonstrate the versatility in the preparation dumbbell-shaped particles with chemical anisotropic properties, the authors have fabricated amphiphilic dumbbell-shaped polymeric particles with pH-responsive properties by surface functionalization of (PS-PDVB)/PS anisotropic particles. During seed formation, (PS-PDVB) seed particles are incorporated with 5 vol% of functional monomers, GMA. Seeded polymerization of styrene is carried out to form anisotropic particles. Consequently, dumbbell-shaped (PS-PDVB)/PS particles are prepared with the seed particle side functionalized by epoxy group of GMA. Surface modification of dumbbell-shaped particles is then achieved by further chemical treatment. Epoxy groups of particle surface are reacted with polyethylenimine and result in forming a layer of hydrophilic PEI on the bulb functionalized by GMA. The surface coating of PEI thus imparts amphiphilicity to the dumbbell-shaped particles. The selective binding of PEI on the anisotropic particles is revealed by fluorescence imaging. From the preliminary result, dumbbell-shaped amphiphilic (PS-PDVB)/PS/PEI is a desirable colloidal surfactant to stabilize water in 1-octanol emulsion.

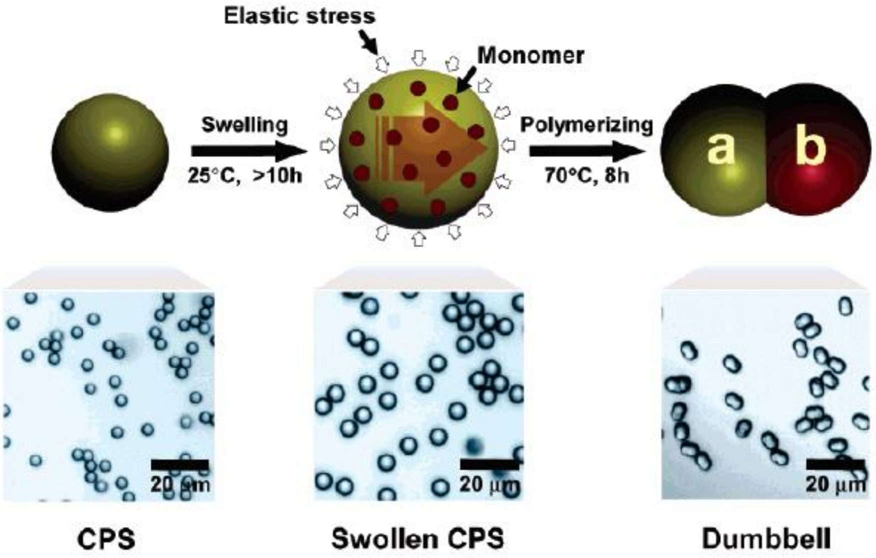

**Fig. 1.39.** Reaction scheme for the synthesis of anisotropic dumbbell-shaped particles by seeded polymerization [152].

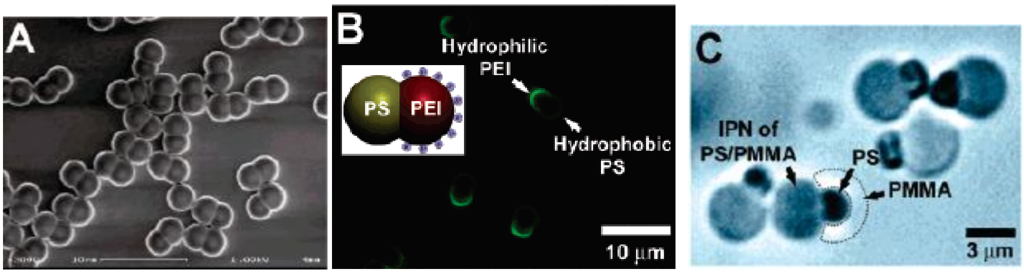

**Fig. 1.40.** SEM micrograph (left) and fluorescence micrograph (right) of amphiphilic dumbbell-shaped (PS-PDVB)/PS/PEI particles; and bright-field image of dumbbell-shaped (PS-PDVB)/PMMA/(PS-PMMA) [152].

Zukoski and coworkers have presented a facile and versatile synthetic strategy to fabricate pH- or thermal-responsive anisotropic polymer particles through two-step seeded emulsion polymerization [154]. Crosslinked PS seed particles are formed at the first stage by seed polymerization of styrene, divinylbenzene (DVB) and 2-(diethylamino)ethyl methacrylate (DEAM). An anionic initiator, potassium persulphate (KPS), is employed in the seed polymerization so that the surface of the resulting seed particles is activated with anionic sulphate groups. Meanwhile, the copolymerization of DEAM monomers also functionalizes the particle surface with amino groups. Upon pH adjustments, the amino groups undergo protonation/deprotonation process and thus contribute to pH-responsive properties of the particles. Monomer swelling at room temperature followed by seeded emulsion polymerization is carried out in the next step to fabricate anisotropic dumbbell-shaped particles. A cationic surfactant, cetyltrimeylammonium bromide (CTAB), is introduced during seeded emulsion to stabilize the protrusion after polymerization. Amphoteric dumbbell-shaped (PS-PDVB-PDEAM)/PS is formed with negatively charged seed particles due to the sulphate groups and positively charged protrusion part due to the CTAB surfactant. The amphoteric character of the particles is investigated by electrophoretic mobility measurement as a function of pH. An isoelectric point on the anisotropic particles is clearly observed at a pH value near 7.5. The particles become unstable and aggregate around this pH.

An extended study on the preparation of dual stimuli-responsive dumbbell-shaped particles is conducted by replacing the second monomer with *N*-isopropylacrlamide (NIPAm). NIPAm monomer and toluene are swollen by the crosslinked PS seed particles followed by seeded emulsion polymerization. Smart dumbbell-shaped (PS-PDVB-PDEAM)/PNIPAm particles with pH- and thermal-responsive properties are fabricated by the proposed synthetic strategy. The success in the fabrication of dumbbell-shaped polymer particles incorporating with stimuli responsive properties should open up new directions in more advanced applications.

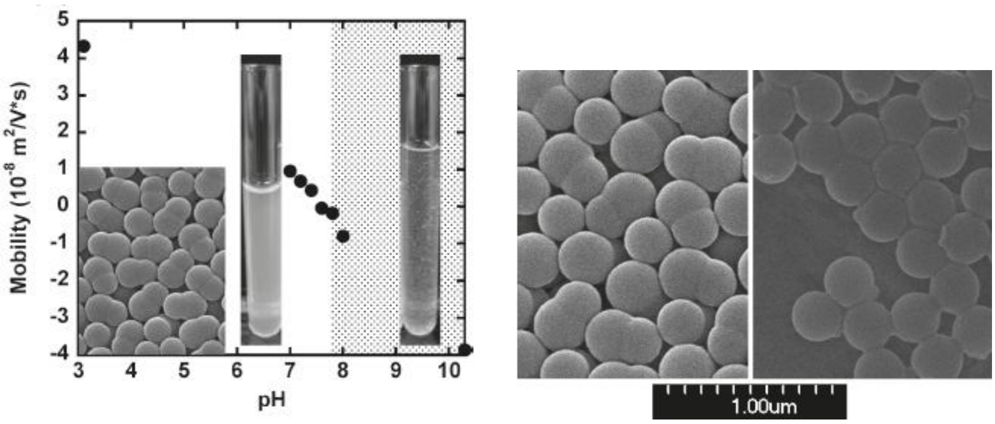

**Fig. 1.41.** Morphology and amphoteric properties of (PS-PDVB-PDEAM)/PS anisotropic particles (left); and SEM micrographs of (PS-PDVB-PDEAM)/PNIPAm anisotropic particles [154].

Traditional approaches towards dumbbell-shaped polymeric particles require crosslinked seed particles as precursor for the protrusion of the polymer formed at the second stage. Dufresne et al have recently overcome this bottleneck on the synthesis of dumbbell-shaped particles. They have successfully facbricated dumbbell-shaped particles in the absence of crosslinked seed particles [155]. According to their publication, they synthesize the dumbbell-shaped PS/(PS-*co*-PTMSPA) particles by two-step seeded emulsion polymerization. Spherical PS particles are formed at the initial step followed by seeded emulsion polymerization of styrene and trimethoxysilylpropylacrylate (TMSPA) monomers. Core-shell particles with hydrophobic PS core and hydrophilic PS-PTMSPA random copolymer shell are subsequently formed. After that, styrene monomers are swollen in the non-crosslinked seed particles and then polymerized, resulting in the formation of dumbbell-shaped polymer particles. The formation of anisotropic particles is caused by local squeezing of styrene monomer through the hydrophilic shell, which preferentially absorbs additional monomer during polymerization. The morphology of the anisotropic particles is examined by SEM. The aspect ratio (length to diameter, L/D ratio) of the particles can be controlled by varying the volume ratio between the monomer and core-shell particles. More importantly, the dumbbell-shaped polymer particles are believed to have high potential in the application of photonic crystals.

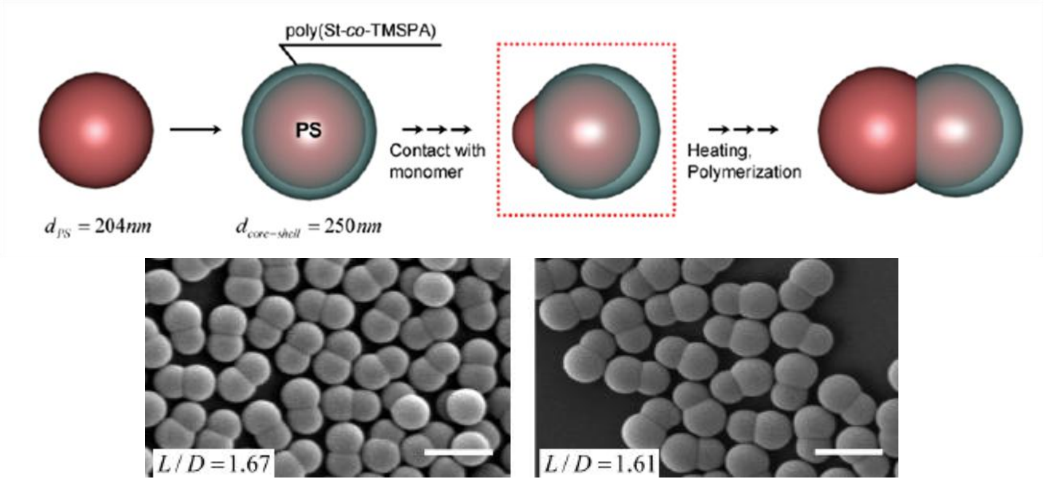

**Fig. 1.42.** Schematic illustration of the synthesis of dumbbell-shaped PS/(PS-*co*-PTMSPA) particles (above); and SEM micrographs of PS/(PS-*co*-PTMSPA) particles (below) [155].

### *Mushroom particles*

Recently, Okubo et al have established a versatile synthetic platform to prepare mushroom-like amphiphilic Janus particles. Two types of dual stimuli-responsive amphiphilic Janus particles, PS/(PMMA-PCMS)-*g*-PDM [156] and PMMA/(PS-PBIEM)-*g*-PDM [157], are reported by utilizing two-step seeded ATRP. In the first step, spherical Janus particles, polystyrene/poly(methyl methacrylate-chloromethylstyrene) (PS/(PMMA-PCMS)) and poly(methyl methacrylate)/poly(styrene-2-(2-bromoisobutyryloxy)ethyl methacrylate) (PMMA/(PS-PBIEM)), are prepared by internal phase separation induced by solvent evaporation from toluene droplets containing both polymers. The halogen rich side of the Janus particles acts as the marcoinitiator in the next stage, ATRP. The second step is generation of surface-initiated activator by electron transfer of 2-(dimethylamino)ethyl methacrylate (DM) monomers with Janus particles macroinitiators in the presence of transition metal catalyst ($CuCl_2$ or $CuBr_2$). Then, seeded ATRP of DM monomers proceeds to produce smart responsive Janus particles. Consequently, a layer of pH- and temperature-sensitive PDM is grafted on the surface of the Janus particles, resulting in the formation of stimuli-responsive amphiphilic Janus particles. Poly[2-(dimethylamino)ethyl methacrylate] is a dual stimuli-responsive polymer which respond to pH and temperature changes. The temperature responsiveness of the particles is governed by lower critical solution temperature at about 34℃. The pH responsiveness of the particles is attributed by the protonation/deprotonation of tertiary amino group at different pH [158]. The morphology of the mushroom-like particles is confirmed by optical microscopy, SEM and TEM. Notably, the monomer conversion of DM is relatively low (< 50%) during seeded ATRP. This phenomenon is contributed by autocatalytical hydrolysis of DM in water. Extensive studies on exploring the applications of mushroom-like amphiphilic Janus particles as particlulate surfactants are conducted [159]. The dual stimuli-responsive mushroom-like particles operate as particulate surfactants that effectively form stable oil -in-water emulsion with 1-octanol. The stability of the emulsion can be altered by adjusting pH and temperature.

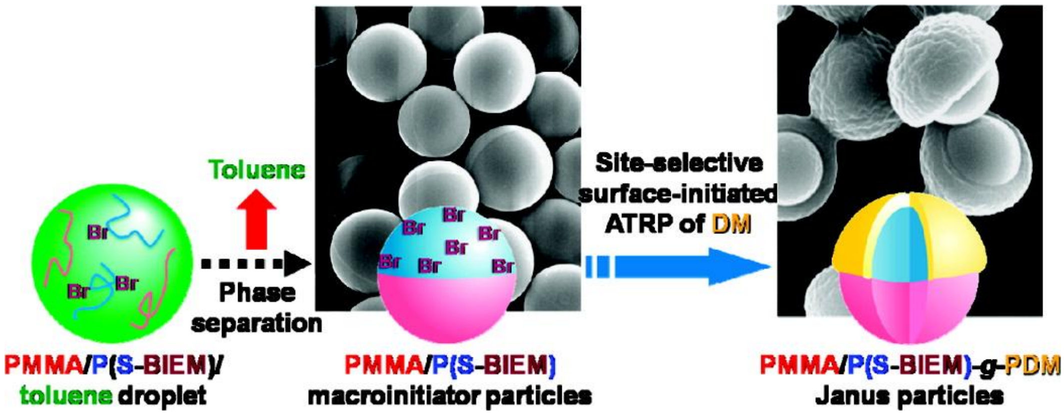

**Fig. 1.43.** Schematic illustration of the preparation of mushroom-like PMMA/(PS-PBIEM)-*g*-PDM particles (left); and SEM micrographs of mushroom-like composite particles (right) [157].

***Snowman particles***

Okubo's research group has successfully prepared snowman-like polymeric particles via solvent evaporation [160]. In this solvent evaporation approach, the preparation of snowman-like particles is based on a solvent absorbing/releasing method. PS and PMMA homopolymers are prepared by solution polymerization. Toluene is selected as solvent and AIBN is applied as initiator. Homogeneous PS/PMMA/toluene solution is then prepared by vigorous stirring an aqueous solution containing polyoxyethylene nonlyphenyl ether (Emulgen 911) surfactant. Due to the presence of the nonionic surfactant Emulgen 911, the polymer-polymer and polymer-aqueous phase interfacial tensions are dramatically reduced (~ $10^{-1}$ mN/m). The extraordinary low interfacial tension facilitates the formation of non-spherical particles. The polymer-polymer interfacial tension is another key factor that contributes to the snowman-like morphology. As solvent is continuously evaporated, the polymer weight fraction is successively increased. This increase leads to successive increase in the polymer-polymer interfacial tension which results in the formation of snowman-like particles. Therefore, with a sufficient amount of Emulgen 911, the morphology of the PS/PMMA/Emulgen 911 particles chang from spherical to snowman-like upon evaporation of toluene. Okubo has compared the experimental result with the Broseta's theoretical model that his results are in good agreement with the theoretical model. In addition, Okubo also reveals that the resulting snowman-like morphology is close to the thermodynamic equilibrium morphology.

Gilbert et al have reported a facile approach to construct snowman-like polymer nanoparticles via a three-step seeded emulsion polymerization [161]. Emulsion polymerization is applied in the initial step to form seed PS particles with dinvinylbenzene (DVB) as crosslinker. Surface of the crosslinked PS seed particles is modified by polymerization of water soluble monomer, vinyl acetate (VAc) of acrylic acid (AA). A layer of hydrophilic polymer is then coated onto the seed particles. The crosslinked seed particles are swollen by the second monomer, styrene, followed by seeded emulsion polymerization. Snowman-like anisotropic (PS-PDVB-PVAc)/PS nanoparticles are formed at the end of polymerization. Anisotropic nanoparticles with one hydrophilic side and one hydrophobic side are fabricated. The morphology of the nanoparticles is revealed under SEM investigation. The snowmanlike morphology is attributed to the presence of hydrophilic polymer shell on the seed particles. The seed polymer-aqueous phase interfacial tension is significantly reduced while the seed polymer-monomer interfacial tension is rapidly increased due to the presence of hydrophilic PVAc or PAA on the seed particle surface. The incompatibility between the seed particles and monomers also promotes phase separation. Based on the consideration of thermodynamics, monomers are preferred to be extruded from seed particles. The prepared anisotropic snowman-like particles exhibit high potential in applications such as photonic band gap materials and sensors.

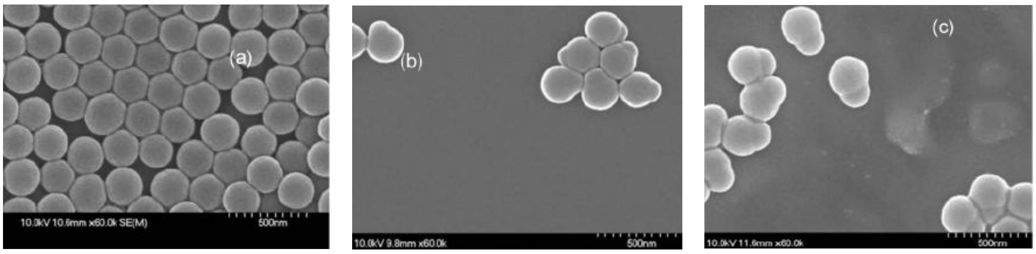

**Fig. 1.44.** SEM micrographs of (PS-PDVB-PVAc) seed particles (left); (PS-PDVB-PVAc)/PS with monomer : seed swelling ratio (w/w) of 5 : 1 (middle) and 9 : 1 (right) [161].

Yang et al also have prepared snowman-like polymer particles by seeded emulsion polymerization [162]. The synthesis of snowman-like particles begins with polystyrene (PS) hollow spheres (HP-433 from Rohm & Haas) as template. Highly crosslinked poly(acrylonitrile-divinylbenzene) hollow spheres are prepared by emulsion polymerization. Linear polymer inside the hollow spheres is removed by washing the hollow particles with excess *N,N'*-dimethylformamide (DMF). Seeded emulsion polymerization is carried out by dropwise addition of comonomer mixture of styrene/DVB to the seed emulsion followed by further polymerization at 80℃ for 6 hours. Snowman-like (PAN-PDVB)/(PS-PDVB) particles with high uniformity and submicronmeter dimension are formed. The formation of anisotropic morphology is typically based on high interfacial tension between PAN and styrene/DVB comonomer. The PS-PDVB polymerized in the second stage of polymerization undergoes phase separation and is extruded from the PAN-PDVB shell due to the crosslinked polymer network elastic-retractile force. The snowman-like particles are further functionalized by selective hydrolysis of the PAN, resulting in the generation of carboxylic acid groups (-COOH) on the particles. These carboxylic acid groups enable the surface modification of the particles by anchoring inorganic materials such as silica, titania and iron oxide onto the modified PAN shell. The success in the formation of anisotropic polymer-inorganic hybrid materials broadens the applications of such functional materials. In addition, Yang's approach also provides a feasible route for large scale synthesis of anisotropic colloidal particles. Preliminary data from Yang's study points out that the functionalized snowman-like particles are desirable colloidal surfactant to emulsify oil/water mixture.

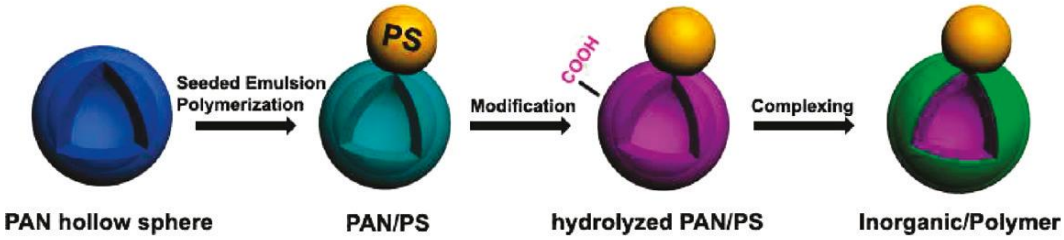

**Fig. 1.45.** Schematic illustration of the synthetic route to prepare (PAN-PDVB)/(PS-PDVB)/inorganic hybrid materials [162].

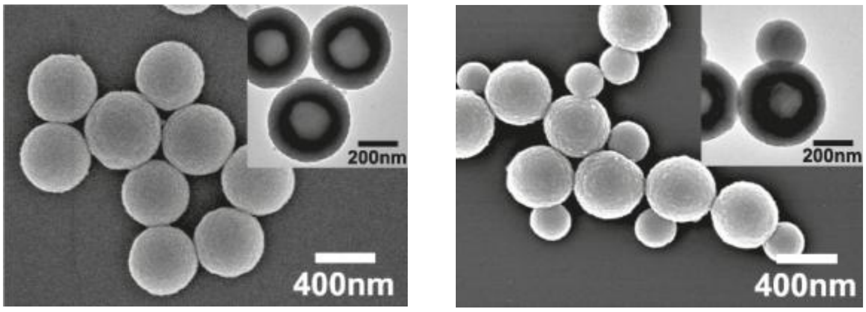

**Fig. 1.46.** SEM and TEM micropraghs of (PAN-PDVB) hollow seed particles (left); and (PAN-PDVB)/(PS-PDVB) anisotropic particles (right) [162].

## 1.5 Limitations of current methods to prepare MCP particles

In chapter 1.4, literatures on the development and fabrication of MCP particles with specific morphology and well-defined nanostructures through various polymerization approaches are summarized. These particles are prepared with sophisticated architectures, specialty functions or stimuli-responsive properties, demonstrating great potential in different applications. Nevertheless, these particles still suffered from different drawbacks such as large particle size, low monomer conversion, additional stabilizer, post-treatment, tedious reaction conditions or low versatility.

### *Large particle size*

Due to sophisticated polymerization process such as multi-stage polymerization, the dimension of MCP particles is inevitably large. The particle size of most MCP particles can reach up to a few micron meters by the end of polymerization. Since the total surface area to volume ratio is inversely proportional to the particle size, the large particle size of MCP particles might limit their application. Compared with latex particles with nanosized dimension, micron-sized latex particles possess smaller total surface area to volume ratio. This eventually leads to lower functionality of the particles and thus limits their applications.

### *Low monomer conversion*

Synthesis of MCP particles involves polymerization of at these two to three polymers. The most common approach to prepare MCP particles is multi-stage polymerization. Due to repeated polymerizations and purifications of the polymer particles, the total monomer conversion of MCP particles is below 60%. The presence of unreacted monomers inside the particles might limit their applications, especially in biological applications. Therefore, further purification of latex particles is required to get rid of any residual monomers.

### *Additional stabilizer*

When MCP particles are prepared in aqueous phase, the produced particles are hydrophobic in nature and easily precipitated. Maintaining the colloidal stability of the particles in the continuous phase is then a problem to be addressed. One approach to tackle this problem is to introduce stabilizers during the polymerization. Surfactant is the most commonly used stabilizer. Surfactants are chemical compounds with one hydrophilic end and one hydrophobic end. The role of surfactants is to assist the dispersion of polymeric particles in the aqueous phase. Surfactants can effectively reduce the polymer/aqueous phase interfacial tension, and thus allow the latex particles to be suspended in aqueous phase. There are basically four categories of surfactants according to the properties of their hydrophilic end. The four types of surfactants are cationic surfactant, anionic surfactant, zwitterionic surfactant and nonionic surfactant. All these surfactants can be utilized in the synthesis of MCP particles with excellent colloidal stability. Nevertheless, the use of surfactant has another potential problem. After polymerization, not all the surfactants are reacted and some of the surfactants remain in the continuous phase. The removal of unreacted surfactants is difficult as they are very stable in water. Moreover, surfactant is not an environmentally benign chemical which is potentially hazardous to animals, ecosystem and humans.

### *Post-treatment*

Some specific nanostructures of MCP particles require further treatment after polymerization. Solvent treatment is the most widely used post-treatment approach. After polymerization and purification, the MCP particles are treated with specific organic solvent. MCP particles are swollen by the solvent at this stage. The swollen particles are treated under specific conditions such as predetermined stirring rate and temperature. After a certain period of time, solvent removal takes place as the structural rearrangement is completed. Organic solvent, which is not environmental benign, is used in solvent treatment. In addition, the solvent treatment process requires harsh reaction condition such as long treatment time and fixed solvent composition. All these result in difficulties in pilot-scale production of MCP particles.

### *Tedious reaction conditions*

To incorporate multiple polymeric components in one particle, different polymerization approaches have been developed. Nevertheless, the polymerization process and synthetic conditions for MCP particles are tedious. Multi-stage polymerization is usually applied in the preparation of MCP particles. In this method, seed particles are prepared by conventional polymerization approach like dispersion polymerization. They are then purified and brought to seeded polymerization to prepare core-shell polymeric particles. Two component polymer particles are formed and purification is carried out again to get rid of any unreacted species. Eventually, the two component particles are further polymerized by seeded emulsion polymerization to fabricate MCP particles. This polymerization approach is tedious and harsh which restirct its terminal applications.

***Low versatility***

MCP particles are fabricated with unique morphology or nanostructure under specific reaction conditions. Once there is a slight adjustment in the synthetic conditions, e.g. monomer is replaced by another one or the reaction temperature is altered, particles with corresponding nanostructure could no longer be prepared. The harsh requirements for the synthetic conditions limit the versatility of the particle preparation.

## 1.6 Our previous work on amphiphilic core-shell particles

Thers is explosive development of polymeric nanoparticles with well-defined core-shell structure in the past few decades because of their unique nanostructure and potential applications in various fields, e.g. photonic crystal [163], dielectric resonator [58, 164], optical data storage [165-167], metallic nanoparticles immobilization as catalyst [168-176], electrically conductive material [177], metal ion detection [178, 179], functional coating [180, 181], superhydrophilic/superhydrophobic colloidal crystal film [182], particulate emulsifier [183], biomolecules carriers [184-186], and enzyme immobilization [187-189]. Stimuli-responsive core-shell particles are the most attractive type due to their potentials in advanced applications. Literatures have reported many approaches to prepare stimuli-responsive core-shell particles and their potential applications recently [190-209]. In the past decade, Li’s research group has developed a simple but versatile platform technology on the preparation of core-shell polymeric particles.  Based on this platform, spherical polymeric nanoparticles with well-defined core-shell nanostructure incorporated with smart properties are synthesized via redox initiated soap-free emulsion polymerization.

### *Particle formation mechanism*

Amphiphilic core-shell nanoparticles are fabricated by graft copolymerization of vinyl monomers from water-soluble polymer chains containing amino groups via redox initiation with the use of redox initiator [3, 210, 211]. A proposed reaction mechanism for the preparation of amphiphilic core-shell nanoparticles is illustrated in Fig. 1.47. The reaction is started with three components, i) a water-soluble polymer which was rich in amino group; ii) an alkyl hydroperoxide redox initiator; and iii) a hydrophobic vinyl monomer in aqueous phase. In the initiation step, alkyl hydroperoxide (ROOH), e.g. *tert*-butyl hydroperoxide or hydrogen peroxide, is interacted with the amino group of the polymer backbone from the water-soluble polymer to form a redox pair. One electron is transferred from the amino nitrogen to ROOH, thus forming cationic nitrogen radical and alkoxyl radical (RO•). The proton on the amino nitrogen is subsequently lost, resulting in the formation of amino radicals. The amino radicals generated on the polymer backbone of the water-soluble polymer are responsible for the initiation of graft copolymerization of vinyl monomers. As the growing chains of the vinylic monomers on the water-soluble polymer reach a hydrophilic-hydrophobic balance, the amphiphilic macro-radicals self-assemble to form micelle-like microdomains. These microdomains are the loci for the subsequent polymerization and particle formation is resulted as polymerization progresses. Simultaneously, the alkoxyl radicals RO• generated also initiate homopolymerization of vinyl monomers inside the polymeric micelles. Besides, alkoxyl radicals RO• possibly undergo backbone abstraction to abstract a hydrogen atom from the polymer backbone of the water-soluble polymer. The backbone abstraction eventually generates additional radicals on the backbone of the water-soluble polymers which are capable for the graft copolymerization of the vinyl monomers. At the end of polymerization, monodispersed amphiphilic core-shell polymeric nanoparticles with a hydrophobic core and a hydrophilic shell are fabricated with nanometer dimension, desirable colloidal stability and well-defined core-shell nanostructures.

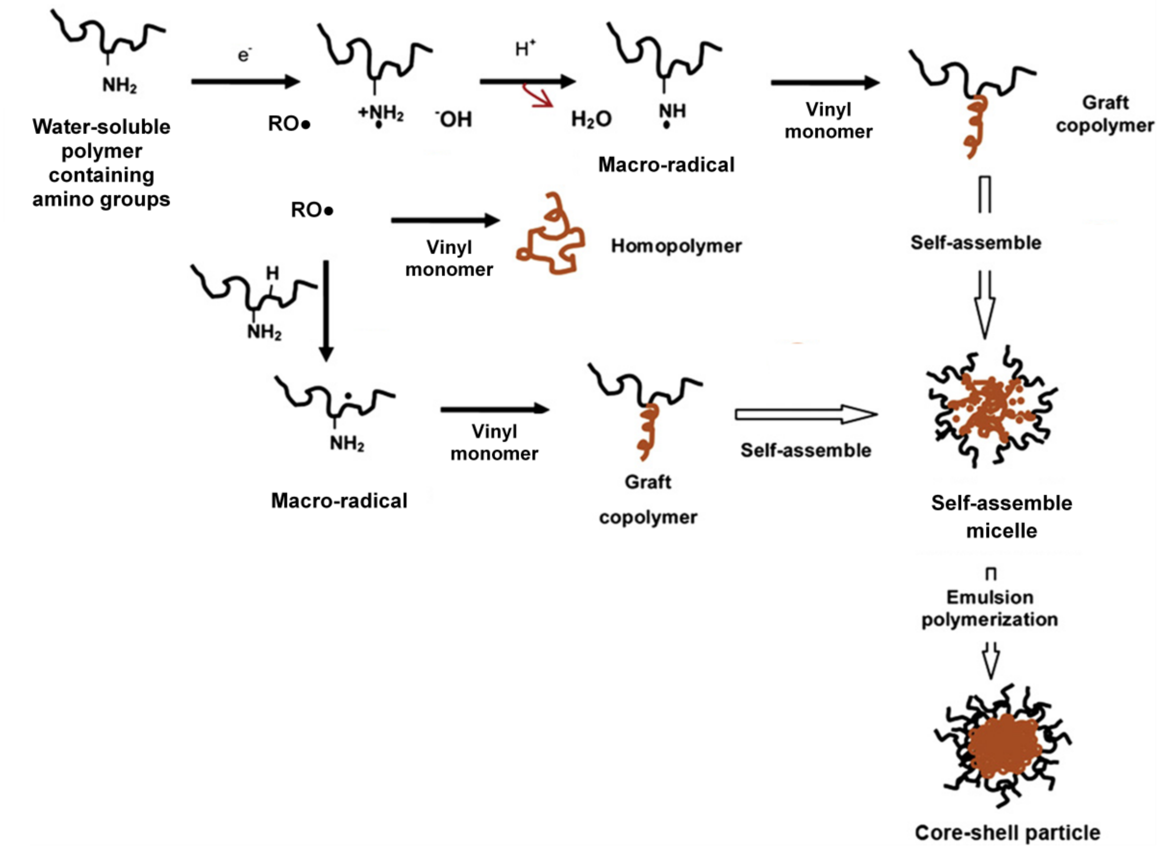

**Fig. 1.47.** Formation mechanism of amphiphilic core-shell nanoparticles [3].

### *Characteristics and unique properties of the amphiphilic core-shell nanoparticles*

The fore-mentioned approach not only provides a facile but also versatile synthetic platform to prepare amphiphilic core-shell particles. Both the shell and core of the nanoparticles can be tailor-made with various properties. The water-soluble polymer shell can be selected from natural biopolymers such as bovine serum albumin [210], casein [212], cellulase [213], chitosan [210] and gelatin [210] to synthetic polymers such as polyethylenimine [210], polyallylamine [210] and polyvinylamine [214]. In addition, the core of the amphiphilic nanoparticles can be selected with a wide variety of vinyl monomers such as methyl methacrylate, *n*-butyl acrylate, styrene, *N*-isopropylacrylamide, *N*-vinylcaprolactam, 2-hydroxy propyl methacrylate. A summary of the amphiphilic core-shell nanoparticles prepared by our platform technology is shown in Fig. 1.48.

The shell component of the nanoparticles can be varied from pH-sensitive, biocompatible to commercially available synthetic water-soluble polymer. The core component of the nanoparticles can be adjusted to have thermal-sensitive, anti-stretching and good film-forming properties. Through combination of different shell and core components, amphiphilic core-shell nanoparticles incorporated with different specific properties are prepared.

The prepared amphiphilic core-shell nanoparticles possess particle sizes ranging from 60 to 500 nm and the particle size distribution is narrow. The core diameter and shell thickness of the amphiphilic core-shell nanoparticles could to be altered by simply adjusting the reaction recipes or reaction parameters. Thus, physical and chemical properties of the nanoparticles are easily tuned. Under SEM and TEM investigation, monodispersed nanoparticles with well-defined core-shell nanostructures are revealed. High uniformity and well-defined architectures allow mass production of amphiphilic core-shell nanoparticles to suit different commercial applications.

The fabrication of amphiphilic core-shell nanoparticles is conducted in aqueous phase, which is an environmental benign approach to fabricate functional polymeric nanoparticles. In addition, this attempt offers a commercial viable process to synthesize nanoparticles with solid content that could reach up to 30% without any addition of surfactants or stabilizers. This implies scale up production of the amphiphilic core-shell nanoparticles is feasible.

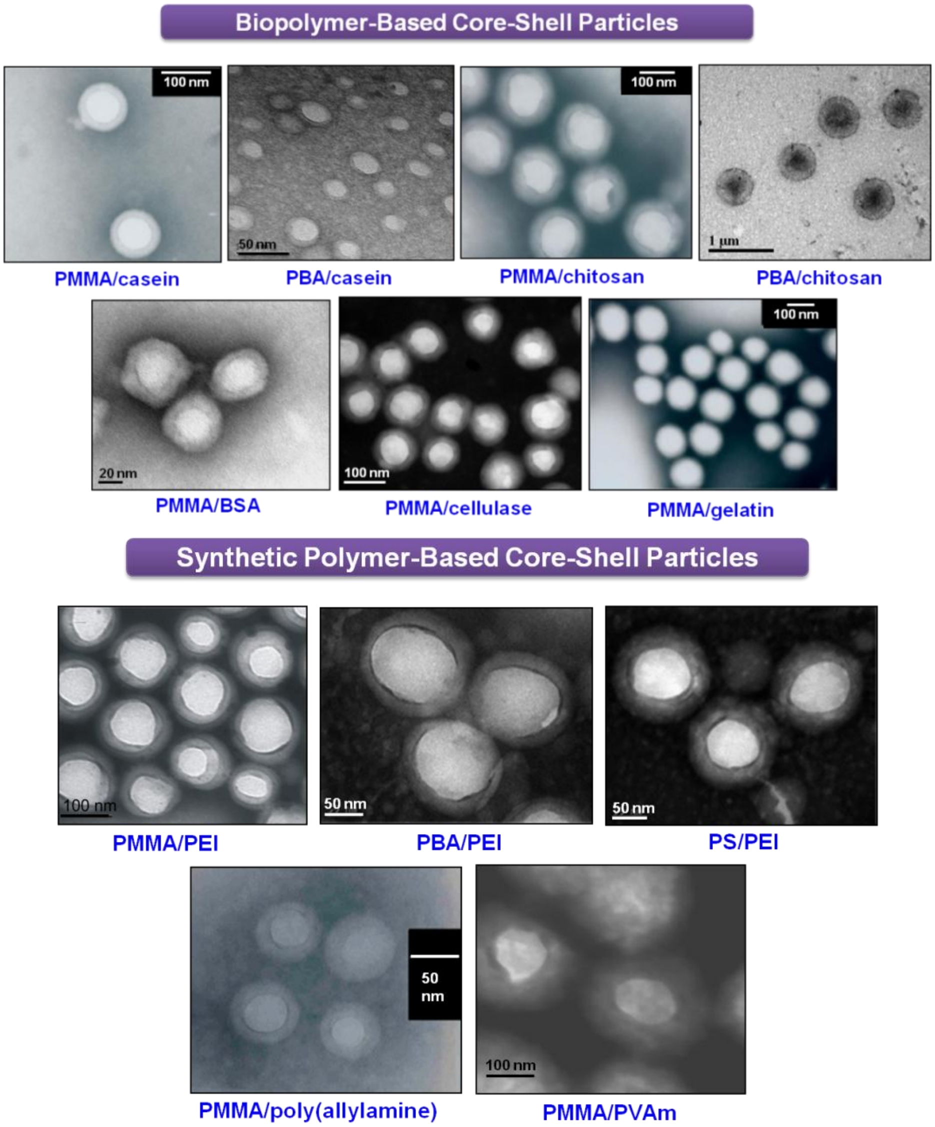

**Fig. 1.48.** Examples of amphiphilic core-shell nanoparticles prepared by the proposed mechanism.

# Chapter 2

## Motivation and Objectives

### 2.1 Project Motivation

Li's group has fabricated various types of amphiphilic core-shell nanoparticles based on the synthetic route mentioned in Chapter 1. Particles prepared by this platform technology have already shown potential applications in diverse fields. As part of our long-term development in core-shell particle platform technology, we aimed to further develop the synthesis of polymer particles containing multiple components and study their complicated nanostructures and properties. Potential applications of these novel types of multi-component particles (MCP) were also explored.

### 2.2 Specific Objectives

1. To develop synthetic routes to multi-component polymer (MCP) particles which contain at least three different polymeric components.

Three different seed particles, PMMA/PEI, MBA-crosslinked PNIPAm/PEI and non-crosslinked PNIPAm/PEI were first synthesized according to Scheme 2.1, 2,2, and 2.3, respectively. The PMMA/PEI seed particles possessed a rigid core, while the PNIPAm/PEI seed particles possessed soft and thermal sensitive core. Effect of type of second monomer; PEI to total monomer ratio; reaction pH on the formation and properties of MCP particles; and degree of crosslinking were systematically studied.

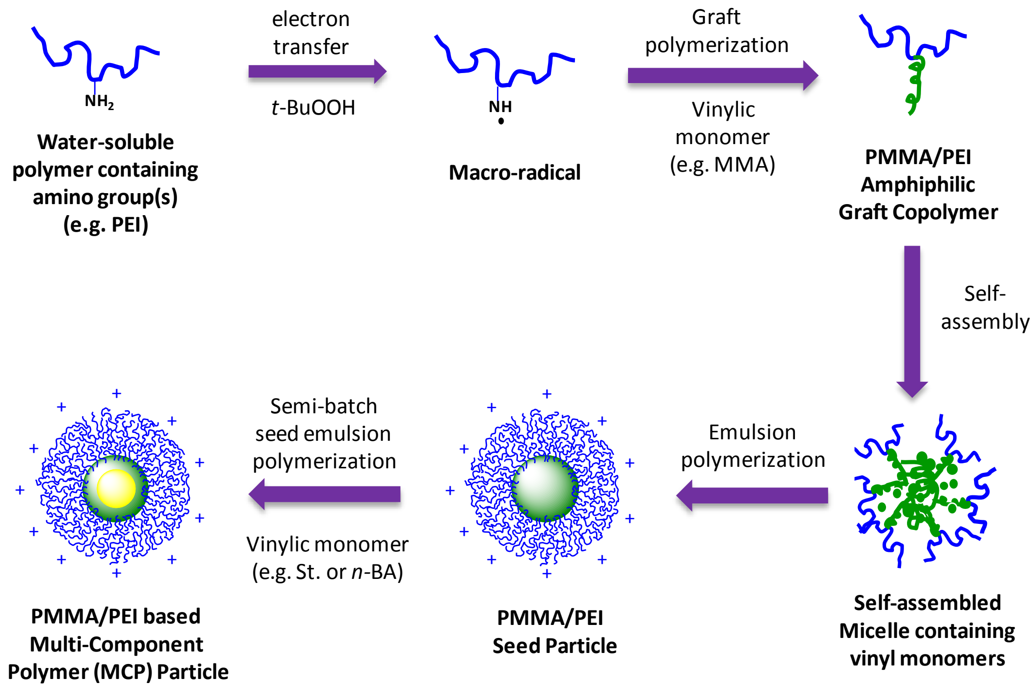

**Scheme 2.1.** Proposed reaction scheme for the formation of PMMA/PEI based MCP particles.

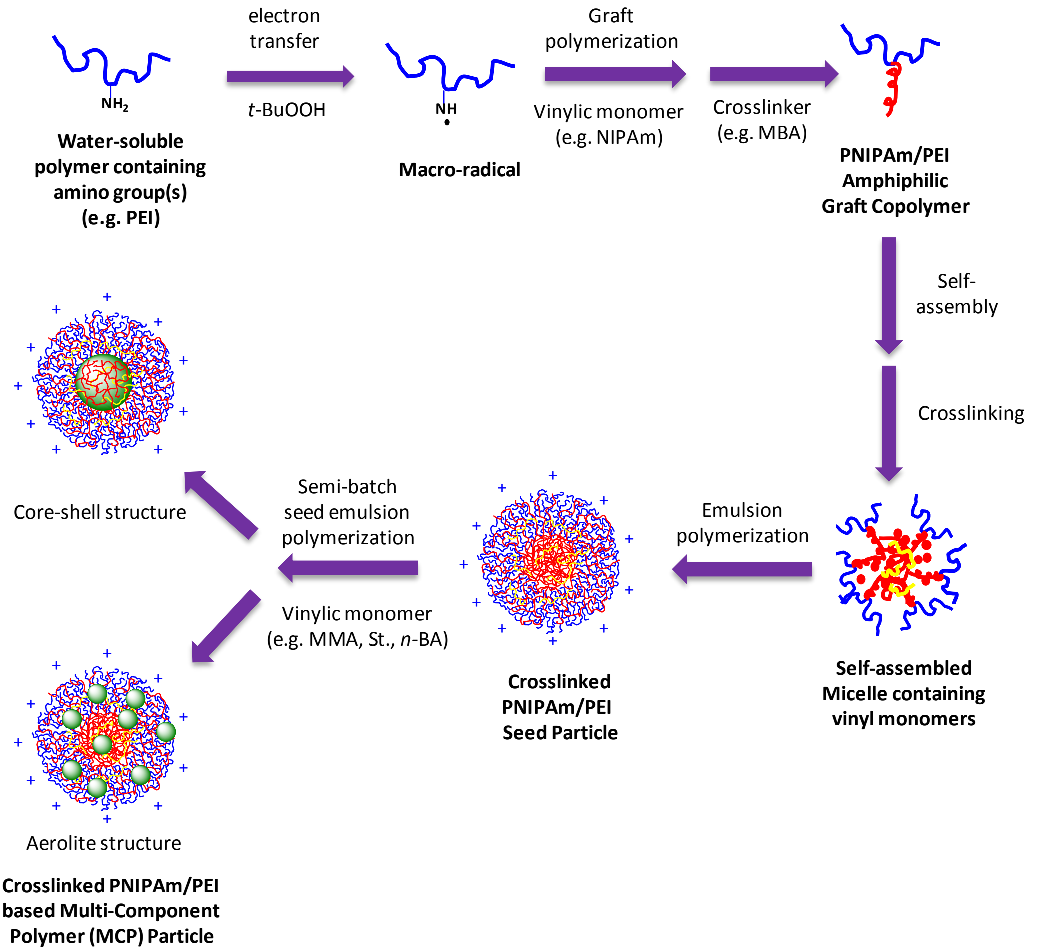

**Scheme 2.2.** Proposed reaction mechanism for the formation of crosslinked PNIPAm/PEI based MCP particles.

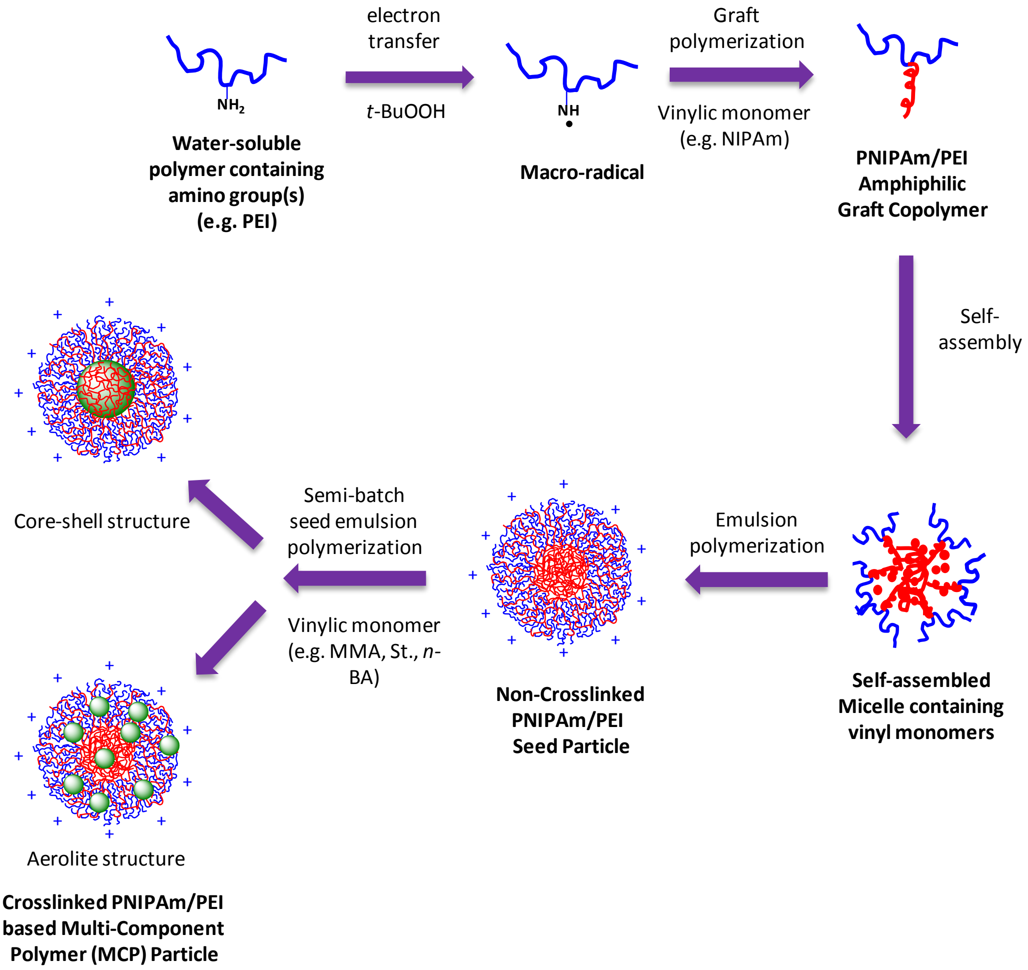

**Scheme 2.3.** Proposed reaction mechanism for the formation of non-crosslinked PNIPAm/PEI based MCP particles.

2. Two types of MCP particles, namely PS/PMMA/PEI and PBA/PMMA/PEI, were fabricated using PMMA/PEI seed particles. Another three types of MCP particles, namely, PMMA/(PNIPAm-MBA)/PEI, PS/(PNIPAm-MBA)/PEI and PBA/(PNIPAm-MBA)/PEI, were fabricated using crosslinked PNIPAm-PEI seed particles with various degree of crosslinking. Moreover, two types of MCP particles, PMMA/PNIPAm/PEI and PS/PNIPAm/PEI, were

fabricated using non-crosslinked PNIPAm/PEI microgel as seed, which were crosslinked through polymerization of the second hydrophobic monomer. Polymerization kinetics on the synthesis of MCP particles and their changes of temperature profile during the reaction were investigated. Properties of the resultant MCP particles were characterized including particle size, particle size distribution, surface charge, chemical compositions, morphologies and nanostructures.

3. Smart properties of the MCP particles using PNIPAm/PEI as seed particles, were systematically investigated including their thermal- and pH-responsive properties, particle sizes, particle size distributions and surface charges.

4. To explore potential applications of PS/(PNIPAm-MBA)/PEI and PMMA/(PNIPAm-MBA)/PEI as temperature-responsive nanocarriers for intracellular uptake.

# Chapter 3

## Synthesis and Characterization of Multi-Component Polymer (MCP) Nanocomposite Particles using PMMA/PEI based Seed Nanoparticles

This chapter describes the synthesis and characterization of multi-component polymer nanocomposite particles using PMMA/PEI as seed nanoparticles. Two types of MCP nanocomposite particles were synthesized, namely PBA/PMMA/PEI and PS/PMMA/PEI, through a semi-batch seeded emulsion polymerization. PMMA/PEI seed nanoparticles were first formed via TBHP induced graft copolymerization of MMA from PEI. Second batch of vinylic monomers, styrene or *n*-BA, was subsequently added and polymerized in the presence of the seed nanoparticles. Scheme 2.1 illustrates the synthetic route and reaction conditions.

Properties of these two types of MCP nanocomposites, including particle size and size distrbution, surface charge, chemical composition and particle morphology were systematically characterized by dynamic light scattering, ζ-potential measurement, FTIR spectroscopy, field emission scanning electron microscopy and transmission electron microscopy.

## 3.1 Experimental Section

### 3.1.1 Materials

Phenolic inhibitors, monomethyl ether hydroquinone (MEHQ), in methyl methacrylate (MMA, 0.936 g/cm$^3$, Sigma Aldrich) and *n*-butyl acrylate (*n*-BA, 0.894 g/cm$^3$, Sigma Aldrich), and phenolic inhibitors in styrene (St., 0.909 g/cm$^3$, Sigma Aldrich) were removed by washing the monomers by three times 10 w/w% sodium hydroxide (NaOH) and then with deionzed water until the water layer dropped to pH 7.

Polyethylenimine (PEI, $M_w$ 750,000 g/mol, 50 w/w% solution in water), *tert*-butyl hydroperoxide (TBHP, 70 w/w% solution in water) were purchased from Sigma Aldrich Co. and used without further purification. Freshly deionized Milli-Q water was used as the dispersion medium.

### 3.1.2 Synthesis of MCP nanocomposite particles using PMMA/PEI based seed nanoparticles

For a total solution of 100 mL, PEI (4 g, 50 w/w% solution) was first dissolved in deionzed water and the pH of the solution was adjusted to 7 with 2 M HCl solution. The diluted PEI solution was then transferred into a three-necked water-jacketed equipped with thermal couple (Testo 735), a condenser, a magnetic stirrer, and a nitrogen inlet. The dispersion was stirred at 350 rpm and purged with nitrogen for 30 mins. Appropriate amount of MMA (4 g) was then added to the dispersion when the temperature of the dispersion reached 80℃. After that, appropriate amount of initiator, TBHP (1 mL, 0.1 M), were added to the reaction mixture and the resulting mixture was continuously stirred at 80 ℃ under nitrogen. Small amount of sample (2 mL) was withdrawn from the reaction mixture after reacting for 30 mins. Second batch of monomer, *n*-BA or St. (4 g), was then added to the reacting mixture. The resulting mixture was allowed to react at 80℃ for 2 hrs under nitrogen. After the reaction, the nanoparticles were purified by repeated centrifugation (18,000 rpm, 1.5 hr), decantation and re-dispersion until the conductivity of the supernatant approached to that of deionzed Milli Q water.

### *3.1.2.1 Determination of monomer conversion and nanoparticle composition*

The monomer conversion of the MCP nanocomposite particles was determined gravimetrically according to the following procedures: 2 mL of the latex dispersion was withdrawn from the reaction mixture and dried overnight at 80 ℃. It was further dried in a vacuum oven (25 inch Hg) at 50 ℃ for 3 days. Assuming that unreacted MMA, *n*-BA and St., and other small molecules such as *t*-BuOOH were removed by the vacuum dry process, the dried solid only contains MCP nanocomposite particles and unreacted PEI. The total solid content of the latex dispersion was determined according to the following equation:

$$Total\ Solid\ Content\ (\%) = \left(\frac{W_{Dried\ Sample} - W_{Container}}{W_{Sample\ Solution} - W_{Container}}\right) \times\ 100\%\ \text{[Eq. 3.1]}$$

Where $W_{Total}$ is the weight of the dried solid, $W_{Sample\ Solution}$ is the weight of latex solution initially added, and $W_{Container}$ is the weight of the container used for the monomer conversion determination. Based on the obtained total solid content, the monomer conversion could be determined by using the following equation:

$$Monomer\ Conversion\ (\%) = \left(\frac{Total\ S.C.\%-S.C.\%_{PEI}-S.C.\%_{HCl}}{S.C.\%_{Total\ monomer}}\right) \times 100\% \text{ [Eq. 3.2]}$$

Where S.C.%$_{PEI}$ was the amount of PEI solution initially added, S.C.%$_{HCl}$ was the amount of HCl initially added for pH adjustment, and S.C.%$_{Total\ Monomer}$ was the total amount of monomer added throughout the reaction.

#### *3.1.2.2 Kinetic study of the polymerization process*

MCP nanoparticles were prepared from seeded emulsion polymerization at 80 ℃ for 2.5 hrs in the presence of 1 X $10^{-3}$ M TBHP. The reaction mixture was continuously stirred at 350 rpm under nitrogen. Throughout the polymerization, 2 mL of the MCP samples were regularly withdrawn from the reaction mixture at various interval times. The samples were quickly placed in an ice bath for 30 mins to quench the polymerization. The monomer conversion of each sample was determined gravimetrically. The withdrawn samples were then purified by repeated centrifugations until the conductivity of the supernatant was close to the deionized water. Particle size and particle size distribution of the intermediate MCP samples were characterized by dynamic light scattering measurement.

#### *3.1.2.3 Effect of PEI to monomer ratio*

The effect of weight ratio between PEI and monomer on the particle stability and properties was studied. The synthetic procedure was the same as described in **3.1.2.** Seed emulsion polymerization of MCP with PEI to total monomer weight ratio at 1 : 2; 1 : 4; 1 : 7 and 1 : 9 were examined, while keeping all other reaction parameters unchanged.

#### *3.1.2.4 Effect of pH of reaction medium*

The effect of pH of the reaction medium on the polymerization kinetics and particle properties was studied through adjusting the solution pH with 2 M HCl. The synthetic procedure was the same as described in **3.1.2.,** except the pH of the reaction mixture was adjusted to 7 and 11 prior to the reaction.

## 3.2 Measurement and Characterization

### 3.2.1 Chemical compositions characterized by FT-IR

Infrared spectra were recorded on a Nicolet 380 Fourier Transform Infrared (FT-IR) Spectrophotometer using KBr disks. MCP nanoparticles were first frozen and then dried overnight in a freeze drier. About 5 mg of the dried samples were grinded with 0.25 g analytical grade anhydrous KBr using a mortar and pestle. A force of 9 tones for 1 minute was exerted on the sample mixture by using a level-screw press in order to obtain a transparent disk with an appropriate thickness for FT-IR measurement.

### 3.2.2 Particle size and size distribution

The particle size and size distribution of MCP nanoparticles were measured on a Beckman Coulter Delsa Nano C Particle Analyzer. The hydrodynamic diameters ($Z_{AVE}$) were measured according to the dynamic laser light scattering (DLLS) experiment with an incident monochromatic laser at 632.8 nm and scattering angle at 165°. Prior measurements, the MCP nanoparticle samples were diluted with deionized water to a concentration between 200 and 300 mg/L. All the measurements were performed at 25 ℃ and repeated thrice.

### 3.2.3 ζ-Potential measurement

ζ-Potential of MCP nanoparticles were measured on a Beckman Coulter Delsa Nano C Particle Analyzer. The ζ-potential measurements were performed with an incident monochromatic laser at 632.8 nm. Samples were diluted to a concentration of 200 mg/L with 1 mM NaCl solution. In addition, the pH of the sample was adjusted to about 7. For each sample, the measurement was repeated thrice at 25 ℃.

### 3.2.4 Particle morphology

#### *3.2.4.1 Field-Emission Scanning Electronic Microscopy (FE-SEM)*

The particle morphologies, sizes and size distributions of the MCP nanoparticles in dried state were examined by a field-emission scanning electron microscope (FE-SEM, JEOL-JSM 6335F). The operating accelerating voltage of FE-SEM was maintained at 5 kV throughout the measurement. SEM samples were prepared by spreading a small drop of dilute MCP nanoparticle dispersion (100 mg/L) on a mica substrate. The particle droplet was allowed to dry overnight in a dust free environment at room temperature. The dried samples were then sputtered with a thin layer of gold under vacuum to a depth of approximately 1 nm.

#### *3.2.4.2 Transmission Electronic Microscopy (TEM)*

The core-shell nanostructures of seeded nanoparticles and MCP nanoparticles were examined by a transmission electron microscope (TEM, JEOL CXII TEM) at an accelerating voltage of 100 kV. TEM samples were prepared by wetting a formvar-coated or carbon-coated copper grid with a small drop of diluted MCP nanoparticle dispersion (10 μL, 50 mg/L). Upon drying, the MCP nanoparticles were stained by 0.5% w/w phosphotungstic acid (PTA) solution for 30 seconds, and then dried at room temperature before analysis.

## 3.3 Results and Discussion

### 3.3.1 PBA/PMMA/PEI MCP nanocomposite particles

The preparation and characterization of PBA/PMMA/PEI nanocomposite particles is discussed in detail in this part. Scheme 3.1 shows the reaction route and conditions.

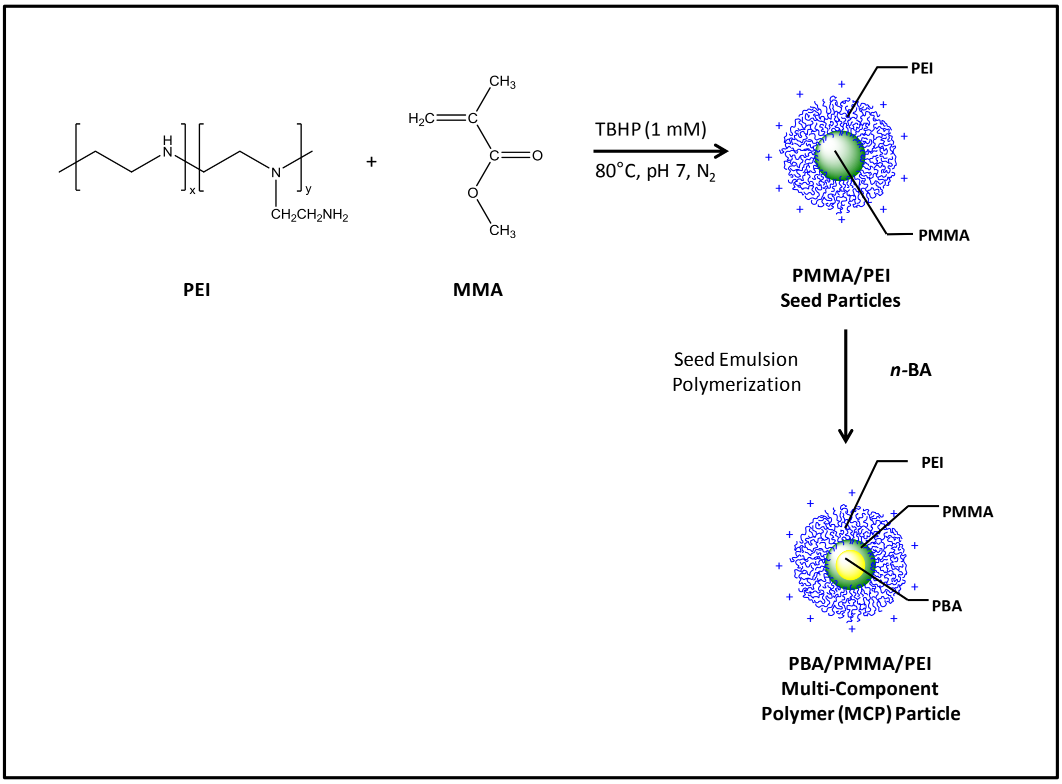

**Scheme 3.1.** Reaction scheme for the synthesis of PBA/PMMA/PEI MCP particles.

The PMMA/PEI seed particles were first formed via a graft copolymerization between PEI and MMA based on our previously established method. After the formation of PMMA/PEI seed nanoparticles, the second monomer, *n*-butyl acrylate (*n*-BA) was introduced into the seed particle dispersion and underwent *in situ* polymerization. The *n*-BA was selected as the second monomer in this study since the polymerized PBA exhibits low glass transition temperature ($T_g$). Variation of glass transition temperature of the resultant MCP particles is very useful for applications in substrate coatings.

#### *3.3.1.1 Kinetic study of the polymerization process*

Figure 3.1 shows the temperature variation during the reaction and conversions as a function of reaction time. The reaction temperature was monitored by a thermal couple (Testo 735) with one temperature recorded per second. After heating up the solution containing both PEI and MMA monomer to around 80°C, an appropriate amount of initiator (TBHP) was added to the reaction mixture to initiate the polymerization. Reaction temperature was found to first drop slightly, and then rose up rapidly. The rapid increase in the temperature was due to an exothermic polymerization of MMA initiated by a redox initiation. When MMA monomers were almost consumed, the solution temperature could drop down and stayed steady at the heating temperature of around 80°C.

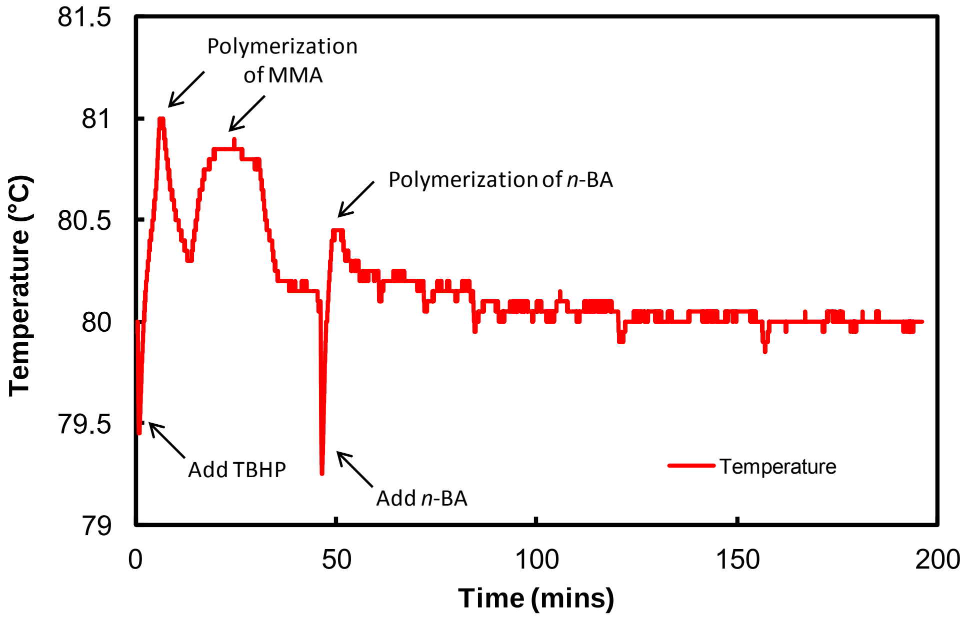

**Fig. 3.1.** Reaction temperature as a function of time of PBA/PMMA/PEI.

When the solution temperature of PEI and MMA monomer in water reached equilibrium (around 80°C), appropriate amount of initiator (TBHP) was added to the mixture to initiate the polymerization. Once TBHP was added, the reaction temperature was first slightly dropped and then increased rapidly. Such rapid rising in solution temperature was caused by a redox initiation between TBHP and PEI followed by an exothermic polymerization of MMA monomer. Graft copolymerization of MMA from PEI was taken place rapidly to generate PEI-g-PMMA amphiphilic copolymer. These molecules could undergo self-assembling to form micelles when reaching hydrophilic-hydrophobic balance. PMMA/PEI core-shell seed particles were formed with further polymerization of MMA monomers in the micelles. When MMA monomers were consumed, the exothermic polymerization was completed and the solution temperature would drop back to the original level.

The second batch of monomer, *n*-BA, was then charged into the reaction mixture to perform seeded emulsion polymerization. Similarly, an increase in solution temperature was detected after the addition of *n*-BA due to the exothermic polymerization of the *n*-BA monomers. However, the increase in temperature was not as vigorous as in the seed forming stage, indicating a slower polymerization of n-BA as compared to the MMA in the first stage. This phenomenon might be due to the low solubility of *n*-BA monomer in water (2 g/L at 25 °C). The diffusion of *n*-BA monomer through the bulk aqueous phase into the growing seed particles was more difficult.

In addition to temperature variation, the polymerization kinetics was also monitored through determining monomer conversions and particle sizes at different stages. A small amount of sample (2 mL) was withdrawn from the reaction mixture at different time interval and monomer conversion was determined gravimetrically. The monomer conversion (based on total amount of

MMA and n-BA added) at different time interval is shown in Table 3.1. At the first stage of polymerization, only MMA was added, and the conversion reached 91% after 30 mins. Average diameter of the seed particles was 199 nm. In the second stage, *n*-BA monomers were polymerized via a seeded emulsion polymerization. The total monomer conversion was 73% at the end of polymerization. Results in Table 3.1 shows that the resultant MCP particles are only 16% larger than the seed particles. Such a small increase in particle size indicates that the seed particles were highly swollen because of the hydrophilic PEI. Increasing the hydrophobic content into the particles resulted in forming more compacted particles in order to reduce their surface energy of the hydrophobic polymer chains.

**Table 3.1.** Total monomer conversion and particle size of MCP particles at different time interval.

| **Reaction time[1] (mins)** | **Type of particle** | **Monomer conversion[2] (%)** | **$Z_{AVE}$[3] (nm)** |
|---|---|---|---|
| 30 | PMMA/PEI seed | 91[4] | 199.0 |
| 36 | PBA/PMMA/PEI MCP | 61[5] | 242.5 |
| 40 | PBA/PMMA/PEI MCP | 64[5] | 233.3 |
| 45 | PBA/PMMA/PEI MCP | 74[5] | 243.0 |
| 90 | PBA/PMMA/PEI MCP | 72[5] | 231.9 |
| 195 | PBA/PMMA/PEI MCP | 73[5] | 230.2 |

[1] The reaction time was counted starting at the time of addition of initiator into the reaction mixture

[2] The total monomer conversion of MCP particles were determined gravimetrically

[3] The hydrodynamic diameter of MCP particles were determined by DLS at 25 °C

[4] The monomer conversion was calculated based on total MMA monomer added

[5] The monomer conversion was calculated based on total monmer added

### *3.3.1.2 Effect of PEI to monomer ratio*

The effect of PEI to total monomer ratios at 1 : 2; 1 : 4; 1 : 7 and 1 : 9 on properties of MCP particles were studied The reaction were all carried out at 80 °C at pH 7 for 150 mins using the same experimental procedure. Results in Table 3.2 indicate that high monomer conversions (from 73% to 99%) generally could be obtained in all these ratios. The hydrodynamic diameters of PMMA/PEI seed particles were ranged from 200 nm to 400 nm, while the hydrodynamic diameters of MCP particles were ranged from 200 nm to 350 nm. In most of the cases, the particle sizes of the PMMA/PEI seed particles were larger than the PBA/PMMA/PEI MCP particles. This effect may attribute to the fact that increasing the hydrophobic content in the particles results in forming more compacted particles in order to reduce their surface energy through packing tightly the hydrophobic polymer chains. All the MCP particles prepared has good colloidal stability with ζ-potential ranging from +29 to + 39 mV. These results suggest that the PEI molecules were predominantly localized as the particle shell, giving high surface charges and providing good colloidal stability of the MCP particles in water.

**Table 3.2.** Effect of PEI to monomer ratio on the properties of MCP particles.

| **w/w ratio between PEI and total monomer**[1] | **Total monomer conversion (%)** | **$Z_{AVE}$**[2] **(nm) of seed** | **PDI of seed** | **$Z_{AVE}$**[2] **(nm) of MCP** | **PDI of MCP** | **ζ-potential**[3] **(mV)** |
|---|---|---|---|---|---|---|
| 1 : 2 | > 99 | 353.5 | 0.066 | 348.8 | 0.062 | +38.37 |
| 1 : 4 | 73 | 199.0 | 0.076 | 230.2 | 0.160 | +28.79 |
| 1 : 7 | 89 | 236.8 | 0.083 | 205.1 | 0.103 | +39.22 |
| 1 : 9 | 91 | 395.2 | 0.066 | 321.7 | 0.059 | +37.31 |

[1] The w/w ratio of MMA to *n*-BA was kept at 1 : 1 in all experiments

[2] The hydrodynamic diameters of MCP particles were measured by DLS at 25 °C

[3] The ζ-potential of MCP particles were measured at 25 °C using 1 mM NaCl as medium

### *3.3.1.3 Effect of solution pH*

The effect of reaction pH on the properties of MCP particles was studied by comparing MCP particle properties at pH 7 and 11, while keeping other synthetic parameters constant. The weight ratio between PEI, MMA and *n*-BA was kept at 1 : 2 : 2. The properties of MCP particles prepared at these two pHs are shown in Table 3.3. The total monomer conversion of MCP particles could reached 80% at the end of polymerization. The hydrodynamic diameter of PMMA/PEI seed particles was bigger at pH 7 due to higher protonation degree of amine groups. The high charge density resulted in stronger electrostatic repulsion.

The the PEI shell became more expanded. At pH 10, the PEI molecule is neutral, thus the seed particles are more compacted, giving smaller seed particles. This study suggest that the polymerization can take The ζ-potential of MCP particles synthesized at pH 7 was + 29 mV which implied the surface charge of this MCP particle was dominated by positively charged $NH_3^+$ group of PEI. On the contrary, the ζ-potential of MCP particles synthesized at pH 11 was - 12 mV, this implied the surface charge of this MCP particle was dominated by negatively charged species which might be caused by the absorption of hydroxyl ions ($OH^-$) onto particle surface under alkaline condition [215].

**Table 3.3.** Effect of pH of reaction medium on the properties of MCP particles[1]

| Reaction pH | Total monomer conversion (%) | $Z_{AVE}$[1] (nm) of seed | PDI of seed | $Z_{AVE}$[2] (nm) of MCP | PDI of MCP | ζ-potential[3] (mV) |
|---|---|---|---|---|---|---|
| 7 | 73 | 199.0 | 0.076 | 230.2 | 0.160 | +28.79 |
| 11 | 80 | 155.2 | 0.028 | 211.2 | 0.126 | -11.94 |

[1] MCP particles were prepared at 80 °C for 150 mins.

[2] The hydrodynamic diameters of MCP particles were measured by DLS at 25 °C.

[3] The ζ-potential of MCP particles were measured at 25 °C using 1 mM NaCl as medium

### 3.3.2 Characterization of PBA/PMMA/PEI nanocomposite particles

#### *3.3.2.1 Composition*

The composition of the PBA/PMMA/PEI MCP particles was investigated by FT-IR spectroscopy. The particles were first purified by repeated centrifugation to get rid of any unreacted PEI and monomers. Figure 3.2a shows the FT-IR spectrum of PMMA/PEI seed particles. A strong carbonyl C=O peak at 1730 cm$^{-1}$ and multiple -C-O- ester peaks between 1150 and 1300 cm$^{-1}$ suggest the presence of PMMA. Both broad amino N-H stretching peak of primary amine at 3400 to 3500 cm$^{-1}$, and C-H stretching and bending at 2900 to 3000 cm$^{-1}$ indicate the presence of PEI. Figure 3.2b shows the FT-IR spectrum of PBA/PMMA/PEI MCP particles. Similar to the spectrum of seed particles, strong C=O peak and –C-O- ester peak suggest the presence of PMMA. Broad amino N-H stretching and C-H stretching indicate the presence of PEI. Besides, an ionized carboxyl –COO$^-$ peak between 1580 cm$^{-1}$ and 1620 cm$^{-1}$ is observed in the spectrum of MCP particles. This indicates the presence of PBA. Presence of this peak is possibly due to the hydrolysis of *n*-BA monomers which will be discussed in details later. We have also attempt DSC to prove for the presence of PBA in MCP particles due to the difference in $T_g$ between PBA, PMMA and PEI. However, the instrument is not capable to determine the composition of MCP particles due to malfunctions in its cooling system. Thus, it’s difficult to further confirm the presence of PBA in MCP particles.

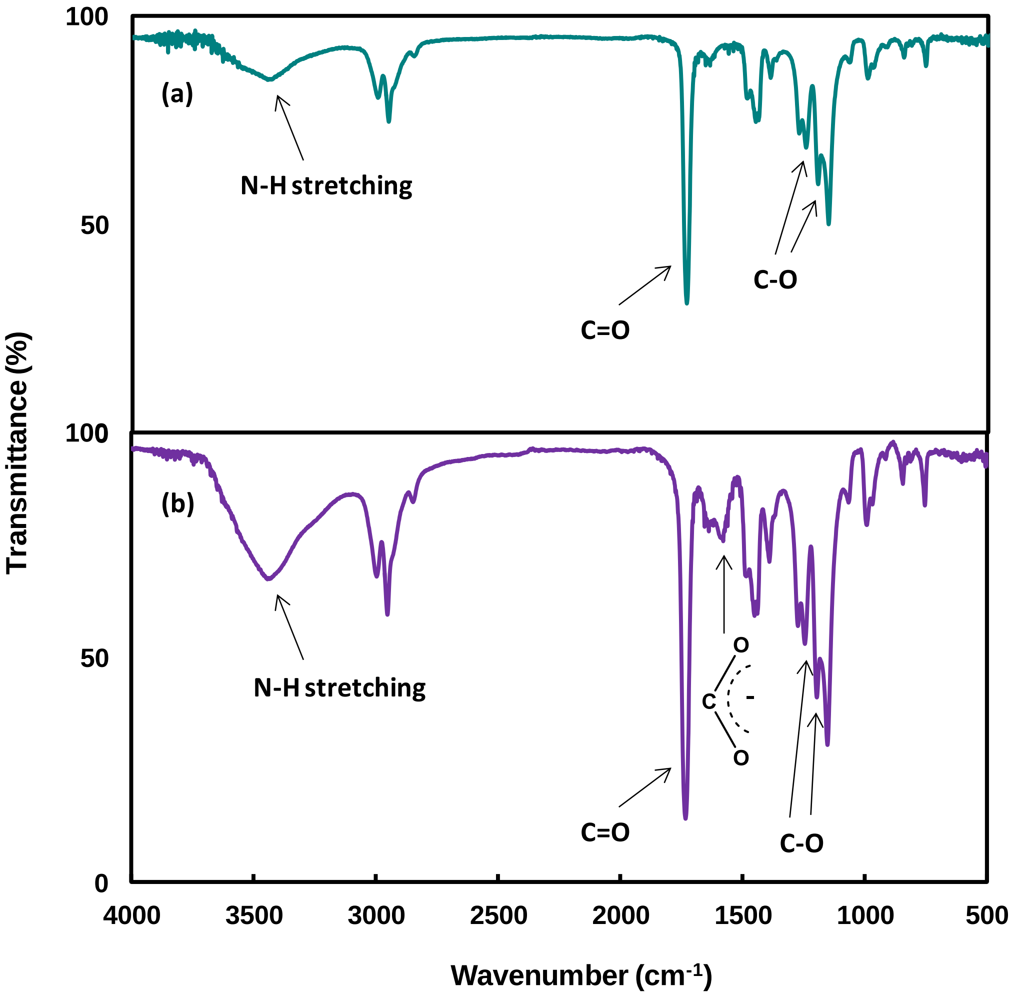

**Fig. 3.2.** FT-IR spectra of a) PMMA/PEI seed; and b) PBA/PMMA/PEI MCP particles.

### *3.3.2.2 Particle size*

The hydrodynamic diameters ($Z_{AVE}$) and particle size distribution (PDI) of seed and MCP particles were determined by the dynamic light scattering (DLS) using Beckman Coulter Delsa Nano C instrument at pH 7. Figure 3.3 Shows that hydrodynamic diameter and size distribution of seed and MCP particles which were 199.0 nm and 230.2 nm, respectively. No additional peak appear after the second batch of nBA. These suggest that the polymerization of n-BA predominantly occurs within the seed particles, leading to the particle growth to bigger size instead of generating new particles. There was only small boarding of the particle size distribution after the second stage reaction. Therefore, the seed polymerization to generate MCP particles is very efficient in this system with good control of particle size and size distribution.

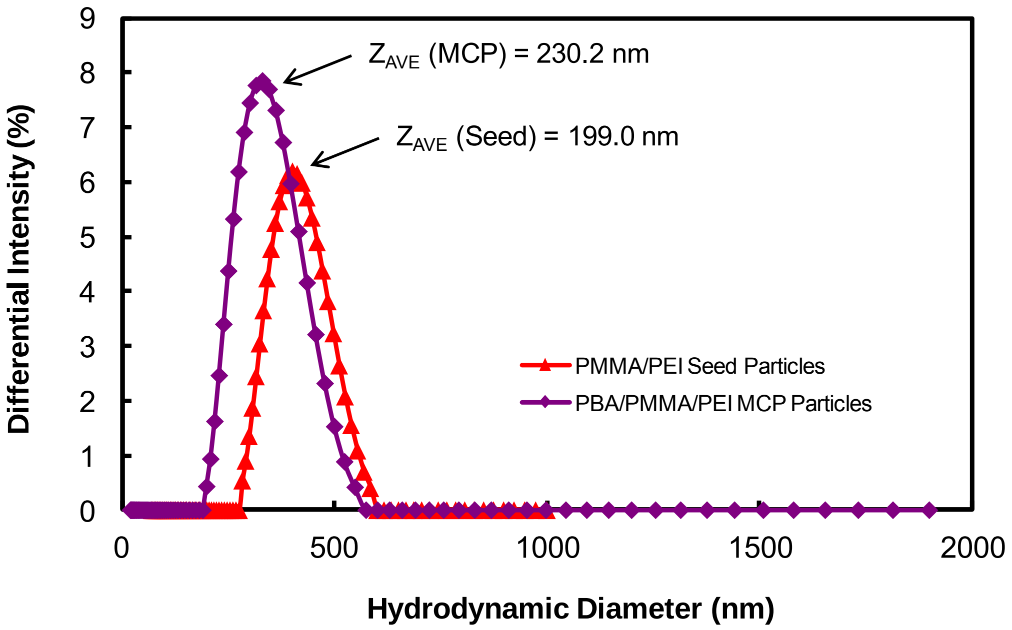

**Figure 3.3.** Particle sizes of PMMA/PEI seed particles (199.0 nm) and PBA/PMMA/PEI MCP particles (230.2 nm).

### *3.3.2.3 Surface charges as a function of pH*

The surface charges of MCP particles were determined by ζ-potential measurement using a Beckman Coulter Delsa Nano C instrument. The variation of ζ-potential of MCP particles at different pH was conducted with the aid of auto-titrator. In all measurements, MCP particles were first diluted to 200 ppm with 1 mM NaCl solution. Results of ζ-potential as a function of pH of MCP particles with different composition are shown in the Figure 3.4.

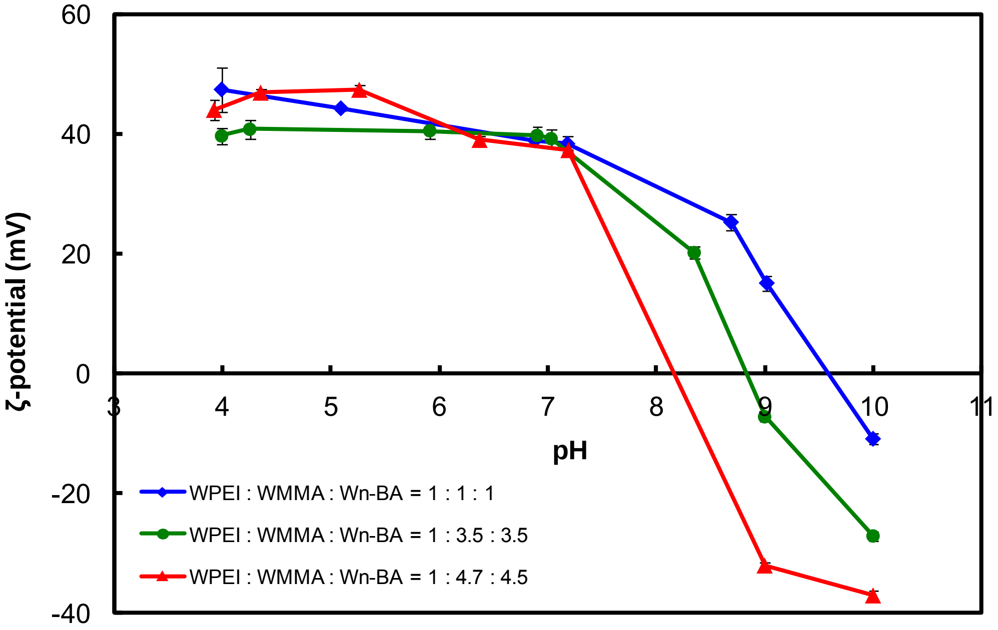

**Fig. 3.4.** ζ-potential values as a function of pH of MCP particles with different compositions.

Three types of MCP particles all possessed high positive charges under acidic medium (pH<7), indicating the presence of PEI component in the particle shells. However, these MCP particles had different isoelectric points under alkaline conditions. The isoeletric point of MCP particles with PEI to monomer ratio of 1 : 2, 1 : 7 and 1 : 9 was at about 9.5, 8.9 and 8.2, respectively. The difference in their isoelectric points was caused by the hydrolysis of *n*-BA monomers during the seeded emulsion polymerization. Upon synthesis of MCP particles, the *n*-BA monomers might be hydrolyzed in the presence of water under high temperature (about 80°C), giving acrylic acid and butyl alcohol (Figure 3.5). During seeded emulsion polymerization, the acrylic acid could also be copolymerized with *n*-BA and residual MMA. Therefore, the hydrophilic particle shell mainly contained amino groups (-$NH_2$) from PEI, but with some carboxylic groups from the copolymer with PAA. Under acidic pHs, some amino groups were protonated to –$NH_3^+$ groups, giving positively charged MCP particles. On the contrary, carboxylic groups were deprotonated to –$COO^-$ under basic pHs, contributing to negatively charges. These results suggest the MCP particles actually possess amphoteric property.

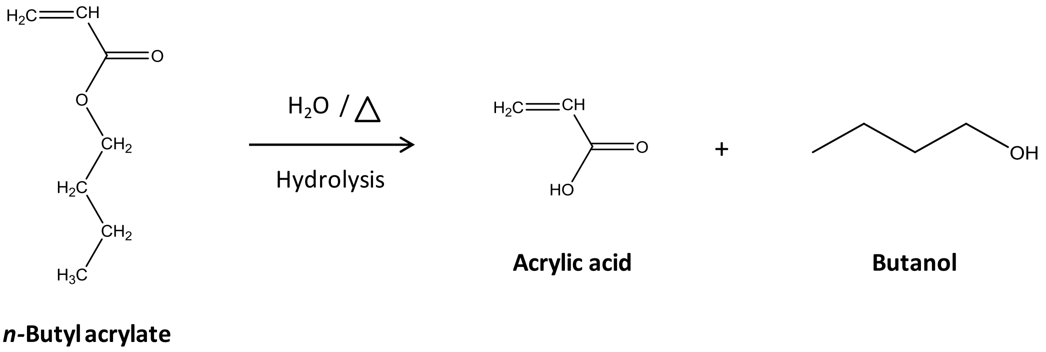

**Fig. 3.5.** Reaction scheme of the hydrolysis of *n*-butyl acrylate.

Results of isoeletric points also indicated that increasing *n*-BA monomers content resulted in lowering isoelectric pH of the MCP particles. This effect is due to increasing the acrylic acid concentration which would neutralize the amino groups.

In addition, the ζ-potential of MCP particles with PEI to monomer ratio of 1 : 2; 1 : 7 and 1 : 9 at pH 10 were - 11 mV, - 27 mV and - 37 mV, respectively. These results further confirm the high carboxylic acid content in the MCP particles with increasing the PEI to monomer ratio.

To minimize the occurrence of hydrolysis as side reaction, one possible approach is to lower the reaction temperature. Reducing the reaction temperature could suppress the hydrolysis of *n*-BA. However, the rate of polymerization of *n*-BA will ineveitably be reduced simultaneously. To achieve this goal, another feasible approach is to replace *n*-BA with another monomer. The monomer selected for the seeded emulsion polymerization containing poor leaving group can reduce the occurrence of water hydrolysis. In addition, selecting monomer with bulky groups will provide steric hindrance to the monomer from being hydrolyzed.  Styrene should be an approapriate choice as second hydrophobic monomer.

### *3.3.2.4 Morphology*

The morphology of MCP particles prepared with different weight ratio of PEI to total monomer (1 : 2, 1 : 4, 1 : 7, 1 : 9) were examined by FE-SEM and TEM. Figure 3.6a shows the SEM microgel of MCP particles prepared using PEI to total monomer of 1 : 4. Spherical and highly uniform nanoparticles were produced. To elucidate the nanostructure of the MCP particles, the particles were stained with 0.5% (w/w) phosphotungstic acid (PTA, $WO_2•H_3PO_4•xH_2O$) for 30 seconds. . The TEM micrographs of Figure 3.6b and c reveal that the MCP particles have core-shell nanostructure However, the spatial distribution between PMMA and PBA were unable to identify since these two polymers possessed similar functional groups that could not be differentiated via chemical staining process.

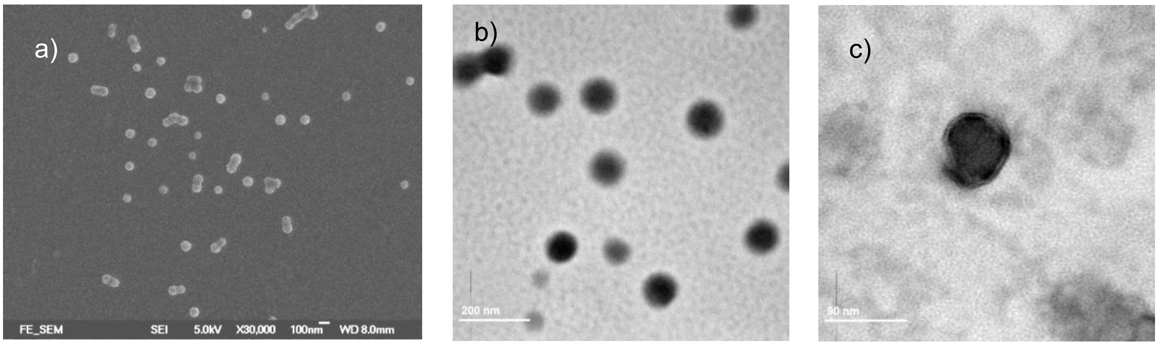

**Fig. 3.6.** Morphology of PBA/PMMA/PEI composite particles: a) FE-SEM micrographs prepared at pH 7; b) TEM image without staining; c) TEM image with staining.

### 3.3.3 PS/PMMA/PEI MCP nanocomposite particles

This part describes the preparation and characterization of PS/PMMA/PEI nanocomposite particles. In fact, styrene has lower water solubility (0.3 g/L) than n-BA. It might be more difficult to undergo seeded polymerization due to the slow diffusion of hydrophobic molecules in water. The success in forming MCP particles containing very hydrophobic component would allow us to prepare a wide range of MCP particles with different compositions.After the formation of PMMA/PEI seed particles, styrene monomer was introduced to undergo seeded emulsion polymerization. Scheme 3.2 shows the synthesis and conditions to prepare these particles.

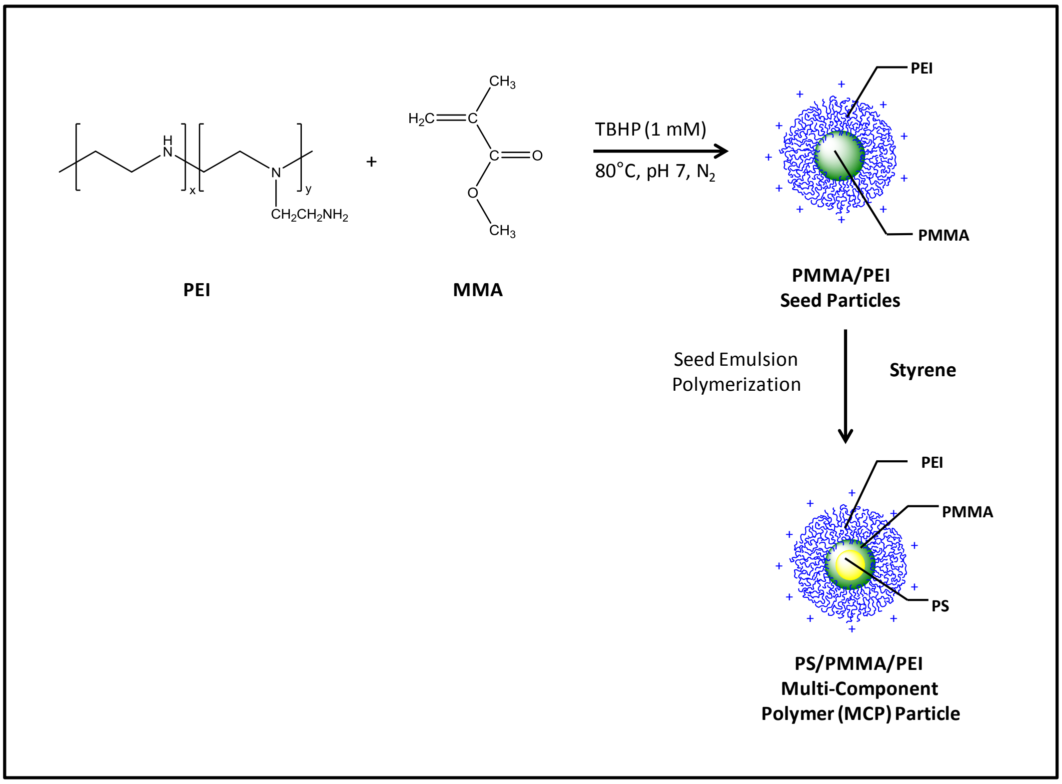

**Scheme 3.2.** Reaction scheme for the synthesis of PS/PMMA/PEI MCP particles.

#### *3.3.3.1 Kinetic study of the polymerization process*

The reaction kinetics of the seeded emulsion polymerization of MCP nanocomposites was monitored by thermal couple (Testo 735) with 1 temperature recorded per second. Figure 3.7 shows the temperature profile of the polymerization at different stages of reaction.

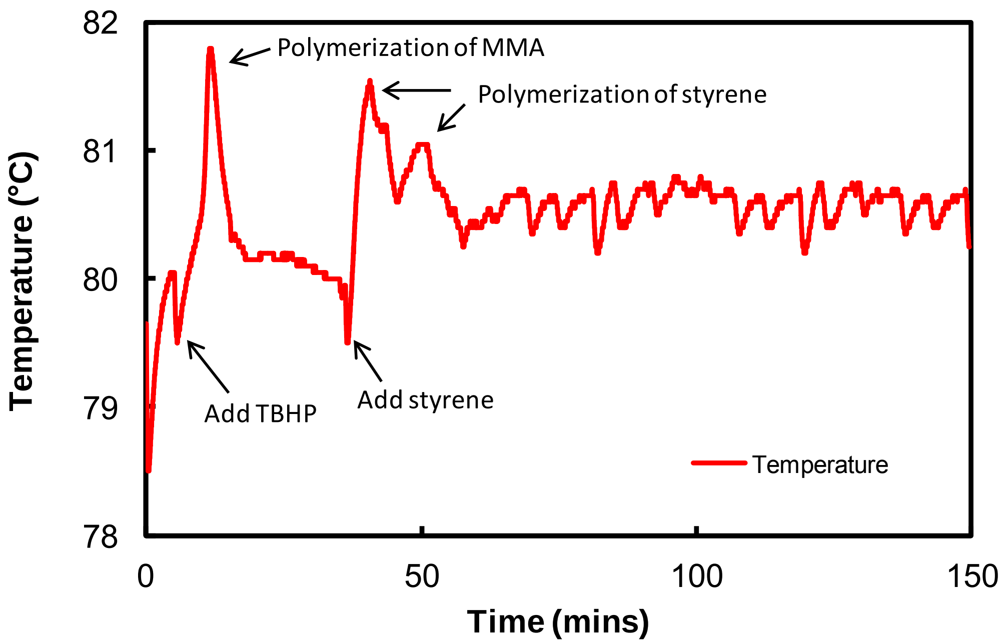

**Fig. 3.7.** Reaction temperature profile during the synthesis of PS/PMMA/PEI MCP particles.

When the temperature of PEI and MMA mixture reached equilibrium (around 80 °C), appropriate amount of initiator (TBHP) was added to the reaction mixture to initiate the polymerization. Once TBHP was added, the reaction temperature was first slightly dropped and then rose up rapidly. After consuming most of the MMA monomers, the exothermic polymerization was almost finished and the temperature of the reaction mixture dropped to the original level.

As the temperature fell back to 80 °C, the second batch of monomer, styrene, was introduced into the reaction mixture by one-shot addition to perform seeded emulsion polymerization. Similarly, an increased in temperature was observed after the addition of styrene. This increase was contributed by an exothermic polymerization of styrene inside PMMA/PEI seed particles. However, the increase in temperature was not as vigorous as in the seed forming stage. Due to extremely low solubility styrene in water (0.3 g/L at 25°C), the diffusion of styrene from bulk aqueous phase into the growing seed particles was significantly hindered. The slow diffusion of hydrophobic monomers into the growing particles leads to slow polymerization. Therefore, compared with the sharp and narrow exothermic peak contributed by MMA polymerization, the exothermic peak of the polymerization of styrene was broad with lower maxima.

In addition to temperature variation, the polymerization kinetics was also monitored by monomer conversion at different stage of polymerization. The total monomer conversion at different time interval is shown in Table 3.4. After the first stage of polymerization, MMA monomer conversion reached 99%. In the second stage of polymerization, styrene monomer was charged to proceed seeded emulsion polymerization. When the exothermic polymerization was completed, the total monomer conversion had reached 98% at the end of polymerization.

The variation of hydrodynamic diameters of MCP particles during the polymerization process was determined through measuring particle size at different time interval. Results are summarized in Table 3.4. Since the styrene monomer is very hydrophobic, it prefers to localize in the hydrophobic region of the seed particle. However, the styrene molecule may be difficult to diffuse into the particle core due to its low solubility in water. From the result of particle size measurement, the hydrodynamic diameters of the seed particles and MCP particles were 205.8 nm and 236.1 nm, respectively. The increment in the hydrodynamic diameter of the particles was about 14.7%.

**Table 3.4.** Total monomer conversion and particle size of MCP particles at different time intervals.

| **Reaction time[1] (mins)** | **Type of particles** | **Monomer conversion[2] (%)** | **$Z_{AVE}$[3] (nm)** |
|---|---|---|---|
| 30 | PMMA/PEI seed | 99%[4] | 205.8 |
| 34 | PS/PMMA/PEI MCP | 67%[5] | 237.2 |
| 40 | PS/PMMA/PEI MCP | 75%[5] | 244.3 |
| 45 | PS/PMMA/PEI MCP | 81%[5] | 258.8 |
| 50 | PS/PMMA/PEI MCP | 87%[5] | 266.4 |
| 90 | PS/PMMA/PEI MCP | 95%[5] | 225.9 |
| 150 | PS/PMMA/PEI MCP | 98%[5] | 236.1 |

[1] The reaction was counted since the addition of initiator into the reaction mixture

[2] The total monomer conversion of MCP particles were determined gravimetrically

[3] The hydrodynamic diameter of MCP particles were determined by DLS at 25 °C

[4] The monomer conversion was calculated based on total MMA monomer added

[5] The monomer conversion was calculated based on total monmer added

### *3.3.3.2 Effect of pH of reaction medium*

The effect of reaction pH on the properties of MCP particles was studied at pH 7 and 11, while keeping other synthetic parameters constant. In these studies, MCP particles were prepared at 80 °C for 150 mins. The weight ratio between PEI, MMA and styrene was kept at 1 : 2 : 2. Results shown in Table 3.5 suggest that the polymerization can effectively take place at both neutral and alkaline conditions. But particle size and size distribution are affected by the solution pH. Both seed and MCP particles obtained at pH 7 are bigger than those produced at pH 11. This is mainly due to higher PEI protonation degree at lower pH, causing stronger electrostatic repulsion. As a result, the size of micelle-like microdomain would be larger. Furthermore, the high charge density gives more expanded PEI shell. It was also noted that size distributions of MCP particles produced at pH 11 are larger than the ones in pH 7. Therefore, the polymerization of PS/PMMA/PEI MCP under neutral pH is more appropriate.

**Table 3.5.** Effect of pH of reaction medium on the properties of MCP particles

| Reaction pH | Total monomer conversion (%) | $Z_{AVE}$[1] (nm) of seed | PDI of seed | $Z_{AVE}$[1] (nm) of MCP | PDI of MCP | ζ-potential[2] (mV) |
|---|---|---|---|---|---|---|
| 7 | 98% | 205.8 | 0.074 | 236.1 | 0.136 | + 38.8 |
| 11 | 88% | 179.6 | 0.251 | 186.3 | 0.183 | + 49.7 |

[1] The hydrodynamic diameters of MCP particles were measured by DLS at 25 °C

[2] The ζ-potential of MCP particles were measured at 25 °C using 1 mM NaCl as medium

\

### 3.3.4 Characterization of PS/PMMA/PEI nanocomposite particles

#### *3.3.4.1 Composition*

The FT-IR spectra of PS/PMMA/PEI particles and PMMA/PEI seed particles are compared in Figure 3.8. The particle dispersions were purified by repeated centrifugation to get rid of any unreacted PEI and monomers. In the FT-IR spectra of both seed and MCP particles, a strong carbonyl C=O peak of PMMA is clearly observed in 1730 cm$^{-1}$. Also, strong -C-O- ester peaks of PMMA appear at 1150 to 1300 cm$^{-1}$. Both broad amino N-H stretching peak of primary amine at 3400 to 3500 cm$^{-1}$, and C-H stretching and bending at 2900 to 3000 cm$^{-1}$ indicate the presence of PEI. In the FT-IR spectrum of PS/PMMA/PEI, additional absorption peaks at 750 cm$^{-1}$ and 700 cm$^{-1}$ are identified, which correspond to aromatic =C-H out-of-plane bending vibration peaks. Enhanced absorption peak at 1500 cm$^{-1}$ regarding to aromatic =C-H stretching vibration of PS is also observed. Enhanced absorption peak also appear at 2950 to 3050 cm$^{-1}$ regarding to =C-H vinylic hydrogen which suggest the presence of PS. These characteristic peaks confirm the presence of polystyrene in the MCP particles. Based on the FTIR results, we can confirm that the MCP particles comprise of PEI, PMMA and polystyrene components.

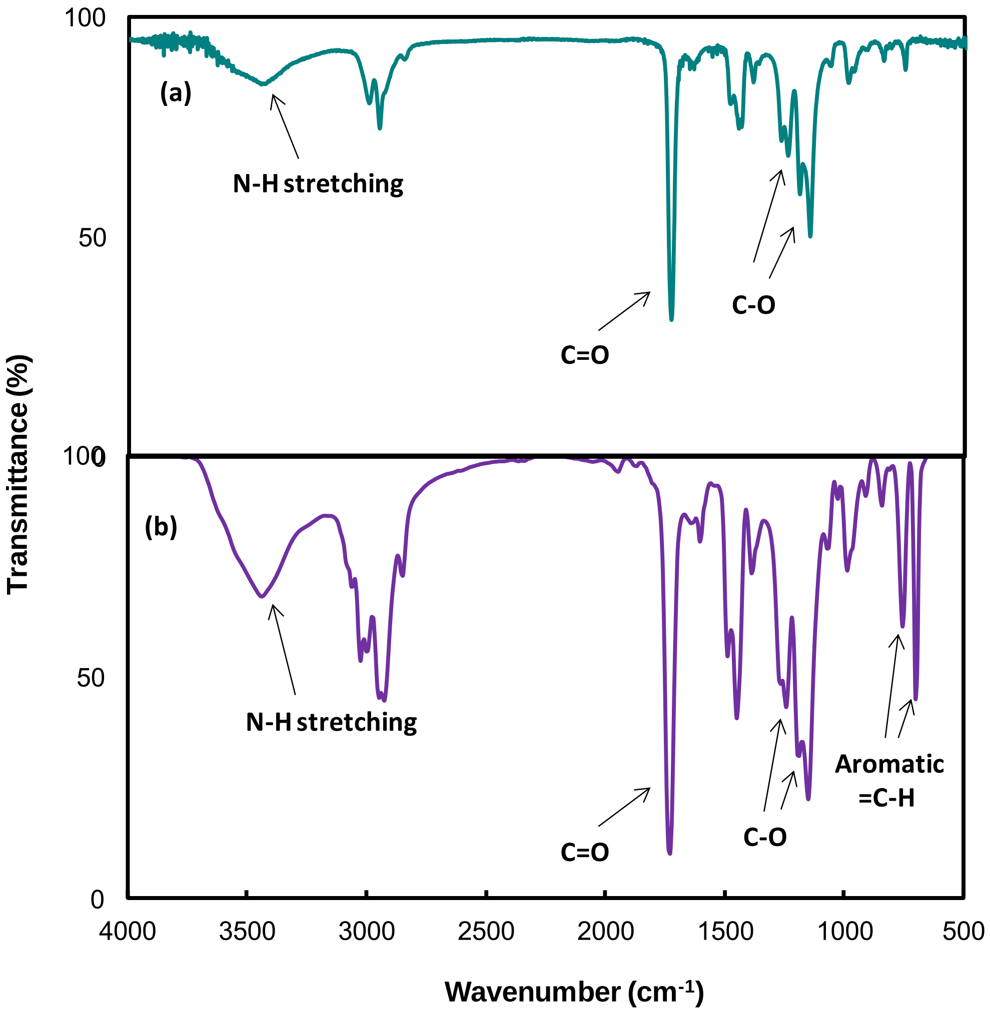

**Fig. 3.8.** FT-IR spectrum of a) PMMA/PEI seed; and b) PS/PMMA/PEI MCP particles.

#### *3.3.4.2 Particle size*

The hydrodynamic diameters ($Z_{AVE}$) and particle size distribution (PDI) of seed and MCP particles were determined by dynamic light scattering (DLS) at pH 7 using a Beckman Coulter Delsa Nano C instrument. Figure 3.8 compares their particle sizes and size distributions. The hydrodynamic diameter and particle size distribution of seed particles were 205.8 nm and 0.074. While the hydrodynamic diameter and particle size distribution of MCP particles were 236.1 nm and 0.136.

These results indicated that the prepared MCP particles were in nano-sized dimension and with narrow size distribution.

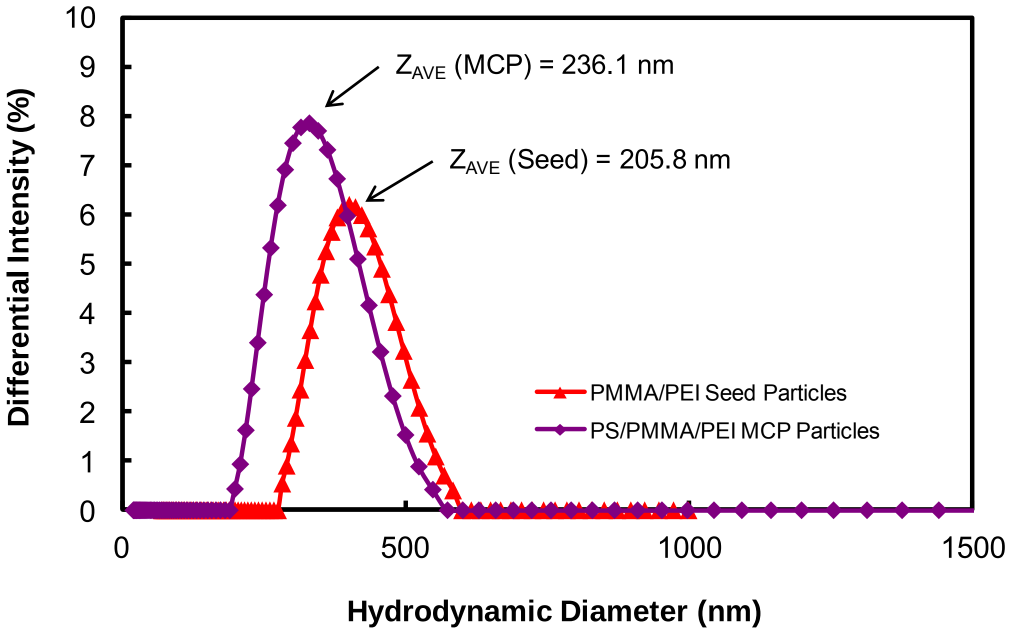

**Fig. 3.9.** Particle size of PMMA/PEI seed particles (205.8 nm) and PS/PMMA/PEI MCP particles (236.1 nm).

### *3.3.4.3 Surface charges of particles as a function of pH*

The surface charges of MCP particles were determined by ζ-potential measurement using a Beckman Coulter Delsa Nano C instrument. The particles were dispersed in 1 mM NaCl solution at pH 7. The ζ-potential value of the MCP particles was + 38.8 mV, indicating that that the MCP particles possessed good colloidal stability in aqueous phase and the particle surface was positively charged. These positive charges were contributed by the protonated amine groups of PEI, confirming that the water soluble PEI was located at the outer shell of MCP particles.

The variation of ζ-potential of MCP particles at different pH was evaluated by ζ-potential measurement using the Delsa Nano C with the aid of auto-titrator. The MCP particles were first diluted to 200 ppm with 1 mM NaCl solution. The variation of ζ-potential of MCP particles as a function of pH is illustrated in Figure 3.10. The ζ-potential of MCP particles was all above + 30 mV below or equal to 7. The results indicate that the MCP particles exhibit good colloidal stability under acidic condition.

When solution pH was above 7, there was an obvious decrease in the ζ-potential of MCP particles due to the deprotonation of the ammonium cations of the PEI. But the ζ-potential of MCP particles still remained about + 20 mV at pH 10. These results suggest that the surface of MCP particles was positively charged and was colloidally stable. The high ζ-potential magnitude of PS/PMMA/PEI MCP particles at high pH (~ + 20 mV) was due to absence of hydrolysis during MCP particle synthesis. Without the formation of carboxylic group due to hyudrolysis, the particle surface of PS/PMMA/PEI was only constructed by positively charged PEI. Therefore, the ζ-potential of PS/PMMA/PEI was not suppressed by the carboxylic acid and kept high at basic pH.

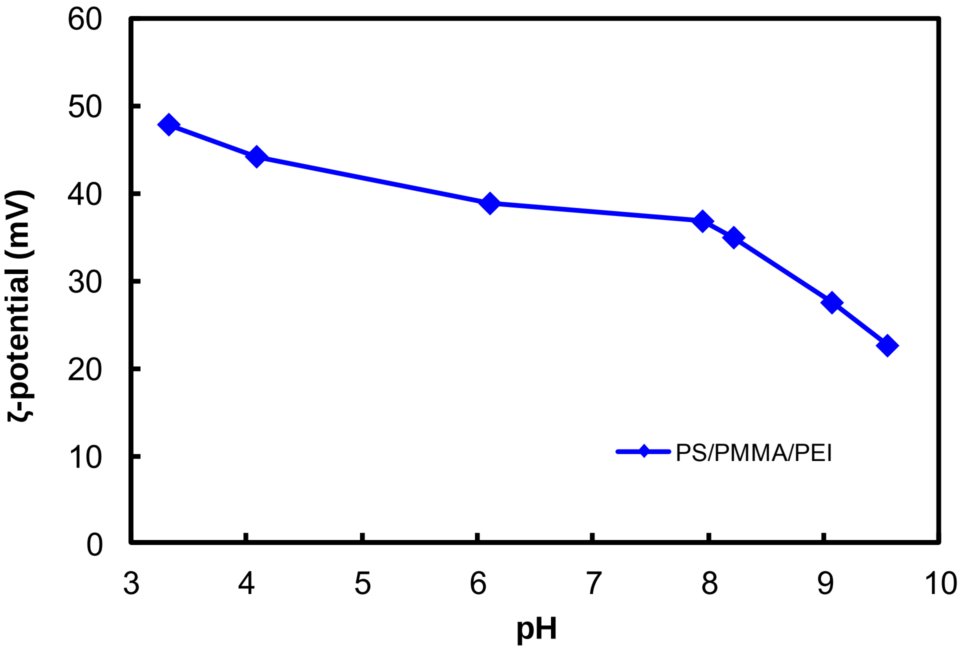

**Fig. 3.10.** ζ-potential as a function of pH of MCP particles.

### *3.3.4.4 Morphology*

The morphology and core-shell nanostructure of PS/PMMA/PEI MCP particles prepared at pH 7 and 11 were examined by TEM. The TEM microgrpahs of PS/PMMA/PEI MCP particles were illustrated in Figure 3.11. The particles were stained with 0.5% w/w phosphotungstic acid (PTA, $WO_2•H_3PO_4•xH_2O$) for 30 seconds. During PTA staining process, only PEI was stained by PTA solution, but not PMMA and PS parts. Thus, we interpreted that the shell of the MCP particles was constructed by PEI and the core of the MCP particles was constructed by PMMA and PS.

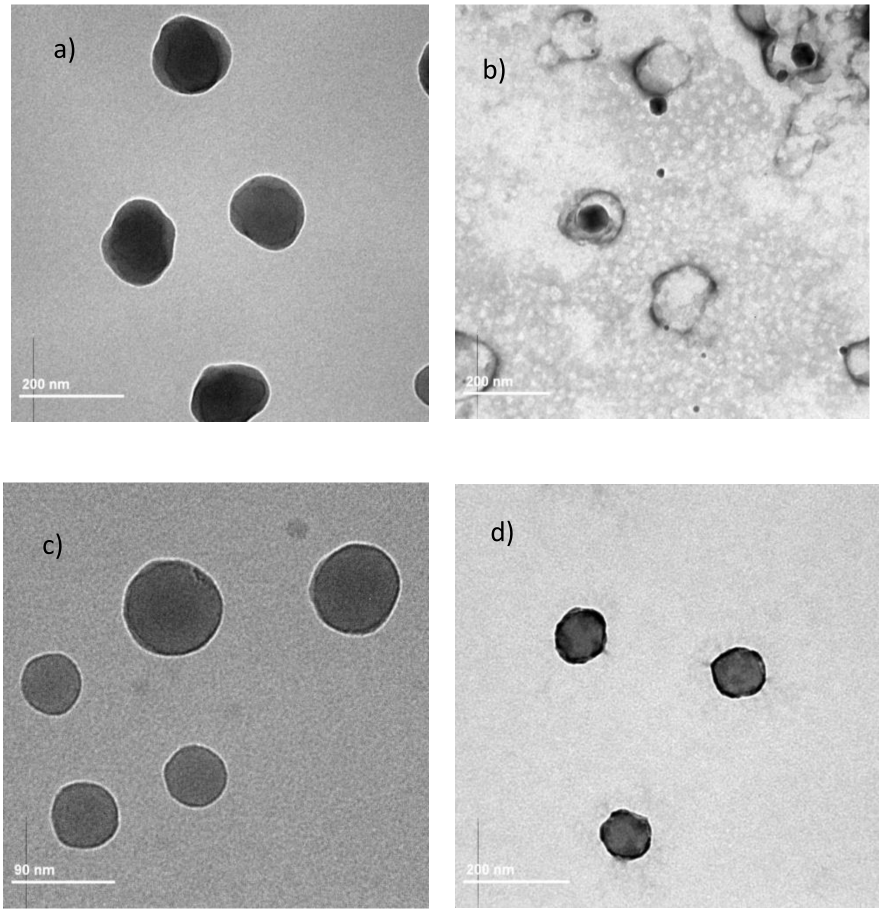

**Fig. 3.11** TEM micrographs of PS/PMMA/PEI MCP particles prepared at pH 7 (a) without staining; b) stained by PTA); and pH 11 (c) without staining; d) stained by PTA)

Above TEM images reveal that morphology of MCP particles are affected by the solution pHs. When the PS/PMMA/PEI was synthesized at basic medium (pH 11), spherical nanoparticles with high uniformity were obtained. The spherical shaped MCP particles had reached thermodynamic favored equilibrium morphology. However, the morphology of PS/PMMA/PEI MCP particles prepared at pH 7 was not perfectly spherical in shape. These MCP particles possessed distorted spherical shape under TEM investigation. This morphology was kinetic favored morphology that the nanoparticles did not achieve a minimum interfacial energy at the end of reaction.

Under neutral pH, amino groups on PEI were partially protonated to ammonium cations. The protonation of amino group on PEI had enhanced the electrostatic stabilization of MCP particles due to the electrostatic repulsion. MCP particles prepared had gained additional electrostatic stability during polymerization that they were stabilized in the continuous phase even thermodynamic morphology was not achieved. As a result, kinetic morphology could be reached, forming distorted spherical MCP particles. On the contrary, amino groups on PEI were deprotonated at basic medium that MCP particles formed were not benefited from the electrostatic stabilization. Without any addition stability, thermodynamic equilibrium morphology was the desirable terminal morphology with minimum interfacial energy. As the polymerization time was sufficient that allowed the rearrangement of components in the particles, equilibrium morphology was achieved at the end.

Monomer conversion is another factor affecting the final morphology of PS/PMMA/PEI MCP particles. The total monomer conversion of PS/PMMA/PEI MCP particles prepared at pH 7 and pH 11 were 98% and 88% respectively. PMMA and PS are rigid polymer possessing high glass transition temperatures ($T_g$ of PMMA is 378 K and $T_g$ of PS is 373 K). Rigid hydrophobic core was constructed in MCP particles immdediately after seeded emulsion polymerization. When the reaction was conducted at pH 7, MMA and styrene monomers are almost completely converted at the end of polyemrization. Reaarangemt of PMMA and PS polymers chains towards equilibrium morphology is prohibited, leading to a kinetically favored morphology (distorted spherical). When the reaction was conducted at pH 11, about 90% monomer conversion was reached at the end of polymerization. PS/PMMA/PEI MCP particles were swelled by unreacted monomers. The presence of residual monomers allowed the migration of high $T_g$ polymers PMMA and PS inside the hydrophobic core. Perfectly spherical particles were obtained at the end of polymerization as thermodynamically favored morphology was achieved. Consequently, perfectly spherical MCP particles were obtained when the polymerization was carried out at basic pH.

## 3.4 Conclusion

Two types of multi-component polymer (MCP) particles, PBA/PMMA/PEI and PS/PMMA/PEI, were successfully synthesized via seeded emulsion polymerization using PMMA/PEI as the seed particles. *n*-BA and styrene monomer were added in the second stage and were polymerized via seed emulsion polymerization. Two stages of exothermic polymerization were observed through online temperature monitoring.Two exothermic peaks were observed in the temperature profiles which corresponded to the seed formation and seed emulsion polymerization. High conversion could be generally achieved via this synthetic route. Characterizations of these two types of MCP particles suggest that they possessed nanosized dimension and uniform size distribution with high positive charges and good colloidal stability. They also possess core-shell nanostructures containing PEI shells. The success in fabrication of MCP particles could solve one major problem which previously encountered in our existing particle formation technology. According to our platform technology in synthesizing core-shell nanoparticles, the nanoparticles could only be formed with monomers which were slightly soluble in water, e.g. MMA. If the monomer used was very hydrophobic and exhibited low solubility in water, e.g. styrene, nanoparticles could not be formed unless the initiator concentration was significantly increased from 1 mM to 2 M. By implementing seed emulsion polymerization strategy, the amphiphilic core-shell seed was formed before the addition of very hydrophobic monomer. This seed particle could facilitate the diffusion of the hydrophobic monomer into the seed core for polymerization. The proposed approach thus provided a facile route to synthesize amiphiphilic nanoparticles containing very hydrophobic polymer core.

It should be emphasized when *n*-BA was used as second monomer in the synthesis of PBA/PMMA/PEI, *n*-BA would undergo hydrolysis during the polymerization process, generating acrylic acid. This side product could also undergo copolymerization to generate amproteric MCP particles. By varying the *n*-BA content, the isoelectric point (IEP) of amproteric MCP particles could be adjusted. As a result, our proposed approach not only provided a possible pathway for the preparation of MCP particles, but also provided a feasible pathway for the preparation of amproteric polymeric particles.

When styrene was used as the second batch monomer for the synthesis of PS/PMMA/PEI MCP particles, reaction medium was an important parameter determining the terminal particle morphology. When MCP particles were prepared at basic pH (pH 11), spherical and highly uniform MCP particles were obtained. When MCP particles were prepared at neutral pH (pH 7), distorted spherical MCP particles were obtained. Although these particles were not perfectly spherical in shape, they were prepared with high uniformity and high stability. Therefore, our synthetic approach also allows us to prepare particle with different morphology through simple turning of solution pH.

# Chapter 4

## Synthesis and Characterization of Multi-Component Polymer (MCP) Nanocomposite Particles using Crosslinked PNIPAm-PEI Seed Microgels

This chapter describes the synthesis and characterization of multi-component polymer nanocomposite particles using crosslinked PNIPAm/PEI as seed nanoparticles. Three types of MCP nanocomposite particles were synthesized, namely PMMA/(PNIPAm-MBA)/PEI, PBA/(PNIPAm-MBA)/PEI and PS/(PNIPAm-MBA)/PEI, through a semi-batch seeded emulsion polymerization. MBA crosslinked PNIPAm/PEI seed nanoparticles were first formed via a TBHP induced graft copolymerization of NIPAm from PEI with MBA as a crosslinker. Second batch of vinylic monomers, MMA, *n*-BA or styrene, was subsequently added and polymerized in the presence of the seed nanoparticles. Scheme 2.2 illustrates the synthetic route and reaction conditions.

Properties of these three types of MCP nanocomposites, including particle size and size distrbution, surface charge, chemical composition and particle morphology were systematically characterized by dynamic light scattering, ζ-potential measurement, FTIR spectroscopy, field emission scanning electron microscopy and transmission electron microscopy.

## 4.1 Experimental Section

### 4.1.1 Materials

Phenolic inhibitors, monomethyl ether hydroquinone (MEHQ), in methyl methacrylate (MMA, 0.936 g/cm$^3$, Sigma Aldrich) and *n*-butyl acrylate (*n*-BA, 0.894 g/cm$^3$, Sigma Aldrich), and phenolic inhibitors in styrene (St., 0.909 g/cm$^3$, Sigma Aldrich) were removed by washing the monomers by three times 10 w/w% sodium hydroxide (NaOH) and then with deionzed water until the water layer dropped to pH 7.

*N*-isopropylacrylamide (NIPAm, 97%, Wako Pure Chemical Industries) was purified by recrystallization method. NIAPm monomers were repeated dissolved and crystallized three times in mixed solvent of toluene and hexane in ratio of 1 : 5 (v/v) to give spindle-like crystals.

Polyethylenimine (PEI, $M_w$ 750,000 g/mol, 50 w/w% solution in water), *tert*-butyl hydroperoxide (TBHP, 70 w/w% solution in water), were purchased from Sigma Aldrich Co., *N,N'*-methylenebis(acrylamide) (MBA, 98%) was obtained from BDH and used without further purification. Freshly deionized Milli-Q water was used as the dispersion medium.

### 4.1.2 Synthesis of MCP nanocomposite particles using crosslinked PNIPAm-PEI based seed microgels

For a total solution of 100 mL, PEI (2 g, 50 w/w% solution) was first dissolved in deionzed water and the pH of the solution was adjusted to 7 with 2 M HCl solution. The diluted PEI solution was then transferred into a three-necked water-jacketed equipped with thermal couple (Testo 735), a condenser, a magnetic stirrer, and a nitrogen inlet. The dispersion was stirred at 350 rpm and purged with nitrogen for 30 mins. Appropriate amount of NIPAm (1.961 g) and crosslinker MBA (0.039 g) were then added to the dispersion when the temperature of the dispersion reached 80°C. After that, appropriate amount of initiator, TBHP (1 mL, 0.1 M), were added to the reaction mixture and the resulting mixture was continuously stirred at 80 °C under nitrogen. Small amount of sample (2 mL) was withdrawn from the reaction mixture after reacting for 30 mins.  Second batch of monomer, MMA, *n*-BA or styrene (2 g), was then added to the reacting mixture. The resulting mixture was allowed to react at 80°C for 2 hrs under nitrogen. After the reaction, the nanoparticles were purified by repeated centrifugation (19,500 rpm, 1.5 hr), decantation and re-dispersion until the conductivity of the supernatant approached to that of deionzed Milli Q water.

#### *4.1.2.1 Determination of monomer conversion and nanoparticle composition*

The monomer conversion of the MCP nanocomposite particles was determined gravimetrically. Measurement procedures were the same as described in **3.1.2.1**. The total solid content was calculated based on **Eq. 3.1**. The monomer conversion was calculated based on **Eq. 3.2**.

#### *4.1.2.2 Kinetic study of the polymerization process*

The polymerization kinetics was monitored by regular withdrawl of samples from reaction mixture at various interval times. The procedures to withdraw samples and characterization methods were the same as described in **3.1.2.2**.

#### *4.1.2.3 Effect of second batch monomer (MMA, n-BA and styrene) on seed emulsion polymerization*

The effect of type of second batch hydrophobic monomer on the polymerization kinetics and particle properties was evaluated by varying the types of second batch hydrophobic monomer to be MMA, *n*-BA or styrene. The synthetic procedure was the same as described in **4.1.2.** except the second batch monomer was varied to be MMA, *n*-BA and styrene.

#### *4.1.2.4 Effect of degree of crosslinking*

The effect of degree of crosslinking of PNIPAm/PEI seed microgel on the polymerization kinetics and particle properties was studied by varying weight ratio between NIPAm monomer and MBA crosslinker in the reaction recipe. The synthetic procedure was the same as described in **4.1.2.** except the weight ratio between NIPAm and MBA was varied to be 90 : 10 (10% crosslinking), 95 : 5 (5% crosslinking), 98 : 2 (2% crosslinking).

**Table 4.1.** Reaction recipe for the effect study of degree of crosslinking.

| **Degree of crosslinking (%)** | **Polymerization recipes**[1] | | | | **MCP particles composition** | |
|---|---|---|---|---|---|---|
| | Weight of PEI (g) | Weight of NIPAm (g) | Weight of MBA (g) | Weight of second batch monomer, St.[2] (g) | w/w ratio of NIPAm to MBA | w/w ratio between PEI and total monomer[3] |
| 10% | 1 | 1.805 | 0.195 | 2 | 90 : 10 | 1 : 4 |
| 5% | 1 | 1.903 | 0.097 | 2 | 95 : 5 | 1 : 4 |
| 2% | 1 | 1.961 | 0.039 | 2 | 98 : 2 | 1 : 4 |

[1] PEI, NIPAm and MBA were reacted in the first step to prepare PNIPAm/PEI seed hydrogel in the presence of 1 mM TBHP. Styrene was added in the second step to form MCP particles. All the reactions were conducted at 80 °C with 350 rpm stirring under nitrogen atmosphere for 2.5 hrs. The pH of the reaction mixture was adjusted to 7 prior to reaction.

[2] Styrene was employed as the second batch monomer for the synthesis of MCP particles. The second batch monomer was ranged from MMA, *n*-BA to styrene. In this table, only the recipe for the synthesis of PS/(PNIPAm-MBA)/PEI MCP particles was shown.

[3] The composition of MCP particles was kept at a weight ratio of 1 : 2 : 2 ($w_{PEI}$ : $w_{NIPAm}$ : $w_{St.}$)

### *4.1.2.5 Effect of seed monomer to second batch monomer ratio*

The effect of seed monomer to second batch monomer ratio on the polymerization kinetics and particle properties was studied by varying the weight ratio between seed monomer and second batch monomer. The synthetic procedure was the same as described in **4.1.2.** except the weight ratio between seed monomer and second batch monomer was varied to be 25 : 75, 50 : 50 and 75 : 25.

**Table 4.2.** Reaction recipe for the effect study of weight ratio between seed monomer and second batch monomer.

| **Monomer composition (seed : hydrophobic)** | **Polymerization recipes**[1] | | | | **MCP particles composition** | |
|---|---|---|---|---|---|---|
| | Weight of PEI (g) | Weight of NIPAm (g) | Weight of MBA[2] (g) | Weight of second batch monomer, St.[3] (g) | w/w ratio of NIPAm to St. | w/w ratio between PEI and total monomer |
| 1 : 3 | 1 | 0.981 | 0.019 | 3 | 25 : 75 | 1 : 4 |
| 1 : 1 | 1 | 1.961 | 0.039 | 2 | 50 : 50 | 1 : 4 |
| 3 : 1 | 1 | 2.941 | 0.059 | 1 | 75 : 25 | 1 : 4 |

[1] PEI, NIPAm and MBA were reacted in the first step to prepare PNIPAm/PEI seed hydrogel in the presence of 1 mM TBHP. Styrene was added in the second step to form MCP particles. All the reactions were conducted at 80 °C with 350 rpm stirring under nitrogen atmosphere for 2.5 hrs. The pH of the reaction mixture was adjusted to 7 prior to reaction.

[2] MBA was employed as crosslinker for the synthesis of the seed hydrogel. The MCP particles contained 2 wt.%, 5 wt.% and 10 wt.% of MBA, based on the weight of NIPAm employed. In this table, only the recipe for the synthesis of 2% MBA crosslinked MCP particles was shown.

[3] Styrene was employed as the second monomer in this study.

## 4.2 Measurement and Characterization

### 4.2.1 Chemical compositions characterized by FT-IR

The chemical composition of MCP particles was characterized by FT-IR spectroscopy. The characterization procedures were the same as described in **3.2.1**.

### 4.2.2 Determination of unbound PEI

The amount of unbound PEI in was determined by titrimetric method. Crude MCP latex dispersion was collected and then purified by repeated centrifugation, decantation and redispersion until the conductivity of the supernatant was close to deionized water. All of the supernatant were collected and combined together. The supernatant was titrated with 0.025 M NaOH solution and the variation of pH and conductivity was monitored by pH and conductometric titration (ThermoOrion 555A integrated pH/conductivity meter). Since conductivity measurement was only sensitive to free ions presented in the measuring solution instead of deprotonation of polyelectrolyte (e.g. PEI), excess NaOH ions would contribute to dramatic increase in conductivity of the solution. Thus, the equivalence point was determined by the pH where dramatic increase in conductivity of the solution began.

A calibration curve for PEI was established first according to the following procedures. Various amounts of PEI solution (50% w/w) were dissolved in water (40 mL), and their pH was adjusted to 7.0 using 2 M HCl solution. The adjusted PEI solution was then titrated with 0.025 M NaOH solution at room temperature under nitrogen atmosphere. The equivalence end point was defined as the pH value where the amount of hydroxide ions completely deprotonate all the protonated amino groups of PEI. The percentage of unbound PEI was determined with reference to the calibration curve, which shown as follows.

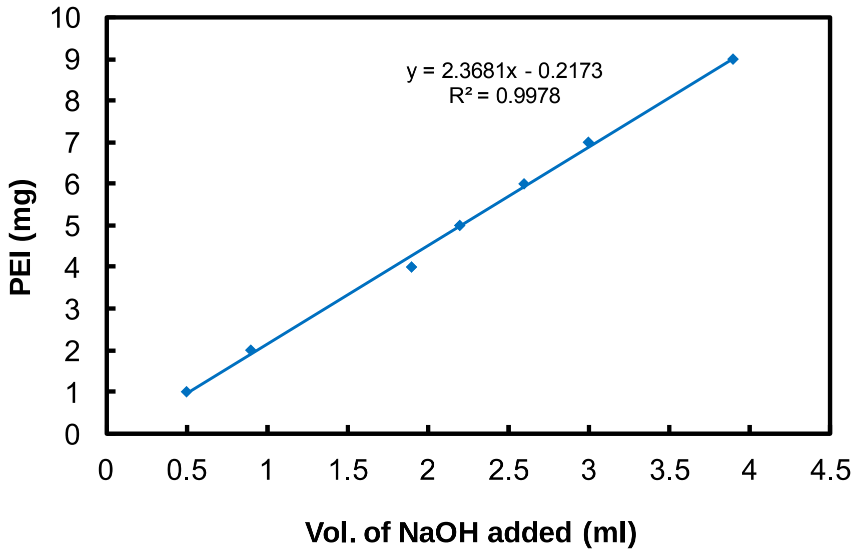

**Fig. 4.1.** Calibration curve for unbound PEI determination.

### 4.2.3 Particle size and size distribution

The particle size and size distribution of MCP nanoparticles were measured on Beckman Coulter Delsa Nano C Particle Analyzer. The measurement procedures were the same as described in **3.2.2**.

### 4.2.4 *ζ*-Potential measurement

ζ-potential of MCP nanoparticles were measured by Beckman Coulter Delsa Nano C Particle Analyzer. The measurement procedures were the same as described in **3.2.3**.

### 4.2.5 pH responsive properties

The effect of pH on the ζ-potential of the MCP nanoparticles was performed on Beckman Coulter Delas Nano C Particle Analyzer with the aid of Delsa Nano AT Auto Titrator. MCP nanoparticle sample was diluted to 200 mg/L by 1 mM NaCl solution for measurements. ζ-potential measurements was repeated thrice at every specific pHs, ranging from pH 4 to 10.

### 4.2.6 Thermal responsive properties

The effect of temperature on the particle size and ζ-potential of the MCP nanoparticles was measured on Beckman Coulter Delas Nano C Particle Analyzer and ALV/DLS/SLS-6000 compact goniometer system with the aid of thermal monitoring device.

For particle size measurement, MCP nanoparticle samples were diluted with deionized water to a concentration between 200 and 300 mg/L. The measurement was conducted at various preset temperatures, ranging from 25℃ to 39℃ and was repeated thrice. Each sample was thermally equilibrated for 10 mins before measurementat the corresponding temperature. Normalized hydrodynamic diameter or hydrodynamic radius was utilized to reflect the thermal responsive properties of MCP particles. The normalized hydrodynamic diameter or hydrodynamic radius was determined as follows.

$$Normalized\ Hydrodynamic\ Diameter = \frac{Dh_{elevated\ temperature}}{Dh_{25°C}} \quad \text{[Eq. 4.1]}$$

$$Normalized\ Hydrodynamic\ Radius = \frac{Rh_{elevated\ temperature}}{Rh_{25°C}} \quad \text{[Eq. 4.2]}$$

Normalized hydrodynamic diameter or normalized hydrodynamic radius was calculated as the ratio of the hydrodynamic diameter or radius at elevated temperature to the hydrodynamic diameter or radius at reference temperature (25 ℃). The calculated normalized hydrodynamic diameter or radius was a ratio illustrating the degree of shrinkage of PNIPAm/PEI based MCP particles.

Dynamic light scattering experiments were done with an ALV/DLS/SLS-6000 compact goniometer system (Peters) equipped with a He-Ne laser (632.8 nm) and a thermostat (Rotilabo, ± 0.1℃) for temperatures between 15 and 45 ℃. The samples were diluted with Milliporewater to give a final concentration of ca. 0.001 wt% and filled into dust free quartz glass cuvettes. Five runs of 60 s were measured at a scattering angle of 90° and the samples were allowed to reach thermal equilibrium for 20 mins. The hydrodynamic radii were obtained by standard cumulative analysis by taking into account the polydispersity of the samples.

For ζ-potential measurement, MCP nanocomposite samples were diluted to a concentration of 200 mg/L with 1 mM NaCl solution. The pH of the samples was adjusted to about 7. The measurement was then conducted at various preset temperatures, ranging from 25℃ to 39℃. Each sample was thermally equilibrated for 10 mins before measurement and the measurement was repeated thrice.

### 4.2.7 Morphology

#### *4.2.7.1 Field-Emission Scanning Electronic Microscopy (FE-SEM)*

The morphologies, particle size and size distribution of the MCP nanoparticles in dried state were examined by field-emission scanning electron microscope (FE-SEM, JEOL-JSM 6335F). The measurement procedures were the same as described in **3.2.4.1**.

#### *4.2.7.2 Transmission Electronic Microscopy (TEM)*

The core-shell nanostructures of the MCP naoparticles were examined by transmission electron microscope (TEM, JEOL CXII TEM). The measurement procedures were the same as described in **3.2.4.2** except the staining conditions. MCP particles samples were stained by 0.5% w/w phosphotungstic acid (PTA) solution for 5 mins for TEM analysis.

## 4.3 Results and Discussion

### 4.3.1 PMMA/(PNIPAm-MBA)/PEI MCP nanocomposite particles

The preparation and characterization of PMMA/(PNIPAm-MBA)/PEI nanocomposite particles is discussed in detail in this part. PNIPAm is a smart polymer which is well-known for its temperature responsive properties (VPTT at 32 °C). The success in forming MCP particles containing pH responsive PEI and thermal responsive PNIPAm would allow us to prepare multi-responsive composite particles for advance applications. After the formation of MBA crosslinked PNIPAm/PEI seed particles, MMA was introduced to undergo seeded emulsion polymerization. Scheme 4.1 shows the reaction route and conditions to prepare these particles.

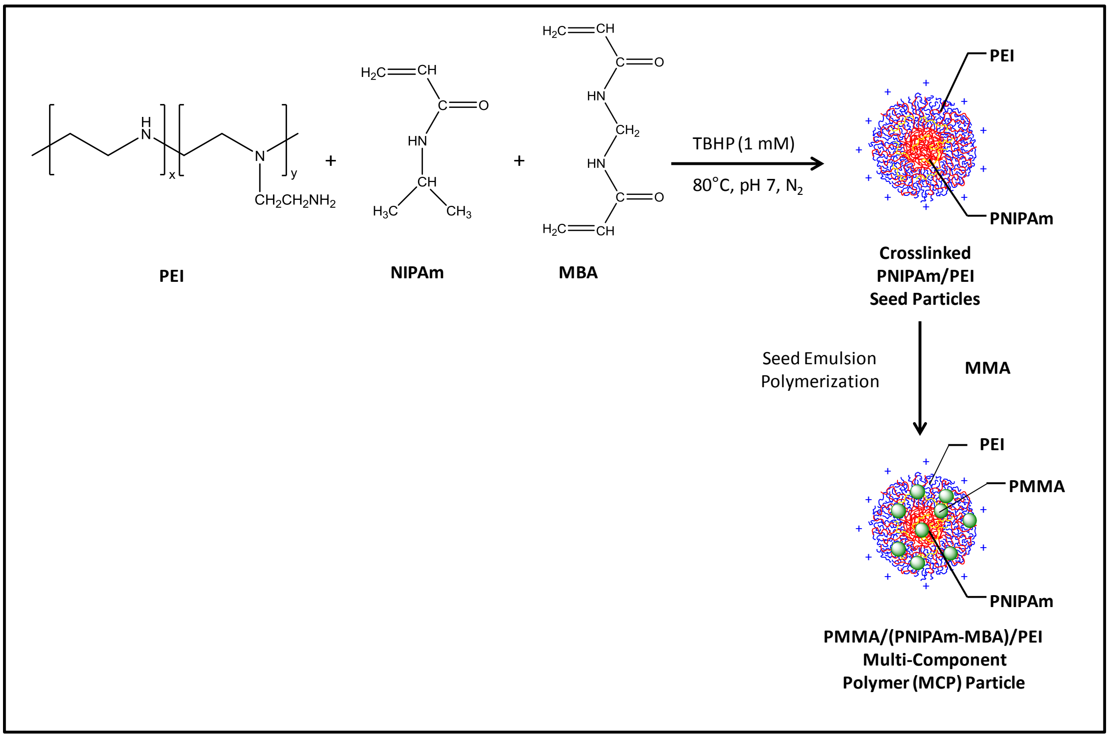

**Scheme 4.1.** Reaction scheme for the synthesis of PMMA/(PNIPAm-MBA)/PEI MCP particles.

### *4.3.1.1 Kinetic study of the polymerization process*

The reaction kinetics of the seeded emulsion polymerization of MCP nanocomposites was monitored by thermal couple (Testo 735) with 1 temperature recorded per second. Figure 4.2 shows the temperature profile of the polymerization at different stages of reaction.

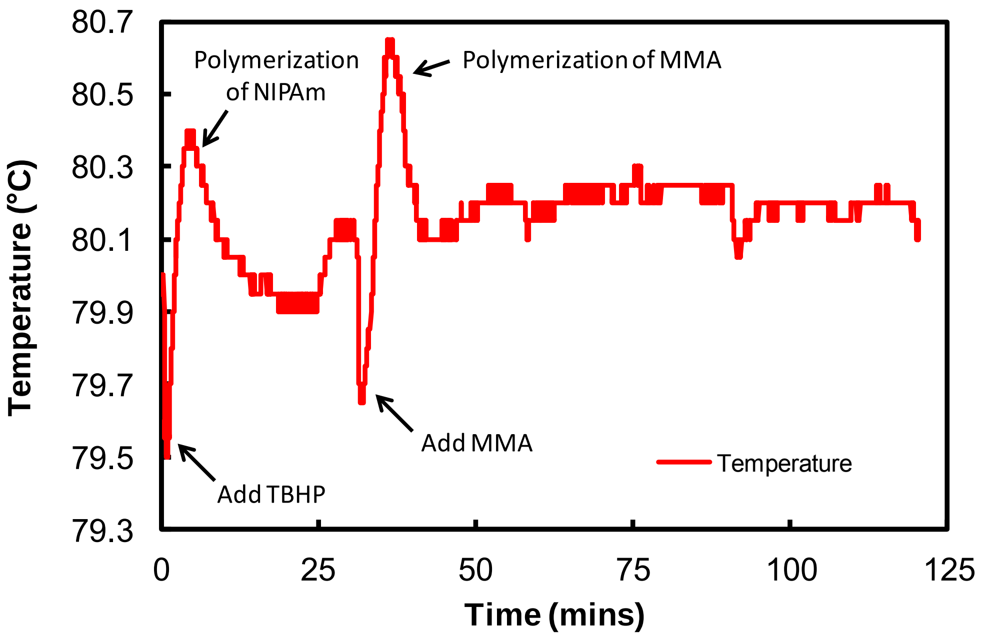

**Fig. 4.2.** Reaction temperature profile during the synthesis of PMMA/(PNIPAm-MBA)/PEI composite particles.

When the temperature of PEI, NIPAm and MBA mixture reached equilibrium (around 80 °C), appropriate amount of initiator (TBHP) was added to the reaction mixture to initiate the polymerization. Once TBHP was added, the reaction temperature was first slightly dropped and then rose up rapidly. After consuming most of the NIPAm monomers, the exothermic polymerization was almost finished and the temperature of the reaction mixture dropped to the original level.

As the temperature fell back to 80 °C, the second batch of monomer, MMA, was introduced into the reaction mixture to perform seeded emulsion polymerization. Similarly, an increased in temperature was observed after the addition of styrene. This increase was contributed by an exothermic polymerization of MMA inside MBA crosslinked PNIPAm/PEI seed particles. Rapid increase in temperature was observed during seeded emulsion polymerization. The solubility MMA monomers in water (15 g/L at 25℃) is sufficient to allow fast diffusion of MMA from bulk aqueous phase into the growing seed particles. The fast diffusion of hydrophobic monomers into the growing particles leads to fast polymerization. Therefore, exothermic peak of the MMA polymerization was as sharp and narrow as the exothermic peak contributed by NIPAm polymerization.

In addition to temperature variation, the polymerization kinetics was also monitored by monomer conversion at different stage of polymerization. The total monomer conversion at different time interval is shown in Table 4.3. After the first stage of polymerization, NIPAm monomer conversion reached 99%. In the second stage of polymerization, MMA monomer was charged to proceed seeded emulsion polymerization. When the exothermic polymerization was completed, the total monomer conversion had reached 90% at the end of polymerization. The variation of hydrodynamic diameters of MCP particles throughout the polymerization process was evaluated by particle size measurement at different time intervals. Upon seed emulsion polymerization, we hypothesized that the hydrodynamic diameter of the MCP particles should be greater than seed particles. Since second batch monomers were hydrophobic, they were more preferred to be diffused into the growing seed particles for polymerization. From the result of particle size measurement, the hydrodynamic diameters of the seed particles ad MCP particles were 307.1 nm and 352.6 nm respectively. The increment in the hydrodynamic diameter of the particles was about 14.8%. Such a small increase in particle size indicates that the seed particles were highly swollen because of the hydrogel structure of the MBA crosslinked PNIPAm/PEI seed particles. Increasing the hydrophobic content into the particles resulted in forming more compacted particles in order to reduce their surface energy of the hydrophobic polymer chains.

**Table 4.3.** Total monomer conversion and particle size of MCP particles at different time intervals.

| **Reaction time[1] (mins)** | **Type of particles** | **Monomer conversion[2] (%)** | **$Z_{AVE}$[3] (nm)** |
|---|---|---|---|
| 30 | MBA crosslinked PNIPAm/PEI seed | 99%[4] | 307.1 |
| 32 | PMMA/(PNIPAm-MBA)/PEI MCP | 58%[5] | 341.4 |
| 34 | PMMA/(PNIPAm-MBA)/PEI MCP | 64%[5] | 361.7 |
| 36 | PMMA/(PNIPAm-MBA)/PEI MCP | 79%[5] | 290.0 |
| 40 | PMMA/(PNIPAm-MBA)/PEI MCP | 82%[5] | 311.6 |
| 75 | PMMA/(PNIPAm-MBA)/PEI MCP | 93%[5] | 291.1 |
| 120 | PMMA/(PNIPAm-MBA)/PEI MCP | 90%[5] | 352.6 |

[1] The reaction was counted since the addition of initiator into the reaction mixture

[2] The total monomer conversion of MCP particles were determined gravimetrically

[3] The hydrodynamic diameter of MCP particles were determined by DLS at 25 °C

[4] The monomer conversion was calculated based on total NIPAm monomer added

[5] The monomer conversion was calculated based on total monmer added

#### *4.3.1.2 Effect of degree of crosslinking*

The effect of MBA crosslinking on the properties of PNIPAm/PEI based MCP particles was studied by varying the weight ratio between NIPAm monomer and MBA crosslinker, keeping other reagents unchanged. The characteristics of PMMA/(PNIPAm-MBA)/PEI MCP particles with different degree of crosslinking were shown in Table 4.4. Independent of the crosslinking degree, all the MCP particles had reached high total monomer conversion at the end of polymerization (over 90%). The hydrodynamic diameter of MBA crosslinked PNIPAm/PEI seed hydrogel was ranged from 250 nm to 400 nm, while the hydrodynamic diameter of PMMA/(PNIPAm-MBA)/PEI MCP particles was ranged from 250 nm to 350 nm. In most of the cases, the hydrodynamic diameter of the seed hydrogels was slightly larger than MCP particles. Since the particle size distribution of PMMA/(PNIPAm-MBA)/PEI was narrow (PDI < 0.2), the smaller hydrodynamic diameter of MCP particles was not caused by secondary nucleation. The larger hydrodynamic diameter of seed hydrogels was contributed by the hydrogel structure of PNIPAm, which was highly extended in aqueous phase at room temperature. After seed emulsion polymerization, second batch monomer was polymerized inside the seed hydrogels. The formation of the third polymeric component in the particle core locked the PNIPAm/PEI hydrogels and thus resulted in smaller hydrodynamic diameter. More importantly, the surface charge of MCP particles was inversely proportional to the crosslinking degree of MBA. Though the ζ-potential of PNIPAm/PEI seed hydrogels was around + 15 mV at 10%, 5% and 2% MBA crosslinking, the effect of MBA crosslinking on the ζ-potential of MCP was significant. A descending trend in the ζ-potential of MCP particles was observed as the degree of MBA crosslinking increased. The ζ-potential of PMMA/(PNIPAm-MBA)/PEI MCP particles with 10%, 5% and 2% MBA crosslinking were + 30.58 mV, + 18.71 mV and + 13.32 mV at pH 7 under room temperature respectively. This trend could be interpreted by the confinement of PNIPAm at different degree of crosslinking which will be further discussed in the later session. PMMA/(PNIPAm-MBA)/PEI MCP particles with high total monomer conversion, nanosized dimension and desirable colloidal stability were successfully prepared with 10%, 5% and 2% MBA crosslinking.

**Table 4.4.** Characteristics of PNIPAm/PEI seed hydrogel and PMMA/(PNIPAm-MBA)/PEI MCP particles with different degree of crosslinking.

| Types of Particles | Degree of crosslinking | Monomer conversion[1] | Hydrodynamic diameter (nm)[2] | | | | ζ-potential (mV)[3] | | | |
|---|---|---|---|---|---|---|---|---|---|---|
| | | | Dh (25°C) | Dh (32°C) | Dh (37°C) | $\mathrm{Dh}_{37^\circ C}/\mathrm{Dh}_{25^\circ C}$ | ζ-potential (pH 7) | ζ-potential (25°C) | ζ-potential (32°C) | ζ-potential (39°C) |
| PNIPAm/PEI seed hydrogel | 10% | 99% | 273.6 | 253.1 | 217.2 | 0.79 | + 15.49 | + 15.49 | + 20.08 | + 30.42 |
| | 5% | 99% | 318.5 | 292.6 | 249.8 | 0.78 | + 14.79 | + 14.79 | + 25.75 | + 38.84 |
| | 2% | 99% | 383.6 | 360.6 | 289.9 | 0.76 | + 12.78 | + 12.78 | + 17.52 | + 38.43 |
| PMMA/(PNIPAm-MBA)/PEI MCP particles | 10% | 93% | 348.8 | 304.4 | 276.3 | 0.79 | + 30.58 | + 30.58 | + 39.25 | + 39.28 |
| | 5% | 91% | 287.9 | 281.5 | 249.0 | 0.86 | + 18.71 | + 18.71 | + 29.13 | + 30.56 |
| | 2% | 90% | 352.6 | 327.3 | 262.9 | 0.75 | + 13.32 | + 13.32 | + 22.44 | + 37.22 |

---

[1] The monomer conversion was determined gravimetrically

[2] The hydrodynamic diameter of MCP particles was determined by DLS at specific temperature and the samples were thermally equilibrated for 10 mins prior measurement

[3] The colloidal stability of MCP particles was determined by ζ-potential measurement using 1 mM NaCl as medium and the samples were thermally equilibrated for 10 mins prior measurement

### 4.3.2 Characterization of PMMA/(PNIPAm-MBA)/PEI nanocomposite particles

#### *4.3.2.1 Composition*

The composition of the PMMA/(PNIPAm-MBA)/PEI MCP particles was investigated by FT-IR spectroscopy. The particles were first purified by repeated centrifugation to get rid of any unreacted PEI and monomers. Figure 4.3a shows the FT-IR spectrum of MBA-crosslinked PNIPAm/PEI seed particles. Strong C=O amide stretching peak observed at 1650 to 1660 $cm^{-1}$, strong N-H amide II bending peak observed at 1535 $cm^{-1}$ and isopropyl C-H peak observed at 1370 to 1390 $cm^{-1}$ suggest the presence of PNIPAm. Both broad amino N-H stretching peak of primary amine at 3400 to 3500 $cm^{-1}$, and C-H stretching and bending at 2900 to 3000 $cm^{-1}$ indicate the presence of PEI. Figure 4.3b shows the FT-IR spectrum of PMMA/(PNIPAm-MBA)/PEI MCP particles. Additional strong carbonyl C=O peak was observed in 1730 $cm^{-1}$ and strong -C-O- ester peak was appeared at 1150 to 1300 $cm^{-1}$, suggesting the presence of PMMA. These characteristic peaks confirm the presence of polystyrene in the MCP particles. Based on the FTIR results, we can confirm that the MCP particles comprise of PEI, PNIPAm and PMMA components.

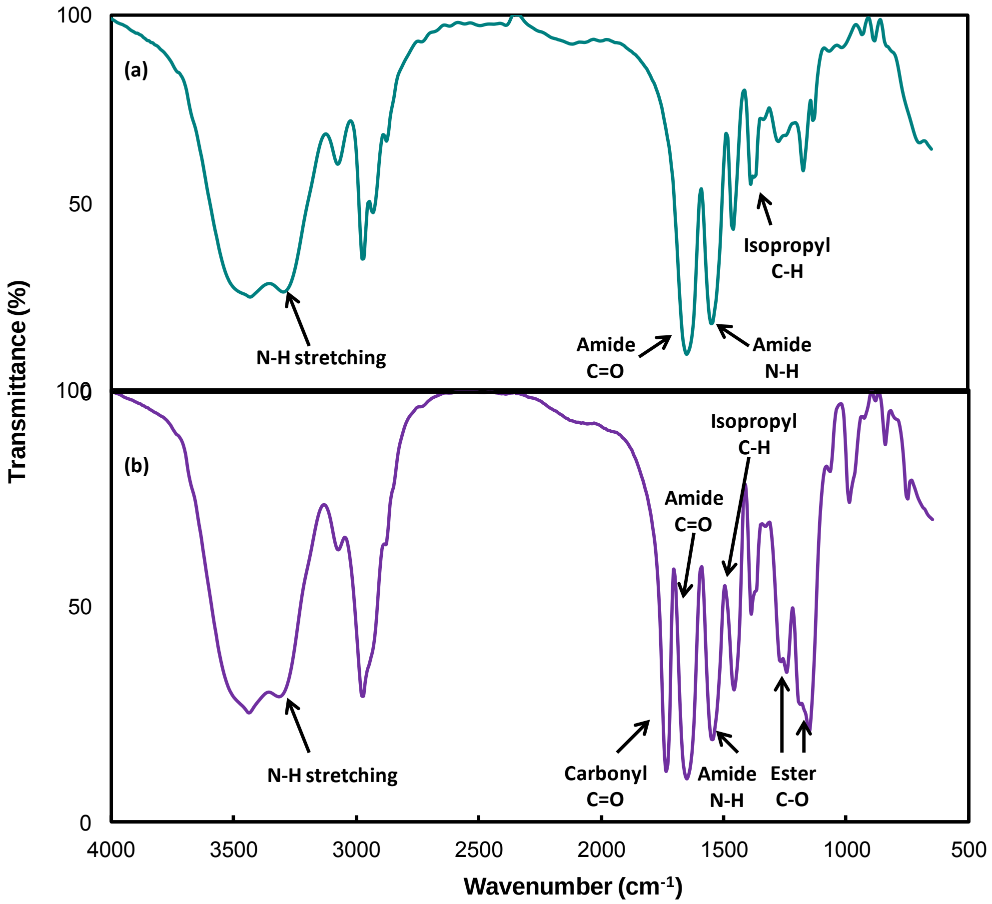

**Fig. 4.3.** FT-IR spectrum of a) 2% MBA crosslinked PNIPAm/PEI seed hydrogel; and b) PMMA/(2% MBA crosslinked PNIPAm-PEI) MCP particles.

### *4.3.2.2 PEI content*

The amount of unbounded PEI in MCP particles was determined by titration method. MCP particles were first purified by repeated centrifugation and all the supernatants were collected. These supernatants were then titrated against 0.025 M NaOH solution and the variation of pH and conductivity was monitored by integrated pH/conductivity meter. Compared with the calibration plot of PEI, the percentage of unreacted PEI in PMMA/(PNIPAm-10% MBA)/PEI, PMMA/(PNIPAm-5% MBA)/PEI and PMMA/(PNIPAm-2% MBA)/PEI were

53.23%, 44.88% and 54.28% respectively. The PEI grafting efficiency was independent of the amount of crosslinker (MBA) added. These results suggested that only 50% of PEI was implemented in the fabrication of PNIPAm/PEI based MCP particles. Assuming the reaction had reached complete conversion at the end of polymerization, the composition of PEI in PMMA/(PNIPAm-MBA)/PEI was ranged from 10% to 12%.

#### *4.3.2.3 Particle size as a function of temperature*

***Particle size***

The hydrodynamic diameters ($Z_{AVE}$) and particle size distribution (PDI) of seed and MCP particles were determined by dynamic light scattering (DLS) at pH 7 using a Beckman Coulter Delsa Nano C instrument. Figure 4.4 compares their particle sizes and size distributions. The hydrodynamic diameter and particle size distribution of seed particles were 383.6 nm and 0.127. While the hydrodynamic diameter and particle size distribution of MCP particles were 352.6 nm and 0.118. These results indicated that the prepared MCP particles were in nano-sized dimension and with narrow size distribution.

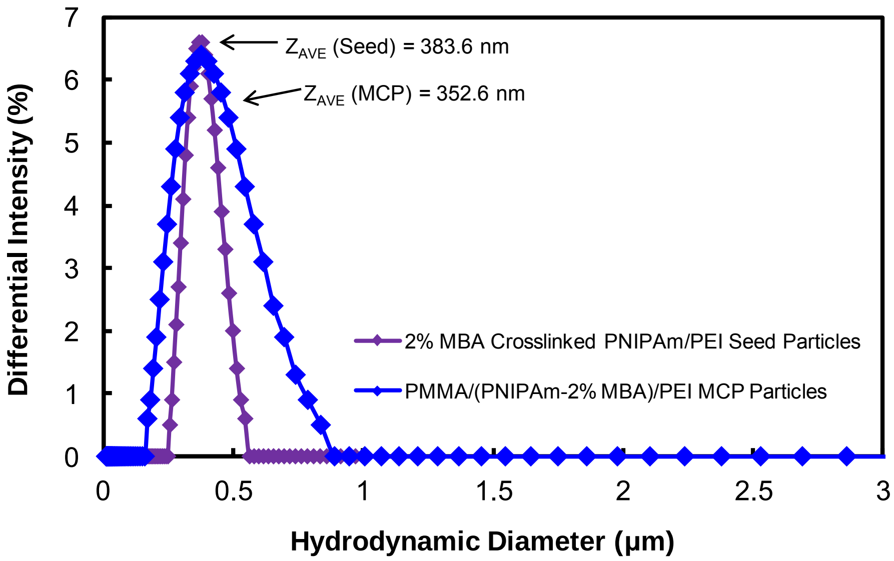

**Fig. 4.4.** Particle sizes of MBA crosslinked PNIPAm/PEI seed particles (383.6 nm) and PMMA/(2% MBA crosslinked PNIPAm-PEI) MCP particles (352.6 nm).

***Particle size as a function of temperature***

The effect of temperature on the hydrodynamic diameter of the PMMA/(PNIPAm-MBA)/PEI MCP particles at different crosslinking degree was evaluated by DLS measurement at different temperatures (25 °C, 27 °C, 29 °C, 32 °C, 35°C, and 37 °C). These MCP particles were thermally equilibrated at the preset temperature for 10 mins prior measurement. The variation of the hydrodynamic diameter of PMMA/(PNIPAm-MBA)/PEI MCP particles as a function of temperature was illustrated in Table 4.5.

Below VPTT (32 °C) of PNIPAm, there was no significant changes in the hydrodynamic diameters of PMMA/(PNIPAm-MBA)/PEI MCP particles. When the temperature was elevated to 32 °C, there was a remarkable drop in the hydrodynamic diameter of the MCP particles. The reduction in the particle size of

MCP particles was attributed to the phase transition of PNIPAm from hydrophilic to hydrophobic. During phase transition, the intermolecular hydrogen bond between PNIPAm and $H_2O$ was broken down, and intramolecular hydrogen bond was formed between the amide oxygen and amide hydrogen in neighbouring PNIPAm instead. This resulted in coil-to-globule transition of PNIPAm and water molecules were expelled from PNIPAm. This eventually caused particle shrinkage which reflected by a reduction in hydrodynamic diameter. As the temperature further increased, there was no significant change in the particle size. This indicated the particle shrinkage was only due to the volume phase transition of PNIPAm. In addition, no shift in the VPTT of PNIPAm was observed. This was due to the formation of PNIPAm/PEI graft copolymer instead of PNIPAm/PEI linear copolymer during the polymerization. Hence, the VPTT of PNIPAm was not affected.

To further evaluate the thermal responsive properties of the MCP particles, the hydrodynamic diameter was re-expressed as normalized hydrodynamic diameter which demonstrated the thermal responsive properties of MCP particles quantitatively. The normalized hydrodynamic diameter of 10%, 5% and 2% PMMA/(PNIPAm-MBA)/PEI MCP particles at 37 °C ($Dh_{37\,°C}/Dh_{25\,°C}$) were 0.79, 0.86 and 0.75 respectively.

The reduction in particle size was more significant in MCP particles at low crosslinking degree. Under higher crosslinking degree, PNIPAm were highly constrained by MBA during phase transition. The coil-to-globule transition of PNIPAm was inhibited which led to little shrinkage in particle size. On the contrary, PNIPAm was less constrained by MBA under low crosslinking degree.

The coil-to-glubole transition of PNIPAm was not inhibited by the crosslinker. Hence, more significant reduction in particle size was observed in MCP particles at lower crosslinking degree.

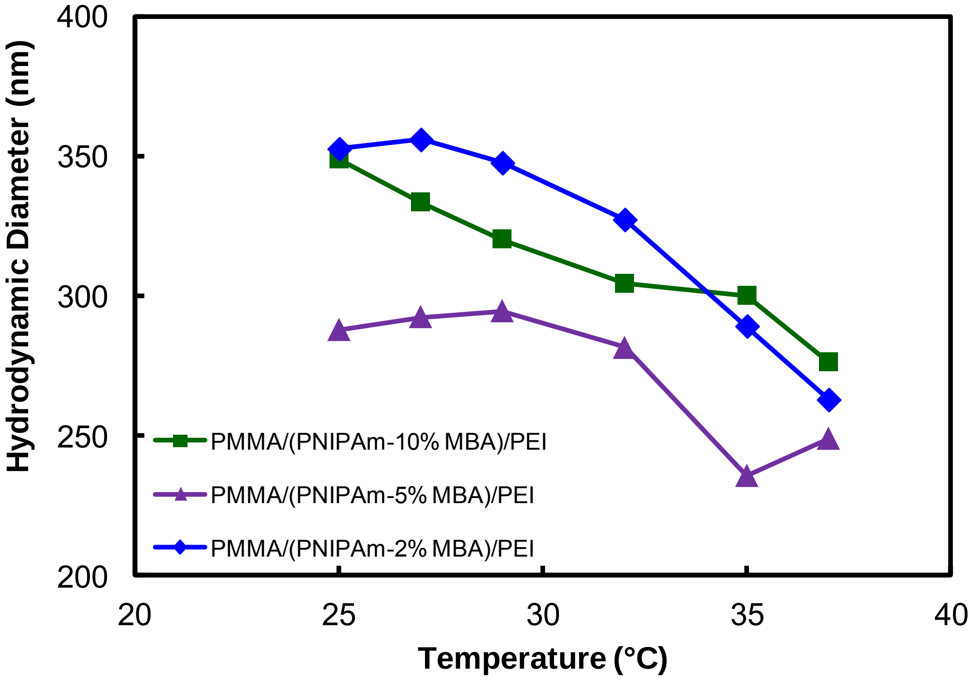

**Fig. 4.5.** Particle size as a function of temperature of PMMA/(PNIPAm-MBA)/PEI MCP particles ($w_{PEI} : w_{NIPAm} : w_{MMA} = 1 : 2 : 2$).

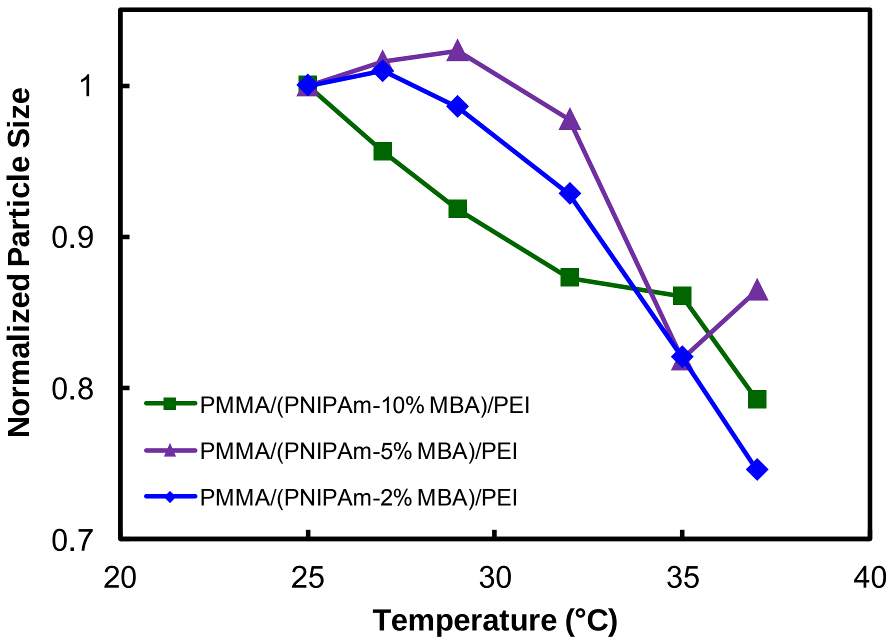

**Fig. 4.6.** Normalized particle size ($Dh/Dh_{25\ °C}$) as a function of temperature of PMMA/(PNIPAm-MBA)/PEI MCP particles ($w_{PEI} : w_{NIPAm} : w_{MMA} = 1 : 2 : 2$).

### *4.3.2.4 Surface charges of particles as a function of pH and temperature*

The surface charge of MCP particles was determined by ζ-potential measurement using a Beckman Coulter Delsa Nano C instrument. Under standard condition, pH 7 with conducting medium of 1 mM NaCl, the ζ-potential of PNIPAm/PEI seed and PMMA/(PNIPAm-MBA)/PEI MCP particles were + 12.78 mV and + 13.72 mV at 25 °C respectively. Generally, Colloidal particles are regarded as stable if the ζ-potential magnitude was greater than +/- 20 mV. The ζ-potential of PNIPAm/PEI seed and MCP particles were lower than this reference value. In fact, these particles still possessed good colloidal stability without formation of aggregates of precipitation. The major reason for this phenomenon was the formation of PNIPAm-PEI interpenetrated shell. PNIPAm was a hydrophilic polymer below its VPTT (32 °C). Hydrophilic PNIPAm was highly extended in the outermost shell of the particles, forming an interpenetrated network with PEI. As a result, the ζ-potential of MCP particles was suppressed due to the charge shielding of PEI by PNIPAm. Though the ζ-potential of the particles suppressed, MCP particles exhibited good colloidal stability because of the presence of hydrophilic PNIPAm in the outermost shell.

### *Surface charges of particles as a function of pH*

The effect of pH on the ζ-potential of MCP particles at was evaluated by ζ-potential measurement using Delsa Nano C with the aid of auto-titrator. In all measurements, MCP particles were first diluted to 200 ppm by 1 mM NaCl solution. The samples were thermally equilibrated at 25 °C for 10 mins before ζ-potential measurement. The variation of ζ-potential as a function of pH of MCP particles with different degree of crosslinking was illustrated in Figure 4.7.

Independent of the crosslinking degree, the surface of PMMA/(PNIPAm-MBA)/PEI MCP particles was positively charged and the ζ-potential almost remains unchanged below pH 7. The positive ζ-potential of MCP particles was contributed by the protonated amino groups of PEI located at the outermost shell of the MCP particles. As the pH of the medium was raised to above 7, there was a drop in the ζ-potential of MCP particles. The drop in ζ-potential was due to the deprotonation of the amino groups. Eventually, the ζ-potential of MCP particles was dropped to about zero as the pH of the medium was approached 9.5, isoelectric point of PEI.

Although PMMA/(PNIPAm-MBA)/PEI MCP particles with different crosslinking degree had the same trend in the variation of ζ-potential against pH, the ζ-potential was decareased as the degree of crosslinking decreased. The ζ-potential of PMMA/(PNIPAm-MBA)/PEI MCP particles with 10%, 5% and 2% crosslinking at pH 7 were + 30.58 mV, + 18.71 mV and + 13.32 mV respectively. The magnitude of ζ-potential of MCP particles was suppressed from + 30.58 mV to + 13.32 mV as the degree of crosslinking decreased from 10% to 2%. The crosslinking degree had significant impact on the formation of interpenetration network in the outermost shell of MCP particles. At low MBA crosslinking, PNIPAm was not confined by the crosslinker and was freely extended in the outermost shell of the particles. Hydrophilic PNIPAm formed an interpenetrated network with PEI, constructing an interpenetrated outer shell. The positive charges on the particle shell were shielded by PNIPAm, resulting in a suppression of the ζ-potential. On the contrary, PNIPAm was constrained by the crosslinker under high MBA content. PNIPAm was slightly interpenetrated with PEI that caused partial shielding on the positive charges of PEI. As a result, there was no significant suppression in ζ-potential of MCP particles under high crosslinking degree.

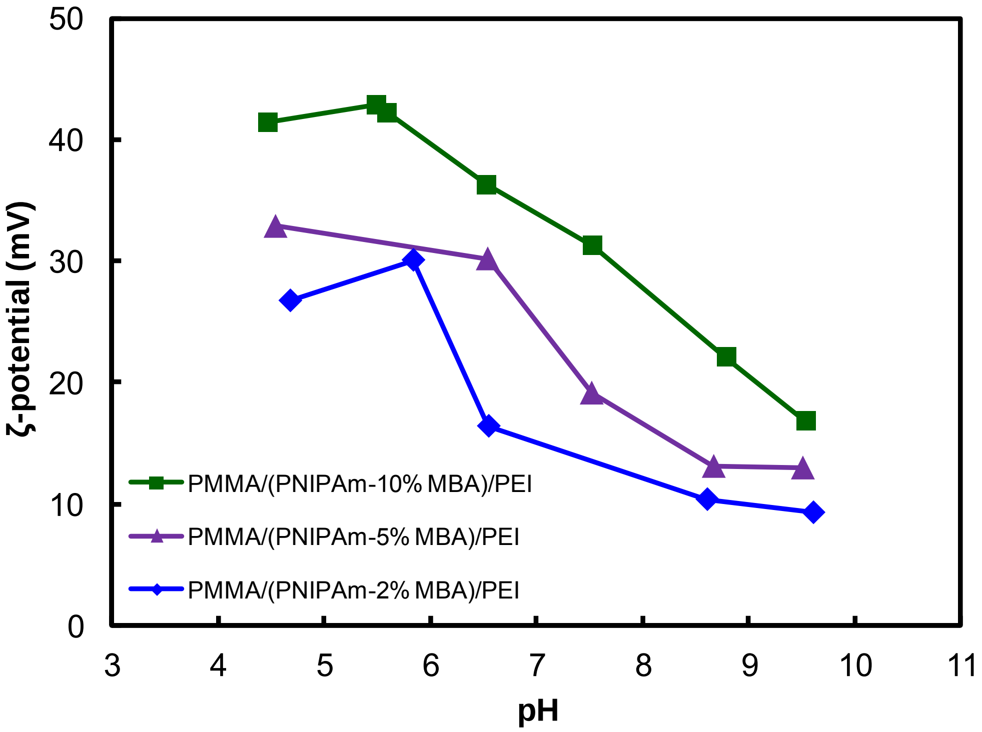

**Fig. 4.7.** ζ-potential as a function of pH of PMMA/(PNIPAm-MBA)/PEI MCP particles ($w_{PEI}$ : $w_{NIPAm}$ : $w_{MMA}$ = 1 : 2 : 2).

### *Surface charge of particles as a function of temperature*

The effect of temperature on the ζ-potential of MCP particles at different crosslinking degree was evaluated by ζ-potential measurement using Delsa Nano C with the aid of thermal monitoring device. In all measurements, MCP particles were first diluted to 200 ppm by 1 mM NaCl solution. The pH of the MCP particle samples was adjusted to 7 for the measurement. The samples were thermally equilibrated at preset temperature (25 °C, 27 °C, 29 °C, 32 °C, 35 °C, 37 °C and 39 °C) for 10 mins before ζ-potential measurement. The variation of ζ-potential as a function of temperature of MCP particles with different degree of crosslinking was illustrated in Figure 4.8.

Regardless of the degree of crosslinking, there was a general trend in the variation of ζ-potential of PMMA/(PNIPAm-MBA)/PEI MCP particles as temperature increaserd. Below VPTT of PNIPAm (32 ℃), MCP particles had positive magnitude in ζ-potential and the ζ-potential was kept constant in this temperature range. As the temperature was raised to the VPTT of PNIPAm, there was an abrupt increase in the ζ-potential. When the temperature was further raised, there was no insignificant increase in the ζ-potential. Eventually, the ζ-potential of MCP particles was approached to + 40 mV at 39 ℃.

The change in ζ-potential of MCP particles was contributed by the phase transition of PNIPAm at its VPTT. Below VPTT of PNIPAm, MCP particles exhibited low magnitude in ζ-potential. PNIPAm was a hydrophilic polymer which was ultimately extended in the outer shell of the particles. The formation of interpenetrated network between PNIPAm and PEI in the outermost shell resulted in charge shielding of PEI.

When the temperature was promoted to VPTT (32 ℃), there was an abrupt increase in the ζ-potential of the MCP particles. PNIPAm underwent phase transition which changed from hydrophilic to hydrophobic. The intermolecular hydrogen bonding between PNIPAm and surrounding water molecules was broken down. Instead, intramolecular hydrogen bonding was formed between the amide oxygen and amide hydrogen of the neighbouring PNIPAm. The coil-to-glubole transition of PNIPAm caused shrinkage of PNIPAm from the outer shell to inner core to minimize the interfacial tension. Positively charged PEI was not shielded by PNIPAm. The charge re-exposure of PEI on the particle surface resulted in an increase in the magnitude of ζ-potential.

As discussed before, the crosslinking degree had an important role in the surface charge of the particles. Below the VPTT, hydrophilic PNIPAm was ultimately extended in the outer shell of the particles. The formation of interpenetrated network resulted in charge shielding of PEI. Thus, the ζ-potential of MCP particles was suppressed. Lower crosslinking degree resulted in greater suppression in ζ-potential. However, PNIPAm changed from hydrophilic to hydrophobic as temperature was above its VPTT. The phase transition of PNIPAm resulted in migration of PNIPAm from outer shell to inner shell. Hence, the positively charged PEI was re-exposed and caused an increase in the ζ-potential. As a result, the outermost shell of the particles was only composed of PEI. At this circumstance, the ζ-potential magnitude of MCP particles under different crosslinking degree was similar to each other as PNIPAm was migrated to the inner core.

The descending order of ζ-potential of PMMA/(PNIPAm-MBA)/PEI at 25 ℃ can be expressed as:

***10% MBA crosslinked MCP > 5% MBA crosslinked MCP > 2% MBA crosslinked MCP***

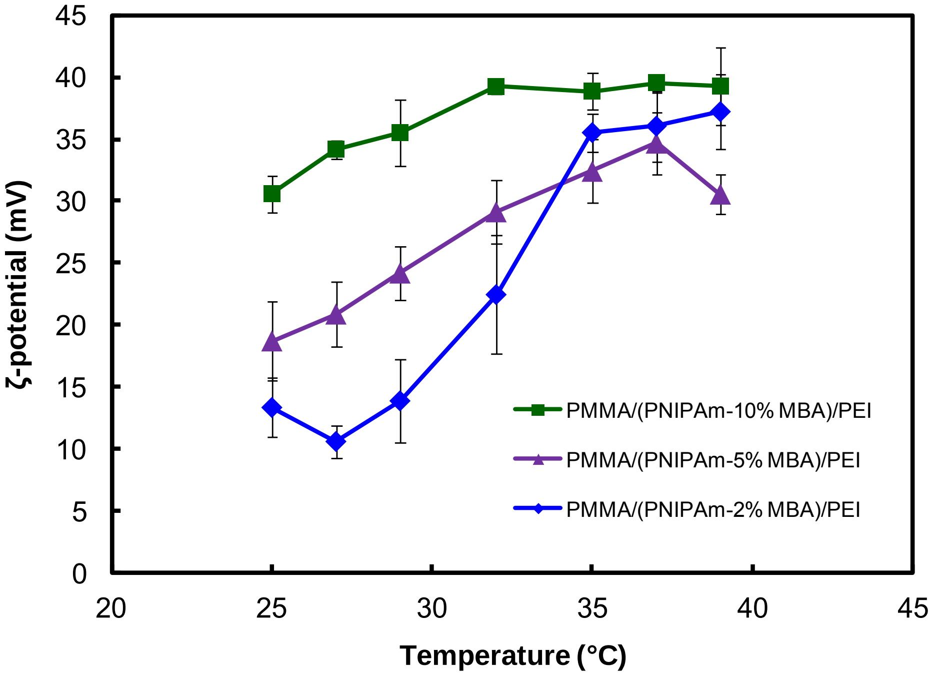

**Fig. 4.8.** ζ-potential as a function of temperature of PMMA/(PNIPAm-MBA)/PEI MCP particles ($w_{PEI} : w_{NIPAm} : w_{MMA} = 1 : 2 : 2$).

### *4.3.2.5 Morphology*

The morphology and core-shell nanostructure of PMMA/(PNIPAm-MBA)/PEI MCP particles with different degree of crosslinking (10%, 5% and 2%) were examined by FE-SEM and TEM. Well-defined core-shell nanostructure of MBA crosslinked PNIPAm/PEI seed particles was observed in TEM micrographs. The dark core of the particles was the heavily stained PNIPAm and the bright shell was the slightly stained PEI.

Highly uniform particles with special aerolite-like morphology was observed in the SEM micrographs of all PMMA/(PNIPAm-MBA)/PEI MCP particles. To elucidate the nanostructure of the MCP particles, these particles were stained with 0.5% (w/w) phosphotungstic acid (PTA, $WO_2 \cdot H_3PO_4 \cdot xH_2O$) for 5 mins. Numerous bright micro-domains were embedded in the dark corona of the aerolite-like MCP particles. The bright micro-domains were solely PMMA and the dark corona was composed of interpenetrated network PNIPAm and PEI. These micro-domains of PMMA were freely distributed inside the MCP particles.

Formation of this special nanostructure was due to high water solubility of MMA. The water solubility of MMA was 15 g/L under room temperature. High solubility of MMA monomer in water effectively facilitated the dissolve and then diffusion from the aqueous continuous phase into the growing particle core. In addition, the rate of initiation of MMA monomers was fast that MMA monomers were initiated once entered the growing particles. Due to the fast polymerization of MMA, numerous micro-domains of PMMA were formed inside PMMA/(PNIPAm-MBA)/PEI MCP particles. As a result, kinetic favored metastable aerolite morphology was achieved.

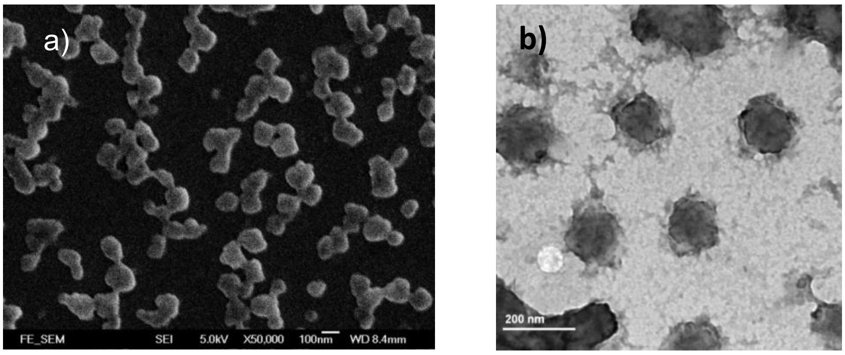

**Fig. 4.9.** Morphology of PMMA/(PNIPAm-10% MBA)/PEI MCP particles: a) FE-SEM image; and b) TEM micrographs.

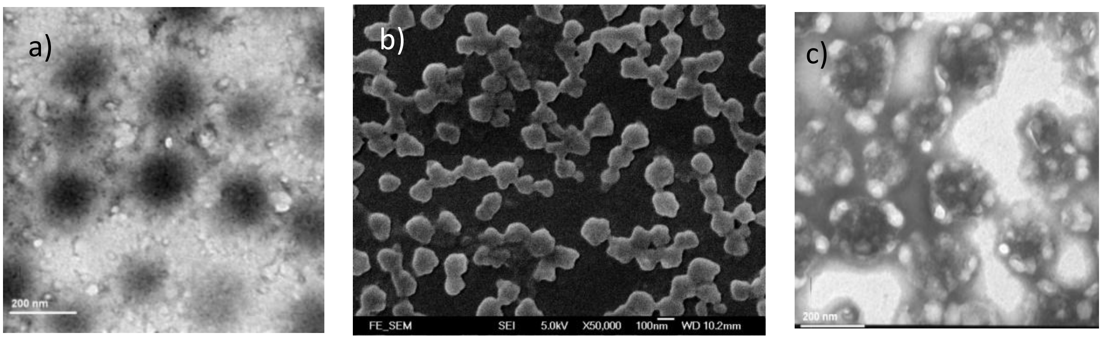

**Fig. 4.10.** Morphology of PNIPAm/PEI seed particles (5% MBA crosslinked): a) TEM image; Morphology of PMMA/(PNIPAm-5% MBA)/PEI MCP particles: b) FE-SEM image; c) TEM image.

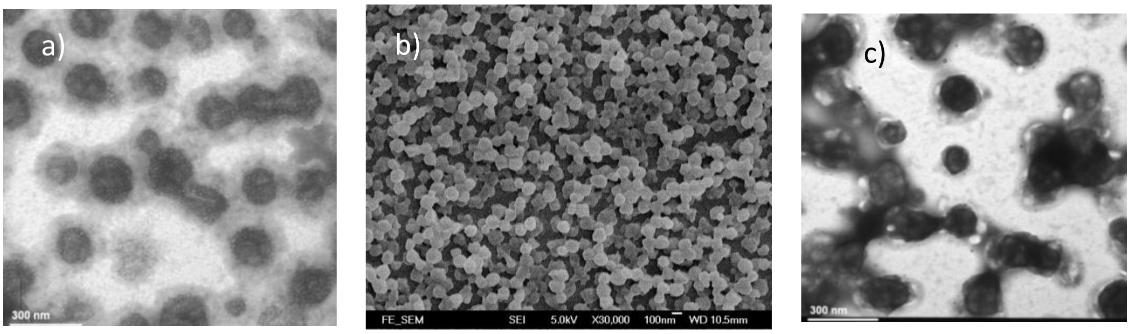

**Fig. 4.11.** Morphology of PNIPAm/PEI seed particles (2% MBA crosslinked): a) TEM image; Morphology of PMMA/(PNIPAm-2% MBA)/PEI MCP particles: b) FE-SEM image; c) TEM image.

### 4.3.3 PBA/(PNIPAm-MBA)/PEI MCP nanocomposite particles

The preparation and characterization of PBA/(PNIPAm-MBA)/PEI nanocomposite particles is discussed in detail in this part. PBA is a polymer with low glass transition temperature ($T_g$ ~ 219 K). The success in incorporating PBA into smart MCP particles allows us to prepare smart MCP particles with good film forming properties for smart coating applications. After the formation of MBA crosslinked PNIPAm/PEI seed particles, *n*-BA was introduced to undergo seeded emulsion polymerization. Scheme 4.2 shows the reaction route and conditions to prepare these particles.

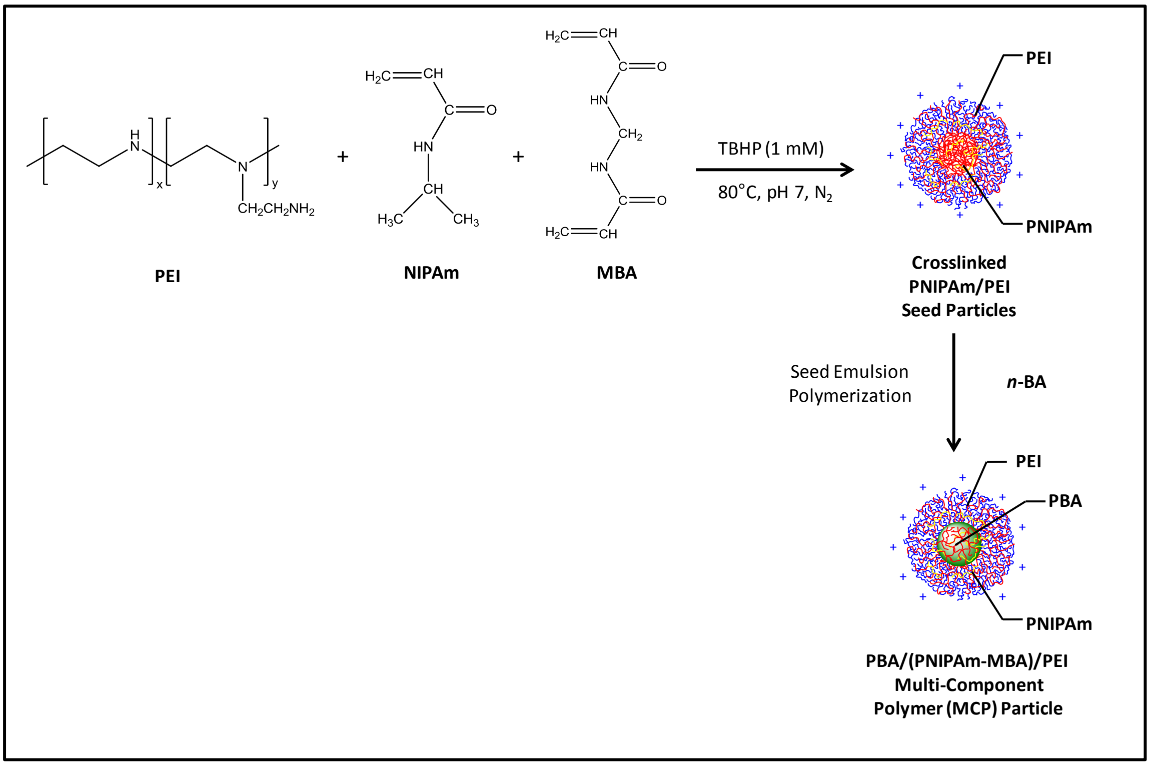

**Scheme 4.2.** Reaction scheme for the synthesis of PBA/(PNIPAm-MBA)/PEI MCP particles.

#### *4.3.3.1 Kinetic study of the polymerization process*

The reaction kinetics of the seeded emulsion polymerization of MCP nanocomposites was monitored by thermal couple (Testo 735) with 1 temperature recorded per second. Figure 4.12 shows the temperature profile of the polymerization at different stages of reaction.

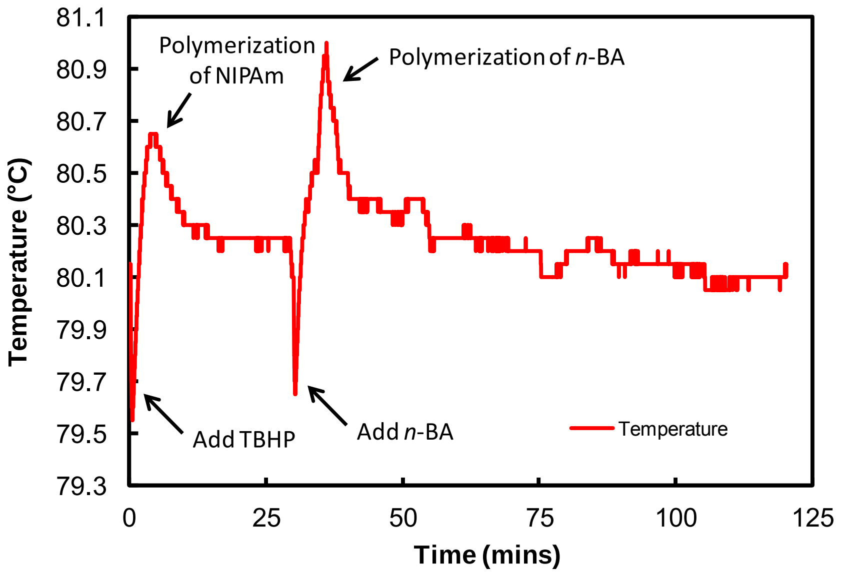

**Fig. 4.12.** Reaction temperature profile during the synthesis of PBA/(PNIPAm-MBA)/PEI composite particles.

When the temperature of PEI, NIPAm and MBA mixture reached equilibrium (around 80 ℃), appropriate amount of initiator (TBHP) was added to the reaction mixture to initiate the polymerization. Once TBHP was added, the reaction temperature was first slightly dropped and then rose up rapidly. After consuming most of the NIPAm monomers, the exothermic polymerization was almost finished and the temperature of the reaction mixture dropped to the original level.

As the temperature fell back to 80 ℃, the second batch of monomer, *n*-BA, was introduced into the reaction mixture to perform seeded emulsion polymerization. Similarly, an increased in temperature was observed after the addition of *n*-BA. This increase was contributed by an exothermic polymerization of *n*-BA inside MBA crosslinked PNIPAm/PEI seed particles. Rapid increase in temperature was observed during seeded emulsion polymerization. This indicated the diffusion of *n*-BA monomers from bulk aqueous phase into the growing seed particles was fast. The fast diffusion of hydrophobic monomers into the growing particles leads to fast polymerization. Therefore, exothermic peak of the *n*-BA polymerization was as sharp and narrow as the exothermic peak contributed by NIPAm polymerization.

In addition to temperature variation, the polymerization kinetics was also monitored by monomer conversion at different stage of polymerization. The total monomer conversion at different time interval is shown in Table 4.5. After the first stage of polymerization, NIPAm monomer conversion reached 99%. In the second stage of polymerization, *n*-BA monomer was charged to proceed seeded emulsion polymerization. When the exothermic polymerization was completed, the total monomer conversion had reached 91% at the end of polymerization. The variation of hydrodynamic diameters of MCP particles throughout the polymerization process was evaluated by particle size measurement at different time intervals. Upon seed emulsion polymerization, we hypothesized that the hydrodynamic diameter of the MCP particles should be greater than seed particles. Since second batch monomers were hydrophobic, they were more preferred to be diffused into the growing seed particles for polymerization. From the result of particle size measurement, the hydrodynamic diameters of the seed particles ad MCP particles were 390.2 nm and 348.3 nm respectively. The hydrodynamic diameter of the seed particles was slightly larger than the MCP particles, which was due to the hydrogel structure of the MBA crosslinked PNIPAm/PEI seed particles. PNIPAm and PEI are hydrophilic polymers which are highly extended in water. *n*-BA was introduced into the reaction system for seeded emulsion polymerization immediately after the formation of seed microgel. This introduced a hydrophobic component, PBA, to the highly extended PNIPAm/PEI microgel. Increasing the hydrophobic content into the particles resulted in forming more compacted particles in order to reduce their surface energy of the hydrophobic polymer chains. As a result, the PNIPAm/PEI was not as highly extended as in seed microgel. Thus, the hydrodynamic diameter of the (PNIPAm-MBA)/PEI seed microgel was slightly larger than the PBA/(PNIPAm-MBA)/PEI MCP particles.

**Table 4.5.** Total monomer conversion and particle size of MCP particles at different time intervals.

| **Reaction time[1] (mins)** | **Type of particles** | **Monomer conversion[2] (%)** | **$Z_{AVE}$[3] (nm)** |
|---|---|---|---|
| 30 | MBA crosslinked PNIPAm/PEI seed | 99%[4] | 390.2 |
| 34 | PBA/(PNIPAm-MBA)/PEI MCP | 74%[5] | 345.1 |
| 36 | PBA/(PNIPAm-MBA)/PEI MCP | 87%[5] | 388.5 |
| 38 | PBA/(PNIPAm-MBA)/PEI MCP | 93%[5] | 324.2 |
| 55 | PBA/(PNIPAm-MBA)/PEI MCP | 97%[5] | 396.9 |
| 75 | PBA/(PNIPAm-MBA)/PEI MCP | 96%[5] | 364.8 |
| 105 | PBA/(PNIPAm-MBA)/PEI MCP | 90%[5] | 375.8 |
| 120 | PBA/(PNIPAm-MBA)/PEI MCP | 91%[5] | 348.3 |

[1] The reaction was counted since the addition of initiator into the reaction mixture

[2] The total monomer conversion of MCP particles were determined gravimetrically

[3] The hydrodynamic diameter of MCP particles were determined by DLS at 25 °C

[4] The monomer conversion was calculated based on total NIPAm monomer added

[5] The monomer conversion was calculated based on total monmer added

### *4.3.3.2 Effect of degree of crosslinking*

The effect of MBA crosslinking on the properties of PNIPAm/PEI based MCP particles was studied by varying the weight ratio between NIPAm monomer and MBA crosslinker, keeping other reagents unchanged. The characteristics of PBA/(PNIPAm-MBA)/PEI MCP particles with different degree of crosslinking were shown in Table 4.6. Stable colloidal dispersion of PBA/(PNIPAm-MBA)/PEI was obtained only at 5% and 2% MBA crosslinking. Although stable coilloidal dispersion was observed during the synthersis of PBA/(PNIPAm-10% MBA)/PEI, it coagulated like curd as the temperature fell back to room temperature after the polymerization. Curdle formation of PBA/(10%MBA-PNIPAm-PEI) should be attributed by low glass transition ($T_g$) of PBA and high MBA content. The $T_g$ of PBA and PEI were 219 K and 213 K respectively, which were far below room temperature (298 K). These polymers behaved like rubbery due to the low $T_g$. In addition, PNIPAm was hydrogel which was swollen with water and soft in nature. Unlike PMMA/(PNIPAm-MBA)/PEI and PS/(PNIPAm-MBA)/PEI, all the major components in PBA/(PNIPAm-MBA)/PEI were soft and this MCP particle did not possess a rigid solid support. As the room temperature was above the $T_g$ of PBA/(PNIPAm-MBA)/PEI, polymer chains were freely migrated to achieve thermodynamically favored equilibrium morphology. Interparticle crosslinking was taken place when the amount of crosslinker was high (i.e. 10% MBA). High extend of interparticle crosslinking eventually resulted in curdle formation.

PBA/(PNIPAm-MBA)/PEI MCP particles at 5% and 2% MBA had reached high total monomer conversion at the end of polymerization (over 90%).

The hydrodynamic diameter of MBA crosslinked PNIPAm/PEI seed hydrogel was ranged from 250 nm to 400 nm, while the hydrodynamic diameter of PBA/(PNIPAm-MBA)/PEI MCP particles was ranged from 350 nm to 450 nm. In most of the cases, the hydrodynamic diameter of the seed hydrogels was slightly larger than MCP particles. Since the particle size distribution of PBA/(PNIPAm-MBA)/PEI was narrow (PDI < 0.2), the smaller hydrodynamic diameter of MCP particles was not caused by secondary nucleation. The larger hydrodynamic diameter of seed hydrogels was contributed by the hydrogel structure of PNIPAm, which was highly extended in aqueous phase at room temperature. After seed emulsion polymerization, second batch monomer was polymerized inside the seed hydrogels. The formation of the third polymeric component in the particle core locked the PNIPAm/PEI hydrogels and thus resulted in smaller hydrodynamic diameter. The ζ-potential of PNIPAm/PEI seed hydrogels was around + 15.49 mV and + 14.79 mV at 5% and 2% MBA crosslinking. And the ζ-potential of PBA/(PNIPAm-MBA)/PEI MCP particles with 5% and 2% MBA crosslinking were + 5.05 mV and + 4.54 mV at pH 7 under room temperature respectively. The extraordinary low magnitudes in ζ-potential of PBA/(PNIPAm-MBA)/PEI MCP particles will be further discussed in the later session. PBA/(PNIPAm-MBA)/PEI MCP particles with high total monomer conversion, nanosized dimension and desirable colloidal stability were successfully prepared with 5% and 2% MBA crosslinking only.

**Table 4.6.** Characteristics of PNIPAm/PEI seed hydrogel and PBA/(PNIPAm-MBA)/PEI MCP particles with different degree of crosslinking.

| Types of Particles | Degree of crosslinking | Monomer conversion[1] | Hydrodynamic diameter (nm)[2] | | | | ζ-potential (mV)[3] | | | |
|---|---|---|---|---|---|---|---|---|---|---|
| | | | Dh (25°C) | Dh (32°C) | Dh (37°C) | $Dh_{37°C}$/ $Dh_{25°C}$ | ζ-potential (pH 7) | ζ-potential (25°C) | ζ-potential (32°C) | ζ-potential (39°C) |
| PNIPAm/PEI seed hydrogel | 10% | 99% | 273.6 | 253.1 | 217.2 | 0.79 | + 15.49 | + 15.49 | + 20.08 | + 30.42 |
| | 5% | 99% | 318.5 | 292.6 | 249.8 | 0.78 | + 14.79 | + 14.79 | + 25.75 | + 38.84 |
| | 2% | 99% | 383.6 | 360.6 | 289.9 | 0.76 | + 12.78 | + 12.78 | + 17.52 | + 38.43 |
| PBA/(PNIPAm-MBA)/PEI MCP particles | 10% | | Formation of curd (unstable) | | | | | | | |
| | 5% | 98% | 437.4 | 412.7 | 384.0 | 0.88 | + 5.05 | + 5.05 | + 10.86 | + 30.49 |
| | 2% | 91% | 348.3 | 306.0 | 266.1 | 0.76 | + 4.54 | + 4.54 | + 10.11 | + 27.58 |

[1] The monomer conversion was determined gravimetrically

[2] The hydrodynamic diameter of MCP particles was determined by DLS at specific temperature and the samples were thermally equilibrated for 10 mins prior measurement

[3] The colloidal stability of MCP particles was determined by ζ-potential measurement using 1 mM NaCl as medium and the samples were thermally equilibrated for 10 mins prior measurement

### 4.3.4 Characterization of PBA/(PNIPAm-MBA)/PEI nanocomposite particles

#### *4.3.4.1 Composition*

The composition of the PBA/(PNIPAm-MBA)/PEI MCP particles was investigated by FT-IR spectroscopy. The particles were first purified by repeated centrifugation to get rid of any unreacted PEI and monomers. Figure 4.13a shows the FT-IR spectrum of MBA-crosslinked PNIPAm/PEI seed particles. Strong C=O amide stretching peak observed at 1650 to 1660 cm$^{-1}$, strong N-H amide II bending peak observed at 1535 cm$^{-1}$ and isopropyl C-H peak observed at 1370 to 1390 cm$^{-1}$ suggest the presence of PNIPAm. Both broad amino N-H stretching peak of primary amine at 3400 to 3500 cm$^{-1}$, and C-H stretching and bending at 2900 to 3000 cm$^{-1}$ indicate the presence of PEI. Figure 4.13b shows the FT-IR spectrum of PBA/(PNIPAm-MBA)/PEI MCP particles. Additional strong carbonyl C=O peak was observed in 1730 cm$^{-1}$ and strong -C-O- ester peak was appeared at 1150 to 1300 cm$^{-1}$, suggesting the presence of PBA. These characteristic peaks confirm the presence of polystyrene in the MCP particles. Based on the FTIR results, we can confirm that the MCP particles comprise of PEI, PNIPAm and PBA components.

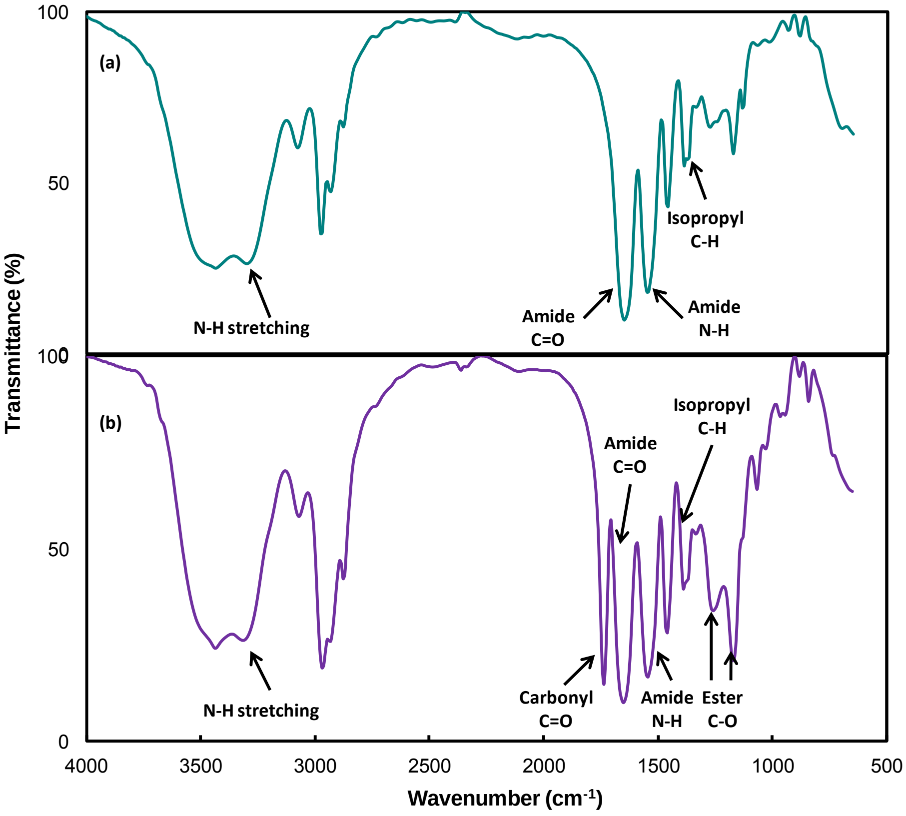

**Fig. 4.13.** FT-IR spectrum of a) 2% MBA crosslinked PNIPAm/PEI seed hydrogel; and b) PBA/(2% MBA crosslinked PNIPAm-PEI) MCP particles

### *4.3.4.2 PEI content*

The amount of unbounded PEI in MCP particles was determined by titration method. MCP particles were first purified by repeated centrifugation and all the supernatants were collected. These supernatants were then titrated against 0.025 M NaOH solution and the variation of pH and conductivity was monitored by integrated pH/conductivity meter. Compared with the calibration plot of PEI, the percentage of unreacted PEI in PBA/(PNIPAm-5% MBA)/PEI and PBA/(PNIPAm-2% MBA)/PEI were 50.24% and 36.88% respectively. The PEI grafting efficiency was independent of the amount of crosslinker (MBA) added.

These results suggested that nearly 60% of PEI was implemented in the fabrication of PNIPAm/PEI based MCP particles. Assuming the reaction had reached complete conversion at the end of polymerization, the composition of PEI in PBA/(PNIPAm-MBA)/PEI was ranged from 11% to 13%.

#### *4.3.4.3 Particle size as a function of temperature*

***Particle size***

The hydrodynamic diameters ($Z_{AVE}$) and particle size distribution (PDI) of seed and MCP particles were determined by dynamic light scattering (DLS) at pH 7 using a Beckman Coulter Delsa Nano C instrument. Figure 4.14 compares their particle sizes and size distributions. The hydrodynamic diameter and particle size distribution of seed particles were 383.6 nm and 0.127. While the hydrodynamic diameter and particle size distribution of MCP particles were 348.3 nm and 0.086. These results indicated that the prepared MCP particles were in nano-sized dimension and with narrow size distribution.

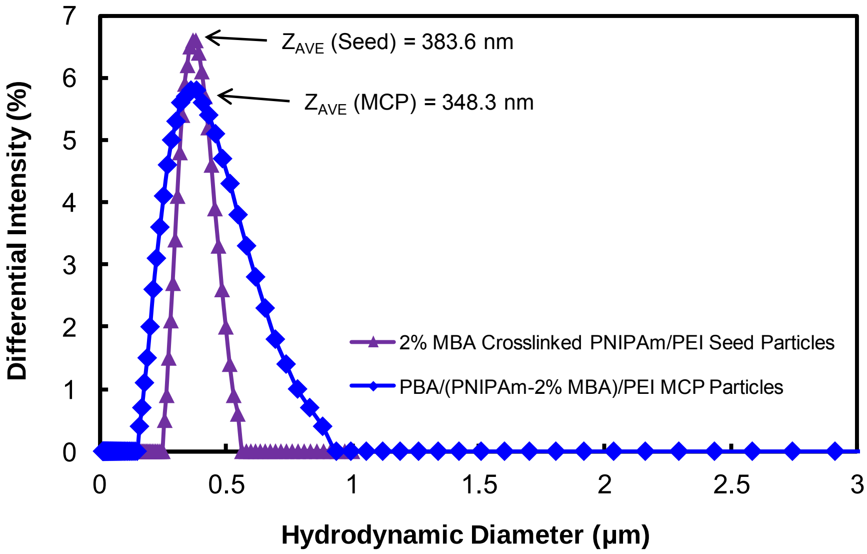

**Fig. 4.14.** Particle sizes of MBA crosslinked PNIPAm/PEI seed particles (383.6 nm) and PBA/(2% MBA crosslinked PNIPAm-PEI) MCP particles (348.3 nm).

### *Particle size as a function of temperature*

The effect of surrounding temperature on the hydrodynamic diameter of the PBA/(PNIPAm-MBA)/PEI MCP particles at different crosslinking degree was evaluated by DLS measurement at different temperatures (25 °C, 27 °C, 29 °C, 32 °C, 35 °C, and 37 °C). The MCP particles were thermally equilibrated at the preset temperature for 10 mins prior measurement. The variation of the hydrodynamic diameter of PBA/(PNIPAm-MBA)/PEI MCP particles as a function of temperature was displayed in Figure 4.15. Below VPTT (32 °C) of PNIPAm, the hydrodynamic diameters of PBA/(PNIPAm-MBA)/PEI MCP particles did not have obvious variation. When the surrounding temperature was elevated to 32 °C, VPTT of PNIPAm, there was a sudden drop in the hydrodynamic diameter of the MCP particles. This implied PNIPAm underwent phase transition which changed from hydrophilic to hydrophobic. The intermolecular hydrogen bond between PNIPAm and $H_2O$ was broken down due to the coil-to-globule transition of PNIPAm. This transition thus caused the shrinkage of the particle size of MCP particles. As the surrounding temperature further increased, there is no significant change in the particle size. This showed that the particle shrinkage was only due to the volume phase transition of PNIPAm. In addition, there was no shift in the VPTT of PNIPAm since PNIPAm/PEI graft copolymer was formed instead of PNIPAm/PEI linear copolymer during seed particle formation.

To further evaluate the thermal responsive properties of the MCP particles, the hydrodynamic diameter was re-expressed as normalized hydrodynamic diameter which demonstrated the thermal responsive properties of MCP particles quantitatively. The normalized hydrodynamic diameter of 5% and 2% PBA/(PNIPAm-MBA)/PEI MCP particles at 37 ℃ ($Dh_{37\,℃}/Dh_{25\,℃}$) were 0.88 and 0.76 respectively. MCP particles exhibited greater thermal responsiveness at lower crosslinking degree. Under higher crosslinking degree, the degree of shrinkage in the particle size was low because PNIPAm was highly crosslinked by MBA. The coil-to-globule transition of PNIPAm was highly constrained by MBA crosslinking. On the contrary, the shrinkage in particle size was more obvious at low crosslinking degree. PNIPAm was not constrained by the MBA crosslinking and underwent coil-to-globule transition as the temperature elevated to above VPTT.

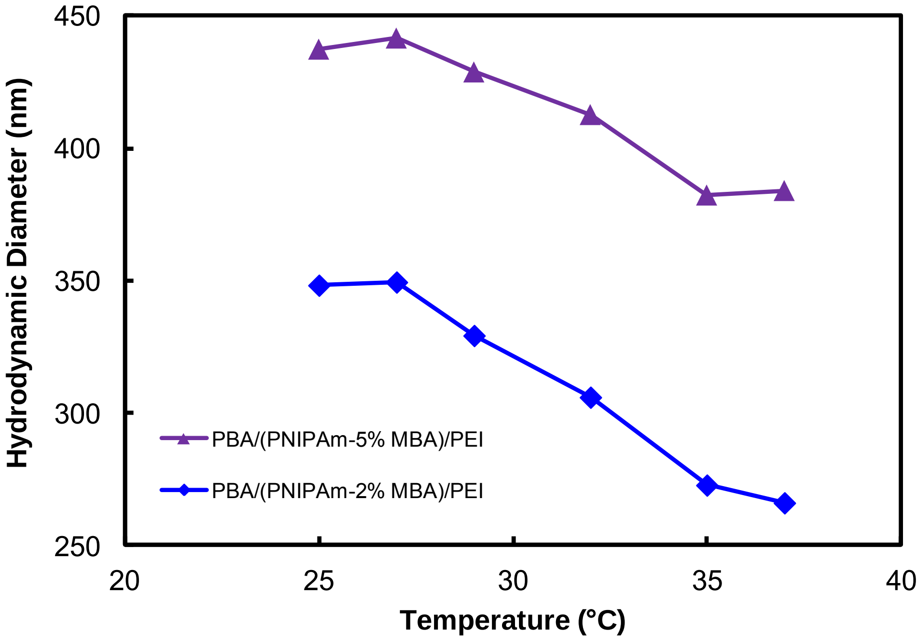

**Fig. 4.15.** Particle size as a function of temperature of PBA/(PNIPAm-MBA)/PEI MCP particles ($w_{PEI} : w_{NIPAm} : w_{n\text{-}BA} = 1 : 2 : 2$).

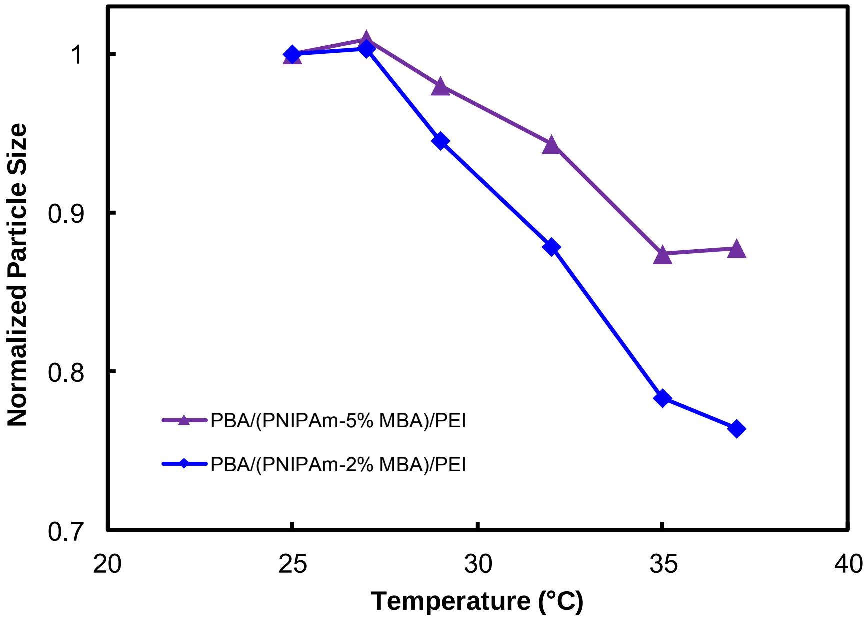

**Fig. 4.16.** Normalized particle size ($Dh/Dh_{25\ °C}$)as a function of temperature of PBA/(PNIPAm-MBA)/PEI MCP particles ($w_{PEI} : w_{NIPAm} : w_{n\text{-}BA} = 1 : 2 : 2$).

### *4.3.4.4 Surface charges of particles as a function of pH and temperature*

#### *Surface charge*

The surface charge of MCP particles was determined by ζ-potential measurement using Beckman Coulter Delsa Nano C instrument. Under standard condition, pH 7 with conducting medium of 1 mM NaCl, the ζ-potential of PNIPAm/PEI seed microgel and PBA/(PNIPAm-MBA)/PEI MCP particles were + 12.78 mV and + 4.54 mV respectively. The low magnitude of ζ-potential of both seed and MCP particles was due to the formation of PNIPAm/PEI interpenetrated network at the outermost shell of the particles as explained in **4.3.2.5**. The charge shielding of PEI by PNIPAm resulted in the suppression of the charge density of the particles.

#### *Surface charge of particles as a function of pH*

The effect of pH on the ζ-potential of MCP particles at was evaluated by ζ-potential measurement using Delsa Nano C with the aid of auto-titrator. The variation of ζ-potential as a function of pH of MCP particles with different degree of crosslinking was illustrated in Figure 4.17.

Independent of the crosslinking degree, the surface of PBA/(PNIPAm-MBA)/PEI MCP particles was positively charged and the ζ-potential almost remains unchanged below pH 7. The positive ζ-potential of MCP particles was contributed by the protonated amino groups of PEI located at the outermost shell of the MCP particles. As the pH of the medium was raised to above 7, there was a drop in the ζ-potential of MCP particles. The drop in ζ-potential was due to the deprotonation of the amino groups. Eventually, the ζ-potential of MCP particles was dropped to about zero as the pH of the medium was approached 9.5, isoelectric point of PEI.

Although PBA/(PNIPAm-MBA)/PEI MCP particles with different crosslinking degree had the same trend in the variation of ζ-potential against pH, the effect of crosslinking degree was reflected by the magnitude of ζ-potential. The ζ-potential of PBA/(PNIPAm-MBA)/PEI MCP particles with 5% and 2% crosslinking at pH 7 were + 22.53 mV and + 6.50 mV respectively. The magnitude of ζ-potential of MCP particles was suppressed from + 22.53 mV to + 6.50 mV as the degree of crosslinking decreased from 5% to 2%. The suppression in the surface charge of the MCP particles was attributed to the formation of interpenetrated network in the outermost shell as explained in **4.3.2.4**. PNIPAm was slightly crosslinked under low crosslinking degree. PNIPAm was not confined at the innermost core and was extended in the outermost shell. The outermost shell of the particles was an interpenetrating network which composed of PNIPAm and PEI. As a result, there was significant shielding of positively charged PEI under low MBA crosslinking.

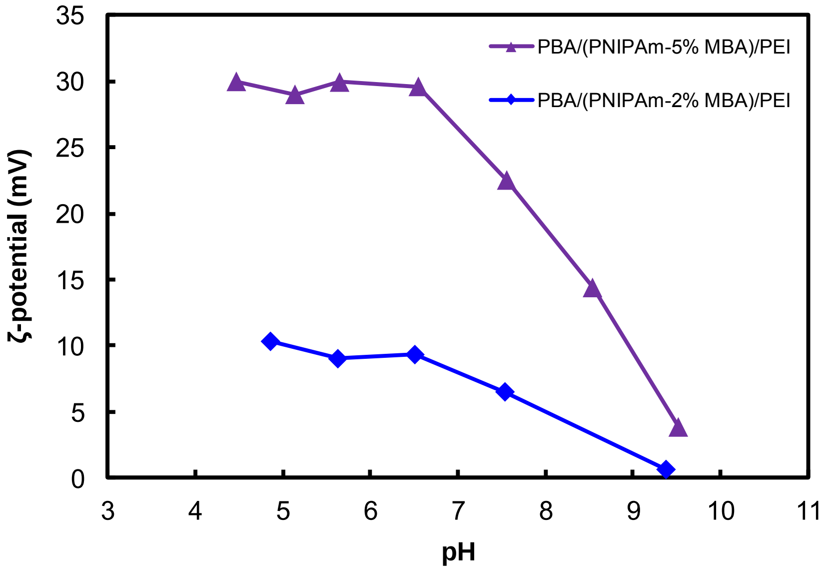

**Fig. 4.17.** ζ-potential as a function of pH of PBA/(PNIPAm-MBA)/PEI MCP particles ($w_{PEI} : w_{NIPAm} : w_{n\text{-}BA} = 1 : 2 : 2$).

***Surface charge of particles as a function of temperature***

The effect of temperature on the ζ-potential of MCP particles at different crosslinking degree was evaluated by ζ-potential measurement using Delsa Nano C with the aid of thermal monitoring device. The variation of ζ-potential as a function of temperature of MCP particles with different degree of crosslinking was illustrated in Figure 4.18.

Regardless of the degree of crosslinking, a general trend in the variation of ζ-potential of PBA/(PNIPAm-MBA)/PEI MCP particles was observed. Below the VPTT of PNIPAm (32 °C), MCP particles had positive ζ-potential and the ζ-potential was kept constant in this temperature range. As the temperature was raised to the VPTT of PNIPAm, there was an obvious jump in the ζ-potential of MCP particles. When the temperature was further raised, there was no insignificant increase in the ζ-potential of MCP particles. Eventually, the ζ-potential of MCP particles was approached to + 30 mV at 39 °C.

This sudden increase in ζ-potential was due to the phase transition of PNIPAm at its VPTT at 32 °C which had been explained in **4.3.2.4**. PNIPAm was hydrophilic at temperature below its VPTT. Hydrophilic PNIPAm was extended in the outermost shell of the particles, forming an interpenetrating network with PEI. This led in charge shielding of PEI and resulted in low magnitude in ζ-potential. At temperature above VPTT, PNIPAm changed from hydrophilic to hydrophobic. This coil-to-glubole transition led to shrinkage of PNIPAm from the outermost shell to the innermost core. As a result, the positive charges on PEI were re-exposed which reflected by a significant increase in the ζ-potential

The effect of MBA crosslinking on the ζ-potential of PBA/(PNIPAm-MBA)/PEI was insignificant. The ζ-potential of 5% and 2% crosslinked PBA/(PNIPAm-MBA)/PEI were + 5.05 mV and + 4.54 mV at 25 °C respectively. The ζ-potential of 5% and 2% crosslinked PBA/(PNIPAm-MBA)/PEI were + 30.49 mV and + 27.58 mV at 39 °C respectively. The ζ-potential of the MCP particles below and above the VPTT of PNIPAm was similar to each other. This might be attributed to the low $T_g$ of the second hydrophobic polymer, PBA. As the $T_g$ of PEI was far below the room temperature (about 213 K) and PNIPAm was a soft hydrogel below its VPTT, the physical properties of the second batch polymer were critical to the final MCP particles nanostructure and thermal responsive properties. When *n*-BA was utilized as the second batch monomer, hydrophobic PBA was polymerized during seed emulsion polymerization. The $T_g$ of the PBA was very low, 219K, which behaved as soft and tacky under room temperature.

Therefore, rearrangement of the polymer chains of all the polymeric components in PBA/(PNIPAm-MBA)/PEI were allowed to reach the thermodynamic equilibrium morphology. As a result, most of the PBA polymer chains were localized at the innermost core of the particles. Without the hindrance of the PBA, PNIPAm was ultimately extended in the outer shell of the particles. Thus, the positive charges of PEI were extensively shielded by PNIPAm which outweigh the effect of crosslinking degree of the particles.

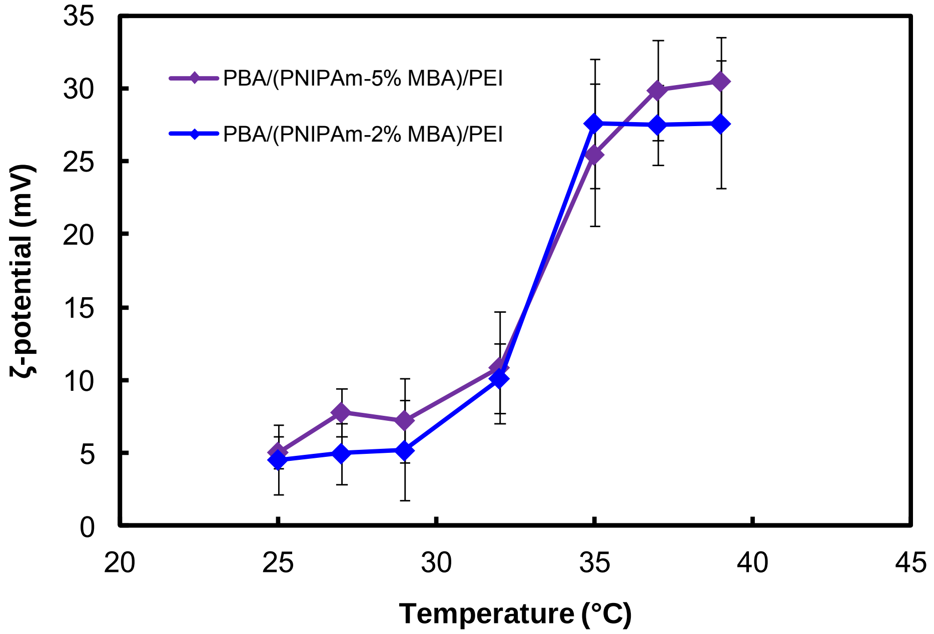

**Fig. 4.18.** ζ-potential as a function of temperature of PBA/(PNIPAm-MBA)/PEI MCP particles ($w_{PEI} : w_{NIPAm} : w_{n\text{-}BA} = 1 : 2 : 2$).

### *4.3.4.5 Morphology*

The morphology and core-shell nanostructure of PBA/(PNIPAm-MBA)/PEI MCP particles prepared at different degree of crosslinking (5% and 2%) were examined by FE-SEM and TEM. Well-defined core-shell nanostructure of

MBA crosslinked PNIPAm/PEI seed particles was observed in TEM micrographs. The dark core of the particles was the heavily stained PNIPAm and the bright shell was the slightly stained PEI.

Highly uniform particles with distorted spherical morphology was observed in the SEM micrographs of all PBA/(PNIPAm-MBA)/PEI MCP particles. To elucidate the nanostructure of the MCP particles, these particles were stained with 0.5% (w/w) phosphotungstic acid (PTA, $WO_2 \bullet H_3PO_4 \bullet xH_2O$) for 5 mins. Well-defined core-shell nanostructured particles were revealed in the TEM micrographs. During PTA staining, PNIPAm was heavily stained by PTA solution while PEI was slightly stained by PTA solution. PBA was not stained by PTA solution. Thus, we interpreted that the bright shell was constructed by PEI and the dark core of the particles was constructed by PNIPAm and PBA.

The distorted spherical morphology of PBA/(PNIPAm-MBA)/PEI MCP particles was due to the lack of rigid solid support. PEI and PBA were polymers with very low glass transition temperature ($T_g$). $T_g$ of PEI and PBA were 213 K and 219 K respectively. PNIPAm was a hydrogel which was soft, too. All the components of the MCP particles were tacky and soft. This resulted in the formation of distorted spherical particles. As previously explained, the PNIPAm was more preferably stained by PTA solution than PEI, while PBA was not stained by PTA solution. The dark region in the micrographs was probably due to heavily stained PNIPAm and the bright region was constructed by the lightly stained PEI and non-stained PBA.

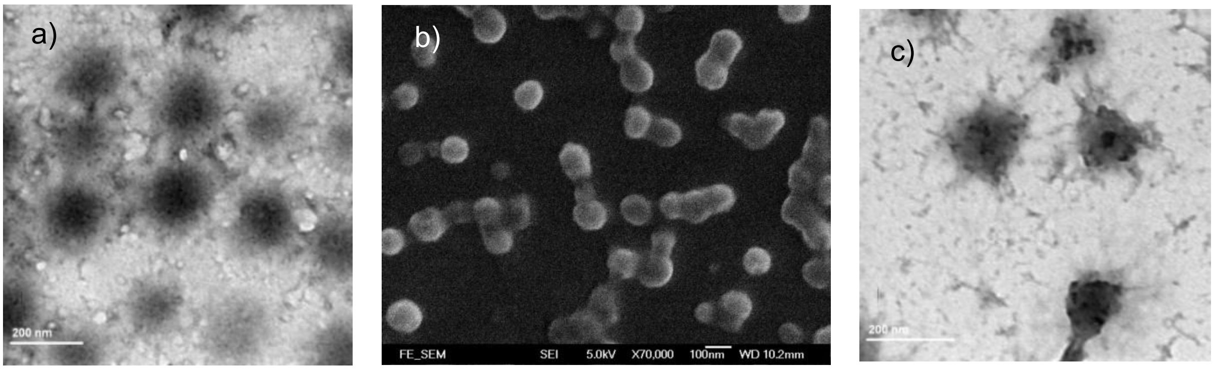

**Fig. 4.19.** Morphology of PNIPAm/PEI seed particles (5% MBA crosslinked): a) TEM image; Morphology of PBA/(PNIPAm-5% MBA)/PEI MCP particles: b) FE-SEM image; c) TEM image.

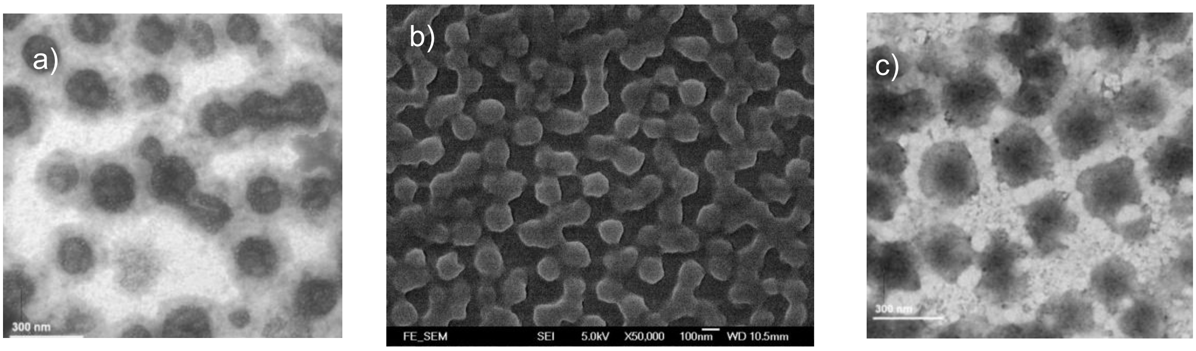

**Fig. 4.20.** Morphology of PNIPAm/PEI seed particles (2% MBA crosslinked): a) TEM image; Morphology of PBA/(PNIPAm-2% MBA)/PEI MCP particles: b) FE-SEM image; c) TEM image.

### 4.3.5 PS/(PNIPAm-MBA)/PEI MCP nanocomposite particles

The preparation and characterization of PS/(PNIPAm-MBA)/PEI nanocomposite particles is discussed in detail in this part. Seeded polymerization of styrene is always a challenege due to its low water solubility in water (0.3 g/L). The diffusion of hydrophobic molecules in water is slow. The success in forming MCP particles containing very hydrophobic component would allow us to prepare a wide range of MCP particles with different compositions.After the formation of MBA crosslinked PNIPAm/PEI seed particles, styrene was introduced to undergo seeded emulsion polymerization. Scheme 4.3 shows the reaction route and conditions to prepare these particles.

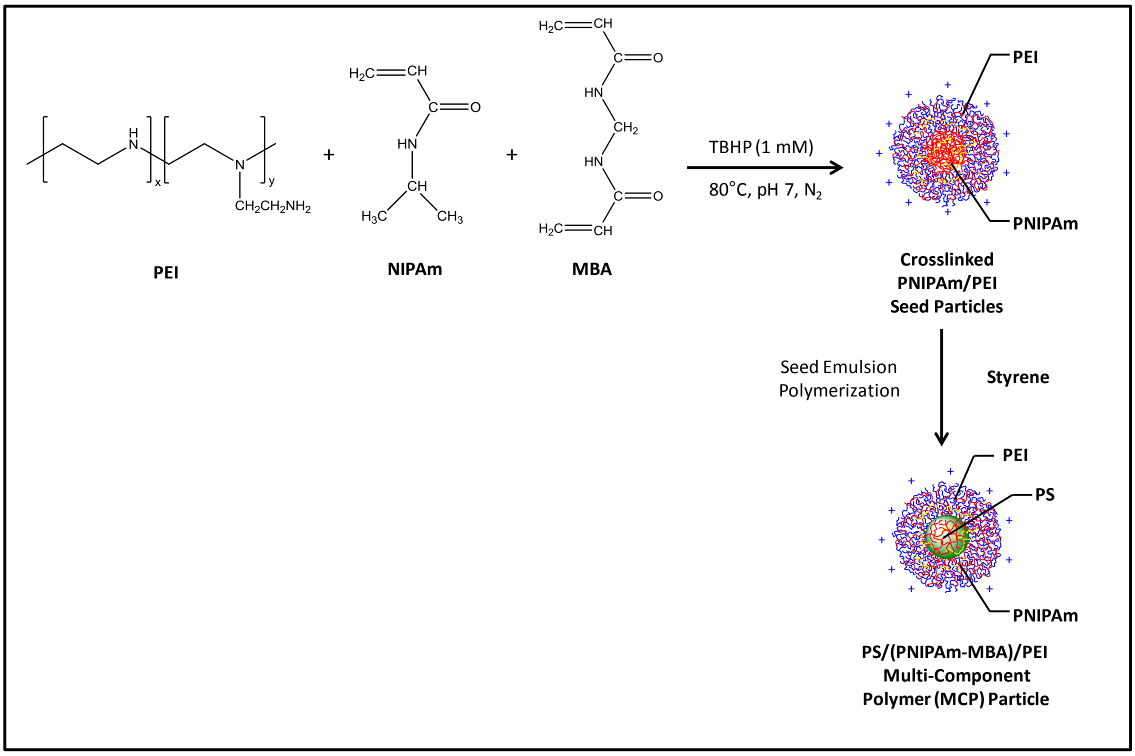

**Scheme 4.3.** Reaction scheme for the synthesis of PS/(PNIPAm-MBA)/PEI MCP particles.

### *4.3.5.1 Kinetic study of the polymerization process*

The reaction kinetics of the seeded emulsion polymerization of MCP nanocomposites was monitored by thermal couple (Testo 735) with 1 temperature recorded per second. Figure 4.21 shows the temperature profile of the polymerization at different stages of reaction.

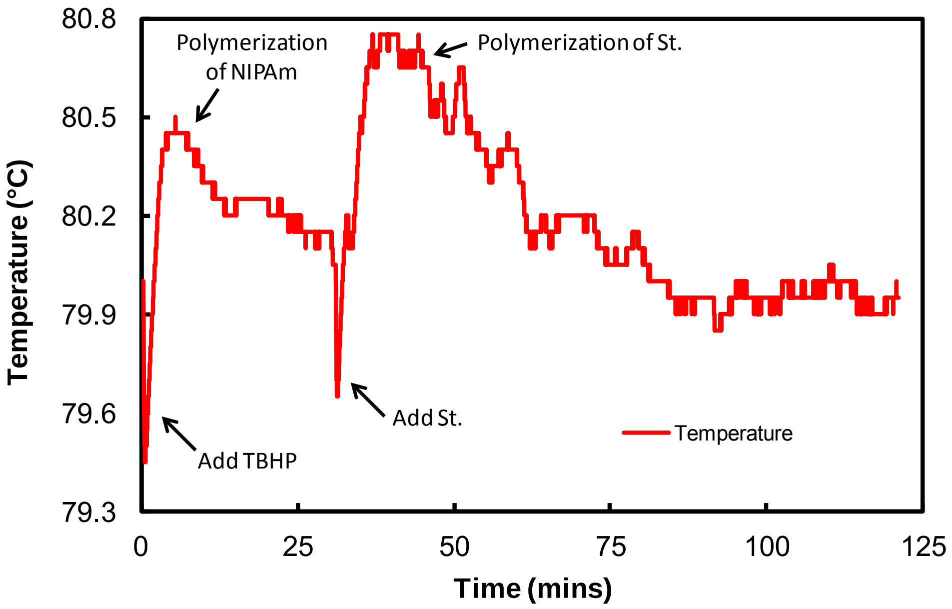

**Fig. 4.21.** Reaction temperature profile during the synthesis of PS/(PNIPAm-MBA)/PEI composite particles.

When the temperature of PEI, NIPAm and MBA mixture reached equilibrium (around 80 °C), appropriate amount of initiator (TBHP) was added to the reaction mixture to initiate the polymerization. Once TBHP was added, the reaction temperature was first slightly dropped and then rose up rapidly. After consuming most of the NIPAm monomers, the exothermic polymerization was almost finished and the temperature of the reaction mixture dropped to the original level.

As the temperature fell back to 80 ℃, the second batch of monomer, styrene, was introduced into the reaction mixture to perform seeded emulsion polymerization. Similarly, an increased in temperature was observed after the addition of styrene. This increase was contributed by an exothermic polymerization of styrene inside MBA crosslinked PNIPAm/PEI seed particles. Rapid increase in temperature was observed during seeded emulsion polymerization. This indicated the fast diffusion of styrene monomers from bulk aqueous phase into the growing seed particles. The fast diffusion of hydrophobic monomers into the growing particles leads to fast polymerization. However, the exothermic peak of seeded emulsion polymerization was broad. This was due to the sow propagation rate of styrene which required longer time to complete the polymerization. Therefore, exothermic peak of the styrene polymerization was sharp but broad as compared with the exothermic peak of NIPAm polymerization.

In addition to temperature variation, the polymerization kinetics was also monitored by monomer conversion at different stage of polymerization. The total monomer conversion at different time interval is shown in Table 4.7. After the first stage of polymerization, NIPAm monomer conversion reached 99%. In the second stage of polymerization, styrene monomer was charged to proceed seeded emulsion polymerization. When the exothermic polymerization was completed, the total monomer conversion had reached 94% at the end of polymerization. The variation of hydrodynamic diameters of MCP particles throughout the polymerization process was evaluated by particle size measurement at different time intervals. Upon seed emulsion polymerization, we hypothesized that the hydrodynamic diameter of the MCP particles should be greater than seed particles.

Since second batch monomers were hydrophobic, they were more preferred to be diffused into the growing seed particles for polymerization. From the result of particle size measurement, the hydrodynamic diameters of the seed particles ad MCP particles were 371.6 nm and 352.3 nm respectively. The hydrodynamic diameter of the seed particles was slightly larger than the MCP particles, which was due to the microgel structure of the MBA crosslinked PNIPAm/PEI seed hydrogel particles. Both the components of seed microgel, PNIPAm and PEI, are hydrophilic polymers which are highly swollen by water. They are highly extended in water which contributed to large particle size. Styrene was added to the reaction system to conduct seeded emulsion polymerization. Hydrophobic component, PS, was formed during the second stage of polymerization. PNIPAm/PEI was not as highly extended as the seed microgel. Increasing the hydrophobic content into the particles resulted in forming more compacted particles in order to reduce their surface energy of the hydrophobic polymer chains. Therefore, the hydrodynamic diameter of the PS/(PNIPAm-MBA)/PEI MCP particles was slightly smaller than (PNIPAm-MBA)/PEI seed microgel.

**Table 4.7.** Total monomer conversion and particle size of MCP particles at different time intervals.

| **Reaction time**[1] **(mins)** | **Type of particles** | **Monomer conversion**[2] **(%)** | **$Z_{AVE}$**[3] **(nm)** |
|---|---|---|---|
| 30 | MBA crosslinked PNIPAm/PEI seed | 99%[4] | 371.1 |
| 34 | PS/(PNIPAm-MBA)/PEI MCP | 59%[5] | 328.6 |
| 38 | PS/(PNIPAm-MBA)/PEI MCP | 65%[5] | 403.9 |
| 45 | PS/(PNIPAm-MBA)/PEI MCP | 76%[5] | 301.1 |
| 60 | PS/(PNIPAm-MBA)/PEI MCP | 88%[5] | 326.7 |
| 75 | PS/(PNIPAm-MBA)/PEI MCP | 88%[5] | 352.8 |
| 90 | PS/(PNIPAm-MBA)/PEI MCP | 94%[5] | 324.7 |
| 120 | PS/(PNIPAm-MBA)/PEI MCP | 94%[5] | 352.3 |

[1] The reaction was counted since the addition of initiator into the reaction mixture

[2] The total monomer conversion of MCP particles were determined gravimetrically

[3] The hydrodynamic diameter of MCP particles were determined by DLS at 25 °C

[4] The monomer conversion was calculated based on total NIPAm monomer added

[5] The monomer conversion was calculated based on total monmer added

### *4.3.5.2 Effect of degree of crosslinking*

The effect of MBA crosslinking on the properties of PS/(PNIPAm-MBA)PEI MCP particles was studied by varying i) the weight ratio between NIPAm and styrene; and ii) the composition of MBA crosslinker, keeping other reagents unchanged. The characteristics of PS/(PNIPAm-MBA)/PEI MCP particles were shown in Table 4.8.

Independent of the crosslinking degree, the total monomer conversion of MCP particles was above 90% at the end of polymerization. The hydrodynamic diameter of MBA crosslinked PNIPAm/PEI seed was ranged from 250 nm to 400 nm, while the hydrodynamic diameter of PS/(PNIPAm-MBA)/PEI MCP particles was ranged from 300 nm to 400 nm. The hydrodynamic diameter of the PNIPAm/PEI seed was generally greater than MCP particles. The particle size distribution of PS/(PNIPAm-MBA)/PEI MCP particles was also narrow (PDI < 0.2). This indicated the MCP particles were prepared with high uniformity and without secondary nucleation.

More importantly, the surface charge of MCP particles was inversely proportional to the crosslinking degree of MBA. Though the ζ-potential of PNIPAm/PEI seed hydrogels was around + 15 mV at 10%, 5% and 2% MBA crosslinking, the effect of MBA crosslinking on the ζ-potential of MCP was significant. A descending trend in the ζ-potential of MCP particles was observed as the degree of MBA crosslinking increased. The ζ-potential of PS/(PNIPAm-MBA)/PEI MCP particles with 10%, 5% and 2% MBA crosslinking were + 31.07 mV, + 28.05 mV and + 16.45 mV at pH 7 under room temperature respectively. This trend could be interpreted by the confinement of PNIPAm at different crosslinking degree which will be further discussed later. PS/(PNIPAm-MBA)/PEI MCP particles with high total monomer conversion, nanosized dimension and desirable colloidal stability were successfully prepared under 10%, 5% and 2% MBA crosslinking.

**Table 4.8.** Characteristics of PNIPAm/PEI seed hydrogel and PS/(PNIPAm-MBA)/PEI MCP particles with different degree of crosslinking.

| **Types of Particles** | **Degree of crosslinking** | **Monomer conversion**[1] | **Hydrodynamic diameter (nm)**[2] | | | | **ζ-potential (mV)**[3] | | | |
|---|---|---|---|---|---|---|---|---|---|---|
| | | | **Dh (25°C)** | **Dh (32°C)** | **Dh (39°C)** | **$Dh_{39°C}/Dh_{25°C}$** | **ζ-potential (pH 7)** | **ζ-potential (25°C)** | **ζ-potential (32°C)** | **ζ-potential (39°C)** |
| **PNIPAm/PEI seed hydrogel** | **10%** | **99%** | **273.6** | **253.1** | **217.2** | **0.79** | **+ 15.49** | **+ 15.49** | **+ 20.08** | **+ 30.42** |
| | **5%** | **99%** | **318.5** | **292.6** | **249.8** | **0.78** | **+ 14.79** | **+ 14.79** | **+ 25.75** | **+ 38.84** |
| | **2%** | **99%** | **383.6** | **360.6** | **289.9** | **0.76** | **+ 12.78** | **+ 12.78** | **+ 17.52** | **+ 38.43** |
| **PS/(PNIPAm-MBA)/PEI MCP particles** | **10%** | **91%** | **378.7** | **362.4** | **349.3** | **0.92** | **+ 31.07** | **+ 31.07** | **+ 34.22** | **+ 39.80** |
| | **5%** | **93%** | **331.6** | **319.0** | **300.9** | **0.91** | **+ 28.05** | **+ 28.05** | **+ 36.83** | **+ 41.43** |
| | **2%** | **91%** | **316.6** | **290.4** | **272.4** | **0.86** | **+ 16.45** | **+ 16.45** | **+ 23.77** | **+ 39.81** |

[1] The monomer conversion was determined gravimetrically

[2] The hydrodynamic diameter of MCP particles was determined by DLS at specific temperatures and the samples were thermally equilibrated for 10 mins prior measurement

[3] The colloidal stability of MCP particles was determined by ζ-potential measurement using 1 mM NaCl as medium and the samples were thermally equilibrated for 10 mins prior measurement

### *4.3.5.3 Effect of seed monomer to second batch monomer ratio*

The effect of weight ratio between the seed monomer (NIPAm) and second batch monomer (styrene) on the properties of the MCP particles was evaluated by varying the composition of NIPAm and styrene, keeping the PEI to total monomer ratio at 1 : 4 (w/w). The weight ratio of NIPAm to styrene changed from 25 : 75 to 75 : 25 under 10%, 5% and 2% MBA crosslinking. The results of these MCP particles were summarized and displayed in Table 4.9.

PS/(PNIPAm-MBA)/PEI MCP particles had achieved total monomer conversion over 90% at the end of polymerization. The hydrodynamic diameter of the prepared MCP particles was ranged from 300 nm to 500 nm. The particle size distribution of these MCP particles was narrow (PDI < 0.2). However, the difference in the hydrodynamic diameter of PS/(PNIPAm-MBA)/PEI MCP particles with different NIPAm/styrene composition was not significant. This was probably due to the presence of PEI in the MCP particles. PEI was a water soluble polymer which was highly extended in the shell due to the charge repulsion. Thus, the MCP particle shell was hairy like structured instead of a compact shell. Thus, the hydrodynamic diameter of MCP particles was not affected by the NIPAm/styrene composition.

The effect of weight ratio between NIPAm and styrene was illustrated in the surface charge of MCP particles. The ζ-potential of MCP particles was gradually decreased as the NIPAm composition in total monomer increased. Applying 2% crosslinked PS/(PNIPAm-MBA)/PEI MCP particles as an example, the ζ-potential of MCP particles with NIPAm to styrene w/w ratio at 1 : 3, 1 : 1 and 3 : 1 were + 30.37

mV, + 16.45 mV and + 14.78 mV respectively. The magnitude of ζ-potential of MCP particles was decreased as the composition of NIPAm increased from 25% to 75% in the total monomer. As the NIPAm composition increased, the shielding of PEI shell became more significant due to formation of interpenetrated network. The formation of interpenetration network significantly shielded the positive charges on PEI, leading to a supression in the ζ-potential of MCP particles.

**Table 4.9.** Characteristics of PS/(PNIPAm-MBA)/PEI MCP particles with NIPAm : St. (w/w) ratio.

| **Types of Particles** | **w/w ratio of NIPAm to St. (NIPAm composition)**[1] | **Monomer conversion**[2] | **Hydrodynamic diameter (nm)**[3] | | | | **ζ-potential (mV)**[4] | | | |
|---|---|---|---|---|---|---|---|---|---|---|
| | | | **Dh (25°C)** | **Dh (32°C)** | **Dh (39°C)** | **Dh$_{39^\circ C}$/ Dh$_{25^\circ C}$** | **ζ-potential (pH 7)** | **ζ-potential (25°C)** | **ζ-potential (32°C)** | **ζ-potential (39°C)** |
| **PS/(PNIPAm-10% MBA)/PEI MCP particles** | **1 : 1 (50%)** | **91%** | **378.7** | **362.4** | **349.3** | **0.92** | **+ 31.07** | **+ 31.07** | **+ 34.22** | **+ 39.80** |
| | **3 : 1 (75%)** | **99%** | **405.8** | **390.9** | **364.6** | **0.90** | **+ 29.38** | **+ 29.38** | **+ 35.65** | **+ 39.17** |
| **PS/(PNIPAm-5% MBA)/PEI MCP particles** | **1 : 3 (25%)** | **94%** | **506.4** | **493.9** | **475.6** | **0.94** | **+ 34.19** | **+ 34.19** | **+ 37.67** | **+ 37.13** |
| | **1 : 1 (50%)** | **93%** | **331.6** | **319.0** | **300.9** | **0.91** | **+ 28.05** | **+ 28.05** | **+ 36.83** | **+ 41.43** |
| | **3 : 1 (75%)** | **93%** | **401.9** | **387.2** | **356.2** | **0.89** | **+ 29.09** | **+ 29.09** | **+ 34.32** | **+ 40.30** |
| **PS/(PNIPAm-2% MBA)/PEI MCP particles** | **1 : 3 (25%)** | **99%** | **406.5** | **392.0** | **379.2** | **0.93** | **+ 30.37** | **+ 30.37** | **+ 40.49** | **+ 40.38** |
| | **1 : 1 (50%)** | **91%** | **316.6** | **290.4** | **272.4** | **0.86** | **+ 16.45** | **+ 16.45** | **+ 23.77** | **+ 39.81** |
| | **3 : 1 (75%)** | **98%** | **415.3** | **383.6** | **339.0** | **0.82** | **+ 14.78** | **+ 14.78** | **+ 24.83** | **+ 39.90** |

[1] The weight ratio between PEI to total monomer was kept at 1 : 4 in this study

[2] The monomer conversion was determined gravimetrically

[3] The hydrodynamic diameter of MCP particles was determined by DLS at specific temperature and the samples were thermally equilibrated for 10 mins prior measurement

[4] The colloidal stability of MCP particles was determined by ζ-potential measurement using 1 mM NaCl as medium and the samples were thermally equilibrated for 10 mins prior measurement

### 4.3.6 Characterization of PS/(PNIPAm-MBA)/PEI nanocomposite particle

#### *4.3.6.1 Composition*

The composition of the PS/(PNIPAm-MBA)/PEI MCP particles was investigated by FT-IR spectroscopy. The particles were first purified by repeated centrifugation to get rid of any unreacted PEI and monomers. Figure 4.22a shows the FT-IR spectrum of MBA-crosslinked PNIPAm/PEI seed particles. Strong C=O amide stretching peak observed at 1650 to 1660 cm$^{-1}$, strong N-H amide II bending peak observed at 1535 cm$^{-1}$ and isopropyl C-H peak observed at 1370 to 1390 cm$^{-1}$ suggest the presence of PNIPAm. Both broad amino N-H stretching peak of primary amine at 3400 to 3500 cm$^{-1}$, and C-H stretching and bending at 2900 to 3000 cm$^{-1}$ indicate the presence of PEI. Figure 4.22b shows the FT-IR spectrum of PS/(PNIPAm-MBA)/PEI MCP particles. Additional absorption peaks at 750 cm$^{-1}$ and 700 cm$^{-1}$ are identified in the spectrum, which correspond to aromatic =C-H out-of-plane bending vibration peaks. Enhanced absorption peak at 1500 cm$^{-1}$ regarding to aromatic =C-H stretching vibration of PS is also observed. Enhanced absorption peak also appear at 2950 to 3050 cm$^{-1}$ regarding to =C-H vinylic hydrogen which suggest the presence of PS. These characteristic peaks confirm the presence of polystyrene in the MCP particles. Based on the FTIR results, we can confirm that the MCP particles comprise of PEI, PNIPAm and PS components.

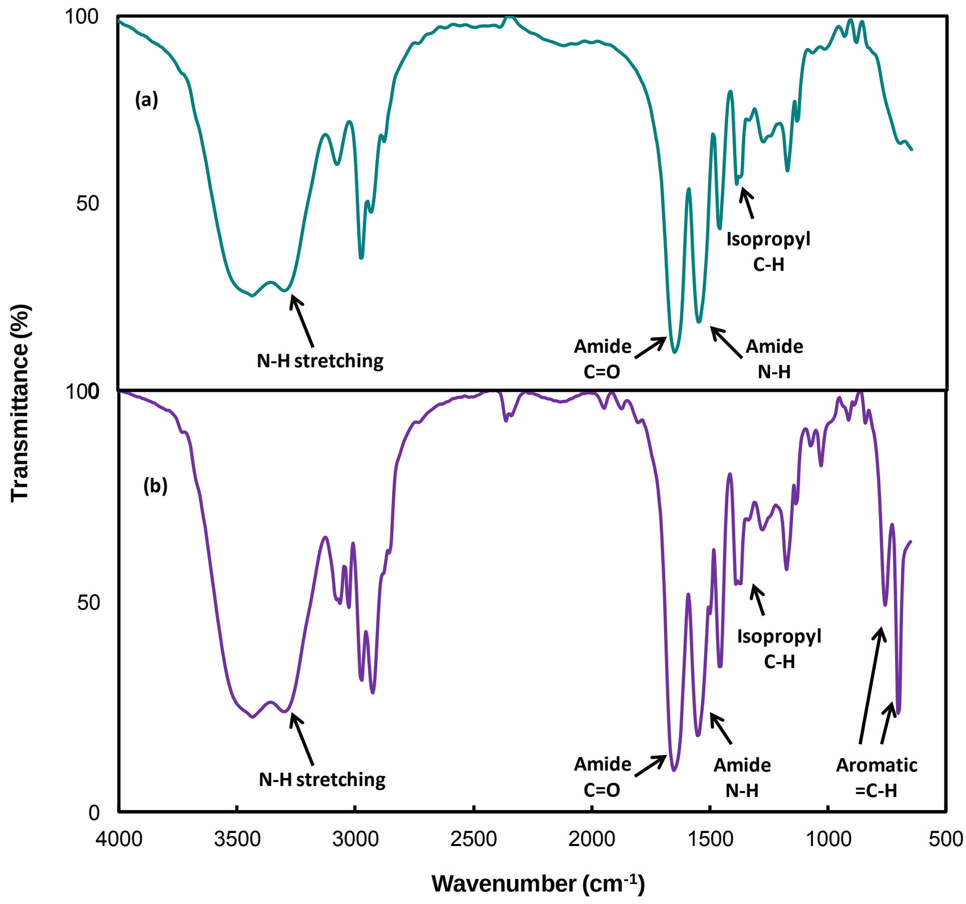

**Fig. 4.22.** FT-IR spectrum of a) 2% MBA crosslinked PNIPAm/PEI seed hydrogel; and b) PS/(2% MBA crosslinked PNIPAm-PEI) MCP particles.

### *4.3.6.2 PEI content*

The amount of unbounded PEI in MCP particles was determined by titration method. MCP particles were first purified by repeated centrifugation and all the supernatants were collected. These supernatants were then titrated against 0.025 M NaOH solution and the variation of pH and conductivity was monitored by integrated pH/conductivity meter. Compared with the calibration plot of PEI, the percentage of unreacted PEI in PS/(PNIPAm-10% MBA)/PEI, PS/(PNIPAm-5% MBA)/PEI and PS/(PNIPAm-2% MBA)/PEI were 43.89%, 53.66% and 47.39% respectively. The PEI grafting efficiency was independent of the amount of crosslinker (MBA) added. These results suggested that only 50% of PEI was implemented in the fabrication of PNIPAm/PEI based MCP particles. Assuming the reaction had reached complete conversion at the end of polymerization, the composition of PEI in PS/(PNIPAm-MBA)/PEI was ranged from 10% to 12%.

### *4.3.6.3 Particle size as a function of temperature*

***Particle size***

The hydrodynamic diameters ($Z_{AVE}$) and particle size distribution (PDI) of seed and MCP particles were determined by dynamic light scattering (DLS) at pH 7 using a Beckman Coulter Delsa Nano C instrument. Figure 4.23 compares their particle sizes and size distributions. The hydrodynamic diameter and particle size distribution of seed particles were 383.6 nm and 0.127. While the hydrodynamic diameter and particle size distribution of MCP particles were 316.6 nm and 0.041. These results indicated that the prepared MCP particles were in nano-sized dimension and with narrow size distribution.

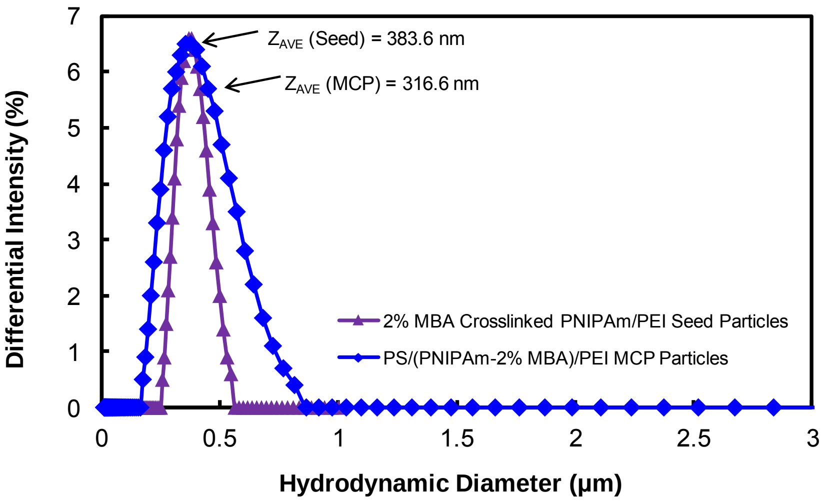

**Fig. 4.23.** Particle sizes of MBA crosslinked PNIPAm/PEI seed particles (383.6 nm) and PS/(2% MBA crosslinked PNIPAm-PEI) MCP particles (316.6 nm).

### *Effect study of degree of MBA crosslinking on particle size as a function of temperature*

The effect of surrounding temperature on the hydrodynamic diameter of the PS/(PNIPAm-MBA)/PEI MCP particles at different crosslinking degree was evaluated by DLS measurement at different temperatures (25 ℃, 27 ℃, 29 ℃, 32 ℃, 35 ℃, 37 ℃ and 39 ℃). The MCP particles were thermally equilibrated at the preset temperature for 10 mins prior measurement. The variation of the hydrodynamic diameter of PS/(PNIPAm-MBA)/PEI MCP particles as a function of temperature was displayed in Figure 4.24.

Below VPTT (32 ℃) of PNIPAm, the hydrodynamic diameters of PS/(PNIPAm-MBA)/PEI MCP particles did not have obvious variation. When the surrounding temperature was elevated to 32 ℃, there was a remarkable drop in the hydrodynamic diameter of the MCP particles. PNIPAm underwent phase transition at this temperature which changed from hydrophilic to hydrophobic. The intermolecular hydrogen bond between PNIPAm and $H_2O$ was broken down and intramolecular hydrogen bonding between amide oxygen and amide hydrogen of neighbouring PNIPAm was formed instead. The coil-to-globule transition of PNIPAm eventually caused the shrinkage of MCP particles. Further increasing the temperature did not introduce significant change in the particle size, indicating the change in particle size was only due to the volume phase transition of PNIPAm. In addition, no shift in the VPTT of PNIPAm was observed. This indicated that PNIPAm/PEI graft copolymer was formed instead of PNIPAm/PEI linear copolymer during polymerization.

To further evaluate the thermal responsive properties of the MCP particles, the hydrodynamic diameter was re-expressed as normalized hydrodynamic diameter which demonstrated the thermal responsive properties of MCP particles quantitatively. The normalized hydrodynamic diameter of 10%, 5% and 2% PS/(PNIPAm-MBA)/PEI MCP particles at 39 ℃ ($Dh_{39\,°C}/Dh_{25\,°C}$) were 0.92, 0.91 and 0.86 respectively. MCP particles exhibited greater thermal responsiveness at lower crosslinking degree. Under higher crosslinking degree, the degree of shrinkage in the particle size was low because PNIPAm was highly crosslinked by MBA. The coil-to-globule transition of PNIPAm was highly constrained by MBA crosslinking. On the contrary, the shrinkage in particle size was more obvious at low crosslinking degree. PNIPAm was not constrained by the MBA crosslinking and underwent coil-to-globule transition as the temperature elevated to above VPTT.

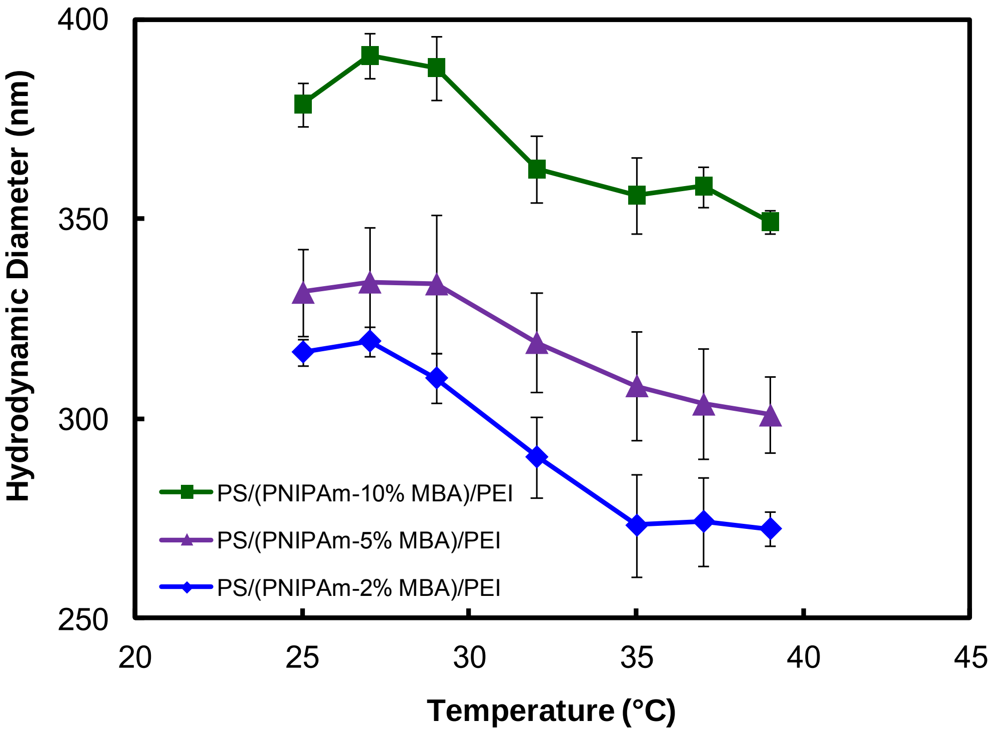

**Fig. 4.24.** Particle size as a function of temperature of PS/(PNIPAm-MBA)/PEI MCP particles ($w_{PEI} : w_{NIPAm} : w_{St.} = 1 : 2 : 2$).

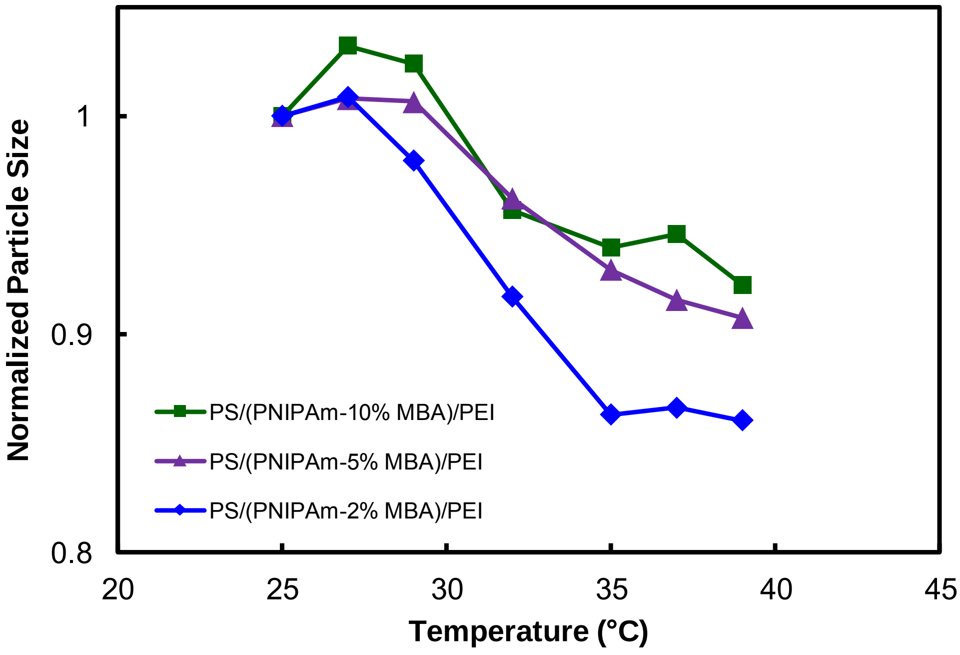

**Fig. 4.25.** Normalized particle size ($Dh/Dh_{25\ °C}$) as a function of temperature of PS/(PNIPAm-MBA)/PEI MCP particles ($w_{PEI} : w_{NIPAm} : w_{St.} = 1 : 2 : 2$).

***Effect study of weight ratio between seed monomer and second batch monomer on particle size as a function of temperature***

The effect of surrounding temperature on the hydrodynamic diameter of the PS/(PNIPAm-MBA)/PEI MCP particles at different NIPAm/styrene weight ratio at 10%, 5% and 2% MBA crosslinking was evaluated by DLS measurement at different temperatures (25 ℃, 27 ℃, 29 ℃, 32 ℃, 35 ℃, 37 ℃ and 39 ℃). The MCP particles were thermally equilibrated at the preset temperature for 10 mins prior measurement. The variation of the hydrodynamic diameter of PS/(PNIPAm-MBA)/PEI MCP particles with different NIPAm/styrene composition as a function of temperature was plotted and displayed according to their crosslinking degree (10%, 5% and 2%).

As explained previously, the variation of the hydrodynamic diameter of PS/(PNIPAm-MBA)/PEI MCP particles was negligible below VPTT of PNIPAm. When the surrounding temperature was elevated to 32 ℃, VPTT of PNIPAm, there was a sudden drop in the hydrodynamic diameter of the MCP particles. PNIPAm underwent volume phase transition which changed from hydrophilic to hydrophobic and caused shrinkage in the particle size of MCP particles. As the surrounding temperature further increased, there is no significant change in the particle size.

To further evaluate the thermal responsive properties of the MCP particles, the hydrodynamic diameter was re-expressed as normalized hydrodynamic diameter which demonstrated the thermal responsive properties of MCP particles quantitatively. At 10% MBA crosslinking, the normalized hydrodynamic diameter of PS/(PNIPAm-MBA)/PEI MCP particles with NIPAm/styrene weight ratio at 1 : 1 and 3 : 1 at 39 ℃ ($Dh_{39\,℃}/Dh_{25\,℃}$) were 0.92 and 0.90 respectively. At 5% MBA crosslinking, the normalized hydrodynamic diameter of PS/(PNIPAm-MBA)/PEI MCP particles with NIPAm/styrene weight ratio at 1 : 3 , 1 : 1 and 3 : 1 at 39 ℃ ($Dh_{39\,℃}/Dh_{25\,℃}$) were 0.94, 0.91 and 0.89 respectively. At 2% MBA crosslinking, the normalized hydrodynamic diameter of PS/(PNIPAm-MBA)/PEI MCP particles with NIPAm/styrene weight ratio at 1 : 3 , 1 : 1 and 3 : 1 at 39 ℃ ($Dh_{39\,℃}/Dh_{25\,℃}$) were 0.93, 0.86 and 0.82 respectively.

Under the same crosslinking degree, a trend was observed that the normalized hydrodynamic diameter ($Dh_{39\,℃}/Dh_{25\,℃}$) of PS/(PNIPAm-MBA)/PEI MCP particles decreased as the NIPAm composition increased. Applying 2% MBA crosslinking system as an example, there was a 7% drop in hydrodynamic diameter when the total monomer consisted of 25% NIPAm by weight. When the total monomer consisted of 50% NIPAm by weight, the drop in the hydrodynamic diameter was raised to 14%. This phenomenon was more obvious as the NIPAm composition was further promoted to 75% by weight. The drop in hydrodynamic diameter was enhanced to 18%. Since the thermal responsive property was depended on the volume phase transition of PNIPAm, increasing NIPAm composition would contribute to the improvement of thermal responsiveness of MCP particles.

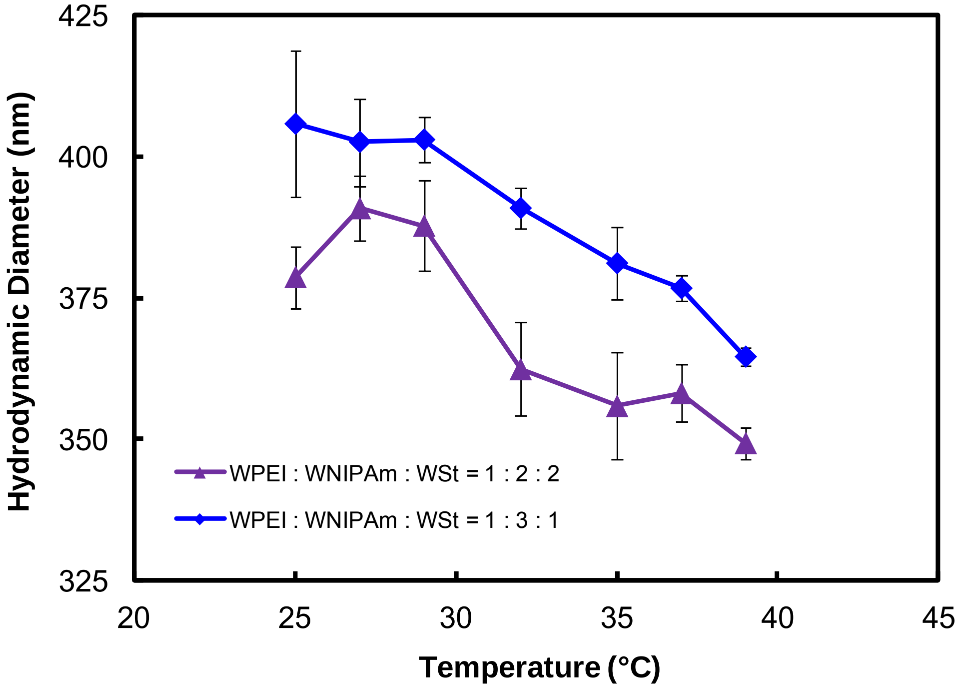

**Fig. 4.26.** Particle size as a function of temperature of PS/(PNIPAm-10% MBA)/PEI MCP particles (10% MBA crosslinking).

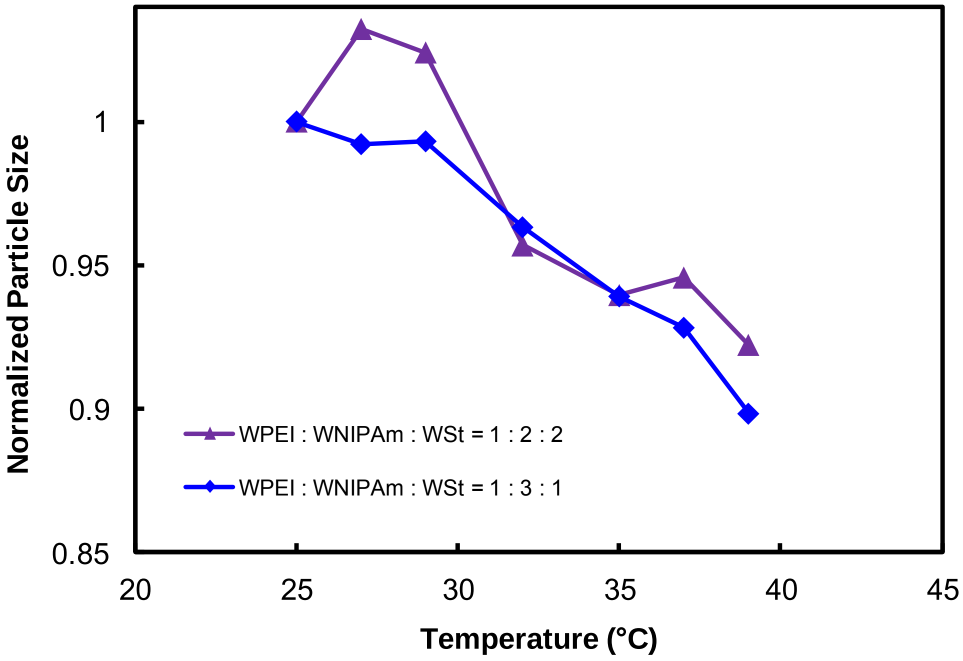

**Fig. 4.27.** Normalized particle size ($Dh/Dh_{25\ °C}$) as a function of temperature of PS/(PNIPAm-10% MBA)/PEI MCP particles (10% MBA crosslinking).

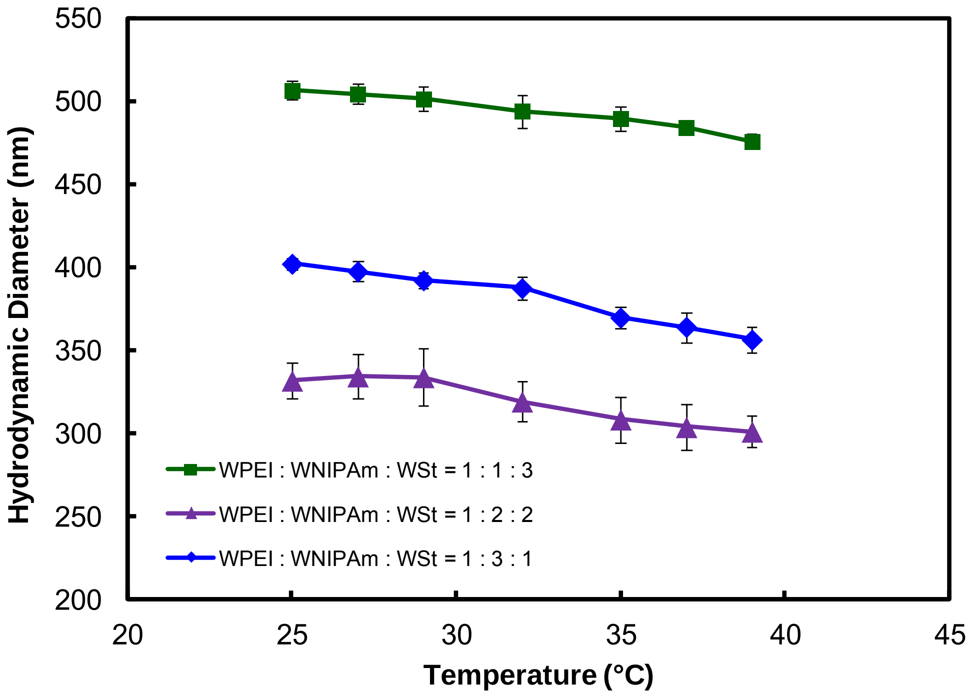

**Fig. 4.28.** Particle size as a function of temperature of PS/(PNIPAm-5% MBA)/PEI MCP particles (5% MBA crosslinking).

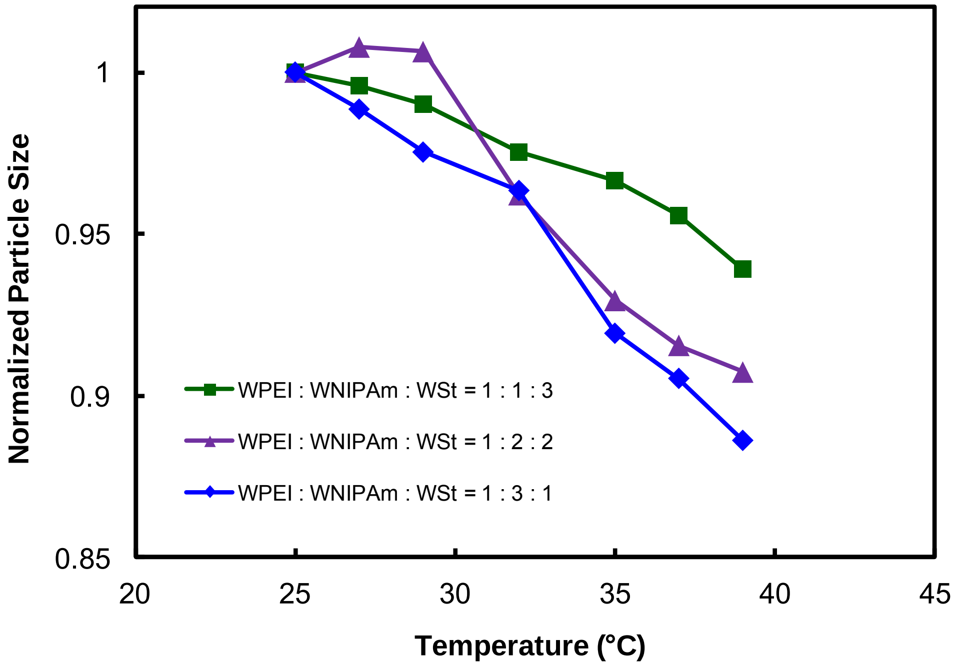

**Fig. 4.29.** Normalized particle size ($Dh/Dh_{25\ °C}$) as a function of temperature of PS/(PNIPAm-5% MBA)/PEI MCP particles (5% MBA crosslinking).

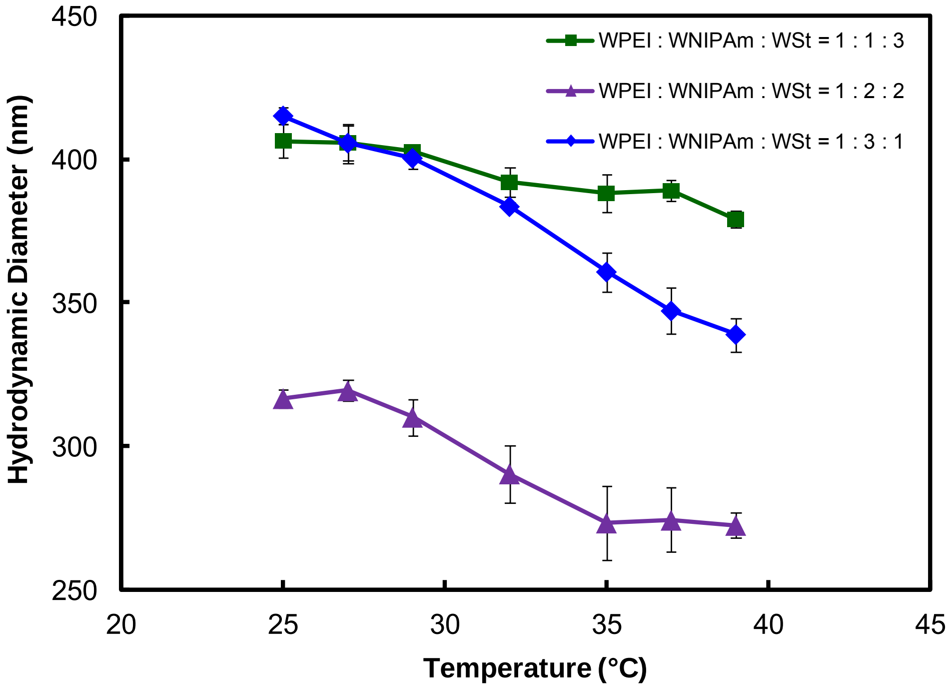

**Fig. 4.30.** Particle size as a function of temperature of PS/(PNIPAm-2% MBA)/PEI MCP particles (2% MBA crosslinking).

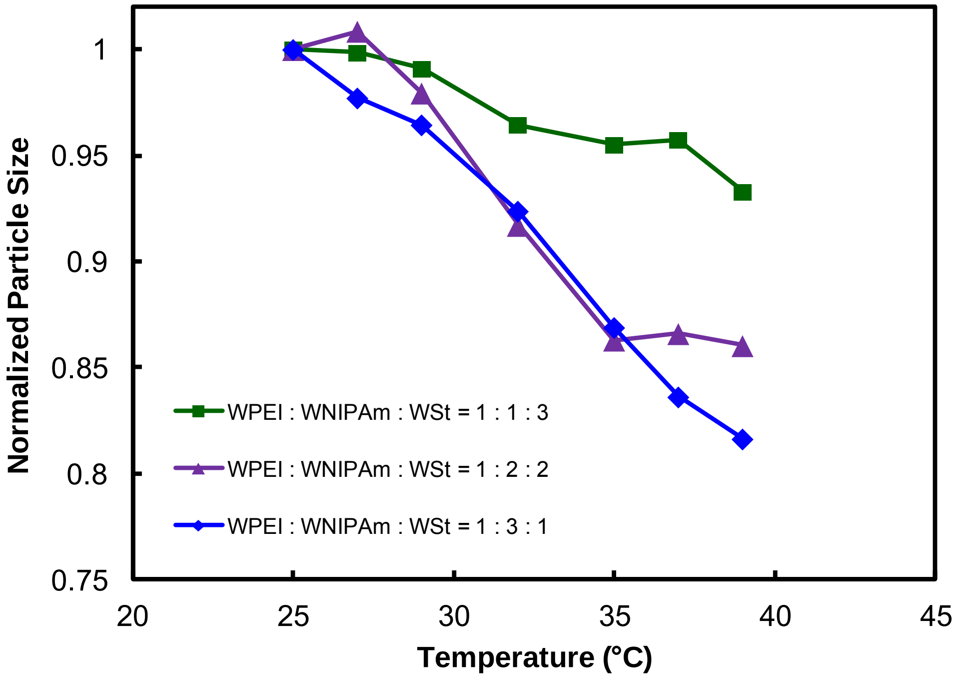

**Fig. 4.31.** Normalized particle size ($Dh/Dh_{25\ °C}$) as a function of temperature of PS/(PNIPAm-2% MBA)/PEI MCP particles (2% MBA crosslinking).

### *4.3.6.4 Surface charges of particles as a function of pH and temperature*

#### *Surface charges*

The surface charge of MCP particles was determined by ζ-potential measurement using Beckman Coulter Delsa Nano C instrument. Under standard condition, pH 7 with conducting medium of 1 mM NaCl, the ζ-potential of PNIPAm/PEI seed microgel and PS/(PNIPAm-MBA)/PEI MCP particles were + 12.78 mV and + 16.45 mV respectively. The low magnitude of ζ-potential of both seed and MCP particles was due to the formation of PNIPAm/PEI interpenetrated network at the outermost shell of the particles as explained in **4.3.2.5**. The charge shielding of PEI by PNIPAm resulted in the suppression of the charge density of the particles.

#### *Effect study of degree of MBA crosslinkingon the surface charges of particles*

The effect of pH on the ζ-potential of MCP particles at was evaluated by ζ-potential measurement using Delsa Nano C with the aid of auto-titrator. The variation of ζ-potential as a function of pH of MCP particles with different degree of crosslinking was illustrated in Figure 4.32.

Independent of the crosslinking degree, the surface of PS/(PNIPAm-MBA)/PEI MCP particles was positively charged and the ζ-potential almost remains unchanged below pH 7. The positive ζ-potential of MCP particles was contributed by the protonated amino groups of PEI located at the outermost shell of the MCP particles. As the pH of the medium was raised to above 7, there was a drop in the ζ-potential of MCP particles. The drop in ζ-potential was due to the deprotonation of the amino groups. Eventually, the ζ-potential of MCP particles was dropped to about zero as the pH of the medium was approached 9.5, isoelectric point of PEI.

Although PS/(PNIPAm-MBA)/PEI MCP particles with different crosslinking degree had the same trend in the variation of ζ-potential against pH, the magnitude of ζ-potential was affected by the degree of crosslinking. The ζ-potential of PS/(PNIPAm-MBA)/PEI MCP particles with 10%, 5% and 2% crosslinking at pH 7 were + 31.07 mV, + 28.08 mV and + 16.45 mV respectively. The magnitude of ζ-potential of MCP particles was suppressed from + 31.07 mV to + 16.45 mV as the degree of crosslinking decreased from 10% to 2%. The suppression in the surface charge of the MCP particles was attributed to the formation of interpenetrated network in the outermost shell as explained in **4.3.2.4**. PNIPAm was slightly crosslinked under low crosslinking degree. PNIPAm was not confined at the innermost core and was extended in the outermost shell. The outermost shell of the particles was an interpenetrating network which composed of PNIPAm and PEI. As a result, there was significant shielding of positively charged PEI under low MBA crosslinking.

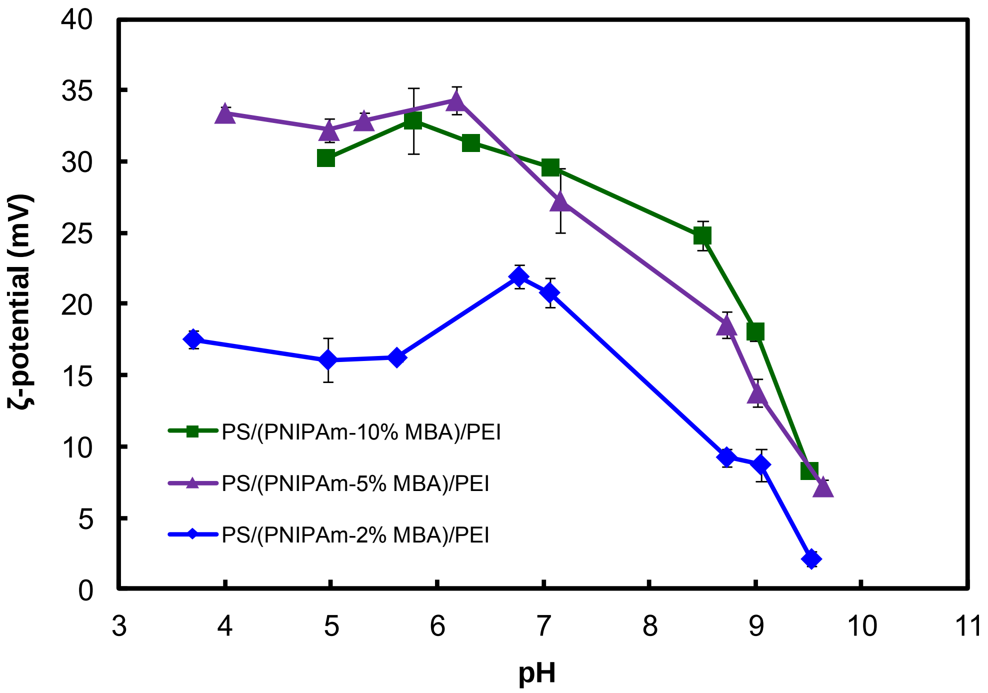

**Fig. 4.32.** ζ-potential as a function of pH of PS/(PNIPAm-MBA)/PEI MCP particles ($w_{PEI} : w_{NIPAm} : w_{St} = 1 : 2 : 2$).

The effect of temperature on the ζ-potential of MCP particles at different crosslinking degree was evaluated by ζ-potential measurement using Delsa Nano C with the aid of thermal monitoring device. In all measurements, MCP particles were first diluted to 200 ppm by 1 mM NaCl solution. The pH of the MCP particle samples was adjusted to 7 for the measurement. The samples were thermally equilibrated at preset temperature (25 °C, 27 °C, 29 °C, 32 °C, 35 °C, 37 °C and 39 °C) for 10 mins before ζ-potential measurement. The variation of ζ-potential as a function of temperature of MCP particles with different degree of crosslinking was illustrated in Figure 4.33.

Regardless of the degree of crosslinking, a general trend in the variation of ζ-potential of PS/(PNIPAm-MBA)/PEI MCP particles was observed. Below the VPTT of PNIPAm (32 °C), MCP particles had positive magnitude in ζ-potential and the ζ-potential was kept constant in this temperature range. As the temperature was raised to the VPTT of PNIPAm, there was an obvious jump in the ζ-potential of MCP particles. When the temperature was further raised, there was no insignificant increase in the ζ-potential of MCP particles. Eventually, the ζ-potential of MCP particles was approached to + 40 mV at 39 °C.

The variation in ζ-potential was regarded as the thermal responsive properties of MCP particles. Within the temperature range for the ζ-potential measurement (from 25 °C to 39 °C), MCP particles had a positive magnitude in ζ-potential. This implied MCP particles was positively charged and the positive charges was contributed by the protonated amino groups on PEI. Below VPTT of PNIPAm, MCP particles had low ζ-potential magnitude because of the interpenetrated shell. PNIPAm was hydrophilic and was extended in the outer shell of the MCP particles. The outermost shell of MCP particles was constructed by an interpenetration network of PNIPAm and PEI. Positively charged PEI was partially shielded by the PNIPAm, leadind to suppression in the ζ-potential of MCP particles.

When the temperature was above VPTT of PNIPAm (32°C), there was an abrupt increase in the ζ-potential of the MCP particles. Further increase in the temperature did not induce significant changes in the ζ-potential. This abrupt increase in the ζ-potential of MCP particles was attributed to the volume phase transition of PNIPAm. Across the VPTT of PNIPAm, the PNIPAm underwent phase transition which changed from hydrophilic to hydrophobic. The intermolecular hydrogen bonding between PNIPAm and water molecules was broken down. Intramolecular hydrogen bond was formed on PNIPAm instead. The coil-to-globule transition of PNIPAm resulted in migration of PNIPAm from the outer shell to inner core in order to minimize the interfacial energy. After volume phase transition of PNIPAm, the outermost shell of the MCP particles was solely composed of PEI. The positive charges on PEI were not shielded by PNIPAm and were fully exposed. The re-exposure of positively charged PEI resulted in significant increase in the ζ-potential to about + 40 mV. Thus, the volume phase transition of PNIPAm across its VPTT not only led to reduction in hydrodynamic diameter, but also contributed to increase in the ζ-potential.

The ζ-potential of PS/(PNIPAm-MBA)/PEI was affected by the degree of MBA crosslinking below VPTT of PNIPAm (32 ℃). The ζ-potential of 10%, 5% and 2% MBA crosslinked PS/(PNIPAm-MBA)/PEI MCP particles were + 31.07 mV, + 28.05 mV and + 16.45 mV at 25 ℃ respectively. MCP particles had the greatest magnitude in ζ-potential under 10% MBA crosslinking. At this circumstance, PNIPAm was tightly confined by the crosslinker from being interpenetrated with PEI in the outer shell. Positively charged PEI was not severely shielded by the PNIPAm. As a result, the ζ-potential of MCP particles was not significantly suppressed and maintained at a high value (> + 30 mV).

Nevertheless, the ζ-potential of MCP particles was obviously affected under 2% MBA crosslinking. At this circumstance, PNIPAm was not confined by the crosslinker and was extensively interpenetrated with PEI in the outermost shell. Positively charged PEI was extensively shielded by PNIPAm which resulted in significant suppression in the ζ-potential of MCP particles. These results indicated that the degree of crosslinking played an important role in the charge surface density of the particles.

The descending order of ζ-potential of PS/(PNIPAm-MBA)/PEI at 25 °C can be expressed as:

***10% MBA crosslinked MCP > 5% MBA crosslinked MCP > 2% MBA crosslinked MCP***

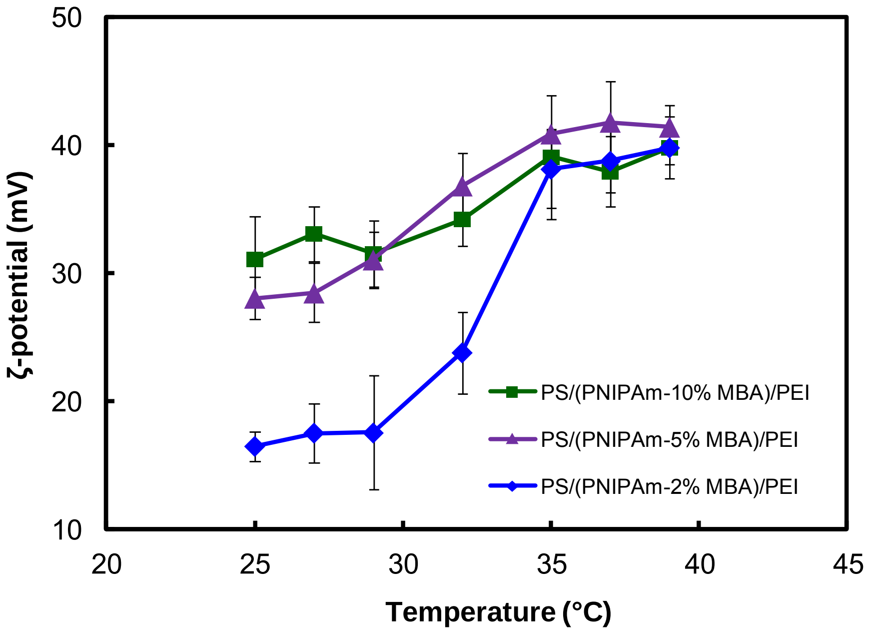

**Fig. 4.33.** ζ-potential as a function of temperature of PS/(PNIPAm-MBA)/PEI MCP particles ($w_{PEI} : w_{NIPAm} : w_{St.} = 1 : 2 : 2$).

***Effect study of weight ratio between seed monomer and second batch monomer on the surface charges of particles***

The effect of weight ratio between NIPAm and styrene on the ζ-potential of PS/(PNIPAm-MBA)/PEI MCP particles at different pH was conducted by ζ-potential measurement using Delsa Nano C with the aid of auto-titrator. The variation of ζ-potential of PS/(PNIPAm-MBA)/PEI MCP particles as a function of pH was plotted and displayed as follows according to their degree of crosslinking (10%, 5% and 2%).

The effect of NIPAm/styrene weight ratio on the ζ-potential of PS/(PNIPAm-MBA)/PEI MCP particles at 10% and 5% MBA crosslinking was not significant. At 10% MBA crosslinking, the ζ-potential of PS/(PNIPAm-MBA)/PEI MCP particles with NIPAm/styrene weight ratio at 1 : 1 and 3 : 1 at pH 7 were + 31.07 mV and + 29.38 mV respectively. At 5% MBA crosslinking, the ζ-potential of PS/(PNIPAm-MBA)/PEI MCP particles with NIPAm/styrene weight ratio at 1 : 3 , 1 : 1 and 3 : 1 at pH 7 were + 34.19 mV, + 28.05 mV and + 29.09 mV respectively. At 10% and 5% MBA crosslinking, PNIPAm was highly crosslinked by the MBA and inhibited from forming interpenetrated network in the outermost shell. PEI was not shielded by PNIPAm and was exposed in the outermost shell. Hence, the weight ratio between PNIPAm and styrene did not exert significant effect on the ζ-potential of the PS/(PNIPAm-MBA)/PEI MCP particles because of high crosslinking degree.

The effect of NIPAm/styrene weight ratio on the ζ-potential of PS/(PNIPAm-MBA)/PEI MCP particles became obvious at 2% MBA crosslinking. At 2% MBA crosslinking, the ζ-potential of PS/(PNIPAm-MBA)/PEI MCP particles with NIPAm/styrene weight ratio at 1 : 3 , 1 : 1 and 3 : 1 at pH 7 were + 30.37 mV, + 16.45 mV and + 14.78 mV respectively. When the total monomer consisted of 25% NIPAm by weight, the ζ-potential of MCP particles was high (> + 30 mV). Although the crosslinking degree was low, the amount of PNIPAm was insufficient to interpenetrate and shield the positively charged PEI in the outer shell. PEI was not completely shielded by PNIPAm and still was the major component in the outermost shell. This resulted in high magnitude in the ζ-potential of the MCP particles. Nevertheless, there was a significant suppression in the ζ-potential of the MCP particles when the NIPAm composition increased.

As the total monomer contained contained more than 50% NIPAm by weight, the amount of PNIPAm was sufficient to form interpenetration network with PEI in the outermost shell. The hydrophilic PNIPAm was highly extended in the outer shell and effectively shielded the positively charged PEI. Due to the charge shielding of PEI, there was a significant suppression in the ζ-potential magnitude of the MCP particles. The surface charge density of MCP particles could be varied by the total monomer compositions.

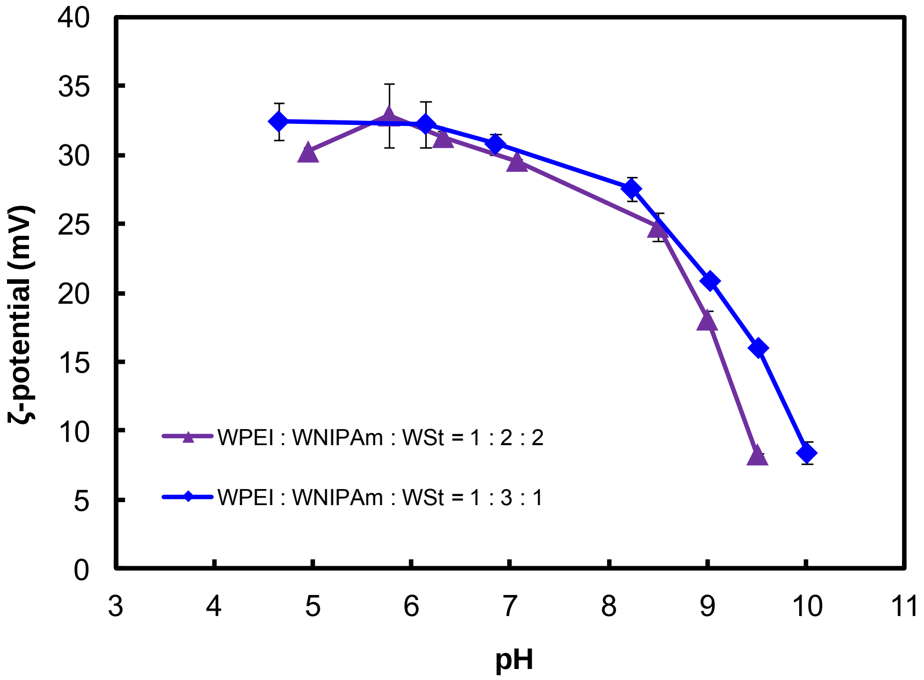

**Fig. 4.34.** ζ-potential as a function of pH of PS/(PNIPAm-10% MBA)/PEI MCP particles (10% MBA crosslinking).

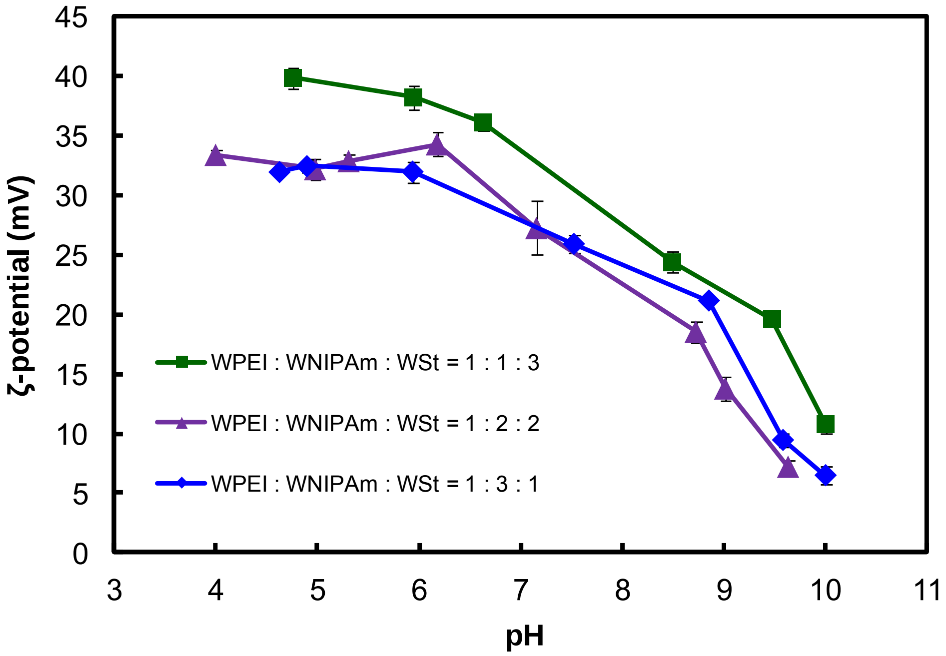

**Fig. 4.35.** ζ-potential as a function of pH of PS/(PNIPAm-5% MBA)/PEI MCP particles (5% MBA crosslinking).

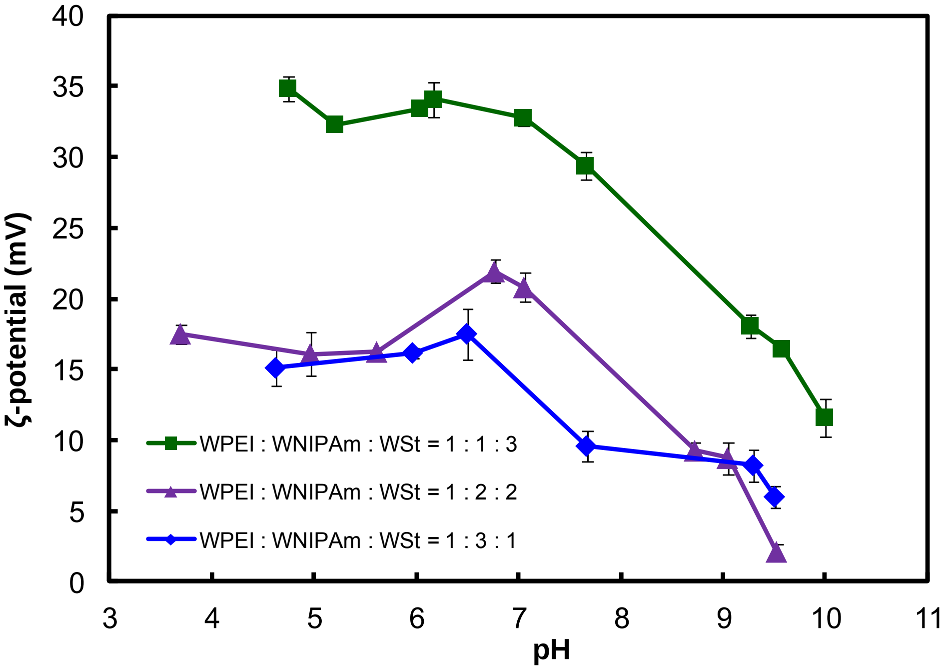

**Fig. 4.36.** ζ-potential as a function of pH of PS/(PNIPAm-2% MBA)/PEI MCP particles (2% MBA crosslinking).

The effect of temperature on the ζ-potential of MCP particles at different NIPAm/styrene weight ratio at 10%, 5% and 2% MBA crosslinking was evaluated by ζ-potential measurement using Delsa Nano C with the aid of thermal monitoring device. In all measurements, MCP particles were first diluted to 200 ppm by 1 mM NaCl solution. The pH of the MCP particle samples was adjusted to 7 for the measurement. The samples were thermally equilibrated at preset temperature (25 ℃, 27 ℃, 29 ℃, 32 ℃, 35 ℃, 37 ℃ and 39 ℃) for 10 mins before ζ-potential measurement. The variation of ζ-potential as a function of temperature of MCP particles with different NIPAm/styrene composition as a function of temperature was plotted and displayed according to their crosslinking degree (10%, 5% and 2%).

Similarly, a general trend in the variation of the ζ-potential was observed in PS/(PNIPAm-MBA)/PEI MCP particles at different NIPAm/styrene composition. Below VPTT of PNIPAm, the ζ-potential of MCP particles was positively charged and almost unchanged. When the temperature was promoted to above VPTT (32 °C), there was an abrupt increase in the ζ-potential due to the volume phase transition of PNIPAm. PNIPAm was hydrophilic below its VPTT which became hydrophobic above its VPTT. The interamolecular hydrogen bond was broken down and intramolecular hydrogen bond was formed instead. To minimize the interfacial energy, PNIPAm was migrated into the inner core. Positively charged PEI was re-exposed which indicated by an increase in the ζ-potential.

Considering the systems of 10% and 5% MBA crosslinking, the effect of NIPAm/styrene composition on the ζ-potential of PS/(PNIPAm-MBA)/PEI as a function of temperature was not significant actually. The plots of ζ-potential with different NIPAm/styrene composition were almost overlapped with each other. This implied the changes in NIPAm/styrene composition did not have significant impact on the thermal responsiveness of MCP particles. High crosslinking degree of MCP particles should be the major reason for this finding. Under high MBA crosslinking, PNIPAm was tightly crosslinked and constrained from forming interpenetrated network with PEI. PEI became the major component in the outer shell where positive charges of PEI were slightly shielded. At this circumstance, the effect crosslinking degree outweighted the effect of NIPAm/styrene composition. Thus, the effect of NIPAm/styrene composition on ζ-potential was insignificant due to limited extension of PNIPAm in the outermost shell by high crosslinking degree.

Nevertheless, the effect of NIPAm/styrene composition on the ζ-potential of the PS/(MBA-PIPAM-PEI) MCP particles became more significant as the crosslinking degree was reduced to 2%. The ζ-potential of PS/(PNIPAm-MBA)/PEI MCP particles with NIPAm/styrene weight ratio at 1 : 3 , 1 : 1 and 3 : 1 were + 30.37 mV, + 16.45 mV and + 14.78 mV at 25 °C respectively. There was suppression in ζ-potential magnitude of MCP particles as the NIPAm composition increased. This was due to the charge shielding of PEI by PNIPAm via the formation of interpenetrated shell. At low crosslinking degree, PNIPAm was not tightly confined and was ultimately extended in the outer shell of the particles. An interpenetrated shell composed of PNIPAm and PEI was then constructed in the outermost shell. Positively charged PEI was shielded by the PNIPAm which led to suppression of ζ-potential. Therefore, the ζ-potential of MCP particles was dropped from + 30.37 mV to + 14.78 mV as the NIPAm composition in the total monomer increased from 25% to 75%. On the other hand, the ζ-potential of

PS/(PNIPAm-MBA)/PEI MCP particles with NIPAm/styrene weight ratio at 1 : 3 , 1 : 1 and 3 : 1 were + 40.38 mV, + 39.81 mV and + 39.90 mV at 39 °C respectively. The ζ-potential of all PS/(PNIPAm-MBA)/PEI MCP particles was approached to + 40 mV at 39 °C. Above VPTT, PNIPAm underwent volume phase transition which changed from hydrophilic to hydrophobic. To minimize the interfacial energy, hydrophobic PNIPAm was migrated to the inner core of the particles. The re-exposure of the positively charged PEI resulted in an increase in the ζ-potential. At this circumstance, PEI was almost completely re-exposed in the outermost shell as all MCP particles possessed the same ζ-potential at 39 °C. Therefore, NIPAm/styrene composition was another parameter to control the thermal responsive properties of MCP particles.

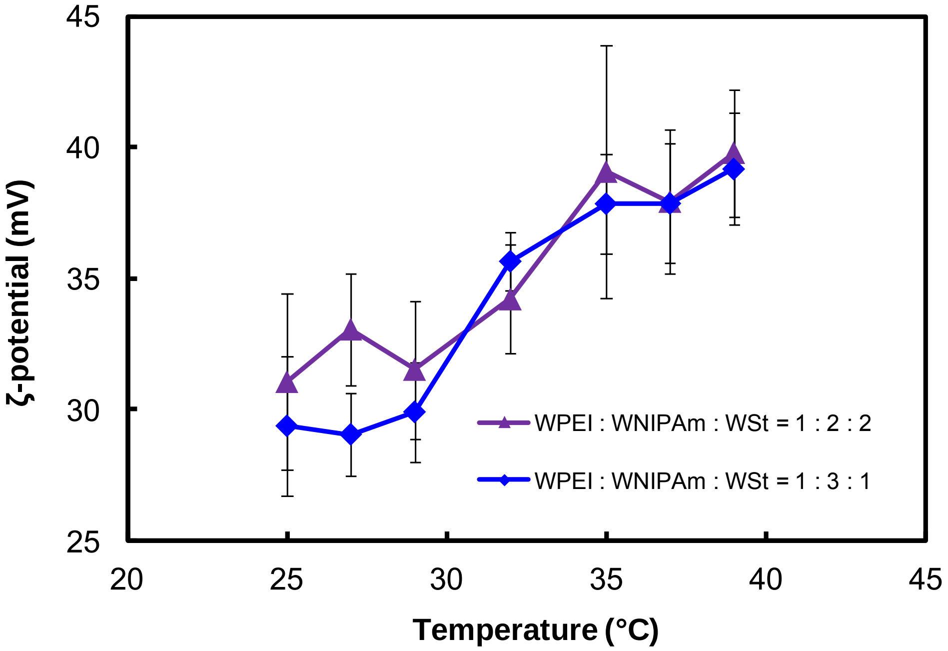

**Fig. 4.37.** ζ-potential as a function of temperature of PS/(PNIPAm-10% MBA)/PEI MCP particles (10% MBA crosslinking).

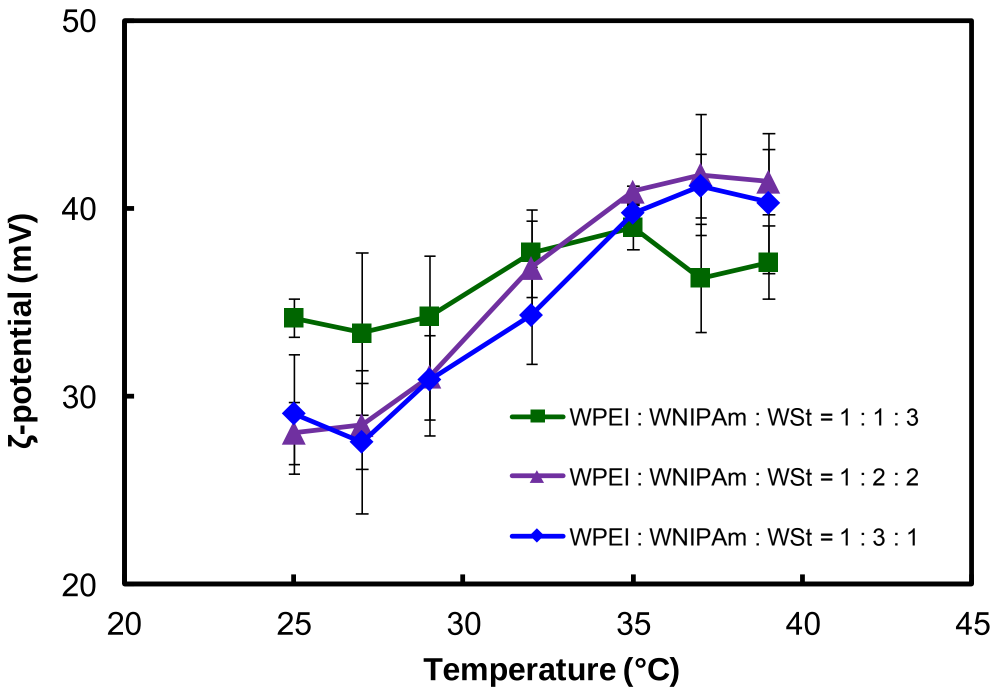

**Fig. 4.38.** ζ-potential as a function of temperature of PS/(PNIPAm-5% MBA)/PEI MCP particles (5% MBA crosslinking).

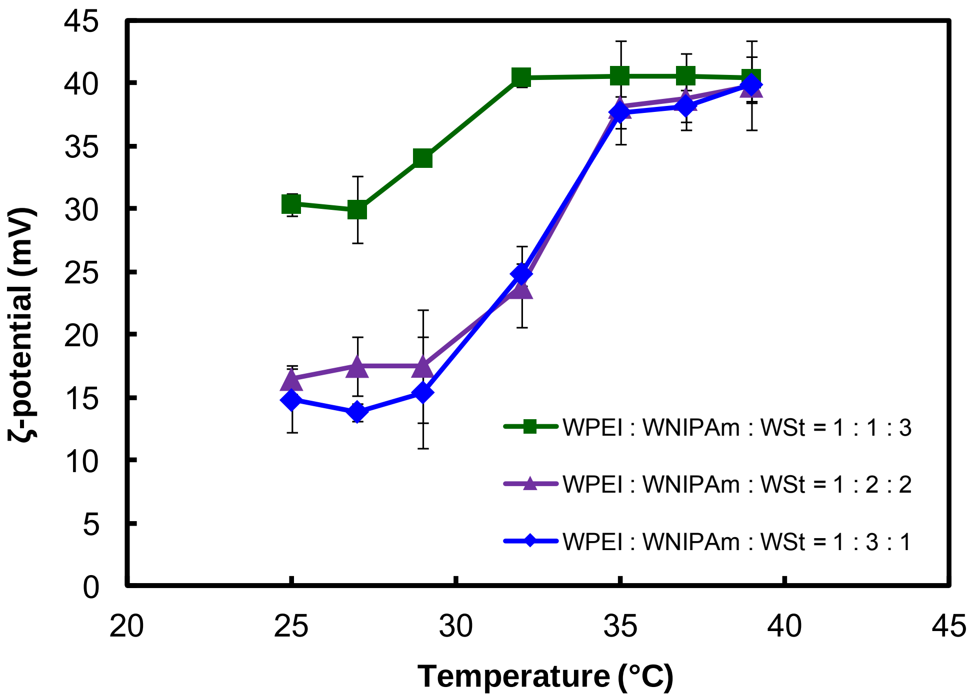

**Fig. 4.39.** ζ-potential as a function of temperature of PS/(PNIPAm-2% MBA)/PEI MCP particles (2% MBA crosslinking).

#### *4.3.6.5 Morphology*

The morphology and core-shell nanostructure of PS/(PNIPAm-MBA)/PEI MCP particles prepared at different degree of crosslinking were examined by FE-SEM and TEM. Well-defined core-shell nanostructure of MBA crosslinked PNIPAm/PEI seed particles was observed in TEM micrographs. The dark core of the particles was the heavily stained PNIPAm and the bright shell was the slightly stained PEI.

Highly uniform particles with spherical morphology was observed in the SEM micrographs of all PS/(PNIPAm-MBA)/PEI MCP particles. To elucidate the nanostructure of the MCP particles, these particles were stained with 0.5% (w/w) phosphotungstic acid (PTA, $WO_2 \cdot H_3PO_4 \cdot xH_2O$) for 5 mins. Well-defined core-shell nanostructured particles were revealed in the TEM micrographs. During PTA staining, PNIPAm was heavily stained by PTA solution while PEI was slightly stained by PTA solution. PS was not stained by PTA solution. Thus, we interpreted that the dark shell was constructed by an interpenetrated network of PEI and PNIPAm and the bright core of the particles was constructed by PS.

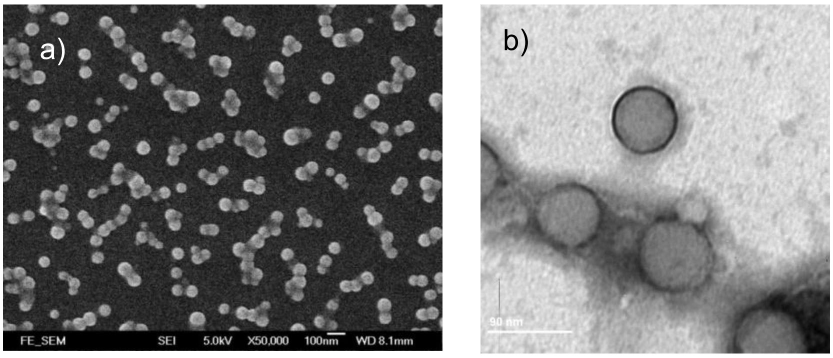

**Fig. 4.40.** Morphology of PS/(PNIPAm-10% MBA)/PEI MCP particles: a) SEM image; b) TEM image.

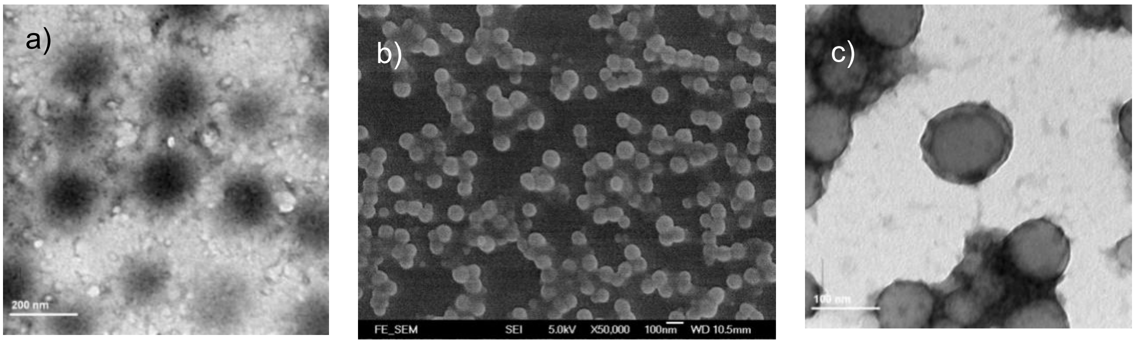

**Fig. 4.41.** Morphology of PNIPAm/PEI seed particles (5% MBA crosslinked): a) TEM image; Morphology of PS/(PNIPAm-5% MBA)/PEI MCP particles: b) FE-SEM image; c) TEM image.

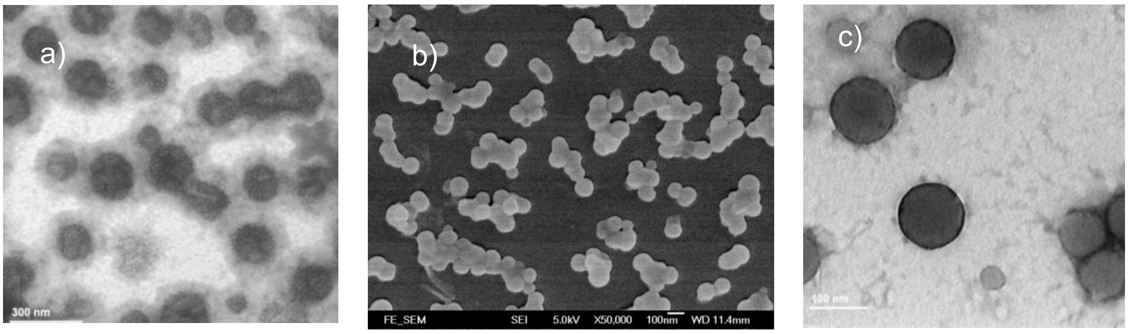

**Fig. 4.42.** Morphology of PNIPAm/PEI seed particles (2% MBA crosslinked): a) TEM image; Morphology of PS/(PNIPAm-2% MBA)/PEI MCP particles: b) FE-SEM image; c) TEM image.

## 4.4 Effect of Second Batch Monomer on the Properties of MCP Nanocomposite Particles

The effect of second batch monomer on the smart properties and nanostructures of MCP particles is discussed in detail in this part. To be consistent, all the MCP particles discussed in this part were crosslinked by 2% MBA. The characteristics of the seed hydrogel and MCP particles were summarized in Table 4.10.

The reaction kinetics of the seeded emulsion polymerization of MCP nanocomposites was monitored by thermal couple (Testo 735) with 1 temperature recorded per second. Fig. 4.2, Fig. 4.12 and Fig. 4.21 showed the temperature profile of the preparation of PMMA/(PNIPAm-MBA)/PEI, PBA/(PNIPAm-MBA)/PEI and PS/(PNIPAm-MBA)/PEI MCP particles respectively. Two obvious exothermic peaks were observed in the temperature profiles. As explained before, the first peak was due to the exothermic polymerization of NIPAm in the seed forming stage. The monomer conversion of NIPAm reached 99%. The second peak was due to the exothermic polymerization of second batch monomer during seeded emulsion polymerization. The total monomer conversions of all MCP particles were over 90% at the end of polymerization.

**Table 4.10.** Characteristics of 2% MBA crosslinked PNIPAm/PEI seed hydrogel and MCP particles.

| Types of Particles | Second batch monomer | Monomer conversion[2] | Hydrodynamic radius (nm)[3] | | | | ζ-potential (mV)[4] | | | |
|---|---|---|---|---|---|---|---|---|---|---|
| | | | Rh (25°C) | Rh (32°C) | Rh (39°C) | $\mathrm{Rh}_{39^\circ\mathrm{C}}/\mathrm{Rh}_{25^\circ\mathrm{C}}$ | ζ-potential (pH 7) | ζ-potential (25°C) | ζ-potential (32°C) | ζ-potential (39°C) |
| **Seed hydrogel** | **N/A** | **99%** | **182.65** | **141.59** | **110.38** | **0.60** | **+ 1.32** | **+ 1.32** | **+ 3.83** | **+ 25.92** |
| **MCP particles[1]** | **MMA** | **90%** | **191.94** | **177.01** | **162.21** | **0.85** | **+ 13.32** | **+ 13.32** | **+ 22.44** | **+ 37.22** |
| | ***n*-BA** | **91%** | **181.52** | **152.22** | **135.42** | **0.75** | **+ 4.54** | **+4.54** | **+ 10.11** | **+ 27.58** |
| | **Styrene** | **94%** | **165.9** | **149.12** | **133.23** | **0.80** | **+ 3.93** | **+ 3.93** | **+ 6.68** | **+ 25.50** |

[1] The weight ratio between PEI to total monomer was kept at 1 : 4; while the weight ratio between NIPAm to second batch hydrophobic monomer was kept at 1 : 1 (NIPAm composition : 50%)

[2] The monomer conversion was determined gravimetrically

[3] The hydrodynamic radius of MCP particles was determined by DLS at specific temperature and the samples were thermally equilibrated for 20 mins prior measurement. Assuming the MCP particles were spherical in shape, the hydrodynamic diameter was calculated as two times the hydrodynamic radius obtained from DLS measurements.

[4] The colloidal stability of MCP particles was determined by ζ-potential measurement using 1 mM NaCl as medium and the samples were thermally equilibrated for 10 mins prior measurement

### 4.4.1 Particle size as a function of temperature

#### *Particle size*

The hydrodynamic radii of seed and MCP particles were determined by ALV/DLS/SLS-6000 compact goniometer system (Peters) equipped with a He-Ne laser (632.8 nm) at pH 7. The hydrodynamic radius of PNIPAm/PEI seed was 182.65 nm at 25℃. The hydrodynamic radius of PMMA/(PNIPAm-MBA)/PEI, PBA/(PNIPAm-MBA)/PEI and PS/(PNIPAm-MBA)/PEI were 191.94 nm, 181.52 nm and 165.90 nm at 25℃ respectively. This indicated both seed and MCP particles were in nano-sized dimension. The difference in hydrodynamic raidus between PNIPAm/PEI seed and MCP particles was insignificant. As explained in **4.3.1.1**, the small difference in particle size was caused by the highly swollen hydrogel structure of PNIPAm/PEI seed and the formation of compact core of MCP particles..

#### *Particle size as a function of temperature*

The thermal responsiveness of seed hydrogel and MCP particles synthesized with different second batch monomer (MMA, *n*-BA and styrene) was evaluated by dynamic light scattering experiments with an ALV/DLS/SLS-6000 compact goniometer system (Peters) equipped with a He-Ne laser (632.8 nm) and a thermostat (Rotilabo, ± 0.1 ℃) for temperatures between 15 and 45 ℃. The MCP particles were allowed to reach thermal equilibrium for 20 mins before DLS measurement. The variation of the hydrodynamic radius of PNIPAm/PEI seed and MCP particles against temperature was plotted in Figure 4.43.

Below VPTT of PNIPAm, there was no significant change in the particle size of both PNIPAm/PEI seed and MCP particles. When the temperature was raised to above 32 ℃ (VPTT of PNIPAm), an abrupt drop in the hydrodynamic radii of both PNIPAm/PEI seed and MCP particles was recorded. This drop was due to the phase transition of PNIPAm from hydrophilic to hydrophobic. The hydrophobic PNIPAm was then migrated to the particle core, leading to shrinkage in the particle size of MCP particles. Further increasing in the temperature did not induce significant change in the particle size. This indicated the reduction in particle size was contributed by volume phase transition of PNIPAm.

To further evaluate the thermal responsive properties of the MCP particles, the hydrodynamic radius was re-expressed as normalized hydrodynamic radius which demonstrated the thermal responsive properties of MCP particles quantitatively. The normalized hydrodynamic radius of PNIPAm/PEI seed, PMMA/(PNIPAm-MBA)/PEI, PBA/(PNIPAm-MBA)/PEI and PS/(PNIPAm-MBA)/PEI MCP particles at 39 ℃, $Rh_{39\,℃}/Rh_{25\,℃}$, were 0.60, 0.85, 0.75 and 0.80 respectively. The degree of shrinkage in particle size of different particles was arranged in descending order as follows.

Degree of shrinkage in particle size:

***PNIPAm/PEI > PBA/(PNIPAm-MBA)/PEI > PS/(PNIPAm-MBA)/PEI > PMMA/(PNIPAm-MBA)/PEI***

PNIPAm/PEI seed exhibited the most remarkable change in hydrodynamic radius as temperature increased. There was 40% reduction in the hydrodynamic radius of PNIPAm/PEI seed at 39 °C. Without any rigid components in the particle core, the migration of PNIPAm from the outer shell to the inner core was not restricted. This resulted in significant shrinkage in the particle size of PNIPAm/PEI seed.

The degree of shrinkage in particle size was less significant if second hydrophobic polymer (e.g. PMMA, PBA or PS) was introduced into the particles. The presence of these polymers retarded the migration of PNIPAm from the outer shell to inner core during its volume phase transition. The shrinkage in particle size strongly depended on the physical properties (e.g. glass transition and spatial arrangement) of the second polymer in the particle. PBA/(PNIPAm-MBA)/PEI MCP particles possessed the greatest thermal responsiveness in particle size among three MCP particles. There was a 25% reduction in the hydrodynamic radius of PBA/(PNIPAm-MBA)/PEI MCP particles at 39 °C. PBA was a soft, tacky polymer under room temperature due to its low $T_g$ (219 K). Soft PBA did not retard the migtration of PNIPAm significantly. As a result, there was a greater extend in the particle size reduction of PBA/(PNIPAm-MBA)/PEI MCP particles.

Oppositely, PMMA and PS were hard and rigid polymer under room temperature. The $T_g$ of PMMA and PS were 378 K and 373 K respectively. The presence of rigid polymer in the particle core had severely retarded the migration of PNIPAm during its phase transition. This resulted in lower degree in the particle shrinkage of PMMA/(PNIPAm-MBA)/PEI and PS/(PNIPAm-MBA)/PEI MCP particles. However, the reduction in hydrodynamic radius of PS/(PNIPAm-MBA)/PEI MCP particles (20%) was greater than PMMA/(PNIPAm-MBA)/PEI MCP particles (15%). The difference in the degree of particle shrinkage between these two MCP particles was attributed to their nanostructures. PS/(PNIPAm-MBA)/PEI MCP particles exhibited a spherical morphology in which PS was located at the inner core. PMMA/(PNIPAm-MBA)/PEI MCP particles exhibited an aero-lite morphology in which PMMA micro-domains were randomly distributed in the particle. The randomly distributed PMMA micro-domains acted as lock which restricted the migration of PNIPAm. This eventually retarded the particle shrinkage of PMMA/(PNIPAm-MBA)/PEI MCP particles. Therefore, PMMA/(PNIPAm-MBA)/PEI exhibited the lowest degree in the shrinkage of the hydrodynamic radius.

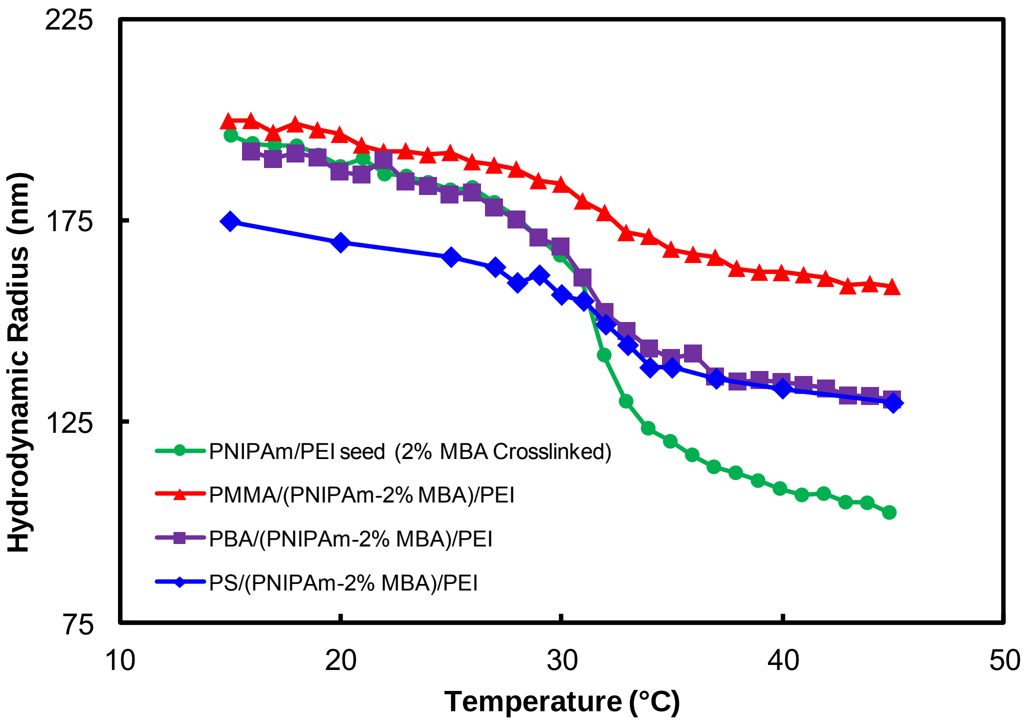

**Fig. 4.43.** Hydrodynamic radius of 2% MBA crosslinked MCP particles as a function of temperature.

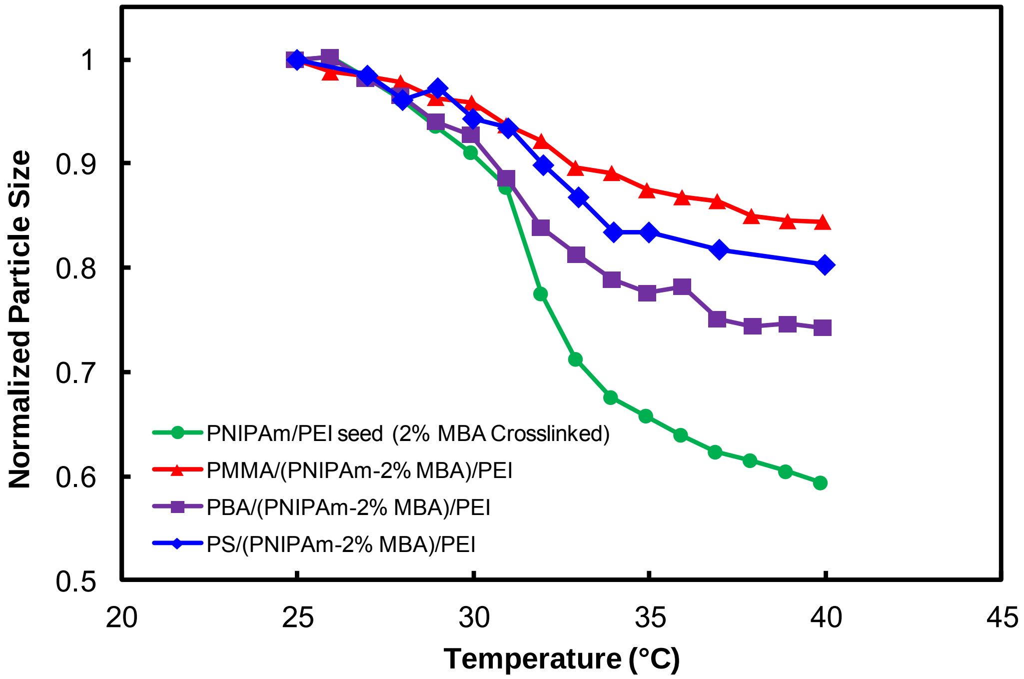

**Fig. 4.44.** Normalized particle size ($Rh/Rh_{25\ °C}$) of 2% MBA crosslinked MCP particles as a function of temperature.

### 4.4.2 Surface charges of particles as a function of pH and temeperature

***Surface charges***

The surface charge of MCP particles was determined by ζ-potential measurement using Beckman Coulter Delsa Nano C instrument. Under standard condition, pH 7 with conducting medium of 1 mM NaCl, the ζ-potential of PNIPAm/PEI seed hydrogel was + 1.32 mV at 25 °C. The ζ-potential of PMMA/(PNIPAm-MBA)/PEI, PBA/(PNIPAm-MBA)/PEI and PS/(PNIPAm-MBA)/PEI were + 13.32 mV, + 4.54 mV and + 3.93 mV at 25 °C respectively. Both PNIPAm/PEI seed and MCP particles had low ζ-potential magnitude. As explained before, the low ζ-potential was due to the formation of PNIPAm/PEI interpenetrated network in the outermost shell of the particles. The positive charges on PEI were shielded by PNIPAm. However, PMMA/(PNIPAm-MBA)/PEI had higher ζ-potential than the other three particles. This was caused by the difference in their nanostructures. All the particles possessed spherical morphology except PMMA/(PNIPAm-MBA)/PEI. PMMA/(PNIPAm-MBA)/PEI MCP particles possessed an aerolite-like nanostructure that numerous PMMA micro-domains were evenly distributed in the particles. These randomly distributed PMMA micro-domains acted as lock and hindered the interpenetration of PNIPAm and PEI. Therefore, the positive charges on PEI were partially shielded by PNIPAm, leading to a higher ζ-potential. PBA/(PNIPAm-MBA)/PEI and PS/(PNIPAm-MBA)/PEI MCP particles possessed spherical core-shell and multi-layered nanostructure where PBA and PS were localized in the particle core. These hydrophobic polymers did not hinder the formation of interpenetrated shell between PNIPAm and PEI. Positive charges on PEI were completely shielded by PNIPAm, leading to lower magnitude in the ζ-potential of MCP particles.

### ***Surface charges of particles as a function of pH***

The effect of pH on the ζ-potential of MCP particles prepared with different second batch monomer was evaluated by ζ-potential measurement using Delsa Nano C with the aid of auto-titrator. The variation of ζ-potential as a function of pH of MCP particles with different second batch monomer was illustrated in Figure 4.45.

MCP particles prepared with different second batch monomers (MMA, *n*-BA and styrene) had similar trend in the variation of ζ-potential as a function of pH. Below pH 7, the ζ-potential of MCP particles was positive and almost unchanged. The positive ζ-potential indicated the presence of PEI on the particle shell. When solution pH was above 7, there was an obvious decrease in the ζ-potential of MCP particles due to the deprotonation of the ammonium cations of the PEI. The ζ-potential of the MCP particles was dropped to below + 10 mV at pH 9.5, the isoelectric point of PEI.

Generally, PMMA/(PNIPAm-MBA)/PEI MCP particles had higher ζ-potential than PBA/(PNIPAm-MBA)/PEI and PS/(PNIPAm-MBA)/PEI MCP particles. As explained before, the high ζ-potential of PMMA/(PNIPAm-MBA)/PEI MCP particles was caused by its special nanostructure. Unlike PBA/(PNIPAm-MBA)/PEI and PS/(PNIPAm-MBA)/PEI, PMMA/(PNIPAm-MBA)/PEI possessed an aero-lite nanostructure that numerous PMMA micro-domains were randomly distributed in the particles. These micro-domains acted as locks which hindered the formation of interpenetrated shell between PNIPAm and PEI. The partial shielding of PEI in the outer shell resulted in high ζ-potential of PMMA/(PNIPAm-MBA)/PEI MCP particles.

PBA/(PNIPAm-MBA)/PEI MCP particles possessed the lowest magnitude in ζ-potential among three MCP particles. Similar to PS/(PNIPAm-MBA)/PEI, PBA/(PNIPAm-MBA)/PEI MCP particles exhibited spherical core-shell nanostructure where the second hydrophobic polymer was localized in the innermost core. However, the glass transition temperature of PBA (219 K) was lower than PS (373 K). PBA was a soft and tacky polymer while PS was a hard and rigid polymer under room temperature. The low $T_g$ of PBA allowed the rearrangement of polymer chains in the particles to reach the thermodynamic equilibrium morphology after the polymerization. Thus, PNIPAm was fully extended in the outer shell of PBA/(PNIPAm-MBA)/PEI, forming an interpenetrated shell with PEI. PEI was nearly completely shielded by PNIPAm, leading to low magnitude in ζ-potential of PBA/(PNIPAm-MBA)/PEI MCP particles.

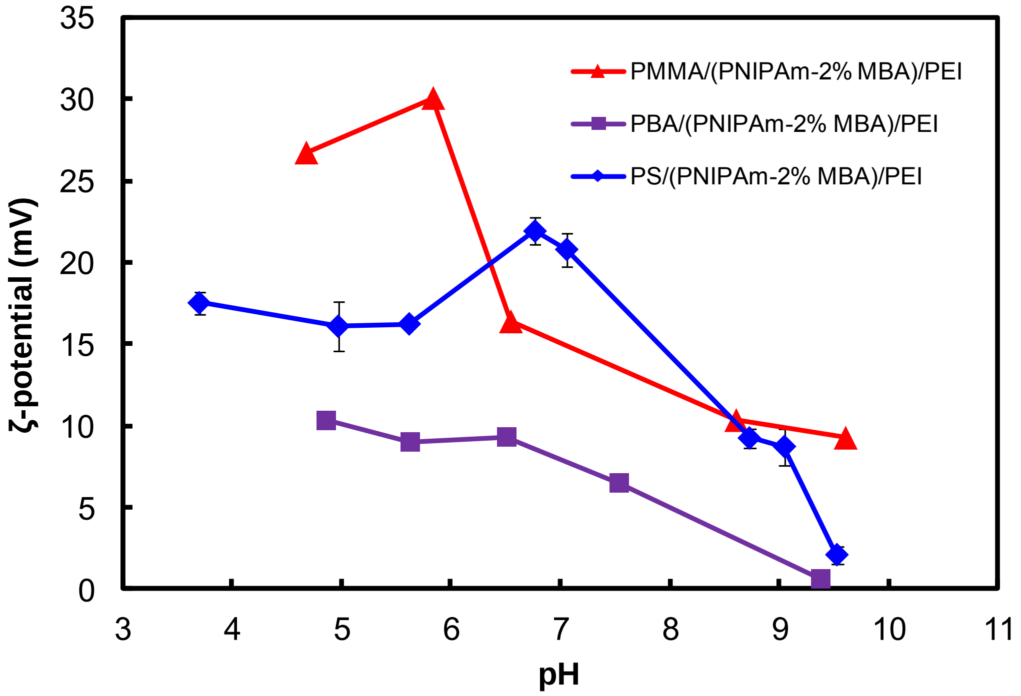

**Fig. 4.45.** ζ-potential as a function of pH of 2% MBA crosslinked MCP particles.

### *Surface charges of particles as a function of temperature*

The effect of temperature on the ζ-potential of MCP particles prepared with different second batch monomer (MMA, *n*-BA and styrene) was evaluated by ζ-potential measurement using Delsa Nano C with the aid of thermal monitoring device. The variation of ζ-potential as a function of temperature of MCP particles with second hydrophobic polymer as a function of temperature was displayed in Figure 4.46.

All the PNIPAm/PEI seed and MCP particles exhibited the same trend in the variation of ζ-potential as temperature increased as explained in **4.3.2.4**. The ζ-potential of seed and MCP particles was positive and kept constant at temperatures below VPTT of PNIPAm. There was an abrupt increase in the magnitude of ζ-potential when the temperature was rasied to above 32 °C. This increase was regarded as charge re-exposure on the particle surface. PNIPAm underwent phase transition at its VPTT which changed from hydrophilic to hydrophobic. Hydrophilic PNIPAm at the interpenetrated shell was shrunk and then migrated into the particle core. Thus, the positive PEI was not shielded by PNIPAm and resulted in an increase in the ζ-potential. This finding also indicated there was a change in the composition of the particle surface. The surface was composed of an interpenetrated network below VPTT of PNIPAm, while the surface was mainly composed of PEI above VPTT.

Nevertheless, PMMA/(PNIPAm-MBA)/PEI MCP particles had larger magnitudes in ζ-potential than the other three particles. This was attributed to the difference in their nanostructures which had been discussed before. PMMA/(PNIPAm-MBA)/PEI MCP particles exhibited a special aero-lite nanostructure that numerous PMMA micro-domains were randomly distributed in the MCP particles. These micro-domains functioned as lock which hindered the formation of interpenetrated network between PNIPAm and PEI. Positively charged PEI was partially shielded by PNIPAm, leading to higher magnitude in ζ-potential of PMMA/(PNIPAm-MBA)/PEI MCP particles. On the other hand, PNIPAm/PEI seed, PBA/(PNIPAm-MBA)/PEI and PS/(PNIPAm-MBA)/PEI MCP particles had spherical core-shell nanostructures. Second hydrophobic polymer (PBA or PS) was confined at particle core. These hydrophobic polymers did not affect the formation of interpenetrated network in the particle shell. Thus, PEI in the outer shell was significantly shielded by PNIPAm, leading to low magnitude in ζ-potential.

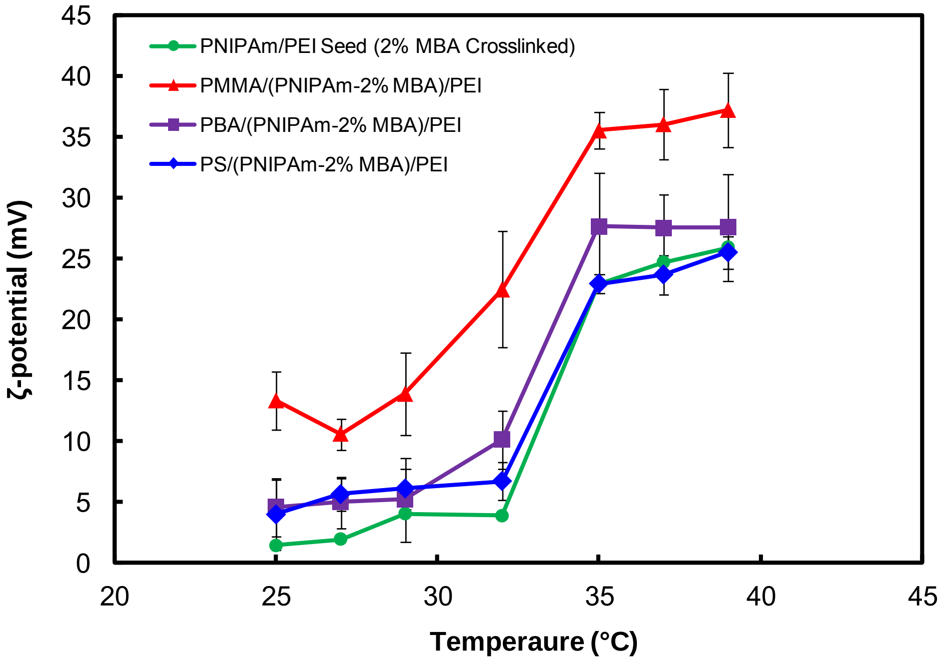

**Fig. 4.46.** ζ-potential as a function of temperature of 2% MBA crosslinked MCP particles.

### 4.4.3 Morphology

The morphology and nanostructure of MBA crosslinked PNIPAm/PEI seed, PMMA/(PNIPAm-MBA)/PEI, PBA/(PNIPAm-MBA)/PEI and PS/(PNIPAm-MBA)/PEI MCP particles were examined by FE-SEM and TEM.

With staining by 0.5% (w/w) phosphotungstic acid for 5 mins, well-defined core-shell nanostructured MBA crosslinked PNIPAm/PEI seed particles were observed in TEM micrographs. The dark core of the particles was the heavily stained PNIPAm and the bright shell was the slightly stained PEI. These seed particles possessed spherical morphology with uniform size distribution.

PMMA/(PNIPAm-MBA)/PEI MCP particles exhibited a special aerolite nanostructure under TEM investigation. Numerous bright micro-domains were randomly distributed in the particles, resulting in the construction of this special morphology. These bright domains were non-stained PMMA while the dark shell were composed of PTA stained PNIPAm and PEI. The formation of this morphology was due to high water solubility of MMA monomers (15 g/L). This facilitated the diffusion of MMA monomers from the continuous phase to the growing seed particles. In addition, MMA had high initiation rate which resulted in fast polymerization. As a result, numerous PMMA micro-doamins were formed and randomly distributed in the MCP particles, contributed to the aerolite nanostructure.

PBA/(PNIPAm-MBA)/PEI MCP particles exhibited a distorted spherical morphology with well-defined core-shell nanostructure. The bright core was PBA while the dark shell was composed of PTA stained PNIPAm and PEI. The formation of distorted spherical particles was attributed to the low $T_g$ of PBA. Unlike PMMA and PS, PBA had a low $T_g$ (219 K) which behaved as soft and tacky polymer under room temperature. In addition, PEI was low $T_g$ (213 K) polymer and PNIPAm was soft hydrogel. All the components in PBA/(PNIPAm-MBA)/PEI MCp particles were soft and tacky. Without rigid solid support, there was slightly distortion in the particle shape and resulted in distorted spherical morphology.

PS/(PNIPAm-MBA)/PEI MCP particles exhibited spherical morphology with well-defined core-shell nanostructure. The bright core was PS while the dark shell was composed of PTA stained PNIPAm and PEI. The confinement of PS at the innermost core resulted in the core-shell nanostructure of the particles. The presence of high $T_g$ (373 K) PS in the particle core provided a rigid solid support to the particles which maintained the spherical morphology from being distorted.

Besides water solubility of the second hydrophobic monomer, the inhomogeneous crosslinking distribution of the MBA crosslinked PNIPAm/PEI seed microgel also played an important role in determining the morphologies of MCP particles. Varga's research group had reported their research work on the distribution crosslinking in PNIPAm microgel latex in a literature [216]. The crosslinking distribution inside PNIPAm microgel latex was not homogeneous. The microgel core was highly crosslinked by MBA while the shell was slightly crosslinked. There was a radial decrease in the crosslinking density from the core to the shell. Thus, the crosslinking of PNIPAm microgel followed Gaussian segment density distribution.

Styrene and *n*-BA were more hydrophobic than MMA, these monomers preferred to be diffused into the more hydrophobic highly crosslinked core for polymerization. Therefore, PS and PBA were polymerized and located at the inner core of the particles. MMA was less hydrophobic than styrene and *n*-BA, which allowed them to be polymerized in the less hydrophobic slightly crosslinked shell. Hence, MMA was polymerized in the shell and core of the seed microgels, forming numerous micro-domains and randomly distributed in the particles.

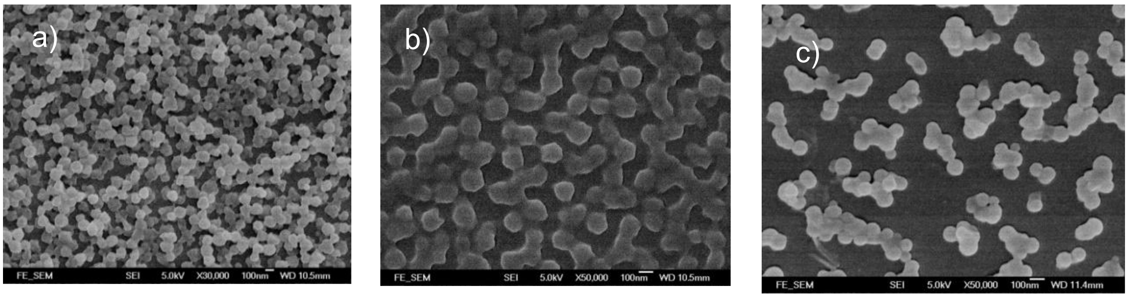

**Fig. 4.47.** SEM micrographs of a) PMMA/(PNIPAm-2% MBA)/PEI; b) PBA/(PNIPAm-2% MBA)/PEI; and c) PS/(PNIPAm-2% MBA)/PEI.

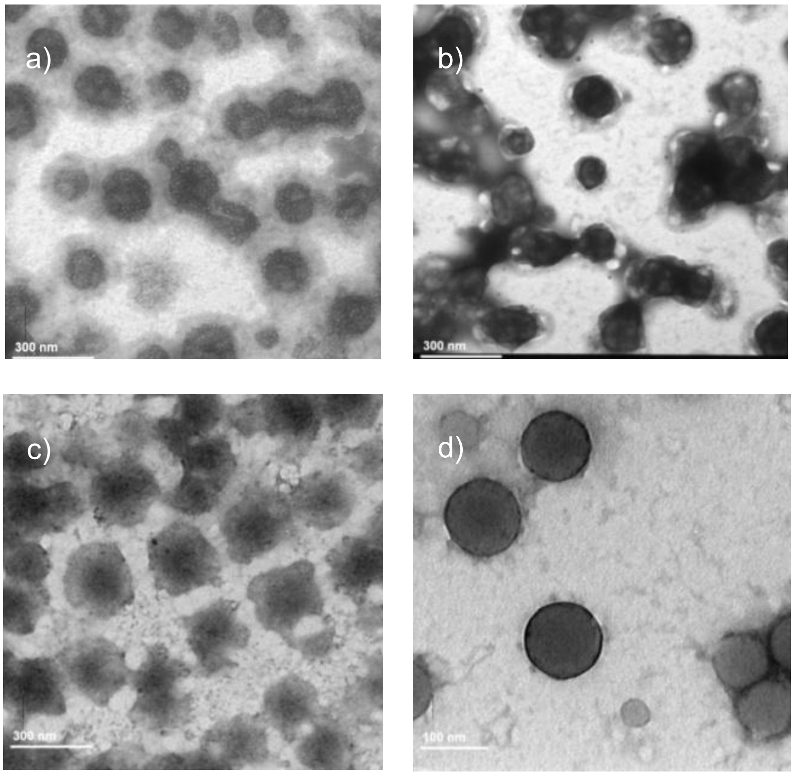

**Fig. 4.48.** TEM micrographs of a) PNIPAm/PEI seed hydrogel (2% MBA crosslinked); b) PMMA/(PNIPAm-2% MBA)/PEI; c) PBA/(PNIPAm-2% MBA)/PEI; and d) PS/(PNIPAm-2% MBA)/PEI.

## 4.5 Conclusion

Three types of multi-component polymer (MCP) particles, namely PMMA/(PNIPAm-MBA)/PEI, PBA/(PNIPAm-MBA)/PEI and PS/(PNIPAm-MBA)/PEI, were successfully prepared via seed emulsion polymerization using MBA crosslinked PNIPAm/PEI microgel as seed particles. MMA, *n*-BA and styrene monomer were added in the second stage and were polymerized via seed emulsion polymerization. Two stages of exothermic polymerization were observed through online temperature monitoring. Two exothermic peaks were observed in the temperature profiles which corresponded to the seed formation and seed emulsion polymerization. High conversion could be generally achieved via this synthetic route. Characterizations of these three types of MCP particles suggest that they possessed nanosized dimension and uniform size distribution with high positive charges and good colloidal stability. More importantly, the outer shell of these MCP particles was composed of PNIPAm/PEI, forming an interpenetrated shell. The presence of PNIPAm/PEI interpenetrated shell was proven by particle size and ζ-potential measurement. Beyond VPTT (32 °C) of PNIPAm, there was a remarkable shrinkage of outer shell PNIPAm, reflected by synergic effect on reduction of hydrodynamic diameter and increase in ζ-potential. The prepared MCP particles were dual stimuli responsive materials which responded to pH and temperature variations. In addition, effect of i) degree of crosslinking; ii) weight ratio between seed monomer and second hydrophobic monomer; and iii) types of second batch monomer on the pH- and thermal-responsive properties of MCP particles were also studied in this chapter.

The degree of MBA crosslinking strongly affects the thermal responsiveness of PNIPAm of MCP particles. When the MBA content decreased from 10% to 2%, the $Rh_{39\,°C}/Rh_{25\,°C}$ of PS/(PNIPAm-MBA)/PEI was decreased from 0.92 to 0.86. This indicated MCP particles had greater temperature responsiveness at lower degree of crosslinking. Also, the ζ-potential of PS/(PNIPAm-MBA)/PEI at pH 7 was + 31.07 mV and + 16.45 mV at 10% and 2% MBA crosslinking respectively. PNIPAm was not tightly confined under low crosslinking degree, allowing them to be extended in the outermost shell and interpenetrated with PEI. It could be concluded that MCP particles with lower crosslinking degree exhibited greater thermal responsive properties. Formation of MCP particles composed of pH and thermal responsive interpenetrated shell could be achieved by simply adjusting the MBA crosslinking degree.

The weight ratio between seed monomer and second batch monomer also affects the pH and thermal responsive properties of MCP particles. The weight ratio between NIPAm and styrene was varied from 1 : 3 to 3 : 1, keeping the PEI to total monomer ratio at 1 : 4. The degree of shrinkage in hydrodynamic diameter, $Rh_{39\,°C}/Rh_{25\,°C}$, of PS/(PNIPAm-2% MBA)/PEI particles decreased from 0.93 to 0.82 as the weight ratio between NIPAm to styrene increased from 1 : 3 to 3 : 1. The thermal responsive properties of MCP particles were improved as the NIPAm content increased. On the other hand, as the weight ratio between NIPAm to styrene increased from 1 : 3 to 3 : 1, the ζ-potential of MCP particles at pH 7 fell from + 30.37 mV to + 14.78 mV. This indicated increasing the NIPAm content had facilitated the formation of PNIPAm-PEI interpenetrated shell, leading to a stronger shielding effect on PEI. Thus the pH responsiveness of MCP particles reduced as the weight ratio between NIPAm to styrene increased from 1 : 3 to 3 : 1. As a result, the pH and thermal responsive properties of MCP particles could be tuned by varying the weight ratio between thermal sensitive seed monomer and hydrophobic second batch monomer.

Second batch hydrophobic monomer has played an important in determining the morphology of MCP particles. MMA, *n*-BA and styrene were selected as the second batch monomer. PS/(PNIPAm-MBA)/PEI and PBA/(PNIPAm-MBA)/PEI had spherical nanostructures where PS or PBA were located at the innermost core. The outermost shell of the particles was constructed by an interpenetrated PNIPAm-PEI shell. PMMA/(PNIPAm-MBA)/PEI was a special case that possessed a non-spherical aerolite-like structure. Although the outermost shell was still composed of PNIPAm-PEI interpenetrated network, numerous PMMA micro domains were formed and randomly distributed inside the particles. These micro domains acts as "lock" for the PNIPAm-PEI seed hydrogels, which hinders the shrinkage of PNIPAm at elevated temperature. The formation of such non-spherical irregular nanostructures was due to relatively high solubility and fast initiation rate of MMA monomers. Thus, different nanostructured MCP particles could be constructed by varying the type of second batch monomers.

# Chapter 5

## Synthesis and Characterization of PNIPAm-PEI based Multi-Component Polymer (MCP) Nanocomposite Particles using Second Batch Monomer as Crosslinker

This chapter describes the synthesis and characterization of multi-component polymer nanocomposite particles using non-crosslinked PNIPAm/PEI as seed nanoparticles. Two types of MCP nanocomposite particles were synthesized, namely PMMA/PNIPAm/PEI and PS/PNIPAm/PEI, through a semi-batch seeded emulsion polymerization. Non-crosslinked PNIPAm/PEI seed nanoparticles were first formed via TBHP induced graft copolymerization of NIPAm from PEI. Second batch of vinylic monomers, MMA or styrene, was subsequently added and polymerized in the presence of the seed nanoparticles. Scheme 2.3 illustrates the synthetic route and reaction conditions.

Properties of these two types of MCP nanocomposites, including particle size and size distrbution, surface charge, chemical composition and particle morphology were systematically characterized by dynamic light scattering, ζ-potential measurement, FTIR spectroscopy, field emission scanning electron microscopy and transmission electron microscopy.

## 5.1 Experimental Section

### 5.1.1 Material

Phenolic inhibitors, monomethyl ether hydroquinone (MEHQ), in methyl methacrylate (MMA, 0.936 g/cm$^3$, Sigma Aldrich) and *n*-butyl acrylate (*n*-BA, 0.894 g/cm$^3$, Sigma Aldrich), and phenolic inhibitors in styrene (St., 0.909 g/cm$^3$, Sigma Aldrich) were removed by washing the monomers by three times 10 w/w% sodium hydroxide (NaOH) and then with deionzed water until the water layer dropped to pH 7.

*N*-isopropylacrylamide (NIPAm, 97%, Wako Pure Chemical Industries) was purified by recrystallization method. NIAPm monomers were repeated dissolved and crystallized three times in mixed solvent of toluene and hexane in ratio of 1 : 5 (v/v) to give spindle-like crystals.

Polyethylenimine (PEI, $M_w$ 750,000 g/mol, 50 w/w% solution in water), *tert*-butyl hydroperoxide (TBHP, 70 w/w% solution in water), were purchased from Sigma Aldrich Co. and used without further purification. Freshly deionized Milli-Q water was used as the dispersion medium.

### 5.1.2 Synthesis of MCP nanocomposite particles using PNIPAm-PEI based seed microgels

For a total solution of 100 mL, PEI (2 g, 50 w/w% solution) was first dissolved in deionzed water and the pH of the solution was adjusted to 7 with 2 M HCl solution. The diluted PEI solution was then transferred into a three-necked water-jacketed equipped with thermal couple (Testo 735), a condenser, a magnetic stirrer, and a nitrogen inlet. The dispersion was stirred at 350 rpm and purged with nitrogen for 30 mins. Appropriate amount of NIPAm (2 g) was then added to the dispersion when the temperature of the dispersion reached 80℃. After that, appropriate amount of initiator, TBHP (1 mL, 0.1 M), were added to the reaction mixture and the resulting mixture was continuously stirred at 80 ℃ under nitrogen. Small amount of sample (2 mL) was withdrawn from the reaction mixture after reacting for 30 mins.  Second batch of monomer, MMA, *n*-BA or styrene (2 g), was then added to the reacting mixture. The resulting mixture was allowed to react at 80℃ for 2 hrs under nitrogen. After the reaction, the nanoparticles were purified by repeated centrifugation (19,500 rpm, 1.5 hr), decantation and re-dispersion until the conductivity of the supernatant approached to that of deionzed Milli Q water.

#### *5.1.2.1 Determination of monomer conversion and nanoparticle composition*

The monomer conversion of the MCP nanocomposite particles was determined gravimetrically. Measurement procedures were the same as described in **3.1.2.1**. The total solid content was calculated based on **Eq. 3.1**. The monomer conversion was calculated based on **Eq. 3.2**.

#### *5.1.2.2 Kinetic study of the polymerization process*

The polymerization kinetics was monitored by regular withdrawl of samples from reaction mixture at various interval times. The procedures to withdraw samples and characterization methods were the same as described in **3.1.2.2**.

### *5.1.2.3 Effect of second batch monomer (MMA, n-BA and styrene) as crosslinker in seed emulsion polymerization*

The effect of type of second batch hydrophobic monomer on the polymerization kinetics and particle properties was evaluated by varying the types of second batch hydrophobic monomer to be MMA, *n*-BA or styrene. The synthetic procedure was the same as described in **5.1.2.** except the second batch monomer was varied to be MMA, *n*-BA and styrene.

### *5.1.2.4 Effect of PEI to monomer ratio*

The effect of the weight ratio between PEI and monomer on the particle stability and properties was studied. The synthetic procedure was the same as described in **5.1.2.** Seed emulsion polymerization of MCP under PEI to total monomer weight ratio at 1 : 1, 1 : 2, 1 : 4, 1 : 7 and 1 : 9 were examined, keeping all other reaction parameters unchanged.

**Table 5.1.** Reaction recipe for the effect study of weight ratio between PEI to total monomer.

| **Monomer composition (PEI : Total monomer)** | **Polymerization recipes**[1] | | | | **MCP particles composition** |
|---|---|---|---|---|---|
| | Weight of PEI (g) | Weight of NIPAm (g) | Weight of second batch monomer, MMA[2] (g) | w/w ratio of NIPAm to MMA[3] | w/w ratio between PEI, NIPAm and MMA |
| 1 : 1 | 2.5 | 1.25 | 1.25 | 50 : 50 | 1 : 0.5 : 0.5 |
| 1 : 2 | 1.67 | 1.67 | 1.67 | 50 : 50 | 1 : 1 : 1 |
| 1 : 4 | 1 | 2 | 2 | 50 : 50 | 1 : 2 : 2 |
| 1 : 7 | 0.63 | 2.19 | 2.19 | 50 : 50 | 1 : 3.5 : 3.5 |
| 1 : 9 | 0.5 | 2.25 | 2.25 | 50 : 50 | 1 : 4.5 : 4.5 |

[1] PEI and NIPAm were reacted in the first step to prepare PNIPAm/PEI seed hydrogel in the presence of 1 mM TBHP. MMA was added in the later step to form MCP particles. All the reactions were conducted at 80 °C with 350 rpm stirring under nitrogen atmosphere for 2.5 hrs. The pH of the reaction mixture was adjusted to 7 prior to reaction.

[2] MMA was employed as the second monomer in this study.

[3] The weight ratio between NIPAm and MMA was kept at 1 : 1 in this study.

#### *5.1.2.5 Effect of seed monomer to second batch monomer ratio*

The effect of seed monomer to second batch monomer ratio on the polymerization kinetics and particle properties was studied by varying the weight ratio between seed monomer and second batch monomer. The synthetic procedure was the same as described in **5.1.2.** except the weight ratio between seed monomer and second batch monomer was varied to be 25 : 75, 50 : 50, 75 : 25 and 90 : 10.

**Table 5.2.** Reaction recipe for the effect study of weight ratio between seed monomer and second batch monomer.

| **Monomer composition (seed : hydrophobic)** | **Polymerization recipes**[1] | | | | **MCP particles composition** |
|---|---|---|---|---|---|
| | Weight of PEI (g) | Weight of NIPAm (g) | Weight of second batch monomer, MMA[2] (g) | w/w ratio of NIPAm to MMA | w/w ratio between PEI and total monomer[3] |
| 1 : 3 | 1 | 1 | 3 | 25 : 75 | 1 : 4 |
| 1 : 1 | 1 | 2 | 2 | 50 : 50 | 1 : 4 |
| 3 : 1 | 1 | 3 | 1 | 75 : 25 | 1 : 4 |
| 9 : 1 | 1 | 3.6 | 0.4 | 90 : 10 | 1 : 4 |

[1] PEI and NIPAm were reacted in the first step to prepare PNIPAm/PEI seed hydrogel in the presence of 1 mM TBHP. MMA was added in the later step to form MCP particles. All the reactions were conducted at 80 °C with 350 rpm stirring under nitrogen atmosphere for 2.5 hrs. The pH of the reaction mixture was adjusted to 7 prior to reaction.

[2] MMA was employed as the second monomer in this study.

[3] The weight ratio between PEI and total monomer was kept at 1 : 4 in this study.

## 5.2 Measurement and Characterization

### 5.2.1 Chemical compositions characterized by FT-IR

The chemical composition of MCP particles was characterized by FT-IR spectroscopy. The characterization procedures were the same as described in **3.2.1**.

### 5.2.2 Particle size and size distribution

The particle size and size distribution of MCP nanoparticles were measured on a Beckman Coulter Delsa Nano C Particle Analyzer. The measurement procedures were the same as described in **3.2.2**.

### 5.2.3 ζ-potential measurement

ζ-potential of MCP nanoparticles were measured by a Beckman Coulter Delsa Nano C Particle Analyzer. The measurement procedures were the same as described in **3.2.3**.

### 5.2.4 pH responsive properties

The effect of pH on the ζ-potential of MCP nanoparticles was measured by a Beckman Coulter Delsa Nano C Particle Analyzer. The measurement procedures were the same as described in **4.2.5**.

### 5.2.5 Thermal responsive properties

The effect of temperature on the particle size and ζ-potential of the MCP nanoparticles was measured by a Beckman Coulter Delas Nano C Particle Analyzer with the aid of thermal monitoring device. The measurement procedures were the same as described in **4.2.6**. The normalized hydrodynamic diameters of MCP particles were calculated based on **Eq.4.1**.

### 5.2.6 Morphology

#### *5.2.6.1 Field-Emission Scanning Electronic Microscope (FE-SEM)*

The morphologies, particle size and size distribution of the MCP nanoparticles in dried state were examined by field-emission scanning electron microscope (FE-SEM, JEOL-JSM 6335F). The measurement procedures were the same as described in **3.2.4.1**.

#### *5.2.6.2 Transmission Electronic Microscope (TEM)*

The core-shell nanostructures of the MCP naoparticles were examined by transmission electron microscope (TEM, JEOL CXII TEM). The measurement procedures were the same as described in **4.2.7.2.**

## 5.3 Results and Discussion

### 5.3.1 PMMA/PNIPAm/PEI MCP nanocomposite particles

The preparation and characterization of PMMA/PNIPAm/PEI nanocomposite particles is discussed in detail in this part. Due to the presence of C=C double bond on both MMA and MBA, we hypothesize that MMA can also crosslink MCP particles during seeded emulsion polymerization via chemical crosslinking. The success in forming MCP particles using MMA as crosslinker allows us to prepare MCP particles using different functional vinyl monomer as crosslinker. After the formation of PNIPAm/PEI seed particles, MMA was introduced to undergo seeded emulsion polymerization. Scheme 5.1 shows the reaction route and conditions to prepare these particles.

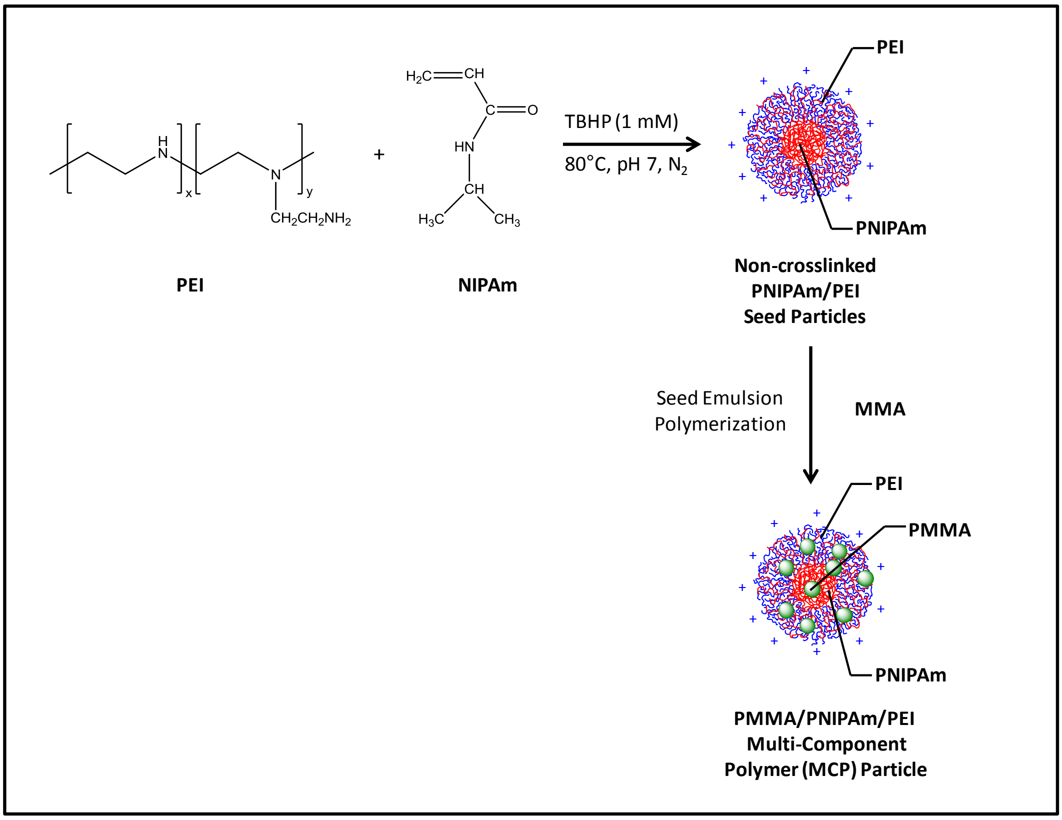

**Scheme 5.1.** Reaction scheme for the synthesis of PMMA/PNIPAm/PEI MCP particles.

### *5.3.1.1 Kinetic study of the polymerization process*

The reaction kinetics of the seeded emulsion polymerization of MCP nanocomposites was monitored by thermal couple (Testo 735) with 1 temperature recorded per second. Figure 5.1 shows the temperature profile of the polymerization at different stages of reaction.

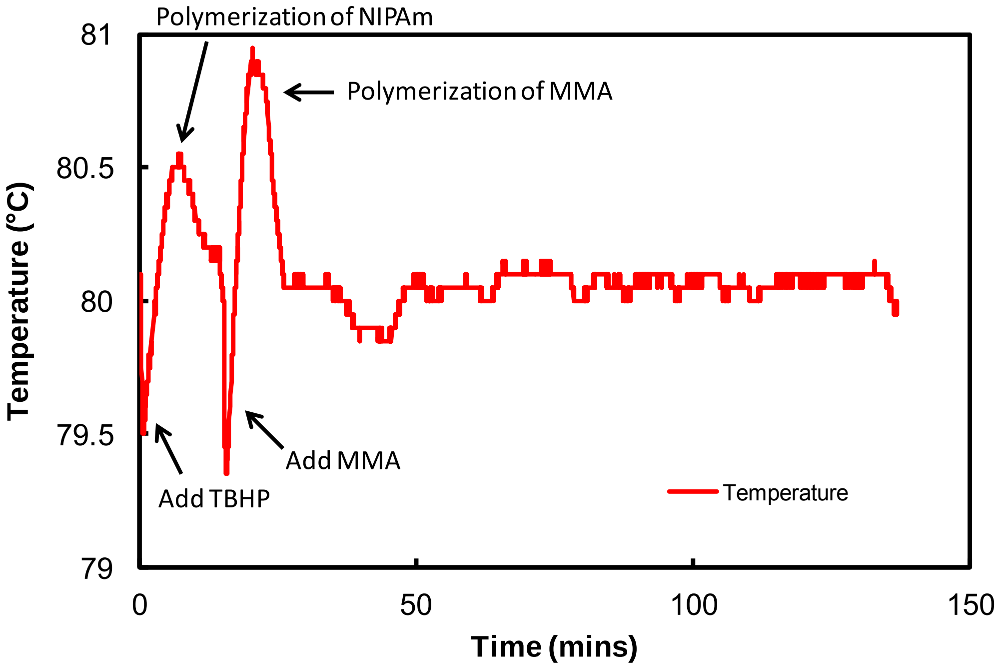

**Fig. 5.1.** Reaction temperature profile during the synthesis of PMMA/PNIPAm/PEI composite particles.

When the temperature of PEI and NIPAm mixture reached equilibrium (around 80 °C), appropriate amount of initiator (TBHP) was added to the reaction mixture to initiate the polymerization. Once TBHP was added, the reaction temperature was first slightly dropped and then rose up rapidly. After consuming most of the NIPAm monomers, the exothermic polymerization was almost finished and the temperature of the reaction mixture dropped to the original level.

As the temperature fell back to 80 ℃, the second batch of monomer, MMA, was introduced into the reaction mixture to perform seeded emulsion polymerization. Similarly, an increased in temperature was observed after the addition of MMA. This increase was contributed by an exothermic polymerization of MMA inside PNIPAm/PEI seed particles. Rapid increase in temperature was observed during seeded emulsion polymerization. The solubility MMA monomers in water (15 g/L at 25 ℃) is sufficient to allow fast diffusion of MMA from bulk aqueous phase into the growing seed particles. The fast diffusion of hydrophobic monomers into the growing particles leads to fast polymerization. Therefore, exothermic peak of the MMA polymerization was as sharp and narrow as the exothermic peak contributed by NIPAm polymerization.

In addition to temperature variation, the polymerization kinetics was also monitored by monomer conversion at different stage of polymerization. The total monomer conversion at different time interval is shown in Table 5.3. After the first stage of polymerization, NIPAm monomer conversion reached 99%. In the second stage of polymerization, MMA monomer was charged to proceed seeded emulsion polymerization. When the exothermic polymerization was completed, the total monomer conversion had reached 99% at the end of polymerization. The variation of hydrodynamic diameters of MCP particles throughout the polymerization process was evaluated by particle size measurement at different time intervals.

From the results of particle size measurement, the hydrodynamic diameter of MCP particles was 480.7 nm. Unfortunately, we are unable to obtain the hydrodynamic diameter of the PNIPAm/PEI seed particles. This was due to the absence of crosslinking in the seed forming stage. The core-shell particle structure of the seed particles was dissociated as temperature dropped to below VPTT of PNIPAm. When MMA was added to conduct seeded emulsion polymerization, vinylic MMA monomers not only proceeded polymerization, but also crosslinked the seed microgel via chemical crosslinking. The particle nanostructure of MCP particles was maintained from dissociation which allowed the determination of their hydrodynamic diameters. Absence of particle dissociation is an evidence to illustrate MMA functioned as crosslinker to keep particle structure of MCP particles.

**Table 5.3.** Total monomer conversion and particle size of MCP particles at different time intervals.

| **Reaction time[1] (mins)** | **Type of particles** | **Monomer conversion[2] (%)** | **$Z_{AVE}$[3] (nm)** |
|---|---|---|---|
| 15 | PNIPAm/PEI seed | 99%[4] | N/A |
| 45 | PMMA/PNIPAm/PEI MCP | 99%[5] | 566.4 |
| 90 | PMMA/PNIPAm/PEI MCP | 99%[5] | 508.9 |
| 135 | PMMA/PNIPAm/PEI MCP | 99%[5] | 480.7 |

[1] The reaction was counted since the addition of initiator into the reaction mixture

[2] The total monomer conversion of MCP particles were determined gravimetrically

[3] The hydrodynamic diameter of MCP particles were determined by DLS at 25 °C

[4] The monomer conversion was calculated based on total NIPAm monomer added

[5] The monomer conversion was calculated based on total monmer added

### *5.3.1.2 Effect of PEI to monomer ratio*

The effect of weight ratio between PEI and total monomer on the properties of the MCP particles was evaluated by varying the composition of PEI and total monomer, keeping the seed monomer to second batch hydrophobic monomer ratio at 1 : 1 (w/w). The weight ratio of PEI to total monomer was changed from 1 : 1 to 1 : 9. The results of these MCP particles were summarized and displayed in Table 5.4.

All MCP particles had achieved total monomer conversion about 90% at the end of polymerization. The hydrodynamic diameter of the prepared MCP particles was ranged from 350 nm to 550 nm. The particle size distribution of the prepared MCP particles was narrow (PDI < 0.2). These indicated the MCP particles were prepared with nanosized dimension with high uniformity.

The effect of weight ratio between PEI and total monomer on the surface charges of PMMA/PNIPAm/PEI MCP particles was obvious. The ζ-potential of PMMA/PNIPAm/PEI MCP particle with NIPAm to styrene w/w ratio at 1 : 1, 1 : 2, 1 : 4, 1 : 7 and 1 : 9 were + 35.93 mV, + 29.38 mV, + 4.12 mV, + 15.07 mV and + 9.77 mV respectively. The magnitude of ζ-potential of MCP particles was decreased as the PEI composition decreased. As previously explained, the outermost shell of the MCP particles was an interpenetrated network constructed by PNIPAm and PEI. At high PEI composition, PEI was dominant component in the outermost shell. PNIPAm was insufficient to shield the PEI in the outer shell. The incomplete partial shielding of PEI resulted in the high ζ-potential of MCP particles. On the contrary, PNIPAm was the dominant component in outer shell as the PEI composition decreased. PEI was completely shielded by PNIPAm, leading to an obvious reduction in the magnitude of ζ-potential. Therefore, the surface charge of MCP particles was highly affected by the composition between PEI and total monomer.

**Table 5.4.** Characteristics of PMMA/PNIPAm/PEI MCP particles with different PEI : Total monomer (w/w) ratio.

| **Types of particles** | **w/w ratio of PEI to Total Monomer (PEI composition)** | **Monomer Conversion[1]** | **Hydrodynamic Diameter (nm)[2]** | | | | **ζ-potential (mV)[3]** | | | |
|---|---|---|---|---|---|---|---|---|---|---|
| | | | **Dh (25°C)** | **Dh (32°C)** | **Dh (39°C)** | **$Dh_{39°C}$/ $Dh_{25°C}$** | **ζ-potential (pH 7)** | **ζ-potential (25°C)** | **ζ-potential (32°C)** | **ζ-potential (39°C)** |
| **PMMA/ PNIPAm/PEI MCP particles** | **1 : 1 (50%)** | **99%** | **483.6** | **467.6** | **458.4** | **0.95** | **+ 35.93** | **+ 35.93** | **+ 52.72** | **+ 55.68** |
| | **1 : 2 (33%)** | **99%** | **544.9** | **524.5** | **512.3** | **0.94** | **+ 29.38** | **+ 29.38** | **+ 49.18** | **+ 51.69** |
| | **1 : 4 (20%)** | **88%** | **368.5** | **318.8** | **278.5** | **0.76** | **+ 4.12** | **+ 4.12** | **+ 11.11** | **+ 32.63** |
| | **1 : 7 (12.5%)** | **99%** | **515.6** | **437.7** | **424.4** | **0.82** | **+ 15.07** | **+ 15.07** | **+ 45.35** | **+ 53.03** |
| | **1 : 9 (10%)** | **99%** | **496.6** | **435.5** | **426.0** | **0.86** | **+ 9.77** | **+ 9.77** | **+ 44.86** | **+ 49.73** |

[1] The weight ratio between NIPAm and MMA was kept at 1 : 1 (NIPAm composition : 50%) in this study

[2] The monomer conversion was determined gravimetrically

[3] The hydrodynamic diameter of MCP particles was determined by DLS at specific temperature and the samples were thermally equilibrated for 10 mins prior measurement

[4] The colloidal stability of MCP particles was determined by ζ-potential measurement using 1 mM NaCl as medium and the samples were thermally equilibrated for 10 mins prior measurement

### *5.3.1.3 Effect of seed monomer to second batch monomer ratio*

The effect of weight ratio between the seed monomer (NIPAm) and second batch monomer (MMA) on the properties of the MCP particles was evaluated by varying the composition of NIPAm and MMA, keeping the PEI to total monomer ratio at 1 : 4 (w/w). The weight ratio of NIPAm to MMA changed from 1 : 3 to 9 : 1. The results of these MCP particles were summarized and displayed in Table 5.5.

All MCP particles had achieved total monomer conversion about 90% at the end of polymerization. The hydrodynamic diameter of the prepared MCP particles was ranged from 350 nm to 950 nm, and the particle size distribution was narrow (PDI < 0.2). The hydrodynamic diameter of PMMA/PNIPAm/PEI was increased as the NIPAm composition was promoted from 25% to 90%. This was due to the hydrogel structure of PNIPAm. PNIPAm was a hydrogel that highly extended in the outermost shell, forming an interpenetrating network with PEI. The composition of PNIPAm in the outermost shell was increased as the NIPAm composition in total monomer was increased. The presence of highly extended PNIPAm in the outermost shell of the particles resulted in larger hydrodynamic diameter. The NIPAm content played an important role in the particle size of MCP particles.

The effect of weight ratio between NIPAm and MMA on the surface charges of PMMA/PNIPAm/PEI MCP particles was also obvious. The ζ-potential of PMMA/PNIPAm/PEI MCP particle with NIPAm to MMA w/w ratio at 1 : 3, 1 : 1 3 : 1 and 9 : 1 were + 34.24 mV, + 4.12 mV, + 11.65 mV and + 6.39 mV respectively. The magnitude of ζ-potential of MCP particles was decreased as the composition of NIPAm increased from 25% to 90% in the total monomer. As explained before, PNIPAm dominated the outermost shell at high PNIPAm content. This resulted in charge shielding of the positively charged PEI and thus led to a suppression of the magnitude of ζ-potential of PMMA/PNIPAm/PEI MCP particles. Therefore, the NIPAm composition in total monomer not only affected the particle size, but also affected the surface cgarges of MCP particles.

**Table 5.5.** Characteristics of PMMA/PNIPAm/PEI MCP particles with different NIPAm : MMA (w/w) ratio.

| **Types of particles** | **w/w ratio of NIPAm to MMA (NIPAm composition)[1]** | **Monomer Conversion[2]** | **Hydrodynamic Diameter (nm)[3]** | | | | **ζ-potential (mV)[4]** | | | |
|---|---|---|---|---|---|---|---|---|---|---|
| | | | **Dh (25°C)** | **Dh (32°C)** | **Dh (39°C)** | **$Dh_{39°C}$/ $Dh_{25°C}$** | **ζ-potential (pH 7)** | **ζ-potential (25°C)** | **ζ-potential (32°C)** | **ζ-potential (39°C)** |
| **PMMA/ PNIPAm/PEI MCP particles** | **1 : 3 (25%)** | **99%** | **473.6** | **456.9** | **445.1** | **0.94** | **+ 34.24** | **+ 34.24** | **+ 40.34** | **+ 40.31** |
| | **1 : 1 (50%)** | **88%** | **368.5** | **318.8** | **278.5** | **0.76** | **+ 4.12** | **+ 4.12** | **+ 11.11** | **+ 32.63** |
| | **3 : 1 (75%)** | **99%** | **775.1** | **715.2** | **564.3** | **0.73** | **+ 11.65** | **+ 11.65** | **+ 42.97** | **+ 50.20** |
| | **9 : 1 (90%)** | **99%** | **931.8** | **803.0** | **575.7** | **0.62** | **+ 6.39** | **+ 6.39** | **+ 38.71** | **+ 48.48** |

[1] The weight ratio between PEI and total monomer was kept at 1 : 4 in this study

[2] The monomer conversion was determined gravimetrically

[3] The hydrodynamic diameter of MCP particles was determined by DLS at specific temperature and the samples were thermally equilibrated for 10 mins prior measurement

[4] The colloidal stability of MCP particles was determined by ζ-potential measurement using 1 mM NaCl as medium and the samples were thermally equilibrated for 10 mins prior measurement

### 5.3.2 Characterization of PMMA/PNIPAm/PEI nanocomposite particles

#### *5.3.2.1 Composition*

The composition of the PMMA/(PNIPAm-MBA)/PEI MCP particles was investigated by FT-IR spectroscopy. The particles were first purified by repeated centrifugation to get rid of any unreacted PEI and monomers. Figure 5.2a shows the FT-IR spectrum of MBA-crosslinked PNIPAm/PEI seed particles. Strong C=O amide stretching peak observed at 1650 to 1660 cm$^{-1}$, strong N-H amide II bending peak observed at 1535 cm$^{-1}$ and isopropyl C-H peak observed at 1370 to 1390 cm$^{-1}$ suggest the presence of PNIPAm. Both broad amino N-H stretching peak of primary amine at 3400 to 3500 cm$^{-1}$, and C-H stretching and bending at 2900 to 3000 cm$^{-1}$ indicate the presence of PEI. Figure 5.2b shows the FT-IR spectrum of PMMA/(PNIPAm-MBA)/PEI MCP particles. Additional strong carbonyl C=O peak was observed in 1730 cm$^{-1}$ and strong -C-O- ester peak was appeared at 1150 to 1300 cm$^{-1}$, suggesting the presence of PMMA. These characteristic peaks confirm the presence of polystyrene in the MCP particles. Based on the FTIR results, we can confirm that the MCP particles comprise of PEI, PNIPAm and PMMA components.

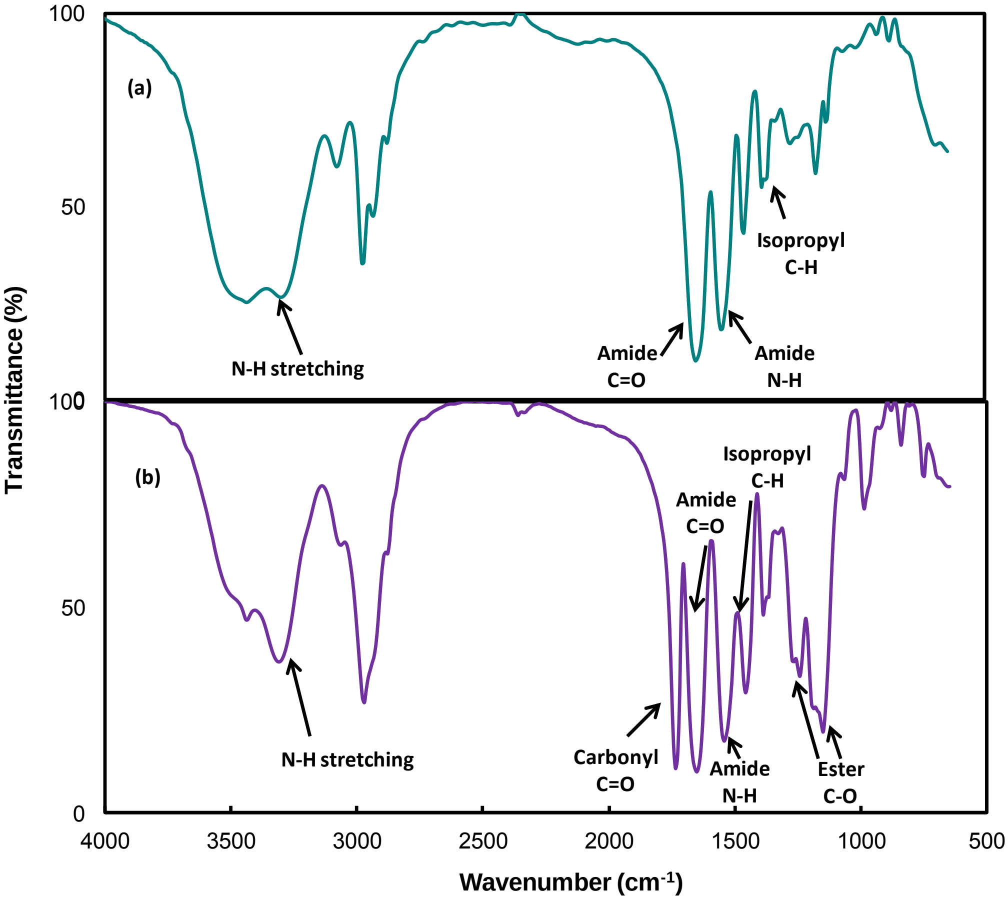

**Fig. 5.2.** FT-IR spectrum of a) PNIPAm/PEI seed; and b) PMMA/PNIPAm/PEI MCP particles.

### *5.3.2.2 Particle size and size distribution*

#### *Particle size*

The hydrodynamic diameters ($Z_{AVE}$) and particle size distribution (PDI) of seed and MCP particles were determined by dynamic light scattering (DLS) at pH 7 using a Beckman Coulter Delsa Nano C instrument. Figure 5.3 shows the particle size and size distribution of PMMA/PNIPAm/PEI MCP particles. The hydrodynamic diameter and particle size distribution of MCP particles were 368.5 nm and 0.059. These results indicated that the prepared MCP particles were in nano-sized dimension and with narrow size distribution. However, the hydrodynamic diameter of PNIPAm/PEI seed could not be determined due to absence of crosslinking which had explained before.

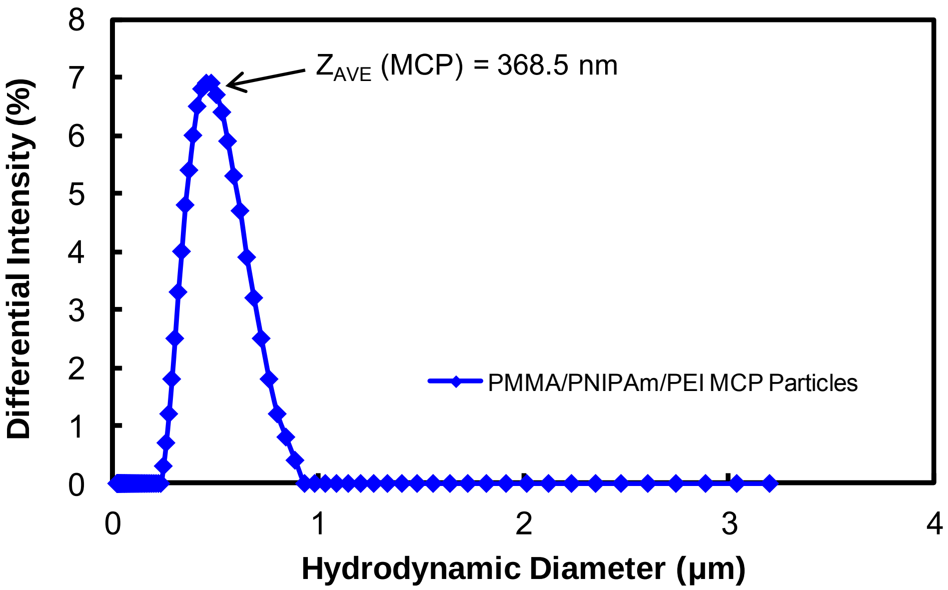

**Fig. 5.3.** Particle sizes of PMMA/PNIPAm/PEI MCP particles (368.5 nm).

### *Effect of PEI to total monomer ratio on the particle size as a function of temperature*

The effect of temperature on the hydrodynamic diameter of the PMMA/PNIPAm/PEI MCP particles at different PEI to total monomer weight ratio was evaluated by DLS measurement at different temperatures (25 °C, 27 °C, 29 °C, 32 °C, 35 °C, 37 °C and 39 °C). The variation in the hydrodynamic diameter of PMMA/PNIPAm/PEI MCP particles at different weight ratio between PEI and total monomer as a function of temperature was plotted and displayed in Figure 5.4.

Generally, the hydrodynamic diameters of MCP particles were ranged from 350 nm to 550 nm. These particles possessed nanosized dimension and narrow size distribution. When the temperature was raised to above 32 °C, there is a decrease in the hydrodynamic diameter of the MCP particles as the temperature increase. This drop was due to the volume phase transition of PNIPAm which had been explained before. The coil-to-globule transition of PNIPAm resulted in particle shrinkage and caused a decrease in the hydrodynamic diameter.

To further evaluate the thermal responsive properties of the MCP particles, the hydrodynamic diameter was re-expressed as normalized hydrodynamic diameter which demonstrated the thermal responsive properties of MCP particles quantitatively. The normalized hydrodynamic diameter of PMMA/PNIPAm/PEI MCP particles with PEI to total monomer weight ratio at 1 : 1, 1 : 2, 1 : 4, 1 : 7 and 1 : 9 at 39 ℃ ($Dh_{39\ ^{\circ}C}/Dh_{25\ ^{\circ}C}$) were 0.95, 0.94, 0.76, 0.82 and 0.86 respectively. The normalized hydrodynamic diameter of MCP particles gradually decreased as the PEI composition reduced from 50% to 10%.

When the weight ratio of PEI to total monomer was kept at 1 : 1, there was a 5% reduction in the hydrodynamic diameter of MCP particles above the VPTT of PNIPAm. The shrinkage of MCP particles became more obvious as the PEI composition decreased. When the weight ratio between PEI and total monomer was changed to 1: 9, the percentage reduction in the hydrodynamic diameter of MCP particles was enhanced to 14%. The thermal responsive properties of MCP particles were enhanced as the PEI composition decreased. As the weight ratio between seed monomer (NIPAm) and second hydrophobic monomer (MMA) was fixed at 1 : 1, there was an increase in the total monomer content when the PEI composition was reduced. Eventually, the composition of PNIPAm in the MCP particles was enhanced. This resulted in more significant particle shrinkage due to the increase in the composition of thermal responsive polymer, PNIPAm. The thermal responsive property of the MCP particles could be adjusted by varying the composition between PEI and the total monomer.

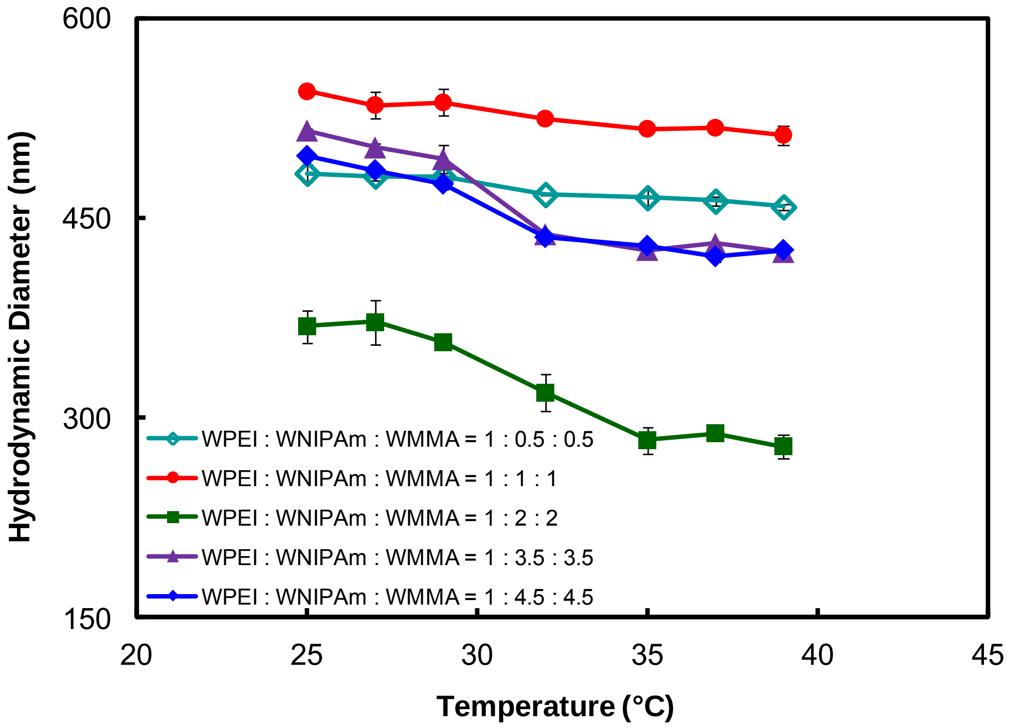

**Fig. 5.4.** Effect of PEI to total monomer ratio on the particle size of PMMA/PNIPAm/PEI MCP particles as a function of temperature.

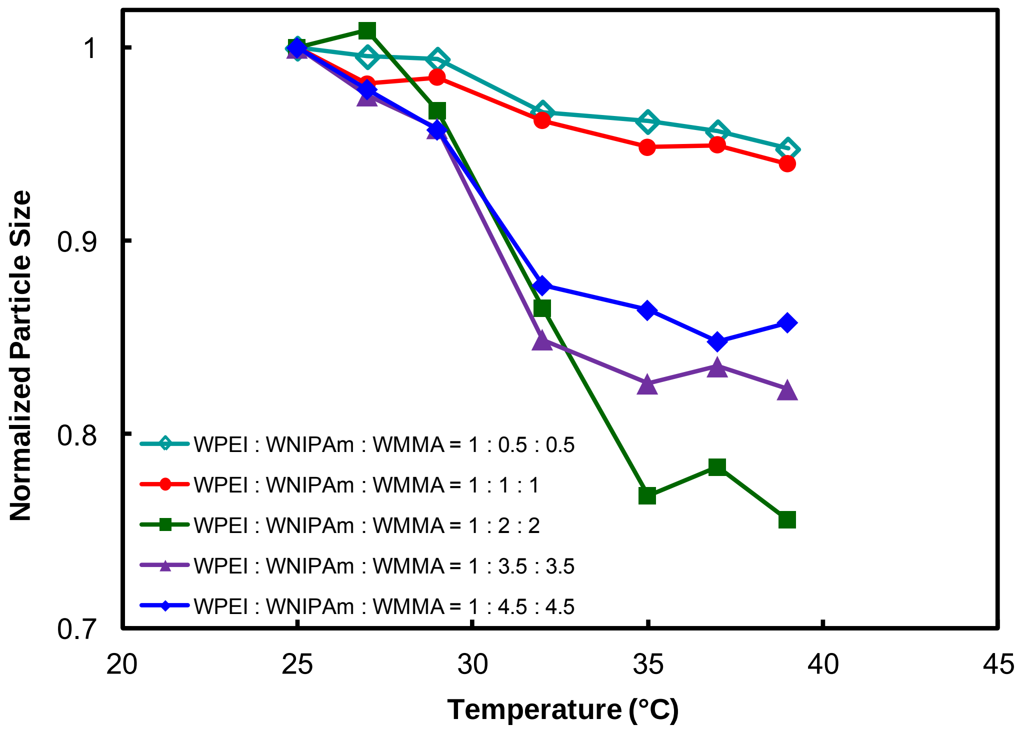

**Fig. 5.5.** Effect of PEI to total monomer ratio on the normalized particle size ($Dh/Dh_{25\,°C}$) of PMMA/PNIPAm/PEI MCP particles as a function of temperature.

### *Effect of seed monomer to second batch monomer ratio on the particle size as a function of temperature*

The effect of surrounding temperature on the hydrodynamic diameter of the PMMA/PNIPAm/PEI MCP particles with different NIPAm/MMA weight ratio was evaluated by DLS measurement at different temperatures (25 °C, 27 °C, 29 °C, 32 °C, 35 °C, 37 °C and 39 °C). The variation of the hydrodynamic diameter of PMMA/PNIPAm/PEI MCP particles with different weight ratio between seed monomer and second batch hydrophobic monomer as a function of temperature was plotted and displayed in Figure 5.6.

The hydrodynamic diameter of MCP particles with NIPAm/MMA weight ratio at 1 : 3, 1 : 1, 3 : 1 and 9 : 1 were 473.6 nm, 368.5 nm, 775.1 nm and 931.8 nm at 25 °C respectively. The hydrodynamic diameter of MCP particles with NIPAm/MMA weight ratio at 1 : 3, 1 : 1, 3 : 1 and 9 : 1 were 445.1 nm, 278.5 nm, 564.3 nm and 575.7 nm at 39 °C respectively. These MCP particles possessed nanosized dimension and narrow size distribution and exhibited a remarkable change in the hydrodynamic diameter as temperature increased. This drop in particle size was due to the volume phase transition of PNIPAm which had explained before. The coil-to-globule transition of PNIPAm resulted in particle shrinkage and resulted in a decrease in the hydrodynamic diameter.

To further evaluate the thermal responsive properties of the MCP particles, the hydrodynamic diameter was re-expressed as normalized hydrodynamic diameter which demonstrated the thermal responsive properties of MCP particles quantitatively. The variation of normalized hydrodynamic diameters of MCP particles as a function of temperature was plotted and displayed in the following figure.

The normalized hydrodynamic diameter of PMMA/PNIPAm/PEI MCP particles with NIPAm/MMA weight ratio at 1 : 3, 1 : 1, 3 : 1, and 9 : 1 at 39 ℃ ($Dh_{39℃}/Dh_{25℃}$) were 0.94, 0.76, 0.73 and 0.62 respectively. The normalized hydrodynamic diameter of MCP particles gradually decreased as the NIPAm composition in the total monomer increased from 25% to 90%. When the total monomer comprised of 25% NIPAm, the normalized hydrodynamic diameter of MCP particles was 0.94, indicating a 6% reduction in the particle size. In fact, the change in particle size was not significant because of the low PNIPAm content. As the NIPAm composition increased substantially from 25% to 90%, the particle size reduction became more obvious. As the total monomer contained 90% of NIPAm, the normalized hydrodynamic diameter of the prepared MCP particles was 0.62. There was a nearly 40% reduction in the hydrodynamic diameter, indicating the remarkable thermal responsive properties of MCP particles. The stimuli responsive properties of MCP particles could be enhanced by adjusting the monomer composition.

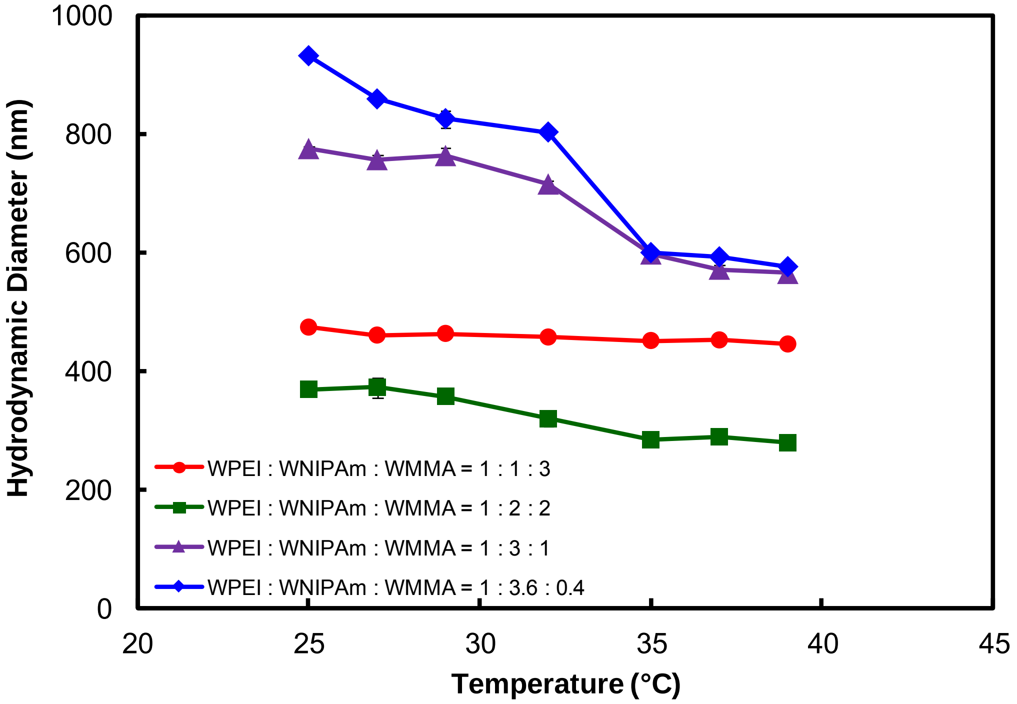

**Fig. 5.6.** Effect of seed monomer to second hydrophobic monomer ratio on the particle size of PMMA/PNIPAm/PEI MCP particles as a function of temperature.

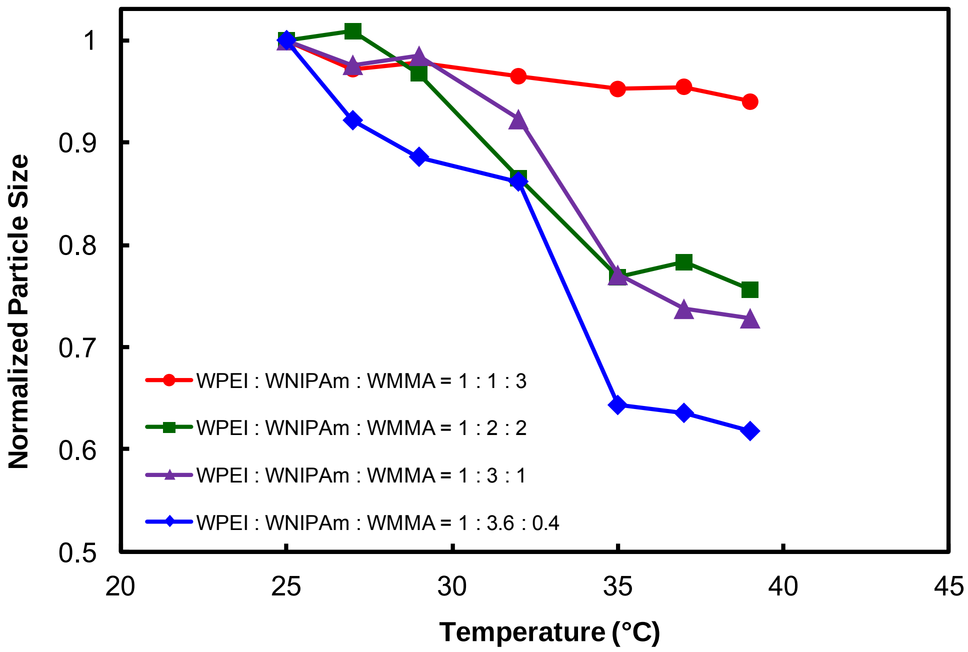

**Fig. 5.7.** Effect of seed monomer to second hydrophobic monomer ratio on the normalized particle size ($Dh/Dh_{25\,°C}$) of PMMA/PNIPAm/PEI MCP particles as a function of temperature.

### *5.3.2.3 Surface charges of particles as a function of pH and temperature*

***Surface charge***

The surface charge of MCP particles was determined by ζ-potential measurement using Beckman Coulter Delsa Nano C instrument. Under standard condition, pH 7 with conducting medium of 1 mM NaCl, only the ζ-potential of PMMA/PNIPAm/PEI MCP particles could be determined. The ζ-potential of PNIPAm/PEI seed could not be determined due to absence of crosslinking of PNIPAm/PEI seed particles. The ζ-potential of PMMA/PNIPAm/PEI MCP particles was and + 4.12 mV respectively. The low magnitude of ζ-potential of both seed and MCP particles was due to the formation of PNIPAm/PEI interpenetrated network at the outermost shell of the particles as explained in **4.3.2.5**. The charge shielding of PEI by PNIPAm resulted in the suppression of the charge density of the particles.

***Effect of PEI to monomer ratio on the surface charges of particles as a function of pH and temperature***

The effect of pH on the ζ-potential of MCP particles at was evaluated by ζ-potential measurement using Delsa Nano C with the aid of auto-titrator. The variation of ζ-potential as a function of pH of MCP particles with different weight ratio between PEI and total monomer was illustrated in Fig. 5.8.

PMMA/PNIPAm/PEI MCP particles possessed a positive ζ-potential, indicating the surface of these particles was positively charged. The positive ζ-potential of MCP particles was due to the protonated amino groups of PEI located at the outermost shell of the MCP particles. As the pH of the medium was subsequently increased, there was a drop in the ζ-potential of MCP particles due to deprotonation of the amino groups. Eventually, the ζ-potential of MCP particles was dropped to about zero as the pH of the medium was approached 9.5, isoelectric point of PEI.

Although PMMA/PNIPAm/PEI MCP particles with different PEI composition had the same trend in the variation of ζ-potential against pH, the effect of PEI to total monomer ratio was reflected by the magnitude of ζ-potential. The ζ-potential of PMMA/PNIPAm/PEI MCP particles with 50%, 33%, 20%, 12.5% and 10% PEI at pH 7 were + 35.93 mV, + 29.38 mV, + 4.12 mV, + 15.07

mV and + 9.77 mV respectively. The ζ-potential magnitude of MCP particles was decreased as the PEI composition decreased from 50% to 10%. Since the weight ratio between seed monomer (NIPAm) and second hydrophobic monomer (MMA) was fixed at 1 : 1, the PNIPAm composition in MCP particles was promoted as the PEI composition decreased. When the MCP particles contained 50% and 33% PEI, the amount of PNIPAm was insufficient to completely shield the protonated amino groups on PEI. Part of protonated amino groups was not shielded by PNIPAm and was exposed in the outermost shell, contributing to high ζ-potential magnitude. When the PEI content in MCP was dropped to 20%, 12.5% and 10%, the protonated amino groups on PEI were almost completely shielded by PNIPAm. The ζ-potential of MCP particles was significantly suppressed to below + 20 mV at acidic pH due to the formation of interpenetrated shell. Hence, the magnitude of ζ-potential of MCP particles was depended on the PEI to total monomer ratio.

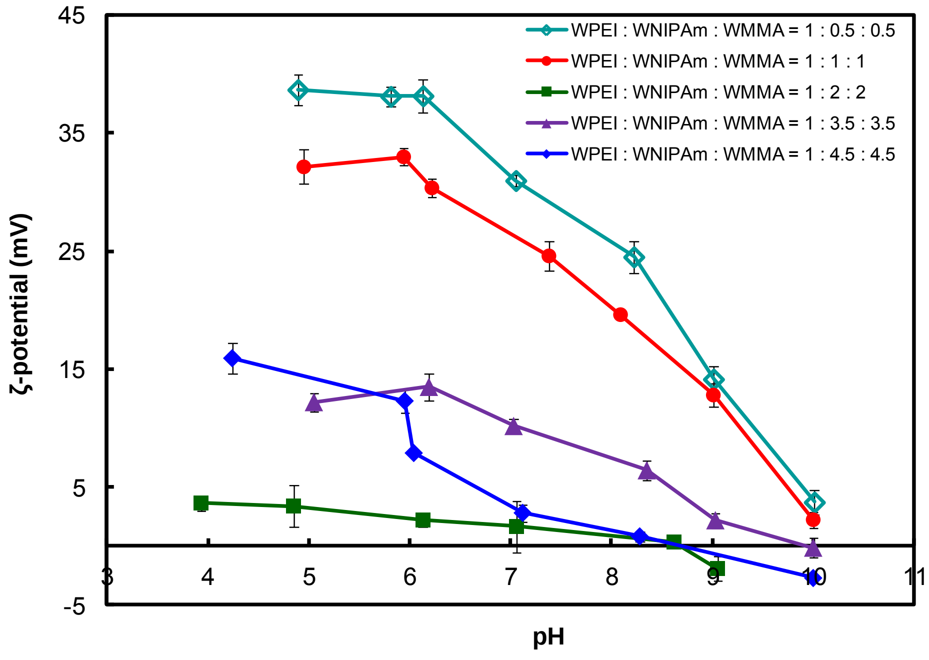

**Fig. 5.8.** Effect of PEI to total monomer ratio on ζ-potential of PMMA/PNIPAm/PEI MCP particles as a function of pH.

The effect of temperature on the ζ-potential of MCP particles at different PEI to monomer ratio was evaluated by ζ-potential measurement using Delsa Nano C with the aid of thermal monitoring device. The variation of ζ-potential as a function of temperature of MCP particles with different NIPAm/MMA composition as a function of temperature was plotted and displayed in Figure 5.9.

Independent of the weight ratio between PEI and total monomer, there is similar trend in the variation of ζ-potential of PMMA/PNIPAm/PEI MCP particles. Below the VPTT of PNIPAm, there was no significant change in the ζ-potential of MCP particles. When the temperature was promoted to above VPTT (32 ℃) of the PNIPAm, there was an abrupt increase in the ζ-potential. This increase in the ζ-potential was due to the volume phase transition of PNIPAm as explained before. The pahse transition of PNIPAm led to charge exposure of PEI in the outermost shell, eventually caused an increase in the ζ-potential of the MCP particles.

Although the trend in the variation of ζ-potential of MCP particles against temperature was the same, there was significant difference in magnitude of ζ-potential in MCP particle with different PEI to total monomer weight ratio. The ζ-potential of MCP particles with PEI/total monomer weight ratio at 1 : 1, 1 : 2, 1 : 4, 1 : 7 and 1 : 9 were + 35.93 mV, + 29.38 mV, + 4.12 mV, + 15.07 mV and + 9.77 mV at 25 ℃ respectively. The ζ-potential magnitude of MCP particles gradually dropped as the PEI composition decreased from 50% to 10%.

When the PEI composition was 50% and 33.3%, the ζ-potential of PMMA/PNIPAm/PEI MCP particles were + 35.93 mV and + 29.38 mV. The magnitude in ζ-potential was high (> + 20 mV) which provided MCP particles with good colloidal stability by charge repulsion. For MCP particles with PEI to total monomer ratio at 1 : 1 and 1 : 2, the PEI content was high that became the major component in the outermost shell. PNIPAm was insufficient to shield protonated amino groups of PEI, leading to incomplete shielding in the positively charged. This eventually resulted in high ζ-potential of the MCP particles. Upon temperature elevation, PNIPAm proceeded volume phase transition across its VPTT. The shrinkage of PNIPAm resulted in the re-exposure of the positive charges of PEI. Due to incomplete charge shielding of PEI, the increase in ζ-potential of MCP particles was less significant (from + 30 mV to + 50 mV).

Nevertheless, the difference between ζ-potential of MCP particles below and above VPTT was boarden with reducing PEI composition. The ζ-potential of MCP particles with PEI composition at 20%, 12.5% and 10% were + 4.12 mV, + 15.07 mV and + 9.77 mV at 25 ℃ respectively. All the MCP particles had ζ-potential below + 15 mV. The low magnitude in ζ-potential of MCP particles was due to extensive shielding of the positively charged PEI on the outermost shell by PNIPAm under low PEI content. When the temperature was above VPTT, volume phase transition of PNIPAm took place. The phase change of PNIPAm from hydrophilic to hydrophobic led to shrinkage of PNIPAm into the inner core. The protonated amino groups of PEI were re-exposed again which resulted in an abrupt increase in the ζ-potential. The ζ-potential of MCP particles was increased from + 10 mV to + 50 mV as temperature was raised from 25 °C to 39 °C. The variation in ζ-potential was significant due to extensive charge shielding of PEI by PNIPAm. Thus, the surface charge density and thermal responsiveness of MCP particles was affected by the PEI to total monomer composition.

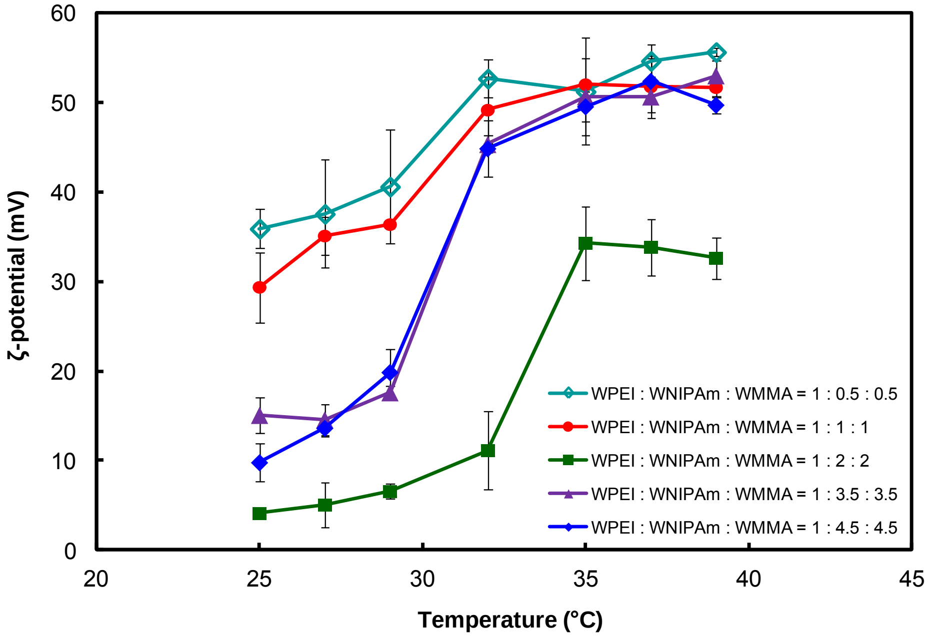

**Fig. 5.9.** Effect of PEI to total monomer ratio on ζ-potential of PMMA/PNIPAm/PEI MCP particles as a function of temperature.

***Effect of seed monomer to second hydrophobic monomer ratio***

The effect of weight ratio between seed monomer and second hydrophobic monomer on the ζ-potential of MCP particles at was evaluated by ζ-potential measurement using Delsa Nano C with the aid of auto-titrator. The variation of ζ-potential as a function of pH of MCP particles with different weight ratio between seed monomer and second hydrophobic monomer was illustrated in Figure 5.10.

Independent of the total monomer composition in MCP particles, the surface of PMMA/PNIPAm/PEI MCP particles was positively charged and the ζ-potential almost remains unchanged below pH 7. The positive ζ-potential of MCP particles was contributed by the protonated amino groups of PEI located at the outermost shell of the MCP particles. As the pH of the medium was raised to above 7, there was a drop in the ζ-potential of MCP particles. The drop in ζ-potential was due to the deprotonation of the amino groups. Eventually, the ζ-potential of MCP particles was dropped to about zero as the pH of the medium was approached 9.5, isoelectric point of PEI.

Although PMMA/PNIPAm/PEI MCP particles with different NIPAm composition had the same trend in the variation of ζ-potential against pH, the effect of weight ratio between NIPAm and MMA was reflected by the magnitude of ζ-potential. The ζ-potential of PMMA/PNIPAm/PEI MCP particles with NIPAm/MMA weight ratio at 1 : 3, 1 : 1, 3 : 1 and 9 : 1 at pH 7 were + 34.24 mV, + 4.12 mV, + 11.65 mV and + 6.39 mV respectively. There was a decrease in the magnitude of ζ-potential as the NIPAm composition increased. When the total monomer contained 25% NIPAm, the ζ-potential of PMMA/PNIPAm/PEI MCP particles was + 34.24 mV. This ζ-potential magnitude was higher than the other three MCP particles. As the total monomer contained more than 50% NIPAm, the magnitude ζ-potential of MCP particles was about + 10 mV. The difference in the ζ-potential of MCP particles was attributed to different extend in the charge shielding of PEI in the outermost shell. Under at high NIPAm content (> 50%), positively charged PEI was almost completely shielded by PNIPAm. The formation of extensively interpenetrated shell led to low ζ-potential of the MCP particles. However, PEI was partially charge shielding of by PNIPAm under low NIPAm content (25%). Incomplete charge shielding of PEI resulted in high ζ-potential of the MCP particles (+ 34.24 mV). The surface charge density of MCP particles could be controlled by adjusting the NIPAm composition.

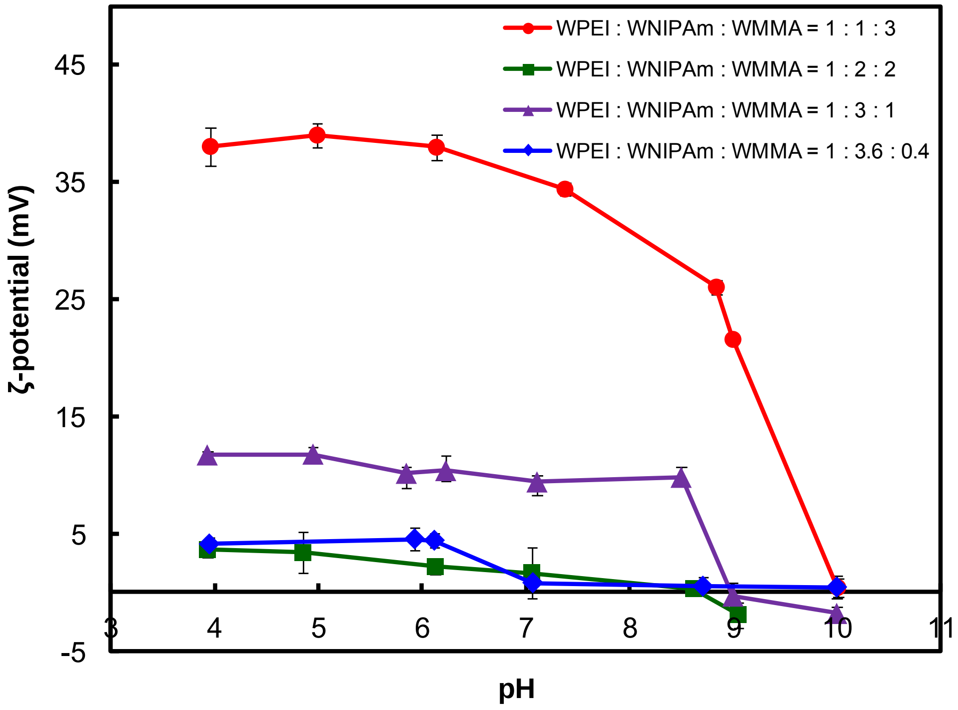

**Fig. 5.10.** Effect of seed monomer to second hydrophobic monomer ratio on ζ-potential of PMMA/PNIPAm/PEI MCP particles as a function of pH.

The effect of temperature on the ζ-potential of MCP particles at different seed monomer to second batch hydrophobic monomer ratio was evaluated by ζ-potential measurement using Delsa Nano C with the aid of thermal monitoring device. The variation of ζ-potential as a function of temperature of MCP particles with different NIPAm/MMA composition as a function of temperature was plotted and displayed in Figure 5.11.

Independent of the weight ratio between seed monomer and second hydrophobic monomer, there was similar trend in the variation of ζ-potential of PMMA/PNIPAm/PEI MCP particles against temperature. Below VPTT of PNIPAm (32 °C), MCP particles had positive ζ-potential and its magnitude was kept constant. As the temperature was raised to the VPTT of PNIPAm, there was a remarkable increase in the ζ-potential of MCP particles. When the temperature was further raised, there was no insignificant increase in the ζ-potential of MCP particles.

Although the trend in the variation of ζ-potential of MCP particles against temperature was the same, there was significant difference in magnitude of ζ-potential in MCP particle with different PEI to total monomer weight ratio. The ζ-potential of MCP particles with NIPAm/MMA weight ratio at 1 : 3, 1 : 1, 3 : 1 and 9 : 1 at 25 ℃ were + 34.24 mV, + 4.12 mV, + 11.65 mV and + 6.39 mV respectively. The ζ-potential magnitude of MCP particles gradually dropped as the NIPAm composition increased from 25% to 90%.

The ζ-potential of MCP particles containing 25% NIPAm in total monomer was + 34.24 mV at 25 °C. The ζ-potential magnitude was positive and high, indicated a positively charged surface of MCP particles. The positive magnitude was contributed by the protonated amino groups on PEI at the outermost shell of particles. Due to the low crosslinking degree of MCP particles, the outermost shell of the particles was an interpenetrated network formed by PNIPAm and PEI. The positively charged PEI was shielded by non-charged PNIPAm, leading to a reduction in the ζ-potential. In fact, the ζ-potential of MCP particles was above + 30 mV, implying the suppression in ζ-potential was not significant. The charge shielding of the positively charged PEI by PNIPAm was not obvious because of the low NIPAm content in the total monomer. The amount of PNIPAm was insufficient to shield all the protonated amino groups of PEI. As a result, the incomplete shielding of the protonated amino groups on PEI led to densely positive charged surface.

Across the VPTT of PNIPAm, there was significant increase in the ζ-potential of MCP particles with NIPAm/MMA weight ratio at 1 : 1, 3 : 1 and 9 : 1. The ζ-potential of MCP particles was increased from +10 mV to + 50 mV. This remarkable increase in the ζ-potential was due to extensive charge shielding of PEI by NIPAm. The positive charges on PEI were ultimately shielded by PNIPAm below its VPTT. The phase change of PNIPAm by coil-to-glubole transition induced its migration to the inner core. Hence, PEI became the mojor component in the outermost shell and the positive charges on PEI were re-exposed as temperature was above VPTT. However, the change in the ζ-potential of MCP particles with NIPAm/MMA weight ratio at 1 : 3 was less significant. This was due to incomplete shielding of PEI by PNIPAm at the outermost shell. The charge re-exposure was less significant as the temperature raised to above VPTT of PNIPAm which led to little change in the ζ-potential of MCP particles. The thermal responsive properties of MCP particles could be altered by the weight ratio between thermal responsive monomer and second hydrophobic monomer.

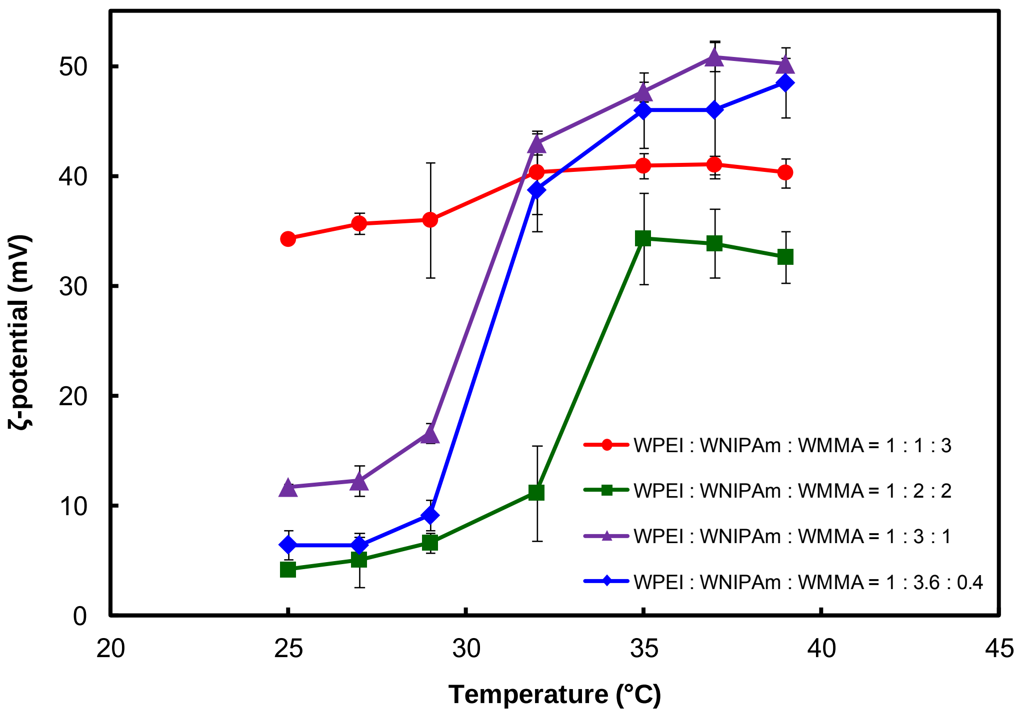

**Fig. 5.11.** Effect of seed monomer to second hydrophobic monomer ratio on ζ-potential of PMMA/PNIPAm/PEI MCP particles as a function of temperature.

### *5.3.2.4 Morphology*

The morphology and core-shell nanostructure of PMMA/PNIPAm/PEI MCP particles prepared at different degree of crosslinking were examined by TEM.

The nanostructure of PMMA/PNIPAm/PEI MCP particles was elucidated by staining with 0.5% (w/w) phosphotungstic acid (PTA, $WO_2•H_3PO_4•xH_2O$) for 5 mins. Numerous bright micro-domains were embedded in the dark corona of the aerolite-like MCP particles. The bright micro-domains were solely PMMA and the dark corona was composed of interpenetrated network PNIPAm and PEI. These micro-domains of PMMA were freely distributed inside the MCP particles.

Formation of this special nanostructure was due to high water solubility of MMA. The water solubility of MMA was 15 g/L under room temperature. High solubility of MMA monomer in water effectively facilitated the dissolve and then diffusion from the aqueous continuous phase into the growing particle core. In addition, the rate of initiation of MMA monomers was fast that MMA monomers were initiated once entered the growing particles. Due to the fast polymerization of MMA, numerous micro-domains of PMMA were formed inside PMMA/PNIPAm/PEI MCP particles. As a result, kinetic favored metastable aerolite morphology was achieved.

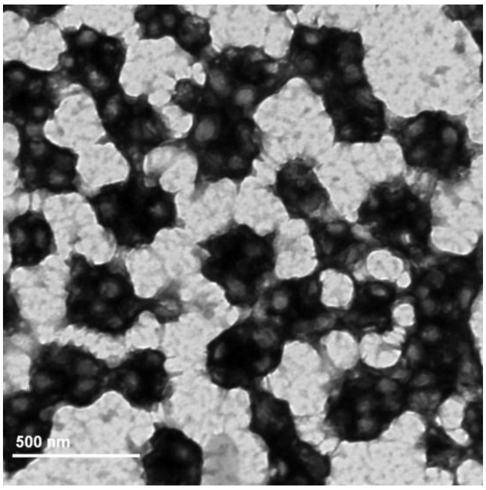

**Fig. 5.12.** TEM image of PMMA/PNIPAm/PEI MCP particles.

### 5.3.3 PS/PNIPAm/PEI MCP nanocomposite particles

The preparation and characterization of PS/(MBA crosslinked PNIPAm-PEI) nanocomposite particles will be discussed in detail in this part. After the formation of PNIPAm-PEI seed microgels, styrene monomers were introduced *in situ* into the reaction mixture to proceed seed emulsion polymerization. The success in forming MCP particles containing of very hydrophobic component could solve the problem encountered in our core-shell nanoparticles technology, i.e. amphiphilic nanoparticles could not be fabricated by monomers with very low water solubility. Also, it would be a desirable model demonstrating the possibility of core-shell nanoparticles fabrication composed of very hydrophobic component in aqueous medium without addition of any additives.

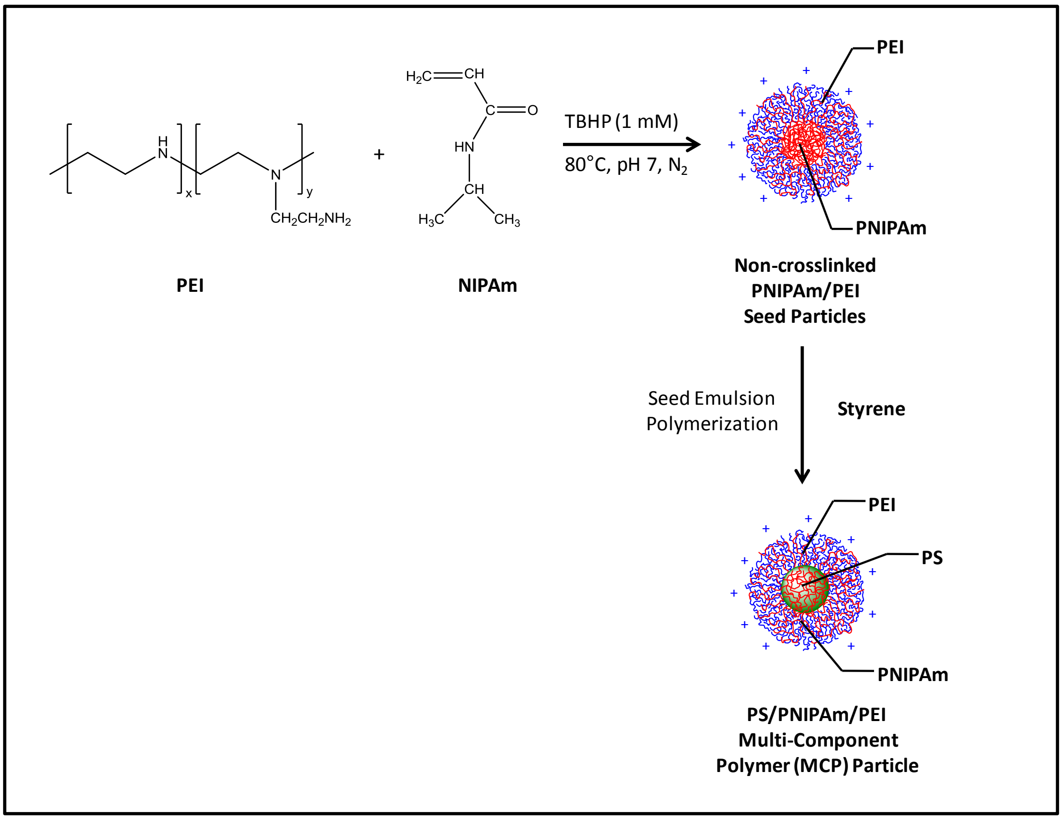

**Scheme 5.2.** Reaction scheme for the synthesis of PS/PNIPAm/PEI MCP particles.

### *5.3.3.1 Kinetic study of the polymerization process*

The reaction kinetics of the seeded emulsion polymerization of MCP nanocomposites was monitored by thermal couple (Testo 735) with 1 temperature recorded per second. The following plots showed the variation of reaction temperature, monomer conversion and hydrodynamic diameter of MCP nanocomposites throughout the polymerization process.

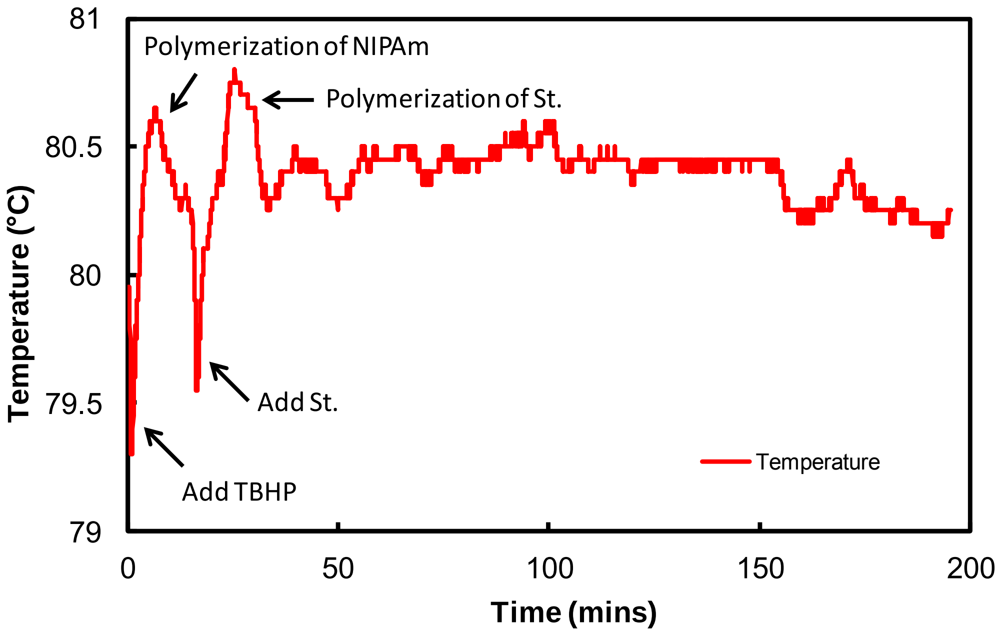

**Fig. 5.13.** Reaction temperature as a function of time of PS/PNIPAm/PEI MCP particles.

When the temperature of PEI and NIPAm mixture reached equilibrium (around 80 °C), appropriate amount of initiator (TBHP) was added to the reaction mixture to initiate the polymerization. Once TBHP was added, the reaction temperature was first slightly dropped and then rose up rapidly. After consuming most of the NIPAm monomers, the exothermic polymerization was almost finished and the temperature of the reaction mixture dropped to the original level.

As the temperature fell back to 80 ℃, the second batch of monomer, styrene, was introduced into the reaction mixture to perform seeded emulsion polymerization. Similarly, an increased in temperature was observed after the addition of styrene. This increase was contributed by an exothermic polymerization of styrene inside PNIPAm/PEI seed particles. Rapid increase in temperature was observed during seeded emulsion polymerization. This indicated the fast diffusion of styrene monomers from bulk aqueous phase into the growing seed particles. The fast diffusion of hydrophobic monomers into the growing particles leads to fast polymerization. Therefore, exothermic peak of the styrene polymerization was as sharp and narrow as the exothermic peak contributed by NIPAm polymerization.

In addition to temperature variation, the polymerization kinetics was also monitored by monomer conversion at different stage of polymerization. The total monomer conversion at different time interval is shown in Table 5.6. After the first stage of polymerization, NIPAm monomer conversion reached 99%. In the second stage of polymerization, styrene monomer was charged to proceed seeded emulsion polymerization. When the exothermic polymerization was completed, the total monomer conversion had reached 98% at the end of polymerization. The variation of hydrodynamic diameters of MCP particles throughout the polymerization process was evaluated by particle size measurement at different time intervals.

From the results of particle size measurement, the hydrodynamic diameter of MCP particles was 515.4 nm. Unfortunately, we are unable to obtain the hydrodynamic diameter of the PNIPAm/PEI seed particles. This was due to the absence of crosslinking in the seed forming stage. The core-shell particle structure of the seed particles was dissociated as temperature dropped to below VPTT of PNIPAm. When styrene was added to conduct seeded emulsion polymerization, vinylic styrene monomers not only proceeded polymerization, but also crosslinked the seed microgel via chemical crosslinking. The particle nanostructure of MCP particles was maintained from dissociation which allowed the determination of their hydrodynamic diameters. Absence of particle dissociation is an evidence to illustrate styrene functioned as crosslinker to keep particle structure of MCP particles.

**Table 5.6.** Total monomer conversion and particle size of MCP particles at different time intervals.

| **Reaction time[1] (mins)** | **Type of particles** | **Monomer conversion[2] (%)** | **$Z_{AVE}$[3] (nm)** |
|---|---|---|---|
| 15 | PNIPAm/PEI seed | 99%[4] | N/A |
| 45 | PS/PNIPAm/PEI MCP | 83%[5] | 499.7 |
| 90 | PS/PNIPAm/PEI MCP | 99%[5] | 514.6 |
| 120 | PS/PNIPAm/PEI MCP | 85%[5] | 435.4 |
| 195 | PS/PNIPAm/PEI MCP | 98%[5] | 515.4 |

[1] The reaction was counted since the addition of initiator into the reaction mixture

[2] The total monomer conversion of MCP particles were determined gravimetrically

[3] The hydrodynamic diameter of MCP particles were determined by DLS at 25 °C

[4] The monomer conversion was calculated based on total NIPAm monomer added

[5] The monomer conversion was calculated based on total monmer added

### *5.3.3.2 Effect of seed monomer to second batch monomer ratio*

The effect of weight ratio between the seed monomer (NIPAm) and second batch monomer (styrene) on the properties of the MCP particles was evaluated by varying the composition of NIPAm and styrene, keeping the PEI to total monomer ratio at 1 : 4 (w/w). The weight ratio of NIPAm to styrene was changed from 1 : 3

to 3 : 1. The results of these MCP particles were summarized and displayed in Table 5.7. In all situations, MCP particles had achieved total monomer conversion over 90% at the end of polymerization. The hydrodynamic diameter of the prepared MCP particles was ranged from 300 nm to 550 nm, indicating nanosized dimension of these particles. PNIPAm was a hydrogel that was extensively swollen with water below its VPTT. Thus we expected the hydrodynamic diameter of the PS/PNIPAm/PEI should be increased as the composition of PNIPAm increased. However, the difference between the hydrodynamic diameter of PS/PNIPAm/PEI MCP particles at different NIPAm/St. ratio was not significant. This was due to the presence of highly extended PEI in the outer shell of MCP particles. Thus, the hydrodynamic diameter of MCP particles was not significantly affected by the PNIPAm content.

The effect of weight ratio between NIPAm and styrene was more obvious in the surface charge of PS/PNIPAm/PEI. The ζ-potential of PS/PNIPAm/PEI MCP particle with NIPAm to styrene w/w ratio at 1 : 3, 1 : 1 and 3 : 1 were + 27.82 mV, + 4.92 mV and + 0.96 mV respectively. The magnitude of ζ-potential of MCP particles was decreased as the composition of NIPAm in the total monomer increased from 25% to 75%. PNIPAm became dominant in the outermost shell with increasing composition of NIPAm in the total monomer. This led to formation of interpenetrated shell between PNIPAm and PEI and resulted in a significant shielding effect on the positively charged PEI. As a result, the magnitude of ζ-potential of PS/PNIPAm/PEI was significantly reduced as the composition of NIPAm increased.

**Table 5.7.** Characteristics of PS/PNIPAm/PEI MCP particles with different NIPAm : St. (w/w) ratio.

| **Types of particles** | **w/w ratio of NIPAm to St. (NIPAm composition)[1]** | **Monomer Conversion[1]** | **Hydrodynamic Diameter (nm)[2]** | | | | **ζ-potential (mV)[3]** | | | |
|---|---|---|---|---|---|---|---|---|---|---|
| | | | **Dh (25°C)** | **Dh (32°C)** | **Dh (39°C)** | **$Dh_{39°C}$/ $Dh_{25°C}$** | **ζ-potential (pH 7)** | **ζ-potential (25°C)** | **ζ-potential (32°C)** | **ζ-potential (39°C)** |
| **PS/ PNIPAm/PEI MCP particles** | **1 : 3 (25%)** | **94%** | **494.7** | **470.2** | **448.8** | **0.91** | **+ 27.82** | **+ 27.82** | **+ 38.82** | **+ 39.45** |
| | **1 : 1 (50%)** | **98%** | **342.4** | **289.6** | **264.2** | **0.77** | **+ 4.92** | **+ 4.92** | **+ 11.10** | **+ 34.96** |
| | **3 : 1 (75%)** | **99%** | **511.1** | **421.1** | **358.3** | **0.70** | **+ 0.96** | **+ 0.96** | **+ 6.81** | **+ 27.25** |

---

[1] The weight ratio between PEI and total monomer was kept at 1 : 4 in this study

[2] The monomer conversion was determined gravimetrically

[3] The hydrodynamic diameter of MCP particles was determined by DLS at specific temperature and the samples were thermally equilibrated for 10 mins prior measurement

[4] The colloidal stability of MCP particles was determined by ζ-potential measurement using 1 mM NaCl as medium and the samples were thermally equilibrated for 10 mins prior measurement

### 5.3.4 Characterization of PS/PNIPAm/PEI nanocomposite particles

#### *5.3.4.1 Composition*

The composition of the PS/PNIPAm/PEI MCP particles was investigated by FT-IR spectroscopy. The particles were first purified by repeated centrifugation to get rid of any unreacted PEI and monomers. Figure 5.14a shows the FT-IR spectrum of MBA-crosslinked PNIPAm/PEI seed particles. Strong C=O amide stretching peak observed at 1650 to 1660 cm$^{-1}$, strong N-H amide II bending peak observed at 1535 cm$^{-1}$ and isopropyl C-H peak observed at 1370 to 1390 cm$^{-1}$ suggest the presence of PNIPAm. Both broad amino N-H stretching peak of primary amine at 3400 to 3500 cm$^{-1}$, and C-H stretching and bending at 2900 to 3000 cm$^{-1}$ indicate the presence of PEI. Figure 5.14b shows the FT-IR spectrum of PS/(PNIPAm-MBA)/PEI MCP particles. Additional absorption peaks at 750 cm$^{-1}$ and 700 cm$^{-1}$ are identified in the spectrum, which correspond to aromatic =C-H out-of-plane bending vibration peaks. Enhanced absorption peak at 1500 cm$^{-1}$ regarding to aromatic =C-H stretching vibration of PS is also observed. Enhanced absorption peak also appear at 2950 to 3050 cm$^{-1}$ regarding to =C-H vinylic hydrogen which suggest the presence of PS. These characteristic peaks confirm the presence of polystyrene in the MCP particles. Based on the FTIR results, we can confirm that the MCP particles comprise of PEI, PNIPAm and PS components.

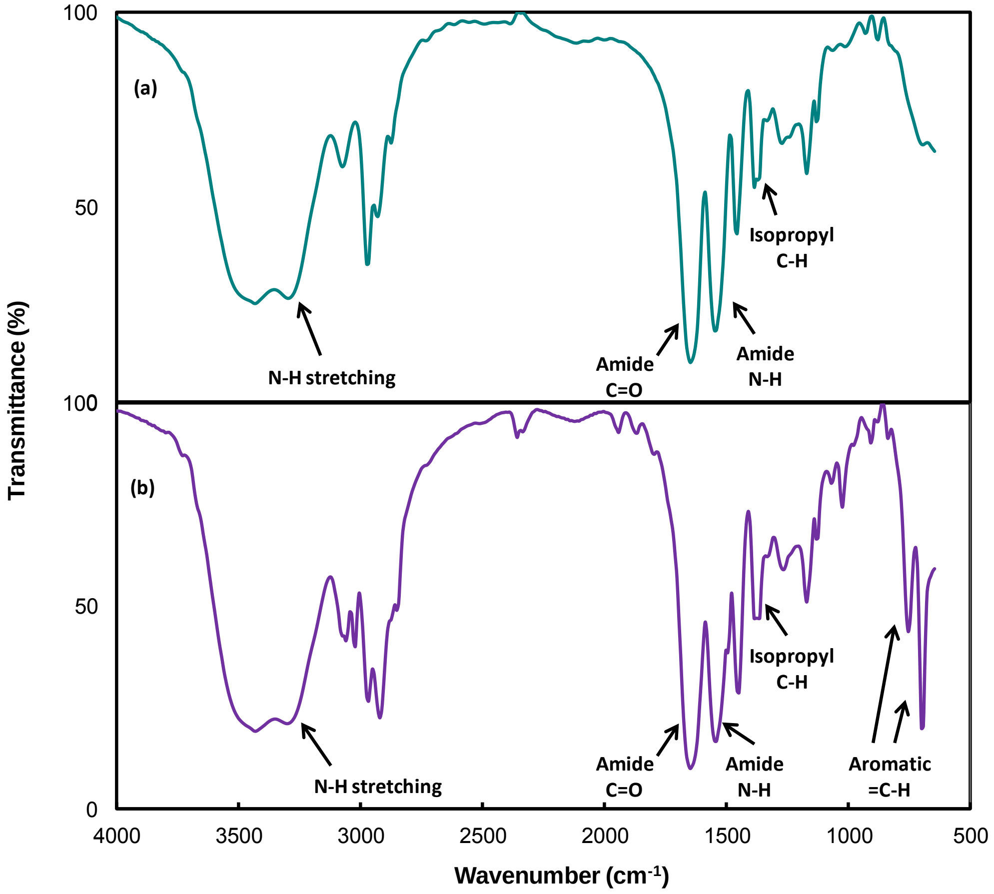

**Fig. 5.14.** FT-IR spectrum of a) PNIPAm/PEI seed; and b) PS/PNIPAm/PEI MCP particles.

### *5.3.4.2 Particle size as a function of temperature*

#### *Particle size*

The hydrodynamic diameters ($Z_{AVE}$) and particle size distribution (PDI) of seed and MCP particles were determined by dynamic light scattering (DLS) at pH 7 using a Beckman Coulter Delsa Nano C instrument. Figure 5.15 shows the particle size and size distribution of PS/PNIPAm/PEI MCP particles. The hydrodynamic diameter and particle size distribution of MCP particles were 342.4 nm and 0.142. These results indicated that the prepared MCP particles were in nano-sized dimension and with narrow size distribution. However, the hydrodynamic diameter of PNIPAm/PEI seed could not be determined due to absence of crosslinking which had explained before.

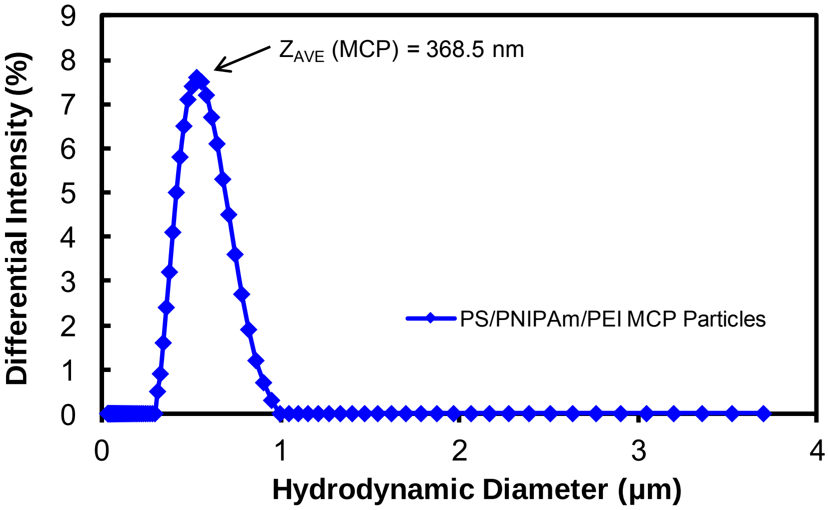

**Fig. 5.15.** Particle size of PS/PNIPAm/PEI MCP particles (342.4 nm).

### *Effect of seed monomer to second monomer ratio on particle size as a function of temperature*

The effect of temperature on the hydrodynamic diameter of the PS/PNIPAm/PEI MCP particles with different NIPAm/styrene weight ratio was evaluated by DLS measurement at different temperatures (25 ℃, 27 ℃, 29 ℃, 32 ℃, 35 ℃, 37 ℃ and 39 ℃). The variation of the hydrodynamic diameter of PS/PNIPAm/PEI MCP particles with different weight ratio between seed monomer and second batch hydrophobic monomer as a function of temperature was plotted and displayed in Figure 5.16.

As explained previously, the variation of the hydrodynamic diameter of PS/PNIPAm/PEI MCP particles was negligible below VPTT of PNIPAm. When the surrounding temperature was elevated to 32 ℃, VPTT of PNIPAm, there was a sudden drop in the hydrodynamic diameter of the MCP particles. PNIPAm underwent volume phase transition which changed from hydrophilic to hydrophobic and caused shrinkage in the particle size of MCP particles. As the surrounding temperature further increased, there is no significant change in the particle size.

At 25℃ (below VPTT of PNIPAm), the hydrodynamic diameter of MCP particles with NIPAm/styrene weight ratio at 1 : 3, 1 : 1 and 3 : 1 were 494.7 nm, 342.4 nm and 511.1 nm respectively. The hydrodynamic diameter of MCP particles was ranged from 350 nm to 500 nm. At 39 ℃ (above VPTT of PNIPAm), the hydrodynamic diameter of MCP particles with NIPAm/styrene weight ratio at 1 : 3, 1 : 1 and 3 : 1 were 448.8 nm, 264.2 nm and 358.3 nm respectively. All the MCP particles exhibited nanosized dimension. PNIPAm underwent volume phase transition which changed from hydrophilic to hydrophobic as the temperature was raised to above its VPTT. The shrinkage of PNIPAm eventually resulted in a reduction in hydrodynamic diameter of MCP particles.

To further evaluate the thermal responsive properties of the MCP particles, the hydrodynamic diameter was re-expressed as normalized hydrodynamic diameter which demonstrated the thermal responsive properties of MCP particles quantitatively. The variation of normalized hydrodynamic diameters of MCP particles as a function of temperature was plotted and displayed in the Figure 5.17.

The normalized hydrodynamic diameter of PS/PNIPAm/PEI MCP particles with NIPAm/MMA weight ratio at 1 : 3, 1 : 1, and 3 : 1 at 39 ℃ ($Dh_{39\ ^{\circ}C}/Dh_{25\ ^{\circ}C}$) were 0.91, 0.77 and 0.70 respectively. The normalized hydrodynamic diameter of MCP particles gradually decreased as the NIPAm composition in the total monomer increased from 25% to 75%. When the total monomer comprised of 25% NIPAm, the normalized hydrodynamic diameter of MCP particles was 0.91, indicating there was a 9% reduction in the particle size. As the NIPAm composition increased substantially from 25% to 75%, the particle size reduction became more obvious. As the total monomer contained 75% of NIPAm by weight, the normalized hydrodynamic diameter of the prepared MCP particles was 0.70. There was a nearly 30% reduction in the hydrodynamic diameter, indicating the MCP particles possessed superior thermal responsive properties. The thermal responsive properties of MCP particles can be adjusted by varying the monomer compositions.

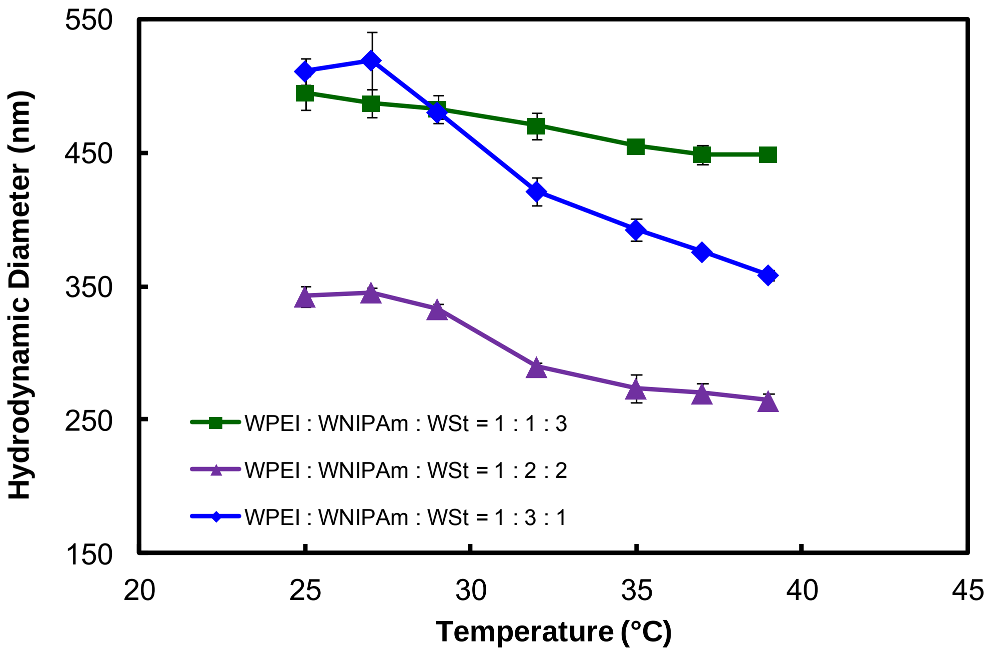

**Fig. 5.16.** Particle size as a function of temperature of PS/PNIPAm/PEI MCP particles ($W_{PEI}$ : $W_{Total\ monomer}$ = 1 : 4).

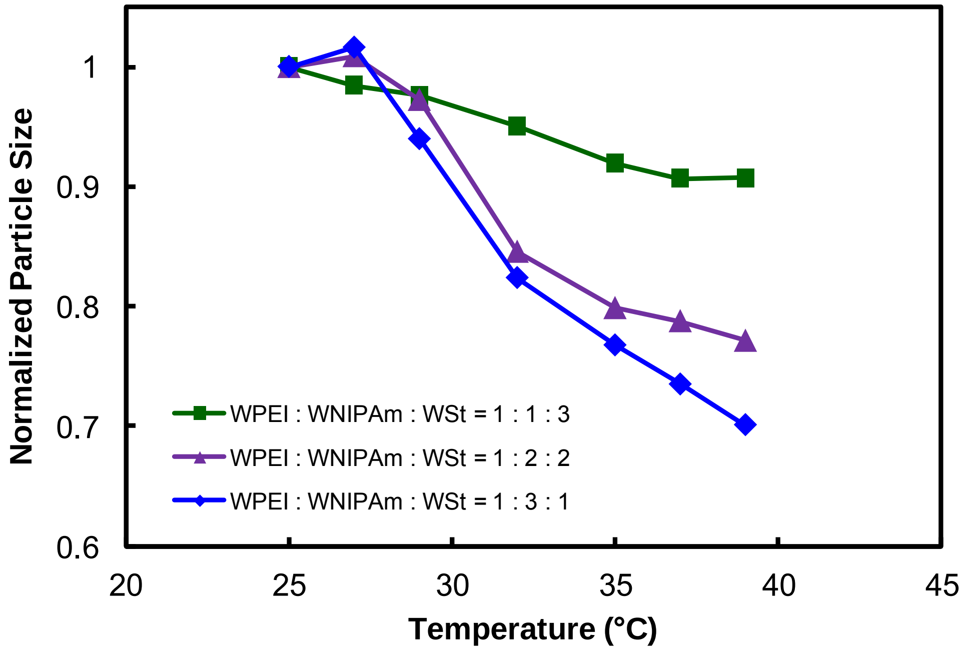

**Fig. 5.17.** Normalized particle size ($Dh/Dh_{25\ °C}$)as a function of temperature of PS/PNIPAm/PEI MCP particles ($W_{PEI}$ : $W_{Total\ monomer}$ = 1 : 4).

### *5.3.4.3 Surface charges of particles as a function of pH and temperature*

#### *Surface charge*

The surface charge of MCP particles was determined by ζ-potential measurement using Beckman Coulter Delsa Nano C instrument. Under standard condition, pH 7 with conducting medium of 1 mM NaCl, only the ζ-potential of PMMA/PNIPAm/PEI MCP particles could be determined. The ζ-potential of PNIPAm/PEI seed could not be determined due to absence of crosslinking of PNIPAm/PEI seed particles. The ζ-potential of PMMA/PNIPAm/PEI MCP particles was and + 4.92 mV respectively. The low magnitude of ζ-potential of both seed and MCP particles was due to the formation of PNIPAm/PEI interpenetrated network at the outermost shell of the particles as explained in **4.3.2.5**. The charge shielding of PEI by PNIPAm resulted in the suppression of the charge density of the particles.

#### *Effect of seed monomer to second monomer ratio on the surface charges of particles as a function of pH and temperature*

The effect of weight ratio between seed monomer and second hydrophobic monomer on the ζ-potential of MCP particles at was evaluated by ζ-potential measurement using Delsa Nano C with the aid of auto-titrator. The variation of ζ-potential as a function of pH of MCP particles with different weight ratio between seed monomer and second hydrophobic monomer was illustrated in Figure 5.18.

Independent of the total monomer composition in MCP particles, the surface of PS/PNIPAm/PEI MCP particles was positively charged and the ζ-potential almost remains unchanged below pH 7. The positive ζ-potential of MCP particles was contributed by the protonated amino groups of PEI located at the outermost shell of the MCP particles. As the pH of the medium was raised to above 7, there was a drop in the ζ-potential of MCP particles. The drop in ζ-potential was due to the deprotonation of the amino groups. Eventually, the ζ-potential of MCP particles was dropped to about zero as the pH of the medium was approached 9.5, isoelectric point of PEI.

Although PS/PNIPAm/PEI MCP particles with different NIPAm composition had the same trend in the variation of ζ-potential against pH, the effect of weight ratio between NIPAm and styrene was reflected by the magnitude of ζ-potential. The ζ-potential of PS/PNIPAm/PEI MCP particles with NIPAm/styrene weight ratio at 1 : 3, 1 : 1 and 3 : 1 at pH 7 were + 27.82 mV, + 4.92 mV and + 0.96 mV respectively. The magnitude of ζ-potential was gradually decreased as the NIPAm composition increased from 25% to 75% in total monomer. The ζ-potential of MCP particles was high (> + 25 mV) when the total monomer contained 25% NIPAm. In this case, the amount of PNIPAm was insufficient to shield the protonated amino groups on PEI though the degree of crosslinking of MCP particles was low. Due to the incomplete shielding of the positive charges of PEI in the outermost shell of the particles, part of the protonated groups were exposed to the continuous phase and contributed to the high magnitude in ζ-potential.

As the NIPAm composition was substantially increased to 50%, there was a significant drop in the magnitude of ζ-potential from + 25 mV to + 5 mV. This drop corresponded to a decrease in the positive charges on the surface of the MCP particles. As the NIPAm composition in total monomer increased to over 50%, the shielding effect of PNIPAm on the protonated amino groups of PEI became more significant. This resulted in an abrupt drop in the magnitude of ζ-potential. Further promoting the NIPAm composition up to 75% caused slightly additional drop in the ζ-potential of MCP particles from + 5 mV to 0 mV. This indicated nearly all the positive charges on PEI were shielded by PNIPAm. Though MCP particles lost the colloidal stability from electrostatic repulsion, it was still dispersed as colloids in the continuous phase. The hydrophilic PNIPAm at the outermost shell provided colloidal stability to the MCP particles. Under low NIPAm compsition, the MCP particles were stabilized by the positively charged PEI via electrostatic repulsion. At high NIPAm composition, the MCP particles were stabilized by the hydrophilic PNIPAm located at the outer shell. Thus, the colloidal stability of the particles was maintained under various NIPAm compositions. The surface charge of the particles could be tuned by varying the NIPAm composition in total monomer.

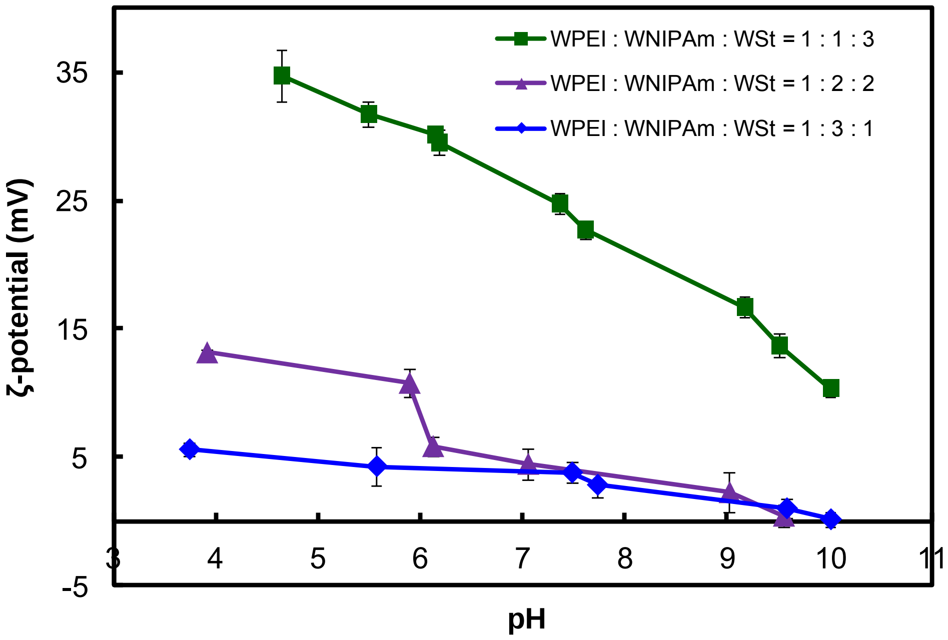

**Fig. 5.18.** ζ-potential as a function of pH of PS/PNIPAm/PEI MCP particles ($W_{PEI}$ : $W_{Total\ monomer}$ = 1 : 4).

The effect of temperature on the ζ-potential of MCP particles at different seed monomer to second batch hydrophobic monomer ratio was evaluated by ζ-potential measurement using Delsa Nano C with the aid of thermal monitoring device. The variation of ζ-potential as a function of temperature of MCP particles with different NIPAm/styrene composition as a function of temperature was plotted and displayed in Figure 5.19.

Independent of the weight ratio between seed monomer and second batch hydrophobic monomer, the trend in the variation of ζ-potential of PS/PNIPAm/PEI MCP particles against temperature was similar. Below the VPTT of PNIPAm (32 °C), MCP particles had positive ζ-potential and the ζ-potential was kept constant in this temperature range. As the temperature was raised to the

VPTT of PNIPAm, there was an obvious jump in the ζ-potential of MCP particles. When the temperature was further raised, there was no insignificant increase in the ζ-potential of MCP particles.

Although the trend in the variation of ζ-potential of MCP particles against temperature was the same, there was significant difference in magnitude of ζ-potential in MCP particle with different PEI to total monomer weight ratio. The ζ-potential of MCP particles with NIPAm/styrene weight ratio at 1 : 3, 1 : 1 and 3 : 1 at 25 °C were + 27.82 mV, + 4.92 mV and + 0.96 mV respectively. The ζ-potential magnitude of MCP particles gradually dropped as the NIPAm composition increased from 25% to 75%. There was a reciprocal relationship between the NIPAm composition and ζ-potential of MCP paricles.

When the total monomer contained 25% NIPAm, the ζ-potential of MCP particles was higher + 25 mV, indicating the charge shielding of PEI was not significant. Protonated amino groups on PEI were only partially shielded by PNIPAm. As the NIPAm content substantially increased to 50%, the ζ-potential of the MCP particles was decreased to + 5 mV. This abrupt drop in the ζ-potential was attributed to significant charge shielding of PEI by PNIPAm. PNIPAm became dominant at the outermost shell of the MCP particles which resulted in charge shielding of the PEI and suppressed the ζ-potential of MCP particles. As the NIPAm content was further raised to 75%, the ζ-potential of MCP particles was slightly dropped and approached to 0 mV. Under this circumstance, PEI was completely shielded by PNIPAm. As a result, the surface charges of the MCP particles could be adjusted by varying the NIPAm composition in the total monomer.

The thermal responsive properties of MCP particles on ζ-potential were demonstrated as the temperature was raised to above VPTT of PNIPAm. Across VPTT of PNIPAm, volume phase transition of PNIPAm was taken place which changed from hydrophilic to hydrophobic. The shrinkage of the PNIPAm caused re-exposure of the positively charged PEI at the outermost shell. Thus, there was a sudden increase in ζ-potential of MCP particles. At the end of the measurement, the ζ-potential of MCP particles was close to + 35 mV. As the NIPAm content in total monomer was gradually increased, the difference between ζ-potential of MCP particles below VPTT and above VPTT was enhanced. This illustrated that the thermal responsiveness of MCP particles could be adjusted by varying the NIPAm composition in total monomer.

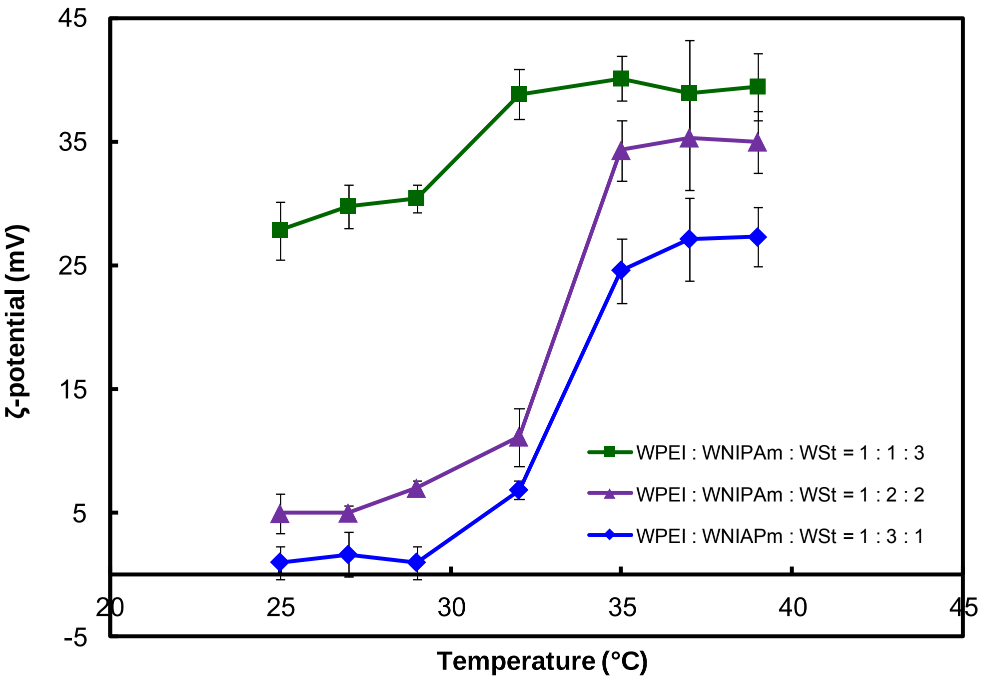

**Fig. 5.19.** ζ-potential as a function of temperature of PS/PNIPAm/PEI MCP particles ($W_{PEI} : W_{Total\ monomer} = 1 : 4$).

### *5.3.4.4 Morphology*

The morphology and core-shell nanostructure of PS/PNIPAm/PEI MCP particles prepared at different degree of crosslinking were examined by TEM.

The nanostructure of PS/PNIPAm/PEI MCP particles was elucidated by staining with 0.5% (w/w) phosphotungstic acid (PTA, $WO_2 \bullet H_3PO_4 \bullet xH_2O$) for 5 mins. Spherical particles with high uniformity were revealed in the TEM micrographs. These MCP particles exhibited well-defined core-shell nanostructured particles. During PTA staining, PNIPAm was heavily stained by PTA solution while PEI was slightly stained by PTA solution. PS was not stained by PTA solution. Thus, we interpreted that the dark shell was constructed by an interpenetrated network of PEI and PNIPAm and the bright core of the particles was constructed by PS.

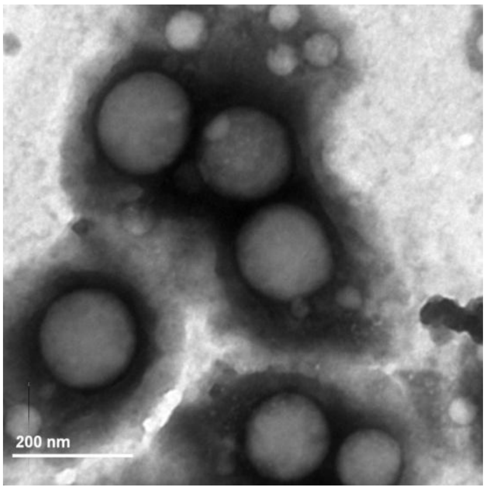

**Fig. 5.20.** TEM image of PS/PNIPAm/PEI MCP particles.

## 5.4 Effect of Second Batch Monomer on the Properties of MCP Nanocomposite Particles

The effect of second batch monomer on the smart properties and nanostructures of MCP particles is discussed in detail in this part. To be consistent, the weight ratio between PEI, NIPAm and second batch monomer of MCP particles discussed in this part was kept at 1 : 2 : 2. The characteristics of the PNIPAm/PEI seed and MCP particles were summarized in the Table 5.8.

MMA, *n*-BA and styrene had been used as second batch monomer in this study. MCP particles were successfully fabricated only when MMA and styrene were used as second batch monomer. However, MCP particles could not be formed when *n*-BA was used as second batch monomer. Particle dissociation of PBA/PNIPAm/PEI occurred at the end of polymerization, indicated by a physical change from milky colloidal dispersion to clear yellow gelatinous solution. Absence of rigid solid support was the major reason for the dissociation of PBA/PNIPAm/PEI particles. The Tg of PBA and PEI are 219 K and 213 K respectively. In addition, PNIPAm exhibits hydrogel structure below its VPTT. All the components of PBA/PNIPAm/PEI particles were soft and tacky. Thus, the particle structure could not be maintained and was dissociated after the polymerization.

The reaction kinetics of the seeded emulsion polymerization of MCP nanocomposites was monitored by thermal couple (Testo 735) with 1 temperature recorded per second. Fig. 5.1 and Fig. 5.13 showed the temperature profile of the preparation of PMMA/(PNIPAm-MBA)/PEI and PS/(PNIPAm-MBA)/PEI MCP particles respectively. Two obvious exothermic peaks were observed in the temperature profiles. As explained before, the first peak was due to the exothermic polymerization of NIPAm in the seed forming stage. The monomer conversion of NIPAm reached 99%. The second peak was due to the exothermic polymerization of second batch monomer during seeded emulsion polymerization. The total monomer conversions of all MCP particles were above 85% at the end of polymerization.

**Table 5.8.** Characteristics of PNIPAm/PEI seed and MCP particles prepared with different second hydrophobic monomer.

| **Types of particles** | **Second batch monomer** | **Monomer Conversion**[2] | **Hydrodynamic Diameter (nm)**[3] | | | | **ζ-potential (mV)**[4] | | | |
|---|---|---|---|---|---|---|---|---|---|---|
| | | | **Dh (25°C)** | **Dh (32°C)** | **Dh (39°C)** | **$Dh_{39^{\circ}C}/Dh_{25^{\circ}C}$** | **ζ-potential (pH 7)** | **ζ-potential (25°C)** | **ζ-potential (32°C)** | **ζ-potential (39°C)** |
| **PNIPAm/PEI seed** | **N/A** | **99%** | **N/A** | **N/A** | **N/A** | **N/A** | **N/A** | **N/A** | **N/A** | **N/A** |
| **MCP particles**[1] | **MMA** | **88%** | **368.5** | **318.8** | **278.5** | **0.76** | **+ 4.12** | **+ 4.12** | **+ 11.11** | **+ 32.63** |
| | ***n*-BA** | **Particle dissociation below VPTT** | | | | | | | | |
| | **Styrene** | **98%** | **342.4** | **289.6** | **264.2** | **0.77** | **+ 4.92** | **+ 4.92** | **+ 11.10** | **+ 34.96** |

[1] The weight ratio between PEI and total monomer was kept at 1 : 4; while the weight ratio between NIPAm and second hydrophobic monomer was kept at 1 : 1 (NIPAm composition : 50%)

[2] The monomer conversion was determined gravimetrically

[3] The hydrodynamic diameter of MCP particles was determined by DLS at specific temperature and the samples were thermally equilibrated for 10 mins prior measurement

[4] The colloidal stability of MCP particles was determined by ζ-potential measurement using 1 mM NaCl as medium and the samples were thermally equilibrated for 10 mins prior measurement

### 5.4.1 Particle size as a function of temperature

#### *Particle size*

The hydrodynamic diameters ($Z_{AVE}$) and particle size distribution (PDI) of seed and MCP particles were determined by dynamic light scattering (DLS) at pH 7 using a Beckman Coulter Delsa Nano C instrument. The hydrodynamic diameter of the PNIPAm/PEI could not be determined by DLS measurement because of dissociation of particle structure. During the seed forming stage, no crosslinker was added to crosslink and maintain the particle structure of the PNIPAm/PEI. The micelle-like structure of PNIPAm/PEI seed was dissociated at temperature below VPTT of PNIPAm in the absence of crosslinker. Therefore, the hydrodynamic diameter of PNIPAm/PEI seed was able to be measured.

During seeded emulsion polymerization, the second hydrophobic monomer (MMA or styrene) was functioned as crosslinker to prevent the MCP particles from particle dissociation. The hydrodynamic diameters of PMMA/PNIPAm/PEI and PS/PNIPAm/PEI at were 368.5 nm and 342.4 nm 25 ℃ respectively. The particle size distribution of PMMA/PNIPAm/PEI and PS/PNIPAm/PEI were 0.059 and 0.142 respectively. These MCP particles were synthesized with nano-sized dimension and narrow size distribution.

#### *Particle size as a function of temperature*

The effect of second batch hydrophobic monomer (MMA and styrene) on the thermal responsive properties of MCP particles was investigated by DLS measurement at different temperatures (25 ℃, 27 ℃, 29 ℃, 32 ℃, 35 ℃, 37 ℃

and 39 ℃). The MCP particles were thermally equilibrated at the preset temperature for 10 mins prior measurement. The variation of the hydrodynamic diameter of MCP particles as a function of temperature was plotted in Figure 5.21.

Below VPTT of PNIPAm, there was no significant change in the particle size of both PNIPAm/PEI seed and MCP particles. When the temperature was raised to above 32 ℃ (VPTT of PNIPAm), an abrupt drop in the hydrodynamic radii of both PNIPAm/PEI seed and MCP particles was recorded. This drop was due to the phase transition of PNIPAm from hydrophilic to hydrophobic. The hydrophobic PNIPAm was then migrated to the particle core, leading to shrinkage in the particle size of MCP particles. Further increasing in the temperature did not induce significant change in the particle size. This indicated the reduction in particle size was contributed by volume phase transition of PNIPAm.

To further evaluate the thermal responsive properties of the MCP particles, the hydrodynamic diameter was re-expressed as normalized hydrodynamic diameter which demonstrated the thermal responsive properties of MCP particles quantitatively. The normalized hydrodynamic diameter of PMMA/PNIPAm/PEI and PS/PNIPAm/PEI MCP particles at 39 ℃, $Rh_{39\ ℃}/Rh_{25\ ℃}$, were 0.76 and 0.77 respectively.

Nearly 25% reduction in the hydrodynamic diameters of PMMA/PNIPAm/PEI and PS/PNIPAm/PEI MCP particles was recorded at temperature above VPTT of PNIPAm. The difference in the particle size reduction between PMMA/PNIPAm/PEI and PS/PNIPAm/PEI was insignificant. However, the results in **4.4.1** suggested that PMMA/(PNIPAm-MBA)/PEI MCP particles exhibited a lower degree of particle shrinkage due to its aerolite-like nanostructure.

This special nanostructure hindered the migration of PNIPAm from the outer shell to the inner core. We believe this should be caused by the low crosslinking degree of the MCP particles. The MCP particles reported in **4.4.1** was crosslinked by 2% MBA. In this study, the MCP particles were crosslinked by second batch monomer during seeded emulsion polymerization. These monomers not only used for crosslinking purpose, but also polymerized to form a rigid solid support in the particles. Thus, the MCP particles were slightly crosslinked by the second batch monomer. The low crosslinking degree of the MCP particles facilitated the extension of PNIPAm in the outer shell to form an interpenetrated network with PEI. As temperature increased, the shrinkage and migration of PNIPAm was not restricted. Therefore, significant reduction (~ 25%) in the hydrodynamic diameters of PMMA/PNIPAm/PEI and PS/PNIPAm/PEI MCP particles was recorded.

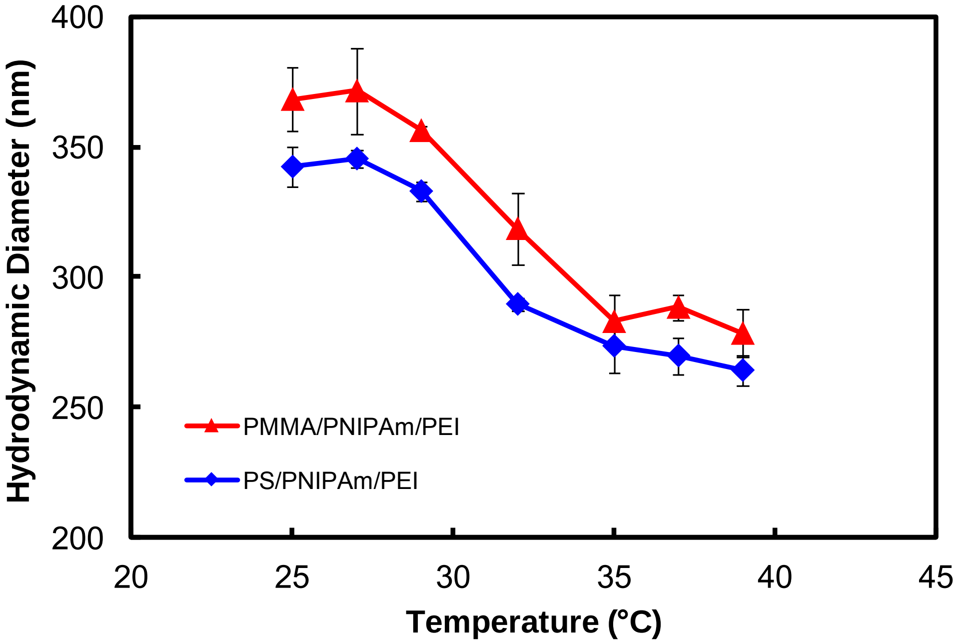

**Fig. 5.21.** Particle size of PNIPAm/PEI based MCP particles as a function of temperature.

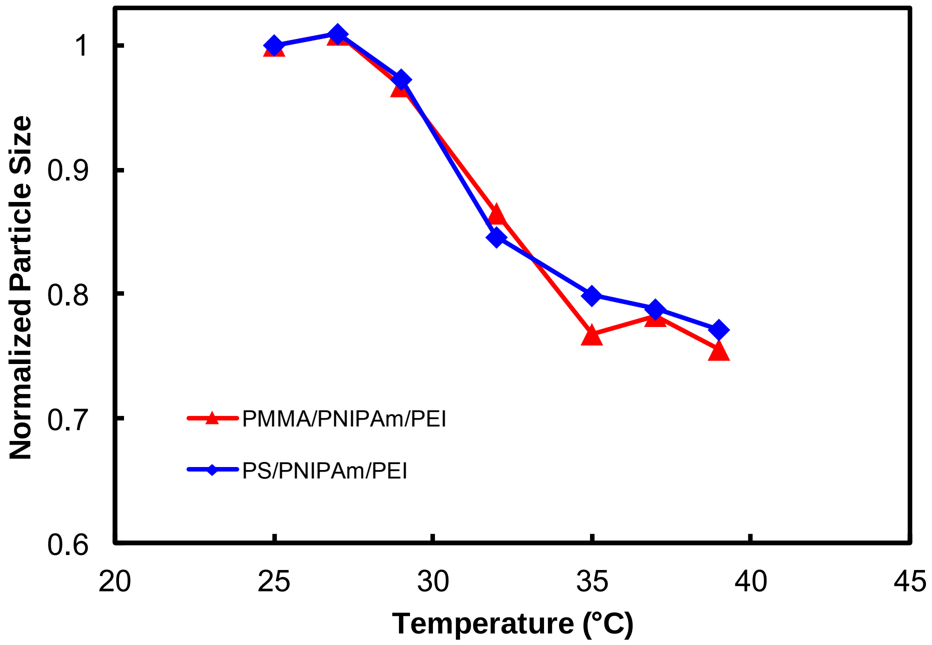

**Fig. 5.22.** Normalized particle size ($Dh/Dh_{25\ °C}$) of PNIPAm/PEI based MCP particles as a function of temperature

### 5.4.2 Surface charge of particls as a function of pH and temperature

***Surface charge***

The surface charge of MCP particles was determined by ζ-potential measurement using Beckman Coulter Delsa Nano C instrument. Under standard condition, pH 7 with conducting medium of 1 mM NaCl, the ζ-potential of PMMA/PNIPAm/PEI and PS/PNIPAm/PEI MCP particles were + 4.12 mV and + 4.92 mV at 25 °C respectively. Similarly, the ζ-potential of PNIPAm/PEI seed could not be measured due to dissociation of particle structure as explained before.

Based on the findings in **4.4.2**, we predict the ζ-potential of PMMA/PNIPAm/PEI MCP particles should be higher than PS/PIPAm/PEI MCP particles due to the difference in their nanostructures. In fact, there was no significant differenece between their ζ-potential. The major reason was low crosslinkg degree of the MCP particles which had been explained before. MCP particles were slightly crosslinked by the second batch monomer during seeded emulsion polymerization. PNIPAm was not restricted to form interpenetrated network with PEI in the outer shell. Due to the formation of interpenetrated shell between PNIPAm and PEI, the positive charges on PEI was shielded by PNIPAm and resulted in low ζ-potential of the MCP particles.

***Surface charges of particles as a function of pH***

The effect of pH on the ζ-potential of MCP particles prepared with different second batch monomer (MMA and styrene) was conducted by ζ-potential measurement using Delsa Nano C with the aid of auto-titrator. The variation of ζ-potential as a function of pH of MCP particles with different second batch monomer was illustrated in Figure 5.23.

MCP particles prepared with different second batch monomers (MMA and styrene) had similar trend in the ζ-potential as a function of pH. Below pH 7, the ζ-potential of MCP particles was positive and almost unchanged. The positive ζ-potential indicated the presence of PEI on the particle shell. When solution pH was above 7, there was an obvious decrease in the ζ-potential of MCP particles due to the deprotonation of the ammonium cations of the PEI. The ζ-potential of the MCP particles was dropped to below + 10 mV at pH 9.5, the isoelectric point of PEI.

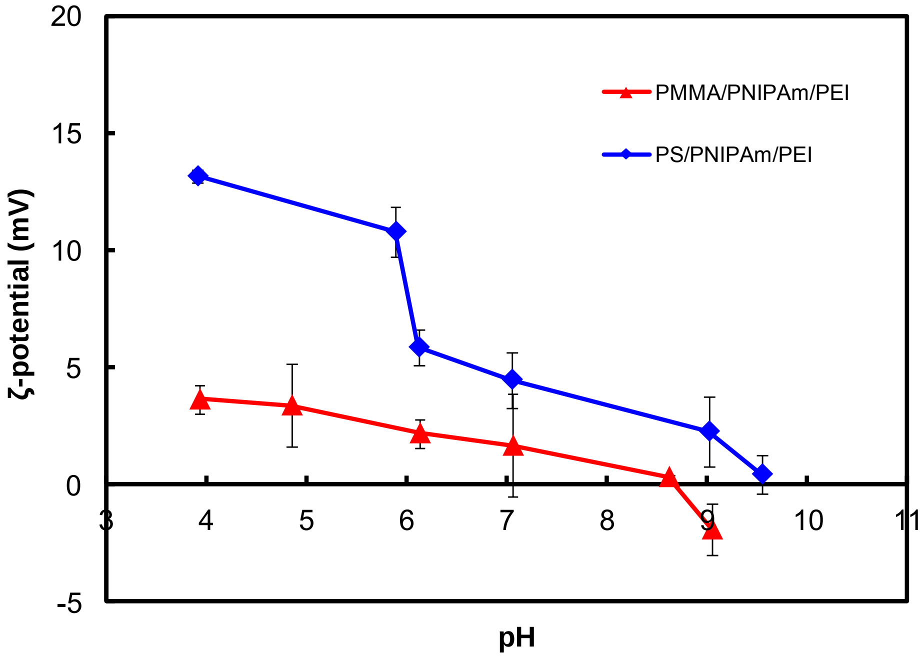

**Fig. 5.23.** ζ-potential as a function of pH of PNIPAm/PEI based MCP particles .

*Surface charges of particles as a function of temperature*

The effect of temperature on the ζ-potential of MCP particles prepared with different second batch monomer (MMA and styrene) was evaluated by ζ-potential measurement using Delsa Nano C with the aid of thermal monitoring device. The variation of ζ-potential as a function of temperature of MCP particles with second hydrophobic polymer (PMMA and PS) as a function of temperature was displayed in Figure 5.24.

PMMA/PNIPAm/PEI and PS/PNIPAm/PEI MCP particles had the same trend in the variation of ζ-potential against temperature as explained in **4.3.2.4**. The ζ-potential of MCP particles was positive and kept constant at temperatures below VPTT of PNIPAm. There was an abrupt increase in the magnitude of ζ-potential when the temperature was rasied to above 32 °C. This increase was regarded as charge re-exposure on the particle surface. PNIPAm underwent phase transition at its VPTT which changed from hydrophilic to hydrophobic. Hydrophilic PNIPAm at the interpenetrated shell was shrunk and then migrated into the particle core. Thus, the positive PEI was not shielded by PNIPAm and resulted in an increase in the ζ-potential. This finding also indicated there was a change in the composition of the particle surface. The surface was composed of an interpenetrated network below VPTT of PNIPAm, while the surface was mainly composed of PEI above VPTT.

In addition, it should be mentioned that there was great amplitude in the increment of the ζ-potential as temperature increased. The ζ-potential of MCP particles was about + 5 mV at 25 °C and + 35 mV at 39 °C. This was probably attributed to the low crosslinking degree of the particles. PNIPAm was extensively extended in the outer shell of MCP particles at temperature below its VPTT, forming a highly interpenetrated network with PEI. PEI was extensively shielded by PNIPAm, leading to a severe suppression in the ζ-potential of the MCP particles. The significant change in the ζ-potential was caused by the interpenetrated shell of MCP particles.

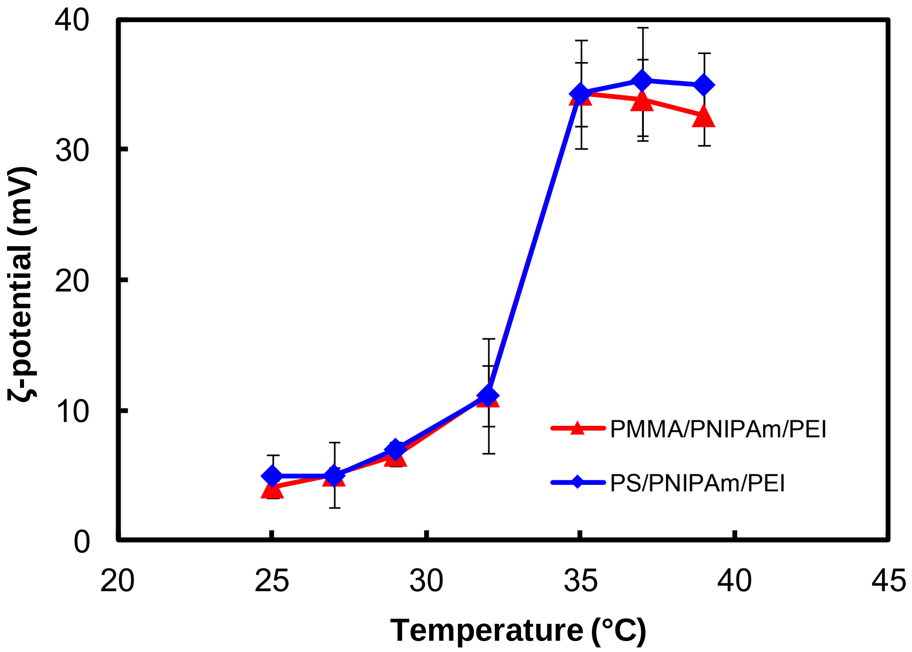

**Fig. 5.24.** ζ-potential as a function of temperature of PNIPAm/PEI based MCP particles.

### 5.4.3 Morphology

The morphology and core-shell nanostructure of PMMA/PNIPAm/PEI, and PS/PNIPAm/PEI MCP particles were examined by TEM.

The nanostructure of the MCP particles was revealed under TEM micrographs by staining the dried particle samples with 0.5% (w/w) phosphotungstic acid (PTA, $WO_2 \cdot H_3PO_4 \cdot xH_2O$) for 5 mins. Different nanostructures were observed in the TEM images of PMMA/PNIPAm/PEI and PS/PNIPAm/PEI MCP particles. PMMA/PNIPAm/PEI exhibited a special aerolite-like structure in which numerous bright micro-domains were freely distributed in the particles. These bright micro-domains were PMMA and the dark region was the PTA-stained PNIPAm and PEI. As explained **4.3.2.5**, the formation of this special nanostructure was due to the high water solubility of MMA monomer (15 g/L). This facilitated the diffusion of MMA from the continuous phase to the growing seed particles for seeded emulsion polymerization. The initiation rate of MMA was high, too. These factors resulted in fast polymerization of MMA and contributed to this kinetic favored morphology.

On the other hand, PS/PNIPAm/PEI MCP particles had a spherical morphology with well-defined core-shell nanostructure. The bright core of the particles was PS and the dark shell was PTA-stained PNIPAm and PEI. The water solubility of styrene (0.31 g/L) was low that allowed slow diffusion of styrene into the growing seed particles. As a result, equilibrium morphology with well-defined core-shell structure was reached at the end of polymerization.

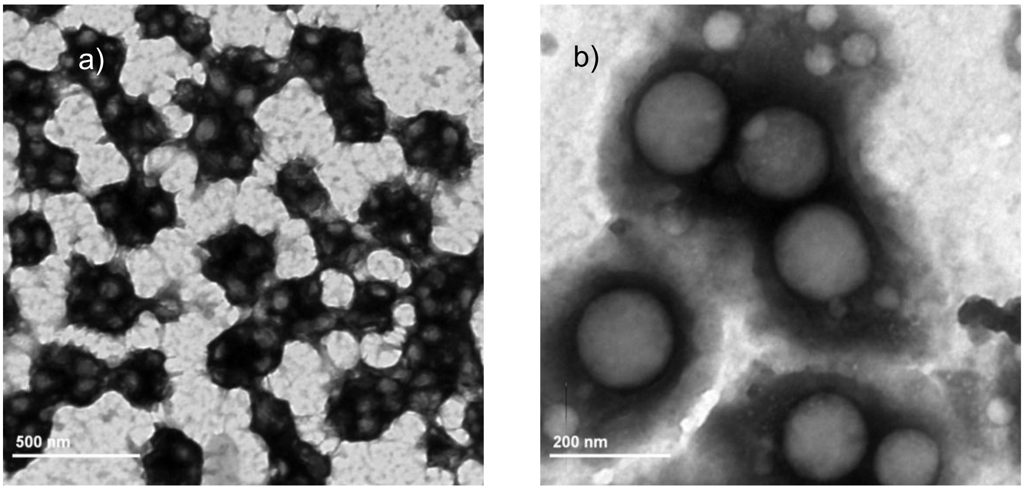

**Fig. 5.25.** TEM micrographs of a) PMMA/PNIPAm/PEI and b) PS/PNIPAm/PEI MCP particles.

## 5.5 Effect of Crosslinker on the Properties of MCP Nanoomposite Particles

The effect of crosslinker type on the smart properties and nanostructures of MCP particles is discussed in detail in this part. To be consistent, the weight ratio between PEI, NIPAm and second batch monomer of MCP particles discussed in this part was kept at 1 : 2 : 2. The characteristics of these MCP particles were summarized in the Table 5.9.

MBA and second hydrophobic monomer (styrene) had been used as crosslinker in this study. The crosslinking degree of MBA for the preparation of MCP particles was 10%. Independent of the crosslinker type, the total monomer conversion of MCP particles was above 90% at the end polymerization. The hydrodynamic diameter of (PNIPAm-10% MBA)/PEI seed hydrogel was 273.6 nm. Nevertheless, the hydrodynamic diameter of PNIPAm/PEI seed hydrogel could be determined due to absence of crosslinking. The self-assembled micelles were dissociated as temperature fell below VPTT. The hydrodynamic diameter of PS/(PNIPAm-10% MBA)/PEI and PS/PNIPAm/PEI MCP particles was ranged from 300 nm to 400 nm. The particle size distribution of PS/(PNIPAm-10% MBA)/PEI and PS/PNIPAm/PEI MCP particles was narrow. This indicated the MCP particles were prepared with high uniformity and without secondary nucleation.

PS/(PNIPAm-10% MBA)/PEI and PS/PNIPAm/PEI possessed positive ζ-potential, indicating the particle surface was constructed by positively charged PEI. Nevertheless, the crosslinker type had significant effect on the ζ-potential magnitiude of MCP particles. The ζ-potential of PS/(PNIPAm-10% MBA)/PEI and PS/PNIPAm/PEI MCP particles were + 31.07 mV and + 4.92 mV at pH 7 under room temperature respectively. The difference in their ζ-potential magnitude was due to the type of crosslinker which will be discussed later. MCP particles with high total monomer conversion, nanosized dimension and desirable colloidal stability were successfully prepared by using MBA or second hydrophobic monomer as crosslinker.

**Table 5.9.** Characterisitics of PS/PNIPAm/PEI MCP particles prepared by different types of crosslinker

| Types of Particles | Crosslinker[1] | Monomer conversion[2] | Hydrodynamic diameter (nm)[3] | | | | ζ-potential (mV)[4] | | | |
|---|---|---|---|---|---|---|---|---|---|---|
| | | | Dh (25°C) | Dh (32°C) | Dh (39°C) | $Dh_{39°C}$/ $Dh_{25°C}$ | ζ-potential (pH 7) | ζ-potential (25°C) | ζ-potential (32°C) | ζ-potential (39°C) |
| (PNIPAm-MBA)/PEI seed hydrogel | MBA | 99% | 273.6 | 253.1 | 217.2 | 0.79 | + 15.49 | + 15.49 | + 20.08 | + 30.42 |
| PS/(PNIPAm-MBA)/PEI MCP particles | MBA | 91% | 378.7 | 362.4 | 349.3 | 0.92 | + 31.07 | + 31.07 | + 34.22 | + 39.80 |
| PNIPAm/PEI seed hydrogel | N/A | 99% | N/A | N/A | N/A | N/A | N/A | N/A | N/A | N/A |
| PS/PNIPAm/PEI MCP particles | Second monomer | 98% | 342.4 | 289.6 | 264.2 | 0.77 | + 4.92 | + 4.92 | + 11.10 | + 34.96 |

[1] The degree of crosslinking of MBA was 10%

[2] The monomer conversion was determined gravimetrically

[3] The hydrodynamic diameter of MCP particles was determined by DLS at specific temperature and the samples were thermally equilibrated for 10 mins prior measurement

[4] The colloidal stability of MCP particles was determined by ζ-potential measurement using 1 mM NaCl as medium and the samples were thermally equilibrated for 10 mins prior measurement

### 5.5.1 Particle size as a function of temperature

#### *Particle size*

The hydrodynamic diameters ($Z_{AVE}$) and particle size distribution (PDI) of seed and MCP particles were determined by dynamic light scattering (DLS) at pH 7 using a Beckman Coulter Delsa Nano C instrument. The hydrodynamic diameters of PS/(PNIPAm-10% MBA)/PEI and PS/PNIPAm/PEI were 378.7 nm and 342.2 nm 25 °C respectively. The particle size distribution of PS/(PNIPAm-10% MBA)/PEI and PS/PNIPAm/PEI were 0.216 and 0.142 respectively. These MCP particles were synthesized with nano-sized dimension and narrow size distribution. More importantly, this indicated the type of crosslinker had insignificant effect on the particle size of MCP particles.

#### *Particle size as a function of temperature*

The effect of crosslinker (MBA and styrene) on the thermal responsive properties of MCP particles was investigated by DLS measurement at different temperatures (25 °C, 27 °C, 29 °C, 32 °C, 35 °C, 37 °C and 39 °C). The MCP particles were thermally equilibrated at the preset temperature for 10 mins prior measurement. The variation of the hydrodynamic diameter of MCP particles as a function of temperature was plotted in the Figure 5.26.

Below VPTT of PNIPAm, there was no significant change in the particle size of PS/(PNIPAm-10% MBA)/PEI and PS/PNIPAm/PEI MCP particles. When the temperature was raised to above 32 °C (VPTT of PNIPAm), an abrupt drop in the hydrodynamic radii of MCP particles was recorded. This drop was due to the phase transition of PNIPAm from hydrophilic to hydrophobic. The hydrophobic

PNIPAm was then migrated to the particle core, leading to shrinkage in the particle size of MCP particles. Further increasing in the temperature did not induce significant change in the particle size. This indicated the reduction in particle size was contributed by volume phase transition of PNIPAm.

To further evaluate the thermal responsive properties of the MCP particles, the hydrodynamic diameter was re-expressed as normalized hydrodynamic diameter which demonstrated the thermal responsive properties of MCP particles quantitatively. The normalized hydrodynamic diameter of PS/(PNIPAm-10% MBA)/PEI and PS/PNIPAm/PEI MCP particles at 39 °C, $Rh_{39\ °C}/Rh_{25\ °C}$, were 0.92 and 0.77 respectively.

There was significant difference in the thermal responsive properties of MCP particles when different types of crosslinker were used. 8% reduction in the hydrodynamic diameter of PS/(PNIPAm-10% MBA)/PEI was recorded when MBA was used as crosslinker. 23% reduction in the hydrodynamic diameter of PS/PNIPAm/PEI was recorded when styrene was used as crosslinker. The shrinakge in the particle size of was more significant in PS/PNIPAm/PEI than PS/(PNIPAm-10% MBA)/PEI. The difference in their thermal responsive properties was probably attributed to the types of crosslinker. When MBA was used as crosslinker, PNIPAm was highly crosslinked which constrained the coil-to-glubole transition across VPTT. When styrene was used as crosslinker, PNIPAm was only slightly croslinked. PNIPAm was not constrined by the styrene and underwent coil-to-glubole transition at elevated temperature.

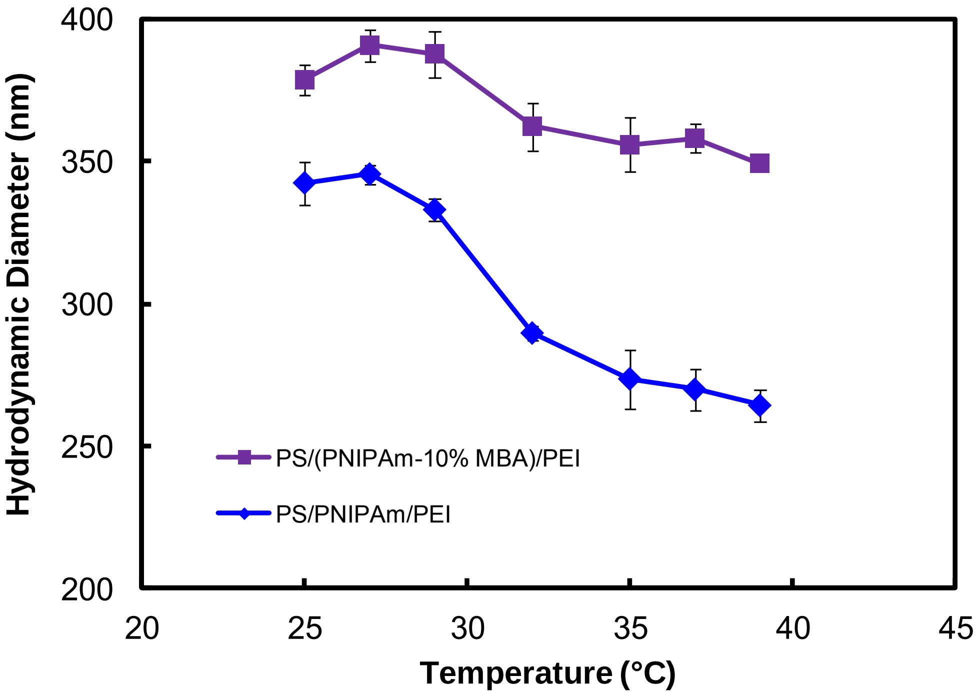

**Fig. 5.26.** Particle size of PS/PNIPAm/PEI MCP particles as a function of temperature.

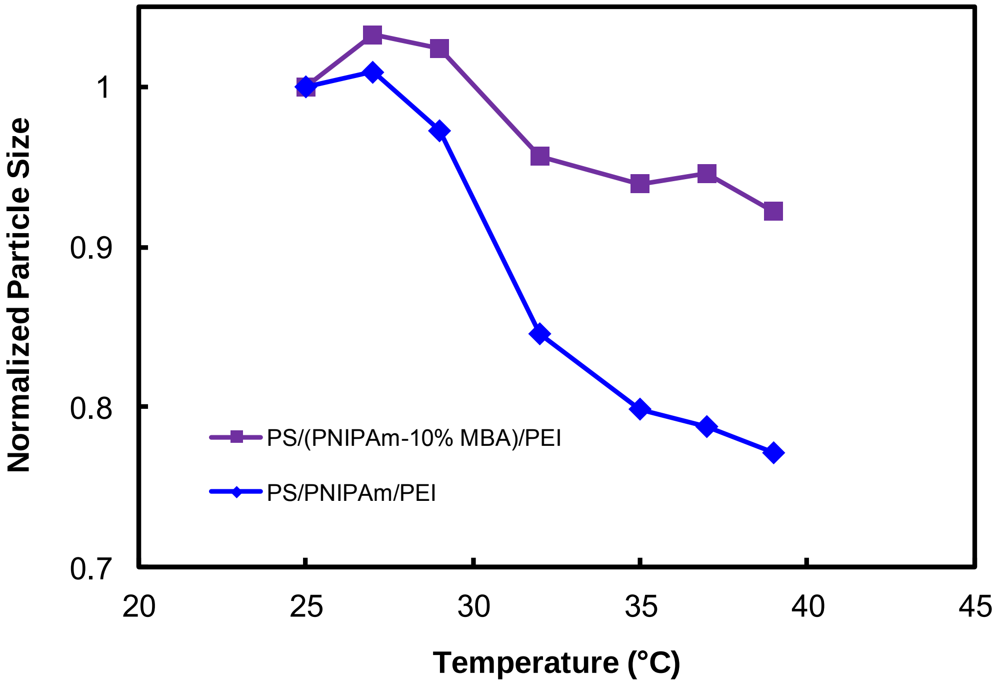

**Fig. 5.27.** Normalized particle size ($Dh/Dh_{25\ °C}$) of PS/PNIPAm/PEI MCP particles as a function of temperature

### 5.5.2 Surface charge as a function of temperature

#### *Surface charge*

The surface charge of MCP particles was determined by ζ-potential measurement using Beckman Coulter Delsa Nano C instrument. Under standard condition, pH 7 with conducting medium of 1 mM NaCl, the ζ-potential of PS/(PNIPAm-10% MBA)/PEI and PS/PNIPAm/PEI MCP particles were + 31.07 mV and + 4.92 mV at 25 ℃ respectively.

There is siginificant difference in the ζ-potential magnitude between PS/(PNIPAm-10% MBA)/PEI and PS/PNIPAm/PEI MCP particles. The major reason was due to the type of crosslinker used. When MBA was used as crosslinker in the synthesis of MCP particles, PNIPAm was highly crosslinked by the crosslinker. The efficient crosslinking was due to the presence of two C=C bonds in MBA which was available for crosslinking. Thus, the formation of interpenetrated network in the outermost shell was restricted. The positively charged PEI was not significantly shielded by PEI, resulting in high ζ-potential of the MCP particles. On the other hand, PNIPAm was slightly crosslinked by the second hydrophobic monomer (styrene). As styrene had only one C=C bond capable for crosslinking, the crosslinking of styrene was less efficient than MBA. This allowed PNIPAm to be extensively interpenetrated with PEI in the outermost shell, formation an interpenetrated network. As a result, the positively charged PEI was significantly shielded by PNIPAm, leading to low ζ-potential of the MCP particles.

***Surface charge as a function of pH***

The effect of pH on the ζ-potential of MCP particles prepared by different types of crosslinker (MBA and styrene) was conducted by ζ-potential measurement using Delsa Nano C with the aid of auto-titrator. The variation of ζ-potential as a function of pH of MCP particles with different second batch monomer was illustrated in the Figure 5.28.

MCP particles prepared by different types of crosslinker (MBA and styrene) had similar trend in the ζ-potential as a function of pH. Below pH 7, the ζ-potential of MCP particles was positive and almost unchanged. The positive ζ-potential indicated the presence of PEI on the particle shell. When solution pH was above 7, there was a drop in the ζ-potential of MCP particles due to the deprotonation of the ammonium cations of the PEI. The ζ-potential of the MCP particles was dropped to below + 10 mV at pH 9.5, the isoelectric point of PEI.

Although the MCP particles prepared by different types of crosslinker the same trend in the variation of ζ-potential against pH, the magnitude of ζ-potential was affected by the crosslinker type. As explained before, the types of crosslinker had significant impact on the formation of interpenetration network between PNIPAm and in the outermost shell. When MBA was used as crosslinker, PNIPAm was highly crosslinked which forbid the formation of interpenetrated shell with PEI. Most of the positive charges on PEI were not shielded which resulted in high ζ-potential below pH 7 (+ 30 mV). When styrene was used as crosslinker, PNIPAm was slightly crosslinked which allowed the formation of interpenetrated shell with PEI. Most of the positive charges on PEI were shielded which resulted in low ζ-potential below pH 7 (+ 10 mV).

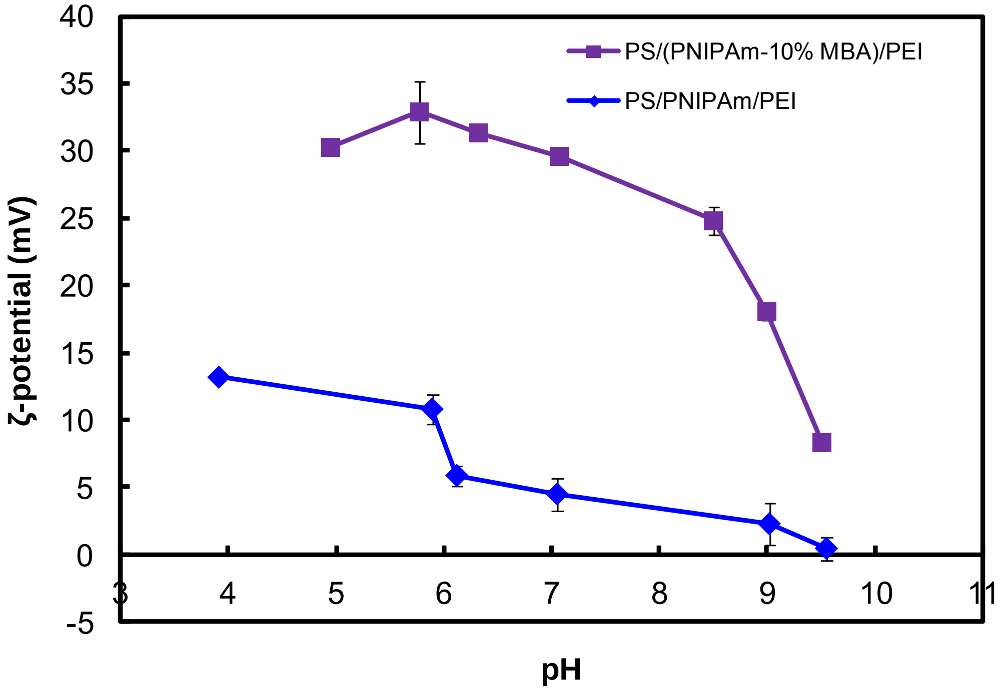

**Fig. 5.28.** ζ-potential as a function of pH of PS/PNIPAm/PEI MCP particles.

***Surface charge as a function of temerpature***

The effect of temperature on the ζ-potential of MCP particles prepared by different types of crosslinker (MBA and styrene) was evaluated by ζ-potential measurement using Delsa Nano C with the aid of thermal monitoring device. The variation of ζ-potential as a function of temperature of MCP particles with second hydrophobic polymer (PMMA and PS) as a function of temperature was displayed in Figure 5.29.

PS/(PNIPAm-10% MBA)/PEI and PS/PNIPAm/PEI MCP particles had the same trend in the variation of ζ-potential against temperature as explained in **4.3.2.4**. The ζ-potential of MCP particles was positive and kept constant at temperatures below VPTT of PNIPAm. There was an abrupt increase in the magnitude of ζ-potential when the temperature was rasied to above 32 °C. This increase was regarded as charge re-exposure on the particle surface. PNIPAm underwent phase transition at its VPTT which changed from hydrophilic to hydrophobic. Hydrophilic PNIPAm at the interpenetrated shell was shrunk and then migrated into the particle core. Thus, the positive PEI was not shielded by PNIPAm and resulted in an increase in the ζ-potential. This finding also indicated there was a change in the composition of the particle surface. The surface was composed of an interpenetrated network below VPTT of PNIPAm, while the surface was mainly composed of PEI above VPTT.

The increment in the ζ-potential of PS/(PNIPAm-10% MBA)/PEI MCP particles across VPTT was insignificant (from + 30 mV to + 40 mV). This was attributed to the selection of MBA as crosslinker. PNIPAm was highly crosslinked and tightly confined from forming interpenetrating metwork with PEI. Positively charge PEI was not severely shielded by PNIPAm, leading to highly positive ζ-potential at temperatures below VPTT. Hence, the increase in the ζ-potential magnitude was not significant at temperature above VPTT. However, there was a remarkable increase in the ζ-potential of PS/PNIPAm/PEI MCP particles across VPTT (from + 5 mV to + 35 mV). PNIPAm was slightly crosslinked by styrene in this case, resulting in the formation of interpenetrated shell with PEI. Positive charges on PEI were severly shielded by PNIPAm, leading to a remarkable suppression in the ζ-potential of the MCP particles. As temperature was raised to above VPTT, PNIPAm was shrunk from the outermost shell to the inner core due to volume phase transition. PEI was not shielded and the positive charges were re-exposed, resulting in an obvious increase in the ζ-potential.

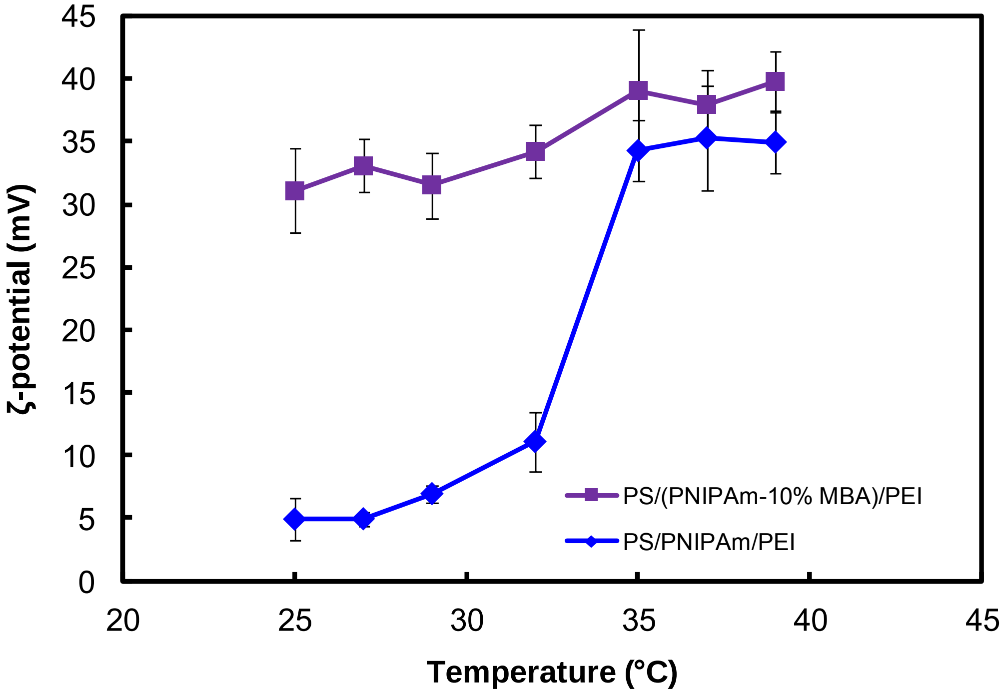

**Fig. 5.29.** ζ-potential as a function of temperature of PS/PNIPAm/PEI MCP particles.

### 5.5.3 Morphology

The morphology and core-shell nanostructure of PS/(PNIPAm-10% MBA)/PEI and PS/PNIPAm/PEI MCP particles were examined by TEM.

The nanostructure of the MCP particles was revealed under TEM micrographs by staining the dried particle samples with 0.5% (w/w) phosphotungstic acid (PTA, $WO_2 \cdot H_3PO_4 \cdot xH_2O$) for 5 mins. Both PS/(PNIPAm-10% MBA)/PEI and PS/PNIPAm/PEI MCP particles had a spherical morphology with well-defined core-shell nanostructure. The bright core of the particles was PS and the dark shell was PTA-stained PNIPAm and PEI.

However, the crosslinker type had affected the nanostructure of MCP particles. Particles with compacted PNIPAm layer was observed in PS/(PNIPAm-10% MBA)/PEI MCP particles. In the presence of 10% MBA, PNIPAm were highly crosslinked which confined their extension in the outermost shell. PEI was slightly interpenetrated with PNIPAm due to high crosslinking degree. On the contrary, particles with diffused PNIPAm layer were observed in PS/PNIPAm/PEI MCP particles. When styrene was used as crosslinker, PNIPAm was slightly crosslinked and highly extended in the outermost shell. This resulted in the formation of highly interpenetrated network between PNIPAm and PEI.

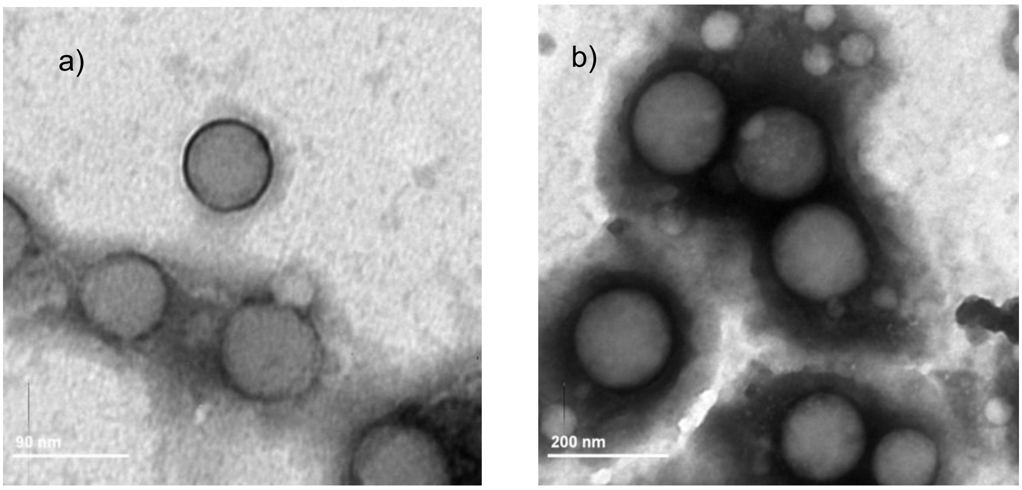

**Fig. 5.30.** TEM micrographs of a) PS/(PNIPAm-10% MBA)/PEI and b) PS/PNIPAm/PEI MCP particles.

## 5.6 Conclusion

Two types of multi-component polymer (MCP) particles, namely PMMA/PNIPAm/PEI and PS/PNIPAm/PEI, were successfully prepared via seed emulsion polymerization using non-crosslinked PNIPAm/PEI microgel as seed particles. MMA and styrene monomer were added in the second stage and were polymerized via seed emulsion polymerization. These hydrophobic monomers not only acted as polymerizable monomers, but also acted as crosslinker to crosslink the MCP particles. Two stages of exothermic polymerization were observed through online temperature monitoring. Two exothermic peaks were observed in the temperature profiles which corresponded to the seed formation and seed emulsion polymerization. High conversion could be generally achieved via this synthetic route. Characterizations of these two types of MCP particles suggest that they possessed nanosized dimension and uniform size distribution with high positive charges and good colloidal stability. More importantly, the outer shell of these MCP particles was composed of PNIPAm/PEI, forming an interpenetrated shell. The presence of PNIPAm/PEI interpenetrated shell was proven by particle size and ζ-potential measurement. Beyond VPTT (32 °C) of PNIPAm, there was a remarkable shrinkage of outer shell PNIPAm, reflected by synergic effect on reduction of hydrodynamic diameter and increase in ζ-potential. The prepared MCP particles were dual stimuli responsive materials which responded to pH and temperature variations. In addition, effect of i) weight ratio between PEI and total monomer; ii) weight ratio between seed monomer and second hydrophobic monomer; and iii) types of second batch monomer were studied in this chapter.

The weight ratio between PEI and total monomer had affected on the thermal and pH properties of MCP particles. The weight ratio between PEI and total monomer was varied from 1 : 1 to 1 : 9, keeping the weight ratio of seed monomer (NIPAm) to second hydrophobic monomer (MMA) at 1 : 1. As the ratio of PEI to total monomer varied from 1 : 1 to 1 : 9, the degree of particle shrinkage, $Dh_{39\,°C}/Dh_{25\,°C}$, was decreased from 0.95 to 0.86. The increase in NIPAm content in the MCP particles resulted in an increase in the thermal responsive properties of MCP particles. In addition, the ζ-potential of MCP particles at 25 °C was dropped from + 35.93 mV to + 9.77 mV as the PEI to total monomer weight ratio changed from 1 : 1 to 1 : 9. This change was contributed by the formation of interpenetration network between PNIPAm and PEI in the outermost shell of MCP particles. Increasing the total monomer content resulted in significant extension of PNIPAm in the outermost shell and contributed to the charge shielding of protonated amino groups on PEI. As a result, the pH responsiveness of MCP particles was suppressed. By varying the composition of PEI and total monomer, the pH and thermal responsive properties of MCP particles could be adjusted.

The weight ratio between seed monomer and second hydrophobic monomer had significant impact on the pH and thermal responsive properties of MCP particles. The composition between the seed monomer and second batch hydrophobic monomer was varied from 1 : 3 to 9 : 1, keeping the weight ratio between PEI and total monomer at 1 : 4. The degree of shrinkage in hydrodynamic diameter, $Rh_{39\,°C}/Rh_{25\,°C}$, of PMMA/PNIPAm/PEI MCP particles decreased from 0.94 to 0.62 as the weight ratio between NIPAm to styrene increased from 1 : 3 to 9 : 1. There was 40% reduction in the hydrodynamic diameter, indicating the thermal responsive property of MCP particles was strong denpended on the NIPAm monomer composition. On the other hand, the ζ-potential of MCP particles decreased from + 34.24 mV to + 6.39 mV as the weight ratio between NIPAm to MMA increased from 1 : 3 to 9 : 1. Increasing the NIPAm monomer composition had facilitated the formation of interpenetration network of PNIPAm and PEI at the outermost shell of the MCP particles, eventually contributed to charge shielding of PEI. Formation of interpenetration shell had enhanced the thermal responsiveness but on the other hand suppressed the pH responsiveness of MCP particles. Thus, the pH and thermal responsive properties of MCP particles could be controlled by optimizing the composition of thermal sensitive seed monomer to second batch hydrophobic monomer.

The second batch hydrophobic monomer also exerted significant effect on the formation and morphoplogy of MCP particles. MMA, *n*-BA and styrene were implemented as the second batch hydrophobic monomer in the preparation of MCP particles. Well characterized and stable colloidal MCP particles were only formed when MMA or styrene were utilized as second batch hydrophobic monomer. Stable MCP particles could not be formed when *n*-BA was used as second batch hydrophobic monomer. This was attributed to the absence of rigid solid support. The $T_g$ of PBA was low (219 K) which could not provide a rigid solid support to the MCP particle. The particle nanostructure could not be maintained and was dissociated eventually. If the second batch monomer was replaced by MMA or styrene, stable colloids of PS/PNIPAm/PEI and PMMA/PNIPAm/PEI MCP particles were obtained at the end of polymerization. In addition, these particles possessed superior thermal responsive properties which reflected from the results of particle size and ζ-potential measurements. However, the morphology of PMMA/PNIPAm/PEI MCP particles was different from PS/PNIPAm/PEI MCP particles. PS/PNIPAm/PEI exhibited spherical particles with well-defined core-shell nanostructure while PMMA/PNIPAm/PEI exhibited non-spherical aerolite-like particles with PMMA micro-domains evenly distributed inside the MCP particles. The difference was mainly contributed by the solubility of the second batch monomer in water mentioned in the previous chapter. The higher water solubility of MMA monomers allowed fast diffusion of the monomers from the bulk aqueous phase into the growing particle core for seed emulsion polymerization and crosslinking. Hence, MCP particles with different nanostructure could be tailor-made by the selection of second batch monomer.

# Chapter 6

## Conclusions

In conclusion, a novel synthetic route had been developed to prepare multi-component polymer (MCP) nanocomposite particles via a robust but versatile one-pot synthesis. Two steps were involved in this synthesis; i) seed particle formation by graft copolymerization of vinyl monomers from amino-containing water soluble polymer through redox initiation; followed by ii) seed emulsion polymerization through *in situ* addition of another hydrophobic vinyl monomer immediately after seed formation. This facile synthetic route allowed MCP particles to be fabricated from wide variety of materials possessing specific functionalities. MCP particles could be prepared from various types of seed particles, ranging from hard (PMMA/PEI) to soft (MBA crosslinked PNIPAm/PEI and non-crosslinked PNIPAm/PEI). The second batch hydrophobic monomers could be selected with various physical and chemical properties, including hard (MMA and styrene), soft (*n*-BA) and temperature sensitive (NIPAm). Combination of appropriate seed particle and second batch monomer might lead to novel smart MCP particles which potentially useful in wide range of applications.

Synthesis and characterization of PMMA/PEI based, MBA-crosslinked PNIPAm/PEI based and non-crosslinked PNIPAm/PEI based MCP particles had been carried out. Several effect studies with respect to total monomer conversion, composition, particle size and size distribution, particle size as a function of temperature, ζ-potential, ζ-potential as a function of pH and temperature, morphology and nanostructure were had been systematically investigated. These effect studies included

a) Types of seed forming monomer (MMA and NIPAm)
b) Types of second batch hydrophobic monomer (MMA, *n*-BA and styrene)
c) PEI to total monomer weight ratio (from 1 : 1 to 1 : 9)
d) Seed monomer to second batch hydrophobic monomer weight ratio (from 1 : 3 to 9 : 1)
e) Degree of MBA crosslinking (from 10% to 2%)
f) Reaction pH (from pH 5.5 to pH 9.0)

High total monomer conversion (> 80%) was achieved at the end of polymerization. The presence of three polymeric components in MCP particles was proved by comparing the FT-IR spectra between the seed particles and the MCP particles. The hydrodynamic diameter of the MCP particles was ranged from 200 nm to 500 nm, indicating a nanosized dimension. The particle size distribution (PDI) of the particles was kept below 0.3, implying a narrow size distribution. The ζ-potential of MCP particles was positive and greater than 20 mV in magnitude in most of the cases. This proved the outermost shell of MCP particles was constructed by positively charged species, PEI. In addition, the magnitude of ζ-potential was greater than 20 mV indicated the MCP particles were colloidally stable. Highly uniform spherical nanoparticles with well-defined core-shell nanostructure were revealed under the SEM and TEM micrographs. The particle size distribution of these MCP particles was narrow which implied no secondary nucleation during the polymerization process.

In the system of PMMA/PEI based MCP particles, amproteric MCP particles could be obtained when *n*-BA was used as second batch hydrophobic monomer. Formation of amproteric particles was observed by a shift in the point of zero charge of MCP particles to lower pH. The amproteric property of MCP particles was due to the presence of side reaction, hydrolysis of *n*-BA. *n*-BA underwent hydrolysis and then dissociated into carboxylic acid and butyl alcohol. The carboxylic acid segment was retained in the MCP particle which underwent protonation/deprotonation upon pH adjustment. The presence of both carboxylic groups and amino groups on the particles resulted in the formation of amproteric MCP particles. This amproteric property was further enhanced as the composition of *n*-BA monomer increased. Thus, our proposed synthetic approach had displayed a facile route to prepare amproteric particles.

In the system of MBA-crosslinked PNIPAm/PEI based MCP particles, particles with different nanostructures were fabricated by varying the types of second batch hydrophobic monomer. Spherical particles with well-defined core-shell structured were obtained when *n*-BA or styrene was applied as second batch hydrophobic monomer. Under this circumstance, the shell of the particles was constructed by PEI and PNIPAm while the core of the particles was constructed by PBA or PS. Multi-layered MCP particles were prepared if the degree of MBA crosslinking was high enough. Polymer chains of PNIPAm was restricted to be extended in the outermost shell and resulted in this hierarchical structure. More importantly, MCP particles with unique aerolite-like nanostructure were prepared when MMA was used as second batch hydrophobic monomer. The outermost shell of this particle was an interpenetrated shell which was composed of PEI and

PNIPAm. Several PMMA micro-domains with similar particle size were evenly distributed in the MCP particles, leading to this special nanostructure. The success in the fabrication of aerolite MCP particles had demonstrated a novel reaction pathway to prepare nanoparticles with different morphologies.

In the system of non-crosslinked PNIPAm/PEI based MCP particles, attempt to utilize the second batch hydrophobic monomer as crosslinker was taken. Vinyl monomer (MMA or styrene) introduced immediately after the seed formation not only took part in seed emulsion polymerization, but also participated in the crosslinking of the PNIPAm/PEI graft copolymer simultaneously. After seed emulsion polymerization, there was no particle dissociation even when the temperature fell back to room temperature (< VPTT of PNIPAm). This phenomenon was essential evidence indicating the second batch hydrophobic monomer was functioned as crosslinker. The presence of crosslinking by second batch hydrophobic monomer in the MCP particles was qualitatively characterized by FT-IR spectroscopy, SEM and TEM. In addition, the thermal responsive property was further promoted in the system of non-crosslinked PNIPAm/PEI based MCP particles. This proved the proposed crosslinkers did not exert adverse effect on the smart properties of the MCP particles. The use of vinyl monomer as organic crosslinker provided an alternative for the crosslinking of PNIPAm/PEI graft copolymer. The proposed crosslinking method was facile and versatile in which the crosslinkers could be selected from a wide range of viyl monomers. Moreover, the physical properties of the MCP particles could be altered by selecting appropriate crosslinkers and adjusting the crosslinking degree.

Other specific key features of different MCP particles were summarized as follows:

a) Well-defined amphiphilic nanoparticles containing three or more polymeric component could be produced without addition of surfactants and stabilizer in aqueous medium

b) The properties of the particles like glass transition temperature could be adjusted by different combination of seed monomer and second batch hydrophobic monomer.

c) pH responsive properties of MCP particles could be adjusted by varying the composition of the amino containing water soluble polymer.

d) Thermal responsive properties of MCP particles could be tuned by varying the composition of temperature sensitive monomer and degree of crosslinking

# Chapter 7

## Recommendations for future work

### 7.1 Design and synthesis of multi-responsive MCP particles

The success in fabrication of PNIPAm/PEI based MCP particles in this project provided us a versatile platform for the preparation of multi-component polymer particles. Future study will be focused on the preparation of multi-responsive MCP particles utilizing functional or stimuli-responsive monomers. Other smart responsive vinyl monomers like acrylic acid, *N*-vinylcaprolactam, are potential candidates for the synthesis of MCP particles. Polymeric particles possessing three responsive properties to external stimuli can be obtained if stimuli-responsive monomers are selected as seed and second hydrophobic monomer. The success in preparation of multi-responsive MCP particles should provide a feasible pathway for the fabrication of functional polymeric particles.

Particle morphologies and nanostructures are essential criteria in determining the applications of particles. They strongly depend on the compatibilities between the polymer components in the particles. Thus, selections of seed monomers and second monomers are critical to their final morphology and nanostructure. Future studies will be focused on the combination of different seed monomer and second monomer to prepare MCP particles with different morphologies and nanostructures.

Reaction parameters such as method of monomer addition, e.g. semi-batch or starve-fed addition, during seed emulsion polymerization might be critical parameter to determine the particle morphologies and nanostructures. Effect of addition method of second monomer on the morphology development of MCP particles should be another focus in the future works.

## 7.2 Applications of MCP particles

1) Protective coating

PBA/PMMA/PEI MCP particles have excellent film formation properties. Continuous and colourless thin film of this MCP particle was formed on most of the substrates under room temperature. Solvent test results had demonstrated the excellent chemical inertness of MCP particle film towards common organic solvents. These superior properties allow MCP particles to be used for protective coating.

2) Multi-responsive polymer-metal nanocomposite catalyst

PNIPAm/PEI based MCP particles have a smart interpenetrating shell composed of PNIPAm and PEI. This interpenetrated shell can respond to external pH and temperature changes. This smart PNIPAm/PEI based MCP particles can be potentially used as a nanocatalyst. Metal ions (e.g. $Ag^+$ or $Au^+$) are first immobilized on MCP particles followed by self reduction at a temperature above its VPTT (32 ℃). Silver or gold nanoparticles are formed and anchored onto the amino groups of PEI of MCP particles. These metal nanoparticles are protected by the interpenetrated shell of MCP particles at room temperature. When the temperature was elevated to above VPTT, the metal nanoparticles are exposed and available for catalytic reactions.

# Chapter 8

## References

1. Stuart, M.A.C., Huck, W.T.S., Genzer, J., Muller, M., Ober, C., Stamm, M., Sukhorukov, G.B., Szleifer, I., Tsukruk, V.V., Urban, M., Winnik, F., Zauscher, S., Luzinov, I., and Minko, S., "Emerging applications of stimuli-responsive polymer materials." *Nat Mater*, **2010**. *9*(2) 101-113.
2. Kawaguchi, H., "Functional polymer microspheres." *Progress in Polymer Science*, **2000**. *25*(8) 1171-1210.
3. Ho, K., Li, W., Wong, C., and Li, P., "Amphiphilic polymeric particles with core–shell nanostructures: emulsion-based syntheses and potential applications." *Colloid and Polymer Science*, **2010**. *288*(16-17) 1503-1523.
4. Champion, J.A., Katare, Y.K., and Mitragotri, S., "Particle shape: A new design parameter for micro- and nanoscale drug delivery carriers." *Journal of Controlled Release*, **2007**. *121*(1–2) 3-9.
5. Ghosh Chaudhuri, R. and Paria, S., "Core/Shell Nanoparticles: Classes, Properties, Synthesis Mechanisms, Characterization, and Applications." *Chemical Reviews*, **2011**. *112*(4) 2373-2433.
6. Schmidt-Thümmes, J., Schwarzenbach, E., and Lee, D.I., Applications in the Paper Industry, in *Polymer Dispersions and Their Industrial Applications*. **2003**, Wiley-VCH Verlag GmbH & Co. KGaA. pp. 75-101.
7. Szabo, B., Applications for Printing Inks, in *Polymer Dispersions and Their Industrial Applications*. **2003**, Wiley-VCH Verlag GmbH & Co. KGaA. pp. 103-122.

8. Richey, B. and Burch, M., Applications for Decorative and Protective Coatings, in *Polymer Dispersions and Their Industrial Applications*. **2003**, Wiley-VCH Verlag GmbH & Co. KGaA. pp. 123-161.

9. Urban, D. and Egan, L., Applications in the Adhesives and Construction Industries, in *Polymer Dispersions and Their Industrial Applications*. **2003**, Wiley-VCH Verlag GmbH & Co. KGaA. pp. 191-252.

10. Chou, C.-S. and Weier, J.E., Applications for Modification of Plastic Materials, in *Polymer Dispersions and Their Industrial Applications*. **2003**, Wiley-VCH Verlag GmbH & Co. KGaA. pp. 355-382.

11. Richard, J., Film Formation, in *Polymeric Dispersions: Principles and Applications*, J. Asua, Editor. **1997**, Springer Netherlands. pp. 397-419.

12. Waters, J., Latex Paint Formulations, in *Polymeric Dispersions: Principles and Applications*, J. Asua, Editor. **1997**, Springer Netherlands. pp. 421-433.

13. Lee, D., Latex Applications in Paper Coating, in *Polymeric Dispersions: Principles and Applications*, J. Asua, Editor. **1997**, Springer Netherlands. pp. 497-513.

14. Pichot, C., Delair, T., and Elaïssari, A., Polymer Colloids for Biomedical and Pharmaceutical Applications, in *Polymeric Dispersions: Principles and Applications*, J. Asua, Editor. **1997**, Springer Netherlands. pp. 515-539.

15. Norde, W., Interaction of Proteins with Polymeric and Other Colloids, in *Polymeric Dispersions: Principles and Applications*, J. Asua, Editor. **1997**, Springer Netherlands. pp. 541-555.

16. Nakai, S., Akiyoshi, M., and Okubo, M., "Preparation of micrometer-sized, multifunctional capsule particles for cosmetic by microsuspension

polymerization utilizing the self-assembling of phase separated polymer method." *Journal of Applied Polymer Science*, **2013**. *127*(4) 2407-2413.

17. Okubo, M., "Control of particle morphology in emulsion polymerization." *Makromolekulare Chemie. Macromolecular Symposia*, **1990**. *35-36*(1) 307-325.
18. Sundberg, D.C., Casassa, A.P., Pantazopoulos, J., Muscato, M.R., Kronberg, B., and Berg, J., "Morphology development of polymeric microparticles in aqueous dispersions. I. Thermodynamic considerations." *Journal of Applied Polymer Science*, **1990**. *41*(7-8) 1425-1442.
19. Chen, Y.-C., Dimonie, V.L., Shaffer, O.L., and El-Aasser, M.S., "Development of morphology in latex particles: The interplay between thermodynamic and kinetic parameters." *Polymer International*, **1993**. *30*(2) 185-194.
20. Sundberg, D.C. and Durant, Y.G., "Latex Particle Morphology, Fundamental Aspects: A Review." *Polymer Reaction Engineering*, **2003**. *11*(3) 379-432.
21. Gonzalez-Ortiz, L.J. and Asua, J.M., "Development of Particle Morphology in Emulsion Polymerization. 1. Cluster Dynamics." *Macromolecules*, **1995**. *28*(9) 3135-3145.
22. González-Ortiz, L.J. and Asua, J.M., "Development of Particle Morphology in Emulsion Polymerization. 2. Cluster Dynamics in Reacting Systems." *Macromolecules*, **1996**. *29*(1) 383-389.
23. González-Ortiz, L.J. and Asua, J.M., "Development of Particle Morphology in Emulsion Polymerization. 3. Cluster Nucleation and

Dynamics in Polymerizing Systems." *Macromolecules*, **1996**. *29*(13) 4520-4527.

24. Herrera, V., Pirri, R., Leiza, J.R., and Asua, J.M., "Effect of in-Situ-Produced Block Copolymer on Latex Particle Morphology." *Macromolecules,* **2006**. *39*(20) 6969-6974.
25. Rios, L., Hidalgo, M., Cavaille, J.Y., Guillot, J., Guyot, A., and Pichot, C., "Polystyrene(1)/poly(butyl acrylate-methacrylic acid)(2) core-shell emulsion polymers. Part I. Synthesis and colloidal characterization." *Colloid and Polymer Science*, **1991**. *269*(8) 812-824.
26. Daniels, E.S., Dimonie, V.L., El-Aasser, M.S., and Vanderhoff, J.W., "Preparation of ABS (acrylonitrile/butadiene/styrene) latexes using hydroperoxide redox initiators." *Journal of Applied Polymer Science*, **1990**. *41*(9-10) 2463-2477.
27. Chen, Y.C., Dimonie, V., and El-Aasser, M.S., "Effect of interfacial phenomena on the development of particle morphology in a polymer latex system." *Macromolecules*, **1991**. *24*(13) 3779-3787.
28. Karlsson, O.J., Stubbs, J.M., Carrier, R.H., and Sundberg, D.C., "Dynamic Modeling of Non-equilibrium Latex Particle Morphology Development During Seeded Emulsion Polymerization." *Polymer Reaction Engineering*, **2003**. *11*(4) 589-625.
29. Joensson, J.-E., Hassander, H., and Toernell, B., "Polymerization Conditions and the Development of a Core-Shell Morphology in PMMA/PS Latex Particles. 1. Influence of Initiator Properties and Mode of Monomer Addition." *Macromolecules*, **1994**. *27*(7) 1932-1937.

30. Stubbs, J., Karlsson, O., Jönsson, J.-E., Sundberg, E., Durant, Y., and Sundberg, D., "Non-equilibrium particle morphology development in seeded emulsion polymerization. 1: penetration of monomer and radicals as a function of monomer feed rate during second stage polymerization." *Colloids and Surfaces A: Physicochemical and Engineering Aspects*, **1999**. *153*(1–3) 255-270.

31. Winzor, C.L. and Sundberg, D.C., "Conversion dependent morphology predictions for composite emulsion polymers: 1. Synthetic latices." *Polymer*, **1992**. *33*(18) 3797-3810.

32. Karlsson, L.E., Karlsson, O.J., and Sundberg, D.C., "Nonequilibrium particle morphology development in seeded emulsion polymerization. II. Influence of seed polymer Tg." *Journal of Applied Polymer Science*, **2003**. *90*(4) 905-915.

33. Nelliappan, V., El-Aasser, M.S., Klein, A., Daniels, E.S., and Roberts, J.E., "Compatibilization of the PBA/PMMA core/shell latex interphase. I. Effect of PMMA macromonomer." *Journal of Polymer Science Part A: Polymer Chemistry*, **1996**. *34*(15) 3173-3181.

34. Nelliappan, V., El-Aasser, M.S., Klein, A., Daniels, E.S., and Roberts, J.E., "Compatibilization of the PBA/PMMA Core/Shell Latex Interphase. II. Effect of PMMA Macromonomer." *Journal of Polymer Science Part A: Polymer Chemistry*, **1996**. *34*(15) 3183-3190.

35. Herrera, V., Pirri, R., Asua, J.M., and Leiza, J.R., "Morphology control in polystyrene/poly(methyl methacrylate) composite latex particles." *Journal of Polymer Science Part A: Polymer Chemistry*, **2007**. *45*(12) 2484-2493.

36. Durant, Y.G., Sundberg, E.J., and Sundberg, D.C., "Effects of Cross-Linking on the Morphology of Structured Latex Particles. 2. Experimental Evidence for Lightly Cross-Linked Systems." *Macromolecules*, **1997**. *30*(4) 1028-1032.

37. Kim, J.-W. and Suh, K.-D., "Monodisperse micron-sized polystyrene particles by seeded polymerization: effect of seed crosslinking on monomer swelling and particle morphology." *Polymer*, **2000**. *41*(16) 6181-6188.

38. Okubo, M., Hosotani, T., and Yamashita, T., "Influences of the locations of monomer and initiator in the seeded polymerization systems on the morphologies of micron-sized monodispersed composite polymer particles." *Colloid and Polymer Science*, **1996**. *274*(3) 279-284.

39. Stubbs, J. and Sundberg, D., "Fundamental studies on morphology control for latex systems with application to waterborne coatings: The effect of polymer radical mobility in latex particles during polymerization." *Journal of Coatings Technology*, **2003**. *75*(938) 59-67.

40. Stubbs, J.M. and Sundberg, D.C., "Nonequilibrium particle morphology development in seeded emulsion polymerization. III. Effect of initiator end groups." *Journal of Applied Polymer Science*, **2004**. *91*(3) 1538-1551.

41. Lee, C.-F., "Effects of surfactants on the morphology of composite polymer particles produced by two-stage seeded emulsion polymerization." *Journal of Polymer Science Part A: Polymer Chemistry*, **2005**. *43*(11) 2224-2236.

42. Saito, N., Kagari, Y., and Okubo, M., "Effect of Colloidal Stabilizer on the Shape of Polystyrene/Poly(methyl methacrylate) Composite Particles

Prepared in Aqueous Medium by the Solvent Evaporation Method†." *Langmuir*, **2006**. *22*(22) 9397-9402.

43. Stubb, J.M. and Sundberg, D.C., "Nonequilibrium morphology development in seeded emulsion polymerization. IV. Influence of chain transfer agent." *Journal of Applied Polymer Science*, **2006**. *102*(2) 945-957.

44. Joensson, J.E.L., Hassander, H., Jansson, L.H., and Toernell, B., "Morphology of two-phase polystyrene/poly(methyl methacrylate) latex particles prepared under different polymerization conditions." *Macromolecules*, **1991**. *24*(1) 126-131.

45. Saito, N., Kagari, Y., and Okubo, M., "Revisiting the Morphology Development of Solvent-Swollen Composite Polymer Particles at Thermodynamic Equilibrium†." *Langmuir*, **2007**. *23*(11) 5914-5919.

46. Duda, Y. and Vázquez, F., "Modeling of Composite Latex Particle Morphology by Off-Lattice Monte Carlo Simulation." *Langmuir*, **2004**. *21*(3) 1096-1102.

47. Stubbs, J., Carrier, R., and Sundberg, D.C., "Monte Carlo Simulation of Emulsion Polymerization Kinetics and the Evolution of Latex Particle Morphology and Polymer Chain Architecture." *Macromolecular Theory and Simulations*, **2008**. *17*(4-5) 147-162.

48. Kirsch, S., Pfau, A., Stubbs, J., and Sundberg, D., "Control of particle morphology and film structures of carboxylated poly (n butylacrylate)/poly (methyl methacrylate) composite latex particles." *Colloids and Surfaces A: Physicochemical and Engineering Aspects*, **2001**. *183–185*(0) 725-737.

49. Stubbs, J.M. and Sundberg, D.C., "The dynamics of morphology development in multiphase latex particles." *Progress in Organic Coatings*, **2008**. *61*(2–4) 156-165.

50. Sundberg, E.J. and Sundberg, D.C., "Morphology development for three-component emulsion polymers: Theory and experiments." *Journal of Applied Polymer Science*, **1993**. *47*(7) 1277-1294.

51. Reyes, Y. and Asua, J.M., "Modeling multiphase latex particle equilibrium morphology." *Journal of Polymer Science Part A: Polymer Chemistry*, **2010**. *48*(12) 2579-2583.

52. Herrera, V., Palmillas, Z., Pirri, R., Reyes, Y., Leiza, J.R., and Asua, J.M., "Morphology of Three-Phase PS/PBA Composite Latex Particles Containing in Situ Produced Block Copolymers." *Macromolecules*, **2010**. *43*(3) 1356-1363.

53. Akhmatskaya, E. and Asua, J., "Dynamic modeling of the morphology of multiphase waterborne polymer particles." *Colloid and Polymer Science*, **2013**. *291*(1) 87-98.

54. Bockstaller, M., Kolb, R., and Thomas, E.L., "Metallodielectric Photonic Crystals Based on Diblock Copolymers." *Advanced Materials*, **2001**. *13*(23) 1783-1786.

55. Urbas, A.M., Maldovan, M., DeRege, P., and Thomas, E.L., "Bicontinuous Cubic Block Copolymer Photonic Crystals." *Advanced Materials*, **2002**. *14*(24) 1850-1853.

56. Yi, G.R., Manoharan, V.N., Klein, S., Brzezinska, K.R., Pine, D.J., Lange, F.F., and Yang, S.M., "Monodisperse Micrometer-Scale Spherical

Assemblies of Polymer Particles." *Advanced Materials*, **2002**. *14*(16) 1137-1140.

57. Babin, V., Garstecki, P., and Holyst, R., "Multiple photonic band gaps in the structures composed of core-shell particles." *Journal of Applied Physics*, **2003**. *94*(7) 4244-4247.

58. Alteheld, A., Gourevich, I., Field, L.M., Paquet, C., and Kumacheva, E., "Multilayer Polymer Particles with Periodic Modulation in Refractive Index." *Macromolecules*, **2005**. *38*(8) 3301-3306.

59. Tanaka, T., Saito, N., and Okubo, M., "Control of Layer Thickness of Onionlike Multilayered Composite Polymer Particles Prepared by the Solvent Evaporation Method†." *Macromolecules*, **2009**. *42*(19) 7423-7429.

60. Hu, R., Dimonie, V.L., El-Aasser, M.S., Pearson, R.A., Hiltner, A., Mylonakis, S.G., and Sperling, L.H., "Multicomponent latex IPN materials. I. Morphology control." *Journal of Polymer Science Part A: Polymer Chemistry*, **1997**. *35*(11) 2193-2206.

61. Hu, R., Dimonie, V.L., El-Aasser, M.S., Pearson, R.A., Hiltner, A., Mylonakis, S.G., and Sperling, L.H., "Multicomponent latex IPN materials: 2. Damping and mechanical behavior." *Journal of Polymer Science Part B: Polymer Physics*, **1997**. *35*(10) 1501-1514.

62. Okubo, M., Takekoh, R., and Sugano, H., "Production of micron-sized, monodispersed, multilayered composite polymer particles by multistep seeded dispersion polymerization." *Colloid and Polymer Science*, **2000**. *278*(6) 559-564.

63. Lee, C.F., "The morphology of composite polymer particles produced by multistage soapless seeded emulsion polymerization." *Colloid and Polymer Science*, **2002**. *280*(2) 116-123.

64. Lee, D.I., "Nanostructured latexes made by a sequential multistage emulsion polymerization." *Journal of Polymer Science Part A: Polymer Chemistry*, **2006**. *44*(9) 2826-2836.

65. Mu, Y., Qiu, T., Li, X., Guan, Y., Zhang, S., and Li, X., "Layer-by-Layer Synthesis of Multilayer Core–Shell Latex and the Film Formation Properties." *Langmuir*, **2011**. *27*(8) 4968-4978.

66. Chen, Y., Ballard, N., Gayet, F., and Bon, S.A.F., "High internal phase emulsion gels (HIPE-gels) from polymer dispersions reinforced with quadruple hydrogen bond functionality." *Chemical Communications*, **2012**. *48*(8) 1117-1119.

67. Fischer, H., "The Persistent Radical Effect: A Principle for Selective Radical Reactions and Living Radical Polymerizations." *Chemical Reviews*, **2001**. *101*(12) 3581-3610.

68. Qiu, J., Charleux, B., and Matyjaszewski, K., "Controlled/living radical polymerization in aqueous media: homogeneous and heterogeneous systems." *Progress in Polymer Science*, **2001**. *26*(10) 2083-2134.

69. Cunningham, M.F., "Controlled/living radical polymerization in aqueous dispersed systems." *Progress in Polymer Science*, **2008**. *33*(4) 365-398.

70. Monteiro, M.J. and Cunningham, M.F., "Polymer Nanoparticles via Living Radical Polymerization in Aqueous Dispersions: Design and Applications." *Macromolecules*, **2012**. *45*(12) 4939-4957.

71. Zetterlund, P.B., Kagawa, Y., and Okubo, M., "Controlled/Living Radical Polymerization in Dispersed Systems." *Chemical Reviews*, **2008**. *108*(9) 3747-3794.

72. Patten, T.E. and Matyjaszewski, K., "Atom Transfer Radical Polymerization and the Synthesis of Polymeric Materials." *Advanced Materials*, **1998**. *10*(12) 901-915.

73. Matyjaszewski, K. and Xia, J., "Atom Transfer Radical Polymerization." *Chemical Reviews*, **2001**. *101*(9) 2921-2990.

74. Matyjaszewski, K. and Tsarevsky, N.V., "Nanostructured functional materials prepared by atom transfer radical polymerization." *Nat Chem*, **2009**. *1*(4) 276-288.

75. Hawker, C.J., Bosman, A.W., and Harth, E., "New Polymer Synthesis by Nitroxide Mediated Living Radical Polymerizations." *Chemical Reviews*, **2001**. *101*(12) 3661-3688.

76. Bertin, D., Gigmes, D., Marque, S.R.A., and Tordo, P., "Kinetic subtleties of nitroxide mediated polymerization." *Chemical Society Reviews*, **2011**. *40*(5) 2189-2198.

77. Nicolas, J., Guillaneuf, Y., Lefay, C., Bertin, D., Gigmes, D., and Charleux, B., "Nitroxide-mediated polymerization." *Progress in Polymer Science*, **2013**. *38*(1) 63-235.

78. Moad, G., Rizzardo, E., and Thang, S.H., "Radical addition–fragmentation chemistry in polymer synthesis." *Polymer*, **2008**. *49*(5) 1079-1131.

79. McCormick, C.L. and Lowe, A.B., "Aqueous RAFT Polymerization: Recent Developments in Synthesis of Functional Water-Soluble

(Co)polymers with Controlled Structures†." *Accounts of Chemical Research*, **2004**. *37*(5) 312-325.

80. Save, M., Guillaneuf, Y., and Gilbert, R.G., "Controlled Radical Polymerization in Aqueous Dispersed Media." *Australian Journal of Chemistry*, **2006**. *59*(10) 693-711.

81. Kagawa, Y., Minami, H., Okubo, M., and Zhou, J., "Preparation of block copolymer particles by two-step atom transfer radical polymerization in aqueous media and its unique morphology." *Polymer*, **2005**. *46*(4) 1045-1049.

82. Kitayama, Y., Yorizane, M., Kagawa, Y., Minami, H., Zetterlund, P.B., and Okubo, M., "Preparation of onion-like multilayered particles comprising mainly poly(iso-butyl methacrylate)-block-polystyrene by two-step AGET ATRP." *Polymer*, **2009**. *50*(14) 3182-3187.

83. Kitayama, Y., Kagawa, Y., Minami, H., and Okubo, M., "Preparation of Micrometer-Sized, Onionlike Multilayered Block Copolymer Particles by Two-Step AGET ATRP in Aqueous Dispersed Systems: Effect of the Second-Step Polymerization Temperature." *Langmuir*, **2010**. *26*(10) 7029-7034.

84. Kagawa, Y., Zetterlund, P.B., Minami, H., and Okubo, M., "Compartmentalization in Atom Transfer Radical Polymerization (ATRP) in Dispersed Systems." *Macromolecular Theory and Simulations*, **2006**. *15*(8) 608-613.

85. Nicolas, J., Ruzette, A.-V., Farcet, C., Gérard, P., Magnet, S., and Charleux, B., "Nanostructured latex particles synthesized by nitroxide-

mediated controlled/living free-radical polymerization in emulsion." *Polymer*, **2007**. *48*(24) 7029-7040.

86. Nicolas, J., Charleux, B., Guerret, O., and Magnet, S., "Novel SG1-Based Water-Soluble Alkoxyamine for Nitroxide-Mediated Controlled Free-Radical Polymerization of Styrene and n-Butyl Acrylate in Miniemulsion." *Macromolecules*, **2004**. *37*(12) 4453-4463.

87. Delaittre, G., Nicolas, J., Lefay, C., Save, M., and Charleux, B., "Surfactant-free synthesis of amphiphilic diblock copolymer nanoparticles via nitroxide-mediated emulsion polymerization." *Chemical Communications*, **2005**(5) 614-616.

88. Delaittre, G., Nicolas, J., Lefay, C., Save, M., and Charleux, B., "Aqueous suspension of amphiphilic diblock copolymer nanoparticles prepared in situ from a water-soluble poly(sodium acrylate) alkoxyamine macroinitiator." *Soft Matter*, **2006**. *2*(3) 223-231.

89. Wei, R., Luo, Y., and Li, Z., "Synthesis of structured nanoparticles of styrene/butadiene block copolymers via RAFT seeded emulsion polymerization." *Polymer*, **2010**. *51*(17) 3879-3886.

90. Zhang, K., Gao, L., Zhang, C., and Chen, Y., "Functional sandwich-like organic/inorganic nanoplates from gelable triblock terpolymers." *Journal of Materials Chemistry*, **2009**. *19*(21) 3482-3489.

91. Zhang, K., Gao, L., Chen, Y., and Yang, Z., "Onion-like microspheres with tricomponent from gelable triblock copolymers." *Journal of Colloid and Interface Science*, **2010**. *346*(1) 48-53.

92. Pérez-Moral, N. and Mayes, A.G., "Molecularly Imprinted Multi-Layer Core-Shell Nanoparticles – A Surface Grafting Approach." *Macromolecular Rapid Communications*, **2007**. *28*(22) 2170-2175.

93. Ali, A.M.I. and Mayes, A.G., "Preparation of Polymeric Core−Shell and Multilayer Nanoparticles: Surface-Initiated Polymerization Using in Situ Synthesized Photoiniferters." *Macromolecules*, **2009**. *43*(2) 837-844.

94. Hossain, M.D.D., Tran, L.T.B., Park, J.M., and Lim, K.T., "Facile synthesis of core-surface crosslinked nanoparticles by interblock RAFT polymerization." *Journal of Polymer Science Part A: Polymer Chemistry*, **2010**. *48*(22) 4958-4964.

95. Ferguson, C.J., Hughes, R.J., Nguyen, D., Pham, B.T.T., Gilbert, R.G., Serelis, A.K., Such, C.H., and Hawkett, B.S., "Ab Initio Emulsion Polymerization by RAFT-Controlled Self-Assembly§." *Macromolecules*, **2005**. *38*(6) 2191-2204.

96. Ganeva, D.E., Sprong, E., de Bruyn, H., Warr, G.G., Such, C.H., and Hawkett, B.S., "Particle Formation in ab Initio RAFT Mediated Emulsion Polymerization Systems." *Macromolecules*, **2007**. *40*(17) 6181-6189.

97. Thickett, S.C. and Gilbert, R.G., "Mechanism of Radical Entry in Electrosterically Stabilized Emulsion Polymerization Systems." *Macromolecules*, **2006**. *39*(19) 6495-6504.

98. Hamasaki, H., Maekawa, Y., Matsuzawa, S., Ohtaka, A., Nakamura, Y., and Fujii, S., "Synthesis of Poly(3,4-ethylenedioxythiophene)&ndash;Palladium Nanocomposite-coated Polymer Particles by Chemical Oxidative Seeded Dispersion Polymerization." *Chemistry Letters*, **2012**. *41*(12) 1658-1659.

99. Fujii, S., Matsuzawa, S., Nakamura, Y., Ohtaka, A., Teratani, T., Akamatsu, K., Tsuruoka, T., and Nawafune, H., "Synthesis and Characterization of Polypyrrole−Palladium Nanocomposite-Coated Latex Particles and Their Use as a Catalyst for Suzuki Coupling Reaction in Aqueous Media*." Langmuir*, **2010**. *26*(9) 6230-6239.

100. Fujii, S., Matsuzawa, S., Hamasaki, H., Nakamura, Y., Bouleghlimat, A., and Buurma, N.J., "Polypyrrole–Palladium Nanocomposite Coating of Micrometer-Sized Polymer Particles Toward a Recyclable Catalyst*." Langmuir*, **2011**. *28*(5) 2436-2447.

101. Okubo, M., Takekoh, R., and Izumi, J., "Preparation of micron-sized, monodispersed, “onion-like” multilayered poly(methyl methacrylate)/polysterene composite particles by reconstruction of morphology with the solvent-absorbing/releasing method*." Colloid and Polymer Science*, **2001**. *279*(5) 513-518.

102. Okubo, M., Izumi, J., Hosotani, T., and Yamashita, T., "Production of micron-sized monodispersed core/shell polymethyl methacrylate/polystyrene particles by seeded dispersion polymerization*." Colloid and Polymer Science,* **1997**. *275*(8) 797-801.

103. Okubo, M., Izumi, J., and Takekoh, R., "Production of micron-sized monodispersed core/shell composite polymer particles by seeded dispersion polymerization*." Colloid and Polymer Science,* **1999**. *277*(9) 875-880.

104. Okubo, M., Takekoh, R., and Saito, N., "Formation mechanism of an “onionlike” multilayered structure by reconstruction of the morphology of micron-sized, monodisperse poly(methyl methacrylate)/polystyrene

composite particles with the solvent-absorbing/solvent-releasing method." *Colloid and Polymer Science*, **2004**. *282*(11) 1192-1197.

105. Okubo, M., Takekoh, R., and Saito, N., "Effect of graft polymer on the formation of micron-sized, monodisperse, "onion-like" alternately multilayered poly(methyl methacrylate)/polystyrene composite particles by reconstruction of morphology with the solvent-absorbing/releasing method." *Colloid and Polymer Science*, **2003**. *281*(10) 945-950.

106. Okubo, M., Yonehara, H., and Kurino, T., "Influence of viscosity within polymerizing particle on the morphology of micron-sized, monodisperse composite polymer particles produced by seeded polymerization for the dispersion of highly monomer-swollen polymer particles." *Colloid and Polymer Science*, **2003**. *281*(10) 1002-1005.

107. Saito, N., Takekoh, R., Nakatsuru, R., and Okubo, M., "Effect of Stabilizer on Formation of “Onionlike” Multilayered Polystyrene-block-poly(methyl Methacrylate) Particles." *Langmuir*, **2007**. *23*(11) 5978-5983.

108. Tanaka, T., Nakatsuru, R., Kagari, Y., Saito, N., and Okubo, M., "Effect of Molecular Weight on the Morphology of Polystyrene/Poly(methyl methacrylate) Composite Particles Prepared by the Solvent Evaporation Method†." *Langmuir*, **2008**. *24*(21) 12267-12271.

109. Okubo, M., Tanaka, A., and Yonehara, H., "Reconstruction of morphology of micron-sized, monodisperse composite polymer particles by the solvent-absorbing/releasing method." *Colloid and Polymer Science*, **2004**. *282*(6) 646-650.

110. Okubo, M., Saito, N., Takekoh, R., and Kobayashi, H., "Morphology of polystyrene/polystyrene-block-poly(methyl methacrylate)/poly(methyl methacrylate) composite particles*." Polymer*, **2005**. *46*(4) 1151-1156.

111. Takekoh, R., Okubo, M., Araki, T., Stöver, H.D.H., and Hitchcock, A.P., "Quantitative Chemical Mapping of Nanostructured “Onionlike” Poly(methyl methacrylate)/Polystyrene Composite Particles by Soft X-ray Microscopy*." Macromolecules*, **2004**. *38*(2) 542-551.

112. Jeon, S.-J., Yi, G.-R., and Yang, S.-M., "Cooperative Assembly of Block Copolymers with Deformable Interfaces: Toward Nanostructured Particles*." Advanced Materials*, **2008**. *20*(21) 4103-4108.

113. Yabu, H., Higuchi, T., and Shimomura, M., "Unique Phase-Separation Structures of Block-Copolymer Nanoparticles*." Advanced Materials*, **2005**. *17*(17) 2062-2065.

114. Higuchi, T., Tajima, A., Yabu, H., and Shimomura, M., "Spontaneous formation of polymer nanoparticles with inner micro-phase separation structures*." Soft Matter*, **2008**. *4*(6) 1302-1305.

115. Yabu, H., "Creation of Functional and Structured Polymer Particles by Self-Organized Precipitation (SORP)*." Bulletin of the Chemical Society of Japan*, **2012**. *85*(3) 265-274.

116. Takekoh, R., Li, W.-H., Burke, N.A.D., and Stöver, H.D.H., "Multilayered Polymer Microspheres by Thermal Imprinting during Microsphere Growth*." Journal of the American Chemical Society*, **2005**. *128*(1) 240-244.

117. Dubé, M.A. and Penlidis, A., "A systematic approach to the study of multicomponent polymerization kinetics—the butyl acrylate/methyl

methacrylate/vinyl acetate example: 1. Bulk copolymerization." *Polymer*, **1995**. *36*(3) 587-598.

118. Dubé, M.A. and Penlidis, A., "A systematic approach to the study of multicomponent polymerization kinetics: the butyl acrylate/methyl methacrylate/vinyl acetate example, 2. Bulk (and solution) terpolymerization." *Macromolecular Chemistry and Physics*, **1995**. *196*(4) 1101-1112.

119. Dubé, M.A. and Penlidis, A., "A systematic approach to the study of multicomponent polymerization kinetics: butyl acrylate/methyl methacrylate/vinyl acetate. III. Emulsion homopolymerization and copolymerization in a pilot plant reactor." *Polymer International*, **1995**. *37*(4) 235-248.

120. Dubé, M.A., Penlidis, A., and Reilly, P.M., "A systematic approach to the study of multicomponent polymerization kinetics: The butyl acrylate/methyl methacrylate/vinyl acetate example. IV. Optimal Bayesian design of emulsion terpolymerization experiments in a pilot plant reactor." *Journal of Polymer Science Part A: Polymer Chemistry*, **1996**. *34*(5) 811-831.

121. Li, Z., Feng, Y., Li, L., Pu, J., and Yang, H., "Preparation and properties of a thermo-sensitive latex film." *European Polymer Journal*, **2008**. *44*(6) 1899-1906.

122. Chen, C.-F., Lee, K.-H., and Chiu, W.-Y., "Synthesis and characterization of poly(butyl acrylate–methyl methacrylate)/polyaniline core–shell latexes." *Journal of Applied Polymer Science*, **2007**. *104*(2) 823-830.

123. Ma, Q., Gu, L., Ma, S., and Ma, G., "Study on synthesis and morphology control of poly(4-vinylpyridine-co-butyl acrylate)/poly(styrene-co-butyl acrylate) composite microspheres." *Journal of Applied Polymer Science*, **2002**. *83*(6) 1190-1203.

124. Lee, C.-F., "The effect of aqueous medium contains poly(acrylic acid) on the morphology of composite polymer particle produced by two stages soapless seeded emulsion polymerization." *Polymer*, **2002**. *43*(21) 5763-5769.

125. Kang, K., Kan, C., Du, Y., Yeung, A., and Liu, D., "Morphology control of soap-free seeded P(St–EA–AA) latex particles." *European Polymer Journal*, **2005**. *41*(7) 1510-1518.

126. Monteiro, M.J. and de Barbeyrac, J., "Free-Radical Polymerization of Styrene in Emulsion Using a Reversible Addition−Fragmentation Chain Transfer Agent with a Low Transfer Constant: Effect on Rate, Particle Size, and Molecular Weight." *Macromolecules*, **2001**. *34*(13) 4416-4423.

127. Monteiro, M.J. and de Barbeyrac, J., "Preparation of Reactive Composite Latexes by 'Living' Radical Polymerization Using the RAFT Process. A New Class of Polymer Materials." *Macromolecular Rapid Communications*, **2002**. *23*(5-6) 370-374.

128. Okubo, M., Yamaguchi, A., and Fujiwara, T., "Thermodynamic aspects of the heterogeneous structure of "golf-ball-like" polymer particles." *Colloid and Polymer Science*, **1999**. *277*(10) 1005-1008.

129. Okubo, M., Wang, Z., Yamashita, T., Ise, E., and Minami, H., "Morphology of micron-sized, monomer-adsorbed, crosslinked polymer particles having snowmanlike shapes prepared by the dynamic swelling

method." *Journal of Polymer Science Part A: Polymer Chemistry*, **2001**. *39*(18) 3106-3111.

130. Okubo, M., Minami, H., Wang, Z., and Ise, E., "Adsorption of styrene on micron-sized, monodisperse, cross-linked polymer particles in a snowman-shaped state by utilizing the dynamic swelling method." *Colloid and Polymer Science*, **2001**. *279*(10) 976-982.

131. Du, Y.-Z., Tomohiro, T., and Kodaka, M., "Synthesis of Hemispherical Poly(2-hydroxylethyl methacrylate-co-methyl methacrylate)/Poly(styrene-co-glycidyl methacrylate) Composite Particles with Heterobifunctional Groups by Soap-Free Seeded Emulsion Polymerization." *Macromolecules*, **2004**. *37*(3) 803-812.

132. Okubo, M., Saito, N., and Fujibayashi, T., "Preparation of polystyrene/poly(methyl methacrylate) composite particles having a dent." *Colloid and Polymer Science*, **2005**. *283*(6) 691-698.

133. Okubo, M., Fujibayashi, T., Yamada, M., and Minami, H., "Micron-sized, monodisperse, snowman/confetti-shaped polymer particles by seeded dispersion polymerization." *Colloid and Polymer Science*, **2005**. *283*(9) 1041-1045.

134. Fujibayashi, T. and Okubo, M., "Preparation and Thermodynamic Stability of Micron-Sized, Monodisperse Composite Polymer Particles of Disc-like Shapes by Seeded Dispersion Polymerization†." *Langmuir*, **2007**. *23*(15) 7958-7962.

135. Wurm, F. and Kilbinger, A.F.M., "Polymeric Janus Particles." *Angewandte Chemie International Edition*, **2009**. *48*(45) 8412-8421.

136. Tolue, S., Moghbeli, M.R., and Ghafelebashi, S.M., "Preparation of ASA (acrylonitrile-styrene-acrylate) structural latexes via seeded emulsion polymerization." *European Polymer Journal*, **2009**. *45*(3) 714-720.

137. Deng, W., Wang, M.Y., Chen, G., and Kan, C.Y., "Morphological evolution of multistage polymer particles in the alkali post-treatment." *European Polymer Journal*, **2010**. *46*(6) 1210-1215.

138. Park, J.H., Kim, K.Y., and Park, J.M., "Polymer hollow particles: Encapsulation of phosphoric acid partial esters and morphology manipulation." *Polymer*, **2010**. *51*(14) 3014-3022.

139. Du, J. and O'Reilly, R.K., "Anisotropic particles with patchy, multicompartment and Janus architectures: preparation and application." *Chemical Society Reviews*, **2011**. *40*(5) 2402-2416.

140. Yang, M., Wang, G., and Ma, H., "An efficient approach for production of polystyrene/poly(4-vinylpridine) particles with various morphologies based on dynamic control." *Chemical Communications*, **2011**. *47*(3) 911-913.

141. Yoon, J., Lee, K.J., and Lahann, J., "Multifunctional polymer particles with distinct compartments." *Journal of Materials Chemistry*, **2011**. *21*(24) 8502-8510.

142. Walther, A. and Müller, A.H.E., "Janus Particles: Synthesis, Self-Assembly, Physical Properties, and Applications." *Chemical Reviews*, **2013**. *113*(7) 5194-5261.

143. Meng, X., Guan, Y., Niu, Z., and Qiu, D., "Facile Preparation Route toward Speckled Colloids via Seeded Polymerization." *Langmuir*, **2013**. *29*(7) 2152-2158.

144. Kaneko, T., Hamada, K., Chen, M.Q., and Akashi, M., "One-Step Formation of Morphologically Controlled Nanoparticles with Projection Coronas." *Macromolecules*, **2003**. *37*(2) 501-506.

145. Huang, H. and Liu, H., "Synthesis of the raspberry-like PS/PAN particles with anisotropic properties via seeded emulsion polymerization initiated by γ-ray radiation." *Journal of Polymer Science Part A: Polymer Chemistry*, **2010**. *48*(22) 5198-5205.

146. Shi, S., Kuroda, S., Tadaki, S., and Kubota, H., "Phase distribution and separation in poly(2-acetoxyethyl methacrylate)/polystyrene latex interpenetrating polymer networks." *Polymer*, **2002**. *43*(26) 7443-7450.

147. Shi, S., Kuroda, S.-i., and Kubota, H., "Anomalous particles formed in two-stage soap-free emulsion polymerization of styrene on poly(2-acetoxyethyl methacrylate)." *Colloid and Polymer Science*, **2003**. *281*(4) 331-336.

148. Shi, S., Kuroda, S., Hosoi, K., and Kubota, H., "Poly(methyl methacrylate)/polyacrylonitrile composite latex particles with a novel surface morphology." *Polymer*, **2005**. *46*(11) 3567-3570.

149. Hoffmann, M., Lu, Y., Schrinner, M., Ballauff, M., and Harnau, L., "Dumbbell-Shaped Polyelectrolyte Brushes Studied by Depolarized Dynamic Light Scattering." *The Journal of Physical Chemistry B*, **2008**. *112*(47) 14843-14850.

150. Hoffmann, M., Siebenburger, M., Harnau, L., Hund, M., Hanske, C., Lu, Y., Wagner, C.S., Drechsler, M., and Ballauff, M., "Thermoresponsive colloidal molecules." *Soft Matter*, **2010**. *6*(6) 1125-1128.

151. Chu, F., Siebenbürger, M., Polzer, F., Stolze, C., Kaiser, J., Hoffmann, M., Heptner, N., Dzubiella, J., Drechsler, M., Lu, Y., and Ballauff, M., "Synthesis and Characterization of Monodisperse Thermosensitive Dumbbell-Shaped Microgels." *Macromolecular Rapid Communications*, **2012**. *33*(12) 1042-1048.

152. Kim, J.-W., Larsen, R.J., and Weitz, D.A., "Synthesis of Nonspherical Colloidal Particles with Anisotropic Properties." *Journal of the American Chemical Society*, **2006**. *128*(44) 14374-14377.

153. Sheu, H.R., El-Aasser, M.S., and Vanderhoff, J.W., "Phase separation in polystyrene latex interpenetrating polymer networks." *Journal of Polymer Science Part A: Polymer Chemistry*, **1990**. *28*(3) 629-651.

154. Mock, E.B. and Zukoski, C.F., "Emulsion Polymerization Routes to Chemically Anisotropic Particles." *Langmuir*, **2010**. *26*(17) 13747-13750.

155. Park, J.-G., Forster, J.D., and Dufresne, E.R., "High-Yield Synthesis of Monodisperse Dumbbell-Shaped Polymer Nanoparticles." *Journal of the American Chemical Society*, **2010**. *132*(17) 5960-5961.

156. Ahmad, H., Saito, N., Kagawa, Y., and Okubo, M., "Preparation of Micrometer-Sized, Monodisperse "Janus" Composite Polymer Particles Having Temperature-Sensitive Polymer Brushes at Half of the Surface by Seeded Atom Transfer Radical Polymerization†." *Langmuir*, **2008**. *24*(3) 688-691.

157. Tanaka, T., Okayama, M., Kitayama, Y., Kagawa, Y., and Okubo, M., "Preparation of "Mushroom-like" Janus Particles by Site-Selective Surface-Initiated Atom Transfer Radical Polymerization in Aqueous Dispersed Systems†." *Langmuir*, **2010**. *26*(11) 7843-7847.

158. Okubo, M. and Ahmad, H., "Synthesis of temperature-sensitive submicron-size composite polymer particles." *Colloid and Polymer Science,* **1995**. *273*(9) 817-821.

159. Tanaka, T., Okayama, M., Minami, H., and Okubo, M., "Dual Stimuli-Responsive "Mushroom-like" Janus Polymer Particles as Particulate Surfactants†." *Langmuir,* **2010**. *26*(14) 11732-11736.

160. Saito, N., Nakatsuru, R., Kagari, Y., and Okubo, M., "Formation of "Snowmanlike" Polystyrene/Poly(methyl methacrylate)/Toluene Droplets Dispersed in an Aqueous Solution of a Nonionic Surfactant at Thermodynamic Equilibrium†." *Langmuir,* **2007**. *23*(23) 11506-11512.

161. Mock, E.B., De Bruyn, H., Hawkett, B.S., Gilbert, R.G., and Zukoski, C.F., "Synthesis of Anisotropic Nanoparticles by Seeded Emulsion Polymerization." *Langmuir,* **2006**. *22*(9) 4037-4043.

162. Tang, C., Zhang, C., Liu, J., Qu, X., Li, J., and Yang, Z., "Large Scale Synthesis of Janus Submicrometer Sized Colloids by Seeded Emulsion Polymerization." *Macromolecules,* **2010**. *43*(11) 5114-5120.

163. Kang, J.-H., Moon, J.H., Lee, S.-K., Park, S.-G., Jang, S.G., Yang, S., and Yang, S.-M., "Thermoresponsive Hydrogel Photonic Crystals by Three-Dimensional Holographic Lithography." *Advanced Materials,* **2008**. *20*(16) 3061-3065.

164. Gourevich, I., Field, L.M., Wei, Z., Paquet, C., Petukhova, A., Alteheld, A., Kumacheva, E., Saarinen, J.J., and Sipe, J.E., "Polymer Multilayer Particles:  A Route to Spherical Dielectric Resonators." *Macromolecules,* **2006**. *39*(4) 1449-1454.

165. Kumacheva, E., Kalinina, O., and Lilge, L., "Three-Dimensional Arrays in Polymer Nanocomposites." *Advanced Materials*, **1999**. *11*(3) 231-234.

166. Siwick, B.J., Kalinina, O., Kumacheva, E., Dwayne Miller, R.J., and Noolandi, J., "Polymeric nanostructured material for high-density three-dimensional optical memory storage." *Journal of Applied Physics*, **2001**. *90*(10) 5328-5334.

167. Gourevich, I., Pham, H., Jonkman, J.E.N., and Kumacheva, E., "Multidye Nanostructured Material for Optical Data Storage and Security Labeling." *Chemistry of Materials*, **2004**. *16*(8) 1472-1479.

168. Chen, C.-W. and Chen, M.-Q., "In situ synthesis and the catalytic properties of platinum colloids on polystyrene microspheres with surface-grafted poly(N-isopropylacrylamide)[double dagger]." *Chemical Communications*, **1998**(7) 831-832.

169. Chen, C.-W., Chen, M.-Q., Serizawa, T., and Akashi, M., "In-Situ Formation of Silver Nanoparticles on Poly(N-isopropylacrylamide)-Coated Polystyrene Microspheres." *Advanced Materials,* **1998**. *10*(14) 1122-1126.

170. Chen, C.-W., Serizawa, T., and Akashi, M., "Preparation of Platinum Colloids on Polystyrene Nanospheres and Their Catalytic Properties in Hydrogenation†." *Chemistry of Materials*, **1999**. *11*(5) 1381-1389.

171. Sharma, G. and Ballauff, M., "Cationic Spherical Polyelectrolyte Brushes as Nanoreactors for the Generation of Gold Particles." *Macromolecular Rapid Communications*, **2004**. *25*(4) 547-552.

172. Lu, Y., Mei, Y., Ballauff, M., and Drechsler, M., "Thermosensitive Core−Shell Particles as Carrier Systems for Metallic Nanoparticles." *The Journal of Physical Chemistry B*, **2006**. *110*(9) 3930-3937.

173. Lu, Y., Mei, Y., Drechsler, M., and Ballauff, M., "Thermosensitive Core–Shell Particles as Carriers for Ag Nanoparticles: Modulating the Catalytic Activity by a Phase Transition in Networks." *Angewandte Chemie International Edition*, **2006**. *45*(5) 813-816.

174. Mei, Y., Lu, Y., Polzer, F., Ballauff, M., and Drechsler, M., "Catalytic Activity of Palladium Nanoparticles Encapsulated in Spherical Polyelectrolyte Brushes and Core−Shell Microgels." *Chemistry of Materials*, **2007**. *19*(5) 1062-1069.

175. Lu, Y., Proch, S., Schrinner, M., Drechsler, M., Kempe, R., and Ballauff, M., "Thermosensitive core-shell microgel as a "nanoreactor" for catalytic active metal nanoparticles." *Journal of Materials Chemistry*, **2009**. *19*(23) 3955-3961.

176. Wu, S., Kaiser, J., Guo, X., Li, L., Lu, Y., and Ballauff, M., "Recoverable Platinum Nanocatalysts Immobilized on Magnetic Spherical Polyelectrolyte Brushes." *Industrial & Engineering Chemistry Research*, **2012**. *51*(15) 5608-5614.

177. Okubo, M., Fujii, S., and Minami, H., "Production of electrically conductive, core/shell polystyrene/polyaniline composite particles by chemical oxidative seeded dispersion polymerization." *Colloid and Polymer Science*, **2001**. *279*(2) 139-145.

178. Chen, J., Zeng, F., Wu, S., Chen, Q., and Tong, Z., "A Core–Shell Nanoparticle Approach to Photoreversible Fluorescence Modulation of a Hydrophobic Dye in Aqueous Media." *Chemistry – A European Journal*, **2008**. *14*(16) 4851-4860.

179. Jian, C., Fang, Z., Shuizhu, W., Junhua, S., Jianqing, Z., and Zhen, T., "A facile approach for cupric ion detection in aqueous media using polyethyleneimine/PMMA core–shell fluorescent nanoparticles." *Nanotechnology*, **2009**. *20*(36) 365502.

180. Dreher, W.R., Jarrett, W.L., and Urban, M.W., "Stable Nonspherical Fluorine-Containing Colloidal Dispersions: Synthesis and Film Formation." *Macromolecules,* **2005**. *38*(6) 2205-2212.

181. Misra, A., Jarrett, W.L., and Urban, M.W., "New Poly(methyl methacrylate)/n-Butyl Acrylate/Pentafluorostyrene/Poly(ethylene glycol) (p-MMA/nBA/PFS/PEG) Colloidal Dispersions: Synthesis, Film Formation, and Protein Adsorption." *Macromolecules*, **2009**. *42*(19) 7299-7308.

182. Wang, J., Wen, Y., Hu, J., Song, Y., and Jiang, L., "Fine Control of the Wettability Transition Temperature of Colloidal-Crystal Films: From Superhydrophilic to Superhydrophobic." *Advanced Functional Materials*, **2007**. *17*(2) 219-225.

183. Fujii, S., Randall, D.P., and Armes, S.P., "Synthesis of Polystyrene/Poly[2-(Dimethylamino)ethyl Methacrylate-stat-Ethylene Glycol Dimethacrylate] Core−Shell Latex Particles by Seeded Emulsion Polymerization and Their Application as Stimulus-Responsive Particulate Emulsifiers for Oil-in-Water Emulsions." *Langmuir,* **2004**. *20*(26) 11329-11335.

184. Okubo, M., Ahmad, H., and Suzuki, T., "Synthesis of temperature-sensitive micron-sized monodispersed composite polymer particles and its application as a carrier for biomolecules." *Colloid and Polymer Science*, **1998**. *276*(6) 470-475.

185. Fang, S.-J. and Kawaguchi, H., "A thermosensitive amphoteric microsphere and its potential application as a biological carrier." *Colloid and Polymer Science*, **2002**. *280*(11) 984-989.

186. Li, Z., Kwok, M.-H., and Ngai, T., "Preparation of Responsive Micrometer-Sized Microgel Particles with a Highly Functionalized Shell." *Macromolecular Rapid Communications*, **2012**. *33*(5) 419-425.

187. Neumann, T., Haupt, B., and Ballauff, M., "High Activity of Enzymes Immobilized in Colloidal Nanoreactors." *Macromolecular Bioscience,* **2004**. *4*(1) 13-16.

188. Haupt, B., Neumann, T., Wittemann, A., and Ballauff, M., "Activity of Enzymes Immobilized in Colloidal Spherical Polyelectrolyte Brushes." *Biomacromolecules,* **2005**. *6*(2) 948-955.

189. Welsch, N., Wittemann, A., and Ballauff, M., "Enhanced Activity of Enzymes Immobilized in Thermoresponsive Core−Shell Microgels." *The Journal of Physical Chemistry B,* **2009**. *113*(49) 16039-16045.

190. Makino, K., Yamamoto, S., Fujimoto, K., Kawaguchi, H., and Ohshima, H., "Surface Structure of Latex Particles Covered with Temperature-Sensitive Hydrogel Layers." *Journal of Colloid and Interface Science,* **1994**. *166*(1) 251-258.

191. Okubo, M. and Ahmad, H., "Effect of shell thickness on the temperature-sensitive property of core-shell composite polymer particles." *Journal of Polymer Science Part A: Polymer Chemistry,* **1996**. *34*(15) 3147-3153.

192. Duracher, D., Sauzedde, F., Elaissari, A., Perrin, A., and Pichot, C., "Cationic amino-containing N-isopropyl- acrylamide–styrene copolymer

latex particles: 1-Particle size and morphology vs. polymerization process." *Colloid and Polymer Science*, **1998**. *276*(3) 219-231.

193. Pelton, R., "Temperature-sensitive aqueous microgels." *Advances in Colloid and Interface Science*, **2000**. *85*(1) 1-33.

194. Senff, H. and Richtering, W., "Influence of cross-link density on rheological properties of temperature-sensitive microgel suspensions." *Colloid and Polymer Science*, **2000**. *278*(9) 830-840.

195. Hellweg, T., Dewhurst, C.D., Eimer, W., and Kratz, K., "PNIPAM-co-polystyrene Core−Shell Microgels: Structure, Swelling Behavior, and Crystallization." *Langmuir*, **2004**. *20*(11) 4330-4335.

196. Ballauff, M., "Spherical polyelectrolyte brushes." *Progress in Polymer Science*, **2007**. *32*(10) 1135-1151.

197. Dai, S., Ravi, P., and Tam, K.C., "pH-Responsive polymers: synthesis, properties and applications." *Soft Matter*, **2008**. *4*(3) 435-449.

198. Tian, P., Wu, Q., and Lian, K., "Preparation of temperature- and pH-sensitive, stimuli-responsive poly(N-isopropylacrylamide-co-methacrylic acid) nanoparticles." *Journal of Applied Polymer Science*, **2008**. *108*(4) 2226-2232.

199. Zhang, F. and Wang, C.-C., "Preparation of thermoresponsive core–shell polymeric microspheres and hollow PNIPAM microgels." *Colloid and Polymer Science*, **2008**. *286*(8-9) 889-895.

200. Dai, S., Ravi, P., and Tam, K.C., "Thermo- and photo-responsive polymeric systems." *Soft Matter*, **2009**. *5*(13) 2513-2533.

201. Tauer, K., Gau, D., Schulze, S., Völkel, A., and Dimova, R., "Thermal property changes of poly(N-isopropylacrylamide) microgel particles and block copolymers." *Colloid and Polymer Science*, **2009**. *287*(3) 299-312.

202. Liu, F. and Urban, M.W., "Recent advances and challenges in designing stimuli-responsive polymers." *Progress in Polymer Science*, **2010**. *35*(1–2) 3-23.

203. Motornov, M., Roiter, Y., Tokarev, I., and Minko, S., "Stimuli-responsive nanoparticles, nanogels and capsules for integrated multifunctional intelligent systems." *Progress in Polymer Science*, **2010**. *35*(1–2) 174-211.

204. Zhang, H., Zhang, X., and Yang, X., "Facile synthesis of monodisperse polymer/SiO2/polymer/TiO2 tetra-layer microspheres and the corresponding double-walled hollow SiO2/TiO2 microspheres." *Journal of Colloid and Interface Science*, **2010**. *348*(2) 431-440.

205. Zhang, L., Daniels, E.S., Dimonie, V.L., and Klein, A., "Synthesis and characterization of PNIPAM/PS core/shell particles." *Journal of Applied Polymer Science*, **2010**. *118*(5) 2502-2511.

206. Lu, Y. and Ballauff, M., "Thermosensitive core–shell microgels: From colloidal model systems to nanoreactors." *Progress in Polymer Science*, **2011**. *36*(6) 767-792.

207. Polzer, F., Heigl, J., Schneider, C., Ballauff, M., and Borisov, O.V., "Synthesis and Analysis of Zwitterionic Spherical Polyelectrolyte Brushes in Aqueous Solution." *Macromolecules*, **2011**. *44*(6) 1654-1660.

208. Rahman, M.M., Chehimi, M.M., Fessi, H., and Elaissari, A., "Highly temperature responsive core–shell magnetic particles: Synthesis,

characterization and colloidal properties." *Journal of Colloid and Interface Science*, **2011**. *360*(2) 556-564.

209. Ramos, J., Imaz, A., and Forcada, J., "Temperature-sensitive nanogels: poly(N-vinylcaprolactam) versus poly(N-isopropylacrylamide)." *Polymer Chemistry*, **2012**. *3*(4) 852-856.

210. Li, P., Zhu, J., Sunintaboon, P., and Harris, F.W., "New Route to Amphiphilic Core−Shell Polymer Nanospheres: Graft Copolymerization of Methyl Methacrylate from Water-Soluble Polymer Chains Containing Amino Groups." *Langmuir*, **2002**. *18*(22) 8641-8646.

211. Ho, K.M., Li, W.Y., Lee, C.H., Yam, C.H., Gilbert, R.G., and Li, P., "Mechanistic study of the formation of amphiphilic core–shell particles by grafting methyl methacrylate from polyethylenimine through emulsion polymerization." *Polymer*, **2010**. *51*(15) 3512-3519.

212. Zhu, J. and Li, P., "Synthesis and characterization of poly(methyl methacrylate)/casein nanoparticles with a well-defined core-shell structure." *Journal of Polymer Science Part A: Polymer Chemistry*, **2003**. *41*(21) 3346-3353.

213. Ho, K.M., Mao, X., Gu, L., and Li, P., "Facile Route to Enzyme Immobilization: Core−Shell Nanoenzyme Particles Consisting of Well-Defined Poly(methyl methacrylate) Cores and Cellulase Shells." *Langmuir*, **2008**. *24*(19) 11036-11042.

214. Li, W. and Li, P., "Synthesis of Well-Defined Amphiphilic Core–Shell Particles Containing Amine-Rich Shells." *Macromolecular Rapid Communications*, **2007**. *28*(23) 2267-2271.

215. Lee, C.H., Wong, C.H., Ouhab, D., Borsali, R., and Li, P., "Synthesis and Characterization of Solvent-Invertible Amphiphilic Hollow Particles." *Langmuir*, **2013**. *29*(25) 7583-7590.

216. Varga, I., Gilányi, T., Mészáros, R., Filipcsei, G., and Zrínyi, M., "Effect of Cross-Link Density on the Internal Structure of Poly(N-isopropylacrylamide) Microgels." *The Journal of Physical Chemistry B,* **2001**. *105*(38) 9071-9076.